Properties of Mechanical Metamaterials

with the Focus on Magnetic Inclusions

Ph.D. Thesis

by

Krzysztof Karol Dudek

Supervised by: Prof. Joseph N. Grima

Co-supervised by: Prof. Krzysztof W. Wojciechowski

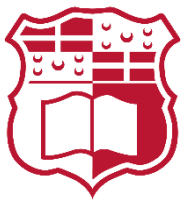

University of Malta

April 2018

Statement of Authenticity

The undersigned declare that the content of this Ph.D. thesis is based on the work carried out by Krzysztof Karol Dudek under the supervision of Professor Joseph N. Grima and Professor Krzysztof W. Wojciechowski.

_____ _____

Krzysztof K. Dudek — Professor Joseph N. Grima

Candidate — *Supervisor*

_____

Professor Krzysztof W. Wojciechowski

Co-Supervisor

Abstract

Mechanical metamaterials are man-made systems having anomalous macroscopic mechanical properties originating primarily from the geometry of the subunits rather than composition of the material at the molecular level. Even though, over the years, mechanical metamaterials have been thoroughly studied, it does not mean that there are not any new aspects related to their behaviour which remain to be discovered such as the capability of these systems to induce their own rotational motion as a result of internal deformation. In this thesis, this novel phenomenon was analysed, optimised and confirmed both by means of a theoretical model and experimental prototype for particular mechanical metamaterials deforming via the rotation of their subunits. It was also proposed that potential prototypes utilising this concept could prove to be useful in applications where control over the rotational motion of the system is of particular importance.

The role of magnetic inclusions inserted into standard mechanical metamaterials was also thoroughly investigated. It is proposed that, as a result of the interaction between subunits constituting the system, such magnetic inclusions have a very important role in modifying the stiffness characteristics of the systems. More specifically, it was shown *via* a theoretical model as well as by means of experimental testing that the smart insertion of magnetic inclusions permits control of the mechanical behaviour of such metamaterials as these inclusions interact with each other as the system deforms. Results suggest that the considered system may not only exhibit negative Poisson's ratio but also negative stiffness, which effect could not be possible without the use of magnetic inclusions. In order to further investigate different physical phenomena which can be exhibited by mechanical metamaterials with magnetic inclusions, through the use of the Ising model, it was shown that such systems make it possible to induce the magnetocaloric effect even in the absence of an external magnetic field. By means of computer simulations, it was also shown that the rate at which such systems are deformed has a large impact on the evolution of magnetic domains within the system. It is also proposed that magnetic inclusions could be useful in inducing the deformation process instead of the 'standard' external forces.

In addition to all this, this thesis has also looked into two metamaterials constructs which are particularly amenable to negative properties. In particular, a mechanical system incorporating a hierarchical design which was investigated through a dynamics approach, where it was shown that such a system makes it possible to obtain a wide range of mechanical properties and deformation patterns solely as a result of the control over the resistance of structural units to the motion promoting the deformation process. Also studied was a novel structure composed of appropriately connected generic triangles which system was reported to exhibit both negative linear compressibility and negative thermal expansion.

Acknowledgements

First and foremost I would like to thank my supervisor, Prof. Joseph N. Grima, who throughout the entire duration of my degree helped me to understand new concepts related to my research and offered his guidance allowing me to finalise my scientific projects. His continuous support also made it possible for me to feel like a member of his research group and focus on my studies. I would also want to thank my co-supervisor, Prof. Krzysztof W. Wojciechowski, who similarly to Prof. Grima allowed me to gain a better understanding of investigated problems and offered me his help whenever it was required.

I would also want to express my gratitude for Prof. Ruben Gatt and Dr Daphne Attard who, despite not being officially assigned as my supervisors or co-supervisors, have helped me with my research and offered to share their knowledge throughout my entire degree. At this point, I would also want to thank all of the former and current members of the Metamaterials Unit, in particular: Dr Luke Mizzi, Roberto Caruana-Gauci, Dr Reuben Cauchi, Darryl Gambin, Dr Jean-Pierre Brincat, Dr Keith Azzopardi and Edera Degabriele who not only helped me with my research but also ensured that I would feel in Malta as at home.

Finally, I would like to thank my parents and my sister for their continuous support.

Table of Contents

List of Figures

Figure 2-19 Systems of thin magnetic films having a potential to exhibit auxetic behaviour shown schematically in the case of (a) a theoretical work reported in and (b) experimental work involving the use of $CoFe_2O_4$.

Figure 2-20 Panels show: (a) different examples of mechanical metamaterials which are potentially suitable to host magnetic inclusions, (b) the model investigated and (c) experimental realisation of the theoretical concept proposed on panel (b).

Figure 2-21 Panels show: (a) elastic Euler beam with a magnet at one of its ends which is being attracted by an external magnet, (b) kagome lattice with magnetic inclusions and (c) cellular structure with magnetic inclusions deformed by an external magnetic field.

Figure 2-22 Different examples of magneto-elastic lattices with magnetic moments represented by blue or red points being oriented in the perpendicular direction to the plane of the figure.

Figure 2-23 Panels show: (a) model of a magnetic vibration damper operating through the principle of negative stiffness and (b) an experimental example of the mechanical metamaterial exhibiting negative stiffness.

Figure 4-1 The panels show (a) the model of the discussed system with schematically drawn blue arrows indicating the positioning of linear actuators inducing a deformation of the system (black arrows indicate all types of rotations exhibited by the system), (b) a diagram presenting a possible connection of the discussed system with an external body, (c) diagrams depicting the concept of global rotation of the system in which the rotation of rigid units results with a decrease of the angle θ_0 and a change in the value of $\Delta\theta_1$. The change in the value of $\Delta\theta_1$ corresponds to the rotation of the structure with respect to its centre of mass.

Figure 4-2 The panels show (a) comparison of the behaviour of systems consisting of a different number of rigid units and (b) the change in the behaviour of the system upon varying the magnitude of the ratio of densities of heavy and light units for a system with a conserved mass. The point where the system stops exhibiting the global rotation, i.e. the values of $\Delta\theta_1$ stop changing, corresponds to the conformation of the system where $2\theta_0 = 0°$.

Figure 5-1 The experimental prototype used in order to investigate the potential of mechanical metamaterials to induce their own rotational motion as the result of the rotation of their subunits.

Figure 5-2 Panels show: (a) the evolution of the system in time from the moment when it was released to the moment when the rigid units collided for the first time and (b) pictures corresponding to (i) the initial configuration assumed by the system and (ii) the configuration assumed by the system at the moment when rigid units collided for the first time. In the case of panel (b), the auxiliary lines indicating the orientation of the system connect two particular points within the structure at different stages of the deformation.

Figure 5-3 The variation in the angle $2\theta_0$ corresponding to the behaviour of of the system after the first collision between the rigid units.

Figure 5-4 Behaviour of the system after the first collision between the rigid units.

Figure 6-1 Panels show: (a) Type I and (b) Type II rotating rectangles systems investigated in this Chapter. Red and blue colours correspond to a different densities of units rotating in the

opposite directions in the case of each of the structures. Note that these systems have different symmetries and profile of pores which result from the different manner how the rectangles are connected together to form the network. In particular, in the Type I four $l_a \times l_b$ rectangles are connected in such a way that the empty spaces between the rectangles form rhombi of size $l_a \times l_a$ and $l_b \times l_b$ whilst the Type II network has parrallelogramic pores of the same size $l_a \times l_b$.

Figure 6-2 A diagram presenting the concept of the global rotation of the Type I rotating rectangle system induced by the rotation of its subunits.

Figure 6-3 Panels (a) and (b) show the variation in the angle of aperture between rigid units $2\theta_0$ plotted with respect to time for Type I and Type II rotating rectangle systems composed of rectangular units associated with different values of the aspect ratio l_a / l_b. Panels (c) and (d) show the variation in the extent of the global rotation exhibited by Type I and Type II respectively for deformation process from panels (a) and (b).

Figure 6-4 Panels (a) and (b) show the variation in I_1 for Type I and Type II rotating rectangle systems during the process of mechanical deformation. Panels (c) and (d) show the variation in the parameter $(5I_H - 4I_L)/I_1$ for Type I and Type II systems associated with different values of l_a / l_b ratio respectively.

Figure 6-5 A diagram presenting the hypothetical concept of the deformation of the rotating square system having electromagnetic hinges connecting adjacent units at vertices. Those pairs of the vertices which form a hinge as a result of the mutual interaction (for example induced by electromagnets or other devices) are highlighted by means of the connected red arrows. It should also be noted that the concept of the global rotation is not shown in this diagram.

Figure 7-1 The panels in this figure present (a) the two-level hierarchical auxetic system with four square-like units corresponding to Level 1 of the structure, where each unit consists of $N_0 \times N_0$ (in the provided example $N_0 = 3$) Level 0 repeat units (bright green), (b) an example of the structure corresponding to $N_0 = 1$ and (c) the permissible angles for θ_0 and θ_1, which conditions ensure that the squares do not overlap with each other and the system retains the same connectivity. This is attained when conditions $\theta_1 > \theta_0$ and $\varepsilon = \pi - 2\theta_1 - 2\theta_0 > 0$ are satisfied.

Figure 7-2 Plots showing the variation in (a) θ_1 (b) θ_0 and (c) Poisson's ratio ν_{xy} as a function of time t for loading in the x direction for systems with K_h values ranging from $0.035\ \mathrm{N \cdot m \cdot deg^{-1}}$ to $2.093\ \mathrm{N \cdot m \cdot deg^{-1}}$ and (d) the relation of θ_1 to θ_0 for a deforming structure having the motion of the hinges governed by harmonic potential. Similarly, plots (e), (f) and (g) show the variation in θ_1, θ_0 and ν_{xy} respectively as a function of time in the case of friction-based hinges corresponding to the value of f ranging between $0\ \mathrm{N \cdot m}$ and $3.5\ \mathrm{N \cdot m}$. (h) shows the relation of θ_1 to θ_0 for a deforming structure having the motion of the hinges governed by friction. In all cases considered, $N_0 = 1$ and F=500 N. It is important to note that in the case of (c) and (g), the scale in the y-axis (incremental Poisson's ratio) was arbitrarily stopped at -2, since this value of the Poisson's ratio tends to $-\infty$ upon approaching the maximum

deformation. A cut-off value of -2 is appropriate in view of the fact that the part of the deformation which is not included in panels (c) and (g) is relatively small, as shown in Table *7-1*. An analogical set of results, plotted with respect to applied strain, is provided in Appendix III.

Figure 7-3 Diagrams showing the final state of the deformation of two systems, where the hinging process is governed by friction, with K_h values of $0.035\ \mathrm{N\cdot m\cdot deg^{-1}}$ and $1.396\ \mathrm{N\cdot m\cdot deg^{-1}}$.

Figure 7-4 A plot showing a comparison of the Poisson's ratios obtained from the numerical solutions presented here for f = 0.5 Nm and f = 3.5 Nm with those calculated from analytical models for uni-level rotating rigid rectangle and square systems.

Figure 8-1 (a) A generalised structure based on Milton's expanders (b) the unit cell of a typical form of the systems studied here.

Figure 8-2 Variation in mechanical properties for three different types of systems. Panels show results for systems where the unit-cell is composed of (a) equilateral triangles having dimensions a = 1 nm, b = 1 nm and c = 1 nm, (b) isosceles triangles corresponding to dimensions a = 1 nm, b = 2 nm and c = 2 nm and (c) scalene triangles where a = 6 nm, b = 3 nm and c = 4 nm. Solid red and dashed blue lines indicate mechanical properties exhibited by the system in the *Ox1* and *Ox2* directions respectively. Different colours on of the background helps to make a distinction between different forms assumed by considered systems.

Figure 8-3 Variation in geometric dimensions of the unit-cell for three different types of systems. Solid red and dashed blue lines indicate mechanical properties exhibited by the system in the *Ox1* and *Ox2* directions respectively. The black dashed line represents the area of the unit-cell corresponding to a given system.

Figure 8-4 Variation of the range of angles in which NLC is exhibited for a particular form on changing the *b*:*a* ratio of an isosceles triangle.

Figure 8-5 Variation of the thermal expansion coefficient with the aspect ratio of isosceles triangles for systems where $b = c > a = 1$ having a form that exists for $180° - 2\gamma < \theta < 2\beta$ and vibrating about an equilibrium angle of $90°$. The temperature was set to be equal to T = 293 K and the value of $I\omega^2$ was set to be equal to $75k_BT$.

Figure 8-6 Panels show: (a) a visualisation of the hypothetical concept related to the self-induced global rotation of mechanical metamaterials composed of triangle motifs having different masses and (b) expected behaviour of the rotating rigid triangle systems with magnetic inclusions.

Figure 9-1 Panels show: (a) the considered system composed of a number of arrowhead units with magnetic inclusions, (b) a single unit of the system, (c)(i) stages of the mechanical deformation in the system with attracting magnets in each unit (ii) stages of the mechanical deformation in the system with attracting magnets in each unit and (d) experimental prototype used in order to investigate mechanical properties of the considered system.

Figure 9-2 Panels show: (a) different stages of the deformation of the experimental prototype associated with: (i) initial, (ii) threshold and (iii) final configuration, (b) Poisson's ratio

exhibited by the system for loading in the vertical direction, (c) force recorded by the tensile loader throughout the entire process of deformation of the experimental prototype, (d) stiffness exhibited by the prototype with attracting and repelling magnets, (e) theoretical results corresponding to the force required to deform the system analogical to the experimental prototype and (f) stiffness exhibited by the system according to the theoretical model.

Figure 9-3 Panels show: (a) the variation in the Poisson's ratio in the loading direction for systems corresponding to a different value of l_b, (b) variation in the (i) magnetic potential energy per unit and (ii) stiffness of the system with attracting magnets for structures corresponding to different values of l_b and (c) graphs analogical to those from panel (b) but generated for systems with repelling magnets.

Figure 9-4 Panels show: (a) the variation in the Poisson's ratio in the loading direction for system with magnets corresponding to different values of μ, (b) variation in (i) magnetic potential energy per unit and (ii) stiffness of the system with attracting magnets for structures corresponding to different values of μ and (c) results analogical to those shown on panel (b) but generated for systems with repelling magnets within structural units.

Figure 10-1 Magneto-auxetic system of 3×3 squares of dimension $a\times a$ with the exemplary configuration of Ising spins $s=\pm1$ denoted by "+" and "-" respectively, located at centre of mass of the squares. L_x and L_y denote linear dimensions of the system in the *x* and *y* directions respectively.

Figure 10-2 Temperature dependence of the isothermal entropy change Δs_M for MAS deformed from θ_i to θ_f at zero magnetic field. The plots representing deformations $89°\rightarrow90°$, $80°\rightarrow90°$, $70°\rightarrow90°$, $45°\rightarrow90°$ are shown (units in degrees). The vertical lines indicate location of T_c for a given value of θ_i and θ_f.

Figure 11-1 The model represented by a set of rigid squares connected at vertices. In this case, signs "+" and "-" located at the centre of each unit, correspond to opposite orientations of magnetic moments within the system. In this diagram, the number of squares was set in a way allowing to conveniently visualise the introduced variables.

Figure 11-2 The panels present (a) the change in the correlation length *r* during the deformation process for different values of ω and (b) the comparison of the evolution of the system corresponding to $\omega=1°/MCs$ to the behaviour of systems in which the distance between the neighbouring spins is not being changed throughout the simulation, i.e. the simulation takes place for a fixed value of θ. The correlation length *r* is expressed in terms of the distance *d*.

Figure 11-3 The panels present (a) diagrams visualising the configuration of the magnetic auxetic system corresponding to a particular value of the angle θ (red lines are used in order to highlight edges forming the aperture of the unit-cell), (b) evolution of magnetic domains for a system in which the angle θ is being changed with the constant angular velocity $\omega=0.5°/MCs$ (relatively low value of ω) and (c) visualisation of the evolution of magnetic domains in the system corresponding to $\omega=10°/MCs$ (relatively high value of ω). In order

to better visualise the domains in the system on panels (b) and (c), only a fragment (100×100 units) of the larger square lattice considered in this work was selected.

Figure 11-4 Energy of spins at the domain boundary per spin for different values of ω.

List of Tables

1. Introduction

1.1 Mechanical Metamaterials

Mechanical metamaterials, which term was probably first formally defined by Grima *et al.* [1], are a class of systems where the macroscopic mechanical properties originate primarily from the geometry of the subunits constituting a given system and not from the composition of the material at the molecular level, i.e. systems exhibiting unusual properties which are composed of standard material components which do not have a propensity to exhibit such characteristic. It also means that in theory, mechanical metamaterials may be constructed at any scale as long as a particular shape of the subunit can be achieved. It also indicates that these systems, irrespective of their size, may exhibit an arbitrary mechanical behaviour including anomalous properties such as negative Poisson's ratio, negative thermal expansion, negative compressibility and negative stiffness which properties are going to be described in the following subsections of this Introduction.

Due to their versatility, mechanical metamaterials may be designed in a variety of conformations to exhibit particular mechanical behaviour. Consequently, over the years, scientists working in the field of materials science have proposed a number of different classes of mechanical metamaterials. Some of the most studied examples of such classes include rotating rigid unit systems [2-4], perforated systems (macro-scale) [5-13], re-entrant [14-23] and chiral honeycomb [24-30] structures (macro-scale) as well as foams (micro-scale) [31-33]. Studies related to these systems are described in more detail in the Literature review section of this thesis.

At this point, it should be highlighted that mechanical metamaterials should not be confused with optical (which include photonic) metamaterials which in literature are also often referred to as metamaterials [34-36]. The latter systems are normally investigated in terms of

their electro-magnetic properties and the way how they interact with different waves. Furthermore, despite the fact that mechanical deformation has been reported to affect properties of optical metamaterials, these systems are not usually the subject of studies related to their mechanical properties. Some excellent reviews on optical metamaterials are given in [37, 38].

Before proceeding any further and discussing the historical progress made in the field of mechanical metamaterials having a propensity to exhibit unusual mechanical properties, it is useful to define some of the basic mechanical properties which are going to be used in order to describe the behaviour of systems investigated in this work, namely: (1) Auxetic Behaviour (Negative Poisson's ratios); (2) Negative thermal expansion; (3) Negative compressibility, and (4) Negative stiffness.

1.2 Different types of mechanical behaviour which may be exhibited by mechanical metamaterials

1.2.1 Auxetic behaviour

Auxetic [39] systems exhibit the counter-intuitive property of expanding laterally when being subjected to a uniaxial strain (see Figure 1-1). On the other hand, in the case of conventional (non-auxetic) materials, the contrary behaviour is expected with these structures getting thinner when uniaxially stretched. The two effects described above, may be quantified by means of the Poisson's ratio, ν_{ij}, which quantity if measured in the $Ox_i - Ox_j$ plane (see Figure 1-1), with Ox_i being the loading direction, may be expressed by means of the formula [40]:

$$\nu_{ij} = -\frac{\varepsilon_j}{\varepsilon_i} \qquad 1\text{-}1$$

where ε_i and ε_j are the axial and transverse strain in the Ox_i and Ox_j direction respectively.

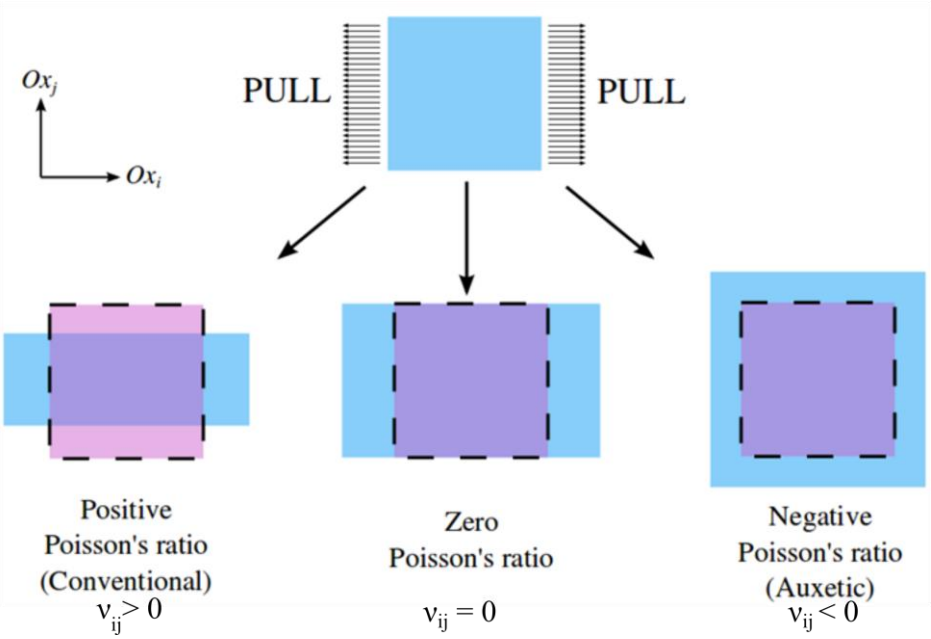

Figure 1-1 A diagram showing the deformation of three different materials, having the same initial shape subjected to a uniaxial load.

Through this definition, a material that exhibits auxetic behaviour would have a negative ν_{ij}. It is also known that in the case of three-dimensional isotropic materials (mechanical properties of a given structure are the same in all directions), the Poisson's ratio assumes a value from the interval: $-1 \leq \nu_{ij} \leq 0.5$ [40]. However, for two-dimensional isotropic materials, the value of the Poisson's ratio ranges between -1 and 1 [41]. It is also important to note that anisotropic systems may have an arbitrary value of the Poisson's ratio in any direction [43]. Furthermore, in recent years, apart from studies related to the possible extent of the Poisson's ratio, a classification [42, 43] was also proposed in order to distinguish between different types of systems with a propensity to exhibit auxetic and conventional behaviour. More specifically, it was proposed that systems exhibiting negative Poisson's ratio in all directions may be referred to as complete auxetics while systems exhibiting negative Poisson's ratio only in specific direction may be called partial auxetics [44, 45]. From this, it follows that materials which exhibit positive Poisson's ratio in all directions should be referred to as non-auxetics.

1.2.2 Thermal expansion

Apart from the negative Poisson's ratio, another unusual macroscopic property exhibited by a number of materials or structures is negative thermal expansion [46-60] (NTE), i.e. shrinkage of the system in at least one dimension when subjected to an increase in temperature. In the case of conventional thermal expansion materials, the contrary is observed with these systems expanding upon being subjected to an increase in temperature (see Figure 1-2). The latter behaviour is typically observed for a majority of materials. The variation in size of the system when subjected to a change in temperature can be quantified by means of the coefficient of thermal expansion (CTE). This quantity assumes either negative or positive values depending on whether the considered system shrinks or expands upon being subjected to an increase in temperature.

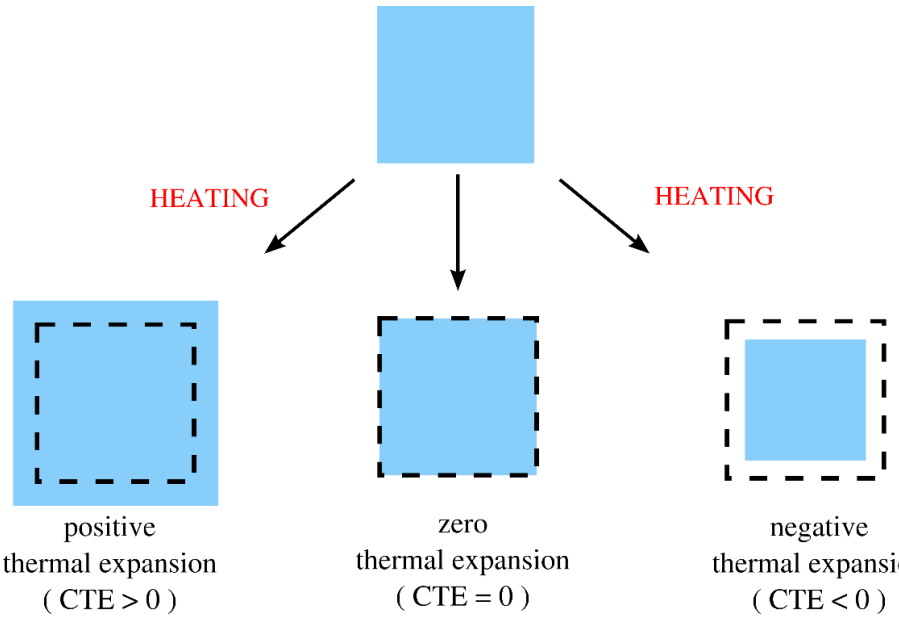

Figure 1-2 A diagram presenting thermal expansion of materials corresponding to different values of CTE. The dashed outline corresponds to the initial shape of the system subjected to an increase in temperature.

The coefficient of thermal expansion corresponding to a deformation of the system in one dimension (α_L) or in the volume of the system (α_V) may be defined as follows [61]:

$$\alpha_L = \frac{1}{L}\left(\frac{dL}{dT}\right)_p \qquad \alpha_V = \frac{1}{V}\left(\frac{dV}{dT}\right)_p \tag{1-2}$$

where, L is the linear dimension of the system in the direction where the thermal expansion is being measured, whilst V, T and p stand for the volume, temperature and pressure respectively. In general, the volumetric coefficient of thermal expansion α_V may be defined both for isotropic as well as for anisotropic systems, in which case, $\alpha_V = \alpha_1 + \alpha_2 + \alpha_3$ where α_1, α_2 and α_3 are the linear thermal expansion coefficients for three mutually orthogonal directions. On the other hand, in the particular case of isotopic materials, $\alpha_V = 3\alpha_L$.

In recent years, scientists have been devoting a lot of attention to materials capable of exhibiting negative thermal expansion. This increasing interest in the field was mostly driven by the large number of potential applications of NTE materials some of which could have an impact on industry and engineering. These studies show that there is a wide range of systems with a propensity to exhibit NTE characteristics, including amongst others: systems made from biomaterials [62], metal-organic frameworks [63-66] (MOFs), metal oxides [46, 48-50, 67-71], zeolites [74-79] and polymers [80, 81]. In a number of these systems, the NTE was explained in terms of rotating rigid units which upon heating rotate to a greater extent relative to each other with the net result that their overall linear dimensions are observed to shrink upon heating.

1.2.3 Linear compressibility

Compressibility is another property of materials which defines the way how systems deform upon being subjected to a hydrostatic pressure p. According to the definition stated by Baughman *et al.* [72], in the case of a constant temperature T, a volumetric compressibility may be defined in the following manner:

$$\beta_V = -\frac{1}{V}\left(\frac{\partial V}{\partial p}\right)_T \tag{1-3}$$

Analogically, the area and linear compressibility (β_A and β_L respectively) are defined by:

$$\beta_A = -\frac{1}{A}\left(\frac{\partial A}{\partial p}\right)_T \qquad \beta_L = -\frac{1}{L}\left(\frac{\partial L}{\partial p}\right)_T . \tag{1-4}$$

To understand better the concept of 'compressibility', one could visualise the volume of the system (or area in the case of two-dimensional structures) as decreasing, remaining the same or increasing when subjected to a hydrostatic pressure. These three different hypothetical scenarios are schematically shown in Figure 1-3. It may also happen that instead of manifesting the particular compressibility in all directions, the system exhibits a given type of compressibility only in a particular direction in which case it is said that it corresponds to a specific linear compressibility. This means that the linear compressibility for a given system may be different depending on the direction in which it is measured. Similar arguments can be made for the area compressibility which can be measured in some particular cross-sectional plane of a three-dimensional system.

In recent years it has been proved that the compressibility might assume negative values even though materials exhibiting such characteristics are still not frequently encountered. The first examples of this phenomenon were reported by Baughman *et al.* [72]. In his work it was shown that certain rare crystal phases may exhibit negative linear (NLC) and negative area compressibility (NAC). Another example is the work of Moore and Lakes [73, 74] on open cell foams. Their work was soon followed by Lakes and Wojciechowski [75] in an attempt of showing that the bulk modulus of an arbitrary system does not have to assume a positive value.

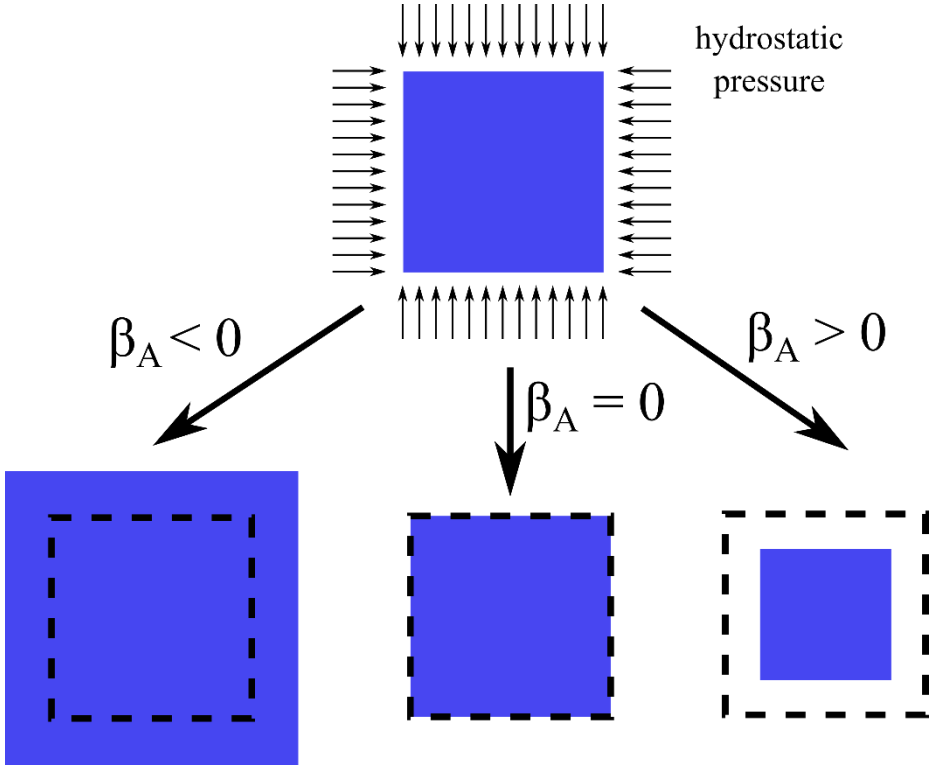

Figure 1-3 A diagram presenting the behaviour of a cross-section of a material corresponding to different values of area compressibility upon being subjected to a hydrostatic pressure.

Here it must be mentioned that Grima *et al.* made the distinction between solid non-porous and porous systems which exhibit negative compressibility. In the first scenario, the system cannot exhibit negative volumetric compressibility as this would be thermodynamically prohibited. However, if the system is porous and the fluid exerting the pressure is entering the system so that the pressure is 'felt' both from the 'inside' and 'outside', then the system could, if smartly designed as in the case of the bimaterial systems [76], manifest an apparent increase in its overall dimension (the equivalent of an overall negative β_V) even if the solid portion of the system would have shrunk (i.e. intrinsically exhibit conventional positive β_V). In other words, the internal components of such a system correspond to a positive compressibility while at the same time the whole system exhibits an apparent negative volumetric compressibility. This is in sharp contrast with nonporous systems where the negative compressibility is not

exhibited as negative β_V but only in specific directions. In order to ensure that scientists working in the field of materials science do not confuse the above concept, the scientific community proposed the distinction between effective volumetric compressibility and volumetric compressibility. As written above, in the case of porous materials, it may happen that a system subjected to a hydrostatic pressure expands in all directions (effective negative compressibility) but its constituting components shrink which corresponds to non-negative compressibility.

1.2.4 Stiffness

Stiffness (often referred to as tangent or tangential stiffness) is a mechanical property describing the way a system responds to deformation. More specifically, when the system is being extended, it is said that it exhibits conventional positive stiffness when it becomes more difficult to deform it further. Conversely, the system exhibits negative stiffness [77-85] when it becomes simpler to continue the extension. This concept is explained schematically in Figure 1-4, where in the case of panel (a), the force required to hold the system at rest at a particular extension equal to l_0, must be increased in order for the system to assume a configuration corresponding to a larger extension equal to $l_0 + \Delta l$, i.e. the systems exhibits positive stiffness. On the other hand, on panel (b) the magnitude of such a force decreases as the material is being extended which according to the above definition means that the system exhibits negative stiffness.

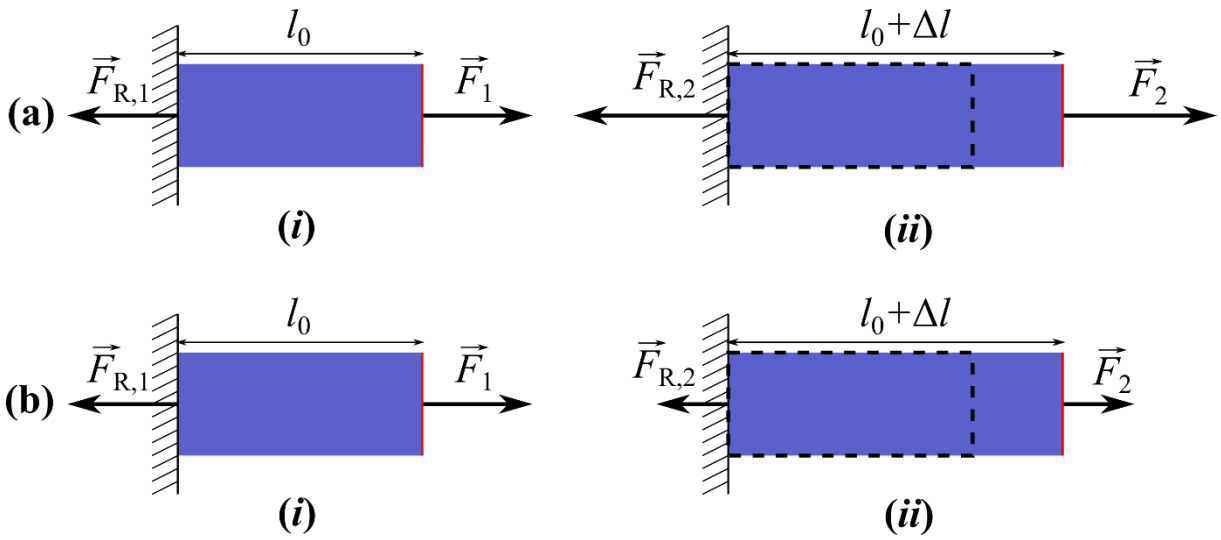

Figure 1-4 Panels show (a) a material exhibiting positive stiffness and (b) a material exhibiting negative stiffness. In both cases, on subpanel the material is extended to a length of (i) l_0 by force $\vec{F}_1$ with one side of this material being fixed to the wall and (ii) $l_0 + \Delta l$ by force $\vec{F}_2$. Quantities $\vec{F}_{R,1}$ and $\vec{F}_{R,2}$ are reaction forces which in terms of the magnitude are equal to $\vec{F}_1$ and $\vec{F}_2$ respectively. The length of the arrows reflect schematically the magnitude of the applied force.

The stiffness of a system in a particular *i*-th direction is defined as the rate of change in the force F_i required to deform the structure by a displacement l_i. Hence it can be written down as follows: stiffness = dF_i / dl_i. In order to explain how to interpret this quantity based on a graph of force *F* plotted with respect to distance *d*, a hypothetical graph is provided in Figure 1-5. In this figure, one can note that between points A and B, the magnitude of the force decreases as the structure is extended, indicating that over this interval, the system exhibits negative stiffness. On the other hand, over the interval between points B and C the contrary is observed, i.e. the system exhibits positive stiffness. In other words, upon extending the system over the interval between points A and B it becomes simpler to stretch and subsequently becomes more difficult over the interval between points B and C.

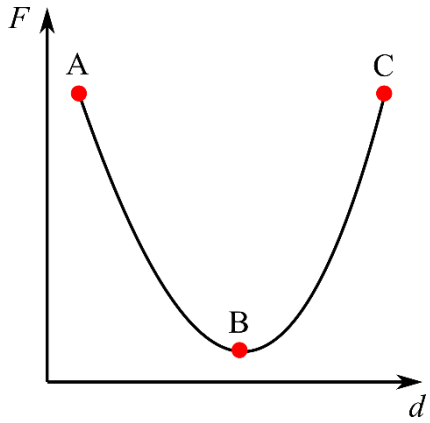

Figure 1-5 A hypothetical auxiliary graph of force *F* plotted with respect to extension length *d* measured in the direction in which the force is applied.

1.3 Current state of the art

As discussed in detail in the next chapter which reviews the historical progress made in the field of mechanical metamaterials, in particular those aspects which are closely related to this thesis, there have been several important discoveries which have transformed the field of mechanical metamaterials and other systems with a potential to exhibit unusual mechanical behaviour. However, despite of these discoveries, there are a number of aspects related to these systems, which as discussed in more detail in the Scope of this Work (see section 3), still remain to be explored. Some of these aspects correspond to different effects which may be observed upon studying the dynamic behaviour of these systems as well as the effect which the use of magnetic inclusions may have on properties of mechanical metamaterials.

1.4 Layout of the thesis

This thesis is divided into twelve chapters meant to describe the state of art in the discussed field as well as the conducted research. More specifically, in Chapter 1, some of the most fundamental of the unusual mechanical properties which are of particular interest from the point of view of this thesis are defined and briefly discussed. In Chapter 2, the Literature Review meant to present the historical progress made in those areas of science which are particularly

related to topics investigated in this thesis is provided. In Chapter 3, the Scope of work is presented in order to state clearly the motivation behind the conducted research. Chapter 4 is the first chapter where original scientific results are being reported. More specifically, in this chapter, the novel concept relating to the potential of mechanical metamaterials to induce their global rotation as a result of the rotation of their subunits is proposed. In Chapter 5, the theoretical concept from Chapter 4 is verified experimentally. In Chapter 6, the theoretical concept from Chapter 4 is further extended to other systems. In chapter 7, the concept of hierarchy is incorporated with rotating square systems in order to analyse their dynamic behaviour. In Chapter 8, the possibility of designing novel mechanical metamaterials composed of triangular units with the propensity to exhibit unusual mechanical behaviour is discussed. In chapter 9, the potential of mechanical metamaterials with magnetic inclusions to exhibit negative stiffness as well as other types of unusual mechanical behaviour is discussed. In Chapter 10, the possibility of inducing the magnetocaloric effect solely as a result of the mechanical deformation of magneto-mechanical systems is analysed. In the last of the chapters related to the original research, i.e. in Chapter 11, the magnetic domain evolution in magneto-mechanical systems at the nano-scale is investigated by means of the Monte Carlo Metropolis algorithm. Finally, in Chapter 12, final conclusions as well as general discussion of all of the reported results are provided.

2. Literature review

As mentioned in the previous chapter, this thesis will focus on novel systems having a potential to exhibit unusual mechanical properties as well as other types of anomalous behaviour. In view of this, the first objective of the literature review will be to discuss the historical development associated with those of the mechanical properties which are going to be the main subject of discussion in the following research chapters, i.e. negative Poisson's ratio, negative compressibility and negative stiffness. In the second part of the literature review, the historical development of mechanical metamaterials and other systems with magnetic inclusions is going to be discussed.

2.1 Unusual mechanical properties

2.1.1 Systems exhibiting auxetic behaviour

General overview

Even though the field of auxetics (negative Poisson's ratio) is still considered to be relatively new, the first mention of systems exhibiting negative Poisson's ratio was reported as early as 1928 by Professor Voigt [86]. The term 'auxetic' itself, originating from the Greek word '*auxetos*' meaning 'to be increased' was first proposed many years later in 1991 by Professor Kenneth E. Evans [39]. In the work published by Prof. Voigt [86], it was proposed that iron pyrites might exhibit auxetic behaviour, which result was proven to be incorrect in subsequent experimental work conducted by Simmons [87] and Benbattouche [88]. In these studies it was argued that in the case of the initial result reported by Voigt, the measured negative Poisson's ratio was a result of crystal twinning. In the following years, a number of independent studies were conducted resulting in numerous publications relating to the auxeticity of various crystalline structures, such as cadmium [89], barium titanite [90], α-quartz

[91, 92], rare gas solids [93-95], face centered cubic (fcc) crystals [93], arsenic [96], metals [94, 95], α-cristobalite [97] and thermally-cracked granite [98]. All of these naturally-occurring structures were a proof to the scientific community that materials exhibiting negative Poisson's ratio indeed exist and thus are worth being investigated. This belief led to further studies on materials with a propensity to exhibit negative Poisson's ratio. One such class of systems are biological structures, amongst which the most representative examples are those of cellulose [99-101], cow teat skin [102, 103] and animal shells [104]. It was also reported that certain parts of a human body may exhibit the discussed characteristics with cancellous bone and a variety of tissues and dentin [105-111] being the most investigated examples. In the following years, thanks to a continuation of these studies, auxeticity was proven to be a property of numerous elements and compounds (including amongst others carbon [112], graphite, graphene [113], calcium carbonate [114], black phosphorus [115-117], molybdenum sulphide and zinc) as well as a wide variety of alloys [118-126] and composites [127, 128].

As described in the above paragraph, despite the fact that the concept of auxetic behaviour might seem to be counter-intuitive as it is not normally observed in the case of materials available in our everyday life, it is possible to find a number of materials exhibiting negative Poisson's ratio in the environment. However, the fact that it is possible to find examples of auxetic materials in the environment does not mean that it is simple to exploit the benefits of auxeticity in real practical applications at an industrial scale. In a majority of cases, in order to use a particular class of materials in the industry, a very large versatility of these systems is required. This in turn is usually reserved for man-made systems where the properties of the given system may be tailored during a production process. A pioneer in this field is Prof. Roderic Lakes who was one of the first scientists to purposely produce a material with a negative Poisson's ratio, i.e. auxetic foam [129]. His discovery was not only of great importance due to its novelty but also because of numerous interesting properties which were later reported

by scientists investigating these materials. Amongst the most significant ones, one should mention increased indentation resistance [32, 130-137], shape memory [148-152], shear stiffness and a potential to be used for damping applications [33, 138-144]. Auxetic foams were also thoroughly investigated from the point of view of a manufacturing process as it could affect the mechanical properties of the material. The approach proposed initially by Lakes *et al.* [129] was associated with the application of pressure (in all three directions of the Cartesian coordinate system) to an open-cell foam while increasing the temperature to soften the material. In the following years, this method was modified in order to allow for a production of larger, more complex foams capable of exhibiting negative Poisson's ratio [13, 145-151]. Amongst the most notable approaches in this respect, it is worth to mention the work of Alderson *et al.* [152] who reported a possibility of fabrication of auxetic open-cell foams in a continuous manner. Some of the other achievements in this field include the work of Friis *et al.* [130] on the fabrication of auxetic metallic foams and the technique proposed by Alderson [153] and Grima [154] to convert a nonauxetic foam into an auxetic one. The last method is analogical to the one reported by Lakes *et al.*, with chemical treatment being used to soften a conventional foam instead of an increase in temperature. Numerous attempts were also made in order to distinguish and quantify a particular mechanism leading to auxetic behaviour of these systems [155-166].

Another important direction of studies on materials exhibiting negative Poisson's ratio was in the field of polymers. The first reports in this field were focused on polytetrafluoroethylene (often referred to as PTFE) which was proven to have a propensity to exhibit auxetic behaviour as early as 1989 [167, 168]. This result was later used by Professors Andrew Alderson, Kim Alderson and Kenneth E. Evans, to lay foundations for the following studies on auxeticity of polymers and materials exhibiting negative Poisson's ratio in general. In the following years, a number of studies relating to these systems were focused on the optimization of the production

process [169-172], mechanisms governing deformation behaviour and a possible range of mechanical properties [173-178].

In addition to the classes of systems described above, another very interesting area of studies on auxetic materials relates to nano-level systems. A pioneer in this field is Professor Anselm C. Griffin whose work was initially focused on the synthesis of liquid crystalline polymers [179-185]. Its significance was magnified by numerous studies conducted in the field of nanotechnology at that time. Over the years, a lot of attention was also devoted to finding a connection between the deformation mechanisms governing the behaviour of systems at nano-scale and at a macro-scale [39, 186-190]. Some of the most prominent examples of systems at nano-level having a capability to exhibit auxetic behaviour are carbon allotropes as well as related structures amongst which it is worth to particularly highlight systems such as benzene, graphene, graphene oxide, a variety of carbon nanotubes and prismanes [191-201]. Over the years, a lot of attention of scientists working in the field of material science who were pursuing novel systems with the propensity to exhibit auxetic behaviour was also devoted to crystalline structures, in particular those occurring naturally. Some of the most studied examples of these systems are zeolites and silicates [189, 202-213] as well as zeolite-type frameworks, frameworks of oxides [91, 92, 97, 153, 214-218] and body centred cubic metals [94].

Last but not least it is important to note that there is a wide range of mechanical metamaterials and related devices which can exhibit auxetic behaviour. Many of these man-made systems were designed based on the theoretical concepts which provided an insight into the possibility of achieving different types of unusual mechanical behaviour. A pioneer in the field of such theoretical models is Prof. Wojciechowski with one of the first examples of system investigated by his group being hard disks [24, 219-232]. Based on his work and subsequent studies of researchers working in this field, various systems have been applied in different branches of the industry.

Different mechanisms leading to auxetic behaviour

Over the years, the rapid development of mechanical metamaterials resulted in a number of separate directions of studies focused on particular types of these systems. Different classes of mechanical metamaterials can be primarily distinguished between each other based on the geometry of the system and the mechanism governing their deformation. Some of the most studied examples of such classes of auxetic mechanical metamaterials include re-entrant structures, chiral and antichiral systems, rotating rigid unit systems, hierarchical structures and mechanical metamaterials with magnetic inclusions. The last three classes of mechanical metamaterials listed above are going to be discussed separately in more detail in the following sections of this thesis. This stems from the fact that these particular systems are closely related to studies conducted as a part of this thesis.

It seems that systems composed of re-entrant honeycombs (see Figure 2-1(a)) are the most studied examples of re-entrant mechanical metamaterials. These systems were proven to have a propensity to exhibit auxetic behaviour as early as 1979 when Abd el-Sayed *et al.* published [233] their novel work. This study was soon followed by Gibson *et al.* [234] who through the theoretical model describing re-entrant honeycombs with a deformation mechanism governed by flexure of ligaments managed to show that such systems indeed exhibit negative Poisson's ratio. In the following years, an attempt was made by a number of researchers to propose a model which would serve as an even more reliable representation of these systems in reality. Of particular importance is here the work published by Masters *et al.* [235], Evans *et al.* [236] and Gibson *et al.* [237], in which studies it was assumed that investigated structures deform via hinging and elongation of ligaments which mechanisms allow to realistically describe the discussed systems. Based on the initial work on re-entrant honeycombs which has formed a foundation for understanding their unusual behaviour, numerous studies were conducted over

the years where these systems were investigated from the point of view of their out-of-plane behaviour [238-241], off-axis mechanical properties [235, 242-246], various geometric designs [247-251] and the way how they respond to the application of a large stress [19, 252, 253].

Apart from re-entrant honeycombs there are also other types of re-entrant systems which may exhibit auxetic behaviour. One such example are structures which are often referred to as STAR-n systems with Attenborough *et al.* [254] being a scientist who initially proposed this concept (see Figure 2-1(b) for an example of such system). In the following years, these structures composed of star-shaped units were investigated in a number of different studies [270-274] where they were primarily used in order to design systems with a potential to exhibit negative Poisson's ratio and negative compressibility. Another interesting example of re-entrant system which can exhibit auxetic behaviour is a so-called arrow-head system proposed by Larsen *et al.* [255] in 1997 (see Figure 2-1(c)). Properties of this system were validated experimentally in a number of studies [255-259] which indicate that this design is also suitable for a design of more complex mechanical metamaterials. It is also worth mentioning that there is a variety of other re-entrant mechanisms which have a propensity to exhibit negative Poisson's ratio. As a matter of fact, such systems can also be designed in three-dimensions with some examples of this approach being studies on a re-entrant version of the tetrakaidecahedron system [139] (see Figure 2-1(d)) and a modified version of hexagonal honeycombs [260-265] (see Figure 2-1(e)). Another type of re-entrant system which can exhibit auxetic behaviour is the so-called "fibril and node" system which concept was initially proposed by Alderson *et al.* [169, 266] in 1993. In the following years, it was reported in a number of studies [267-269] that similarly to their two-dimensional counterparts, these systems can exhibit similar characteristic in three dimensions (see Figure 2-1(f) for an example of such a system).

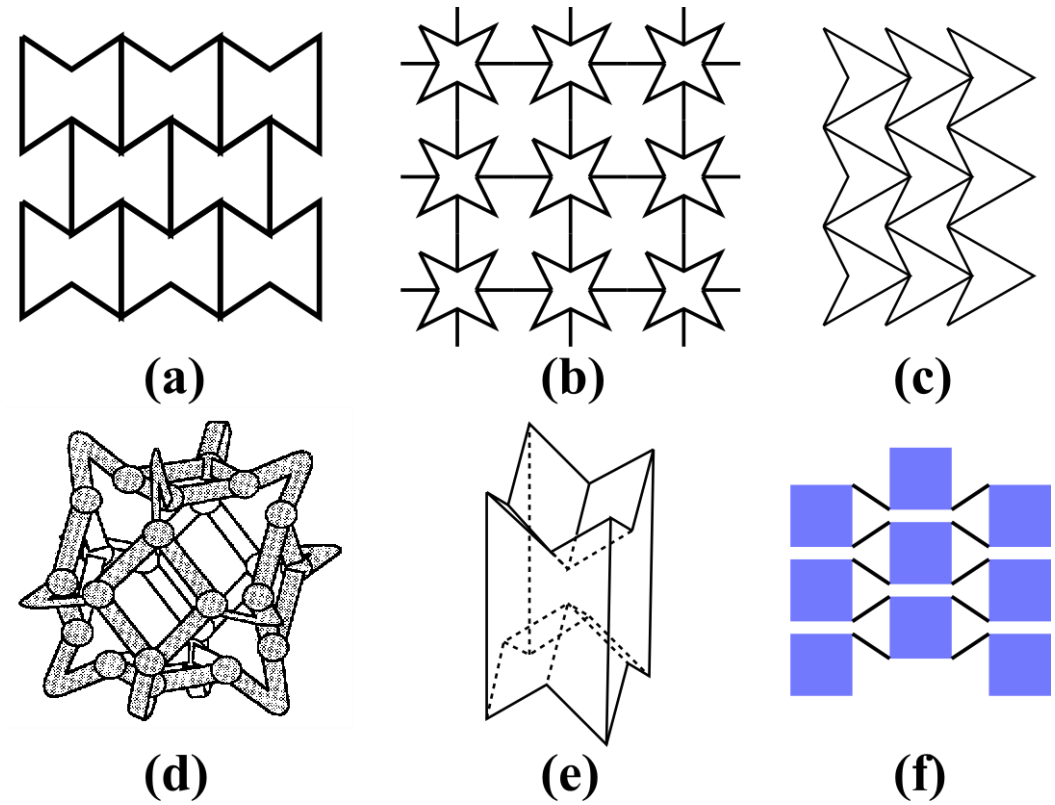

Figure 2-1 Examples of re-entrant systems. Panels show: (a) re-entrant honeycomb system [233], (b) STAR-4 system [254], (c) arrow-head system [255], (d) re-entrant configuration of the tetrakaidecahedron system, (e) a 3D arrangement of re-entrant honeycomb cells [Replicated from [260]] and (f) an example of the so-called "fibril and node" system [267].

Apart from systems described above, there are also other classes of structures which were proven to have a potential to exhibit auxetic behaviour and have been of particular interest among scientists working in the field of material science. One such class of systems corresponds to chiral re-entrant honeycombs which concept was initially proposed by Prof. Wojciechowski in 1989 [24]. These systems are composed of units (commonly they have a cylindrical shape but in general these units may also assume other shapes) which are connected to each other by means of ligaments with these ligaments being tangent to the surface of each of the units to which they are connected. The deformation mechanism associated with these systems is normally related to the flexure of ligaments where the extent of this effect depends on the geometry of a given structure.

In the pioneering work of Prof. Wojciechowski [24], the concept of the particular chiral system having a six-fold symmetry was proposed (see Figure 2-2(c)). In the years following this publication, this system, which is commonly referred to as a hexachiral system, was investigated experimentally by Lakes [25] and Prall *et al.* [26] in order to verify its potential to exhibit auxetic behaviour. As a result of these studies, it was proven that this system exhibits an isotropic Poisson's ratio equal to -1. Another fundamental development in this field was made by Sigmund *et al.* [27, 28], who proposed a novel system where square-like units were connected by means of ligaments in a way resembling the diagram shown in Figure 2-2(e). This geometry, despite being seemingly similar to the structure mentioned above, deforms in a way resulting in units assuming alternate positions within the system rotating in opposite directions. This is very different from the behaviour observed in the case of the hexachiral system described above where all of the units rotate in the same direction during the process of deformation. In order to make a distinction between these two types of structures, more specifically systems corresponding to one of the two types of deformation described above, in 2000 it was proposed by Prof. Grima to refer to such systems as anti-chiral systems. At this point it is also worth to mention that in addition to geometries described above, the concept of trichiral and anti-trichiral re-entrant honeycombs (see Figure 2-2) was proposed in 2010 by Alderson *et al.* [29].

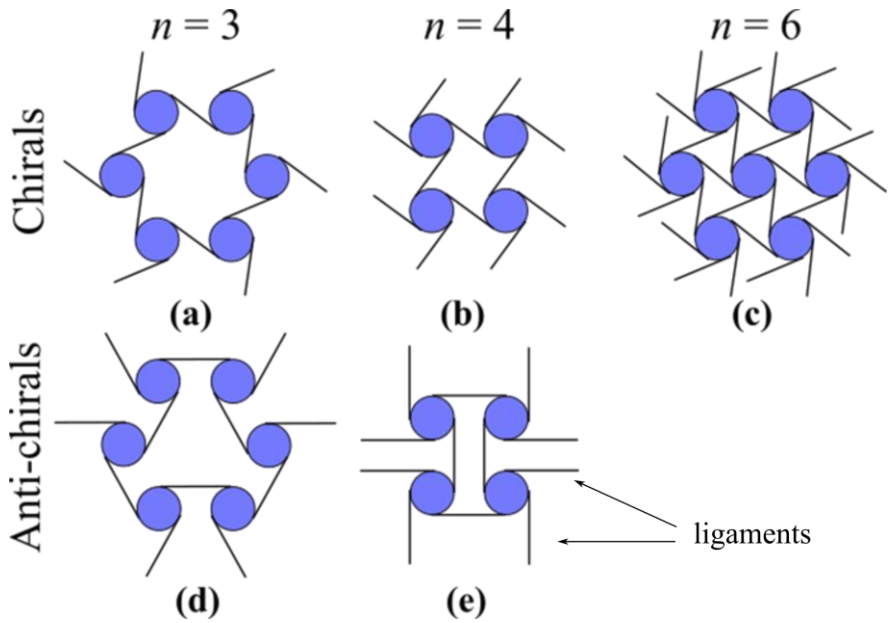

Figure 2-2 All of the possible space-filling configurations of chiral and anti-chiral honeycomb systems. More specifically, panels (a), (b) and (c) show tri-, tetra- and hexachiral honeycomb systems. Panels (d) and (e) correspond to anti-trichiral and anti-tetrachiral structures.

Even though both chiral and anti-chiral systems may assume complex shapes, there is a very limited number of designs of these systems which may form space-filling configurations. As a matter of fact, as discussed by Alderson *et al.* [270], space-filling chiral systems may only assume *n*-fold symmetries which correspond to $n = 3, 4, 6$ (see Figure 2-2(a)). On the other hand, as discussed by Grima *et al.* [271], the anti-chiral systems may only form a space-filling configuration for $n = 3, 4$.

Apart from the studies on the design of chiral and anti-chiral honeycomb systems, these structures were also a subject of numerous [26, 270-275] studies focused on the analysis of their potential to exhibit auxetic behaviour. Another aspect which was thoroughly investigated is the effect which the variation in the thickness of ligaments and other geometric parameters has on mechanical properties of discussed systems [270-273]. Chiral honeycomb systems were also analysed in terms of their out-of-plane mechanical properties. This direction of studies turned out to be very successful as among other results it was reported that the discussed systems possess an enhanced resistance to transverse shear [276] and that due to the presence of nodes

they also exhibit a large resistance to the in-plane compression as their ligaments buckle out of plane [277-280]. In 2012, it was also reported that these systems have a propensity to exhibit negative Poisson's ratio in the case of large strains [281]. This result indicates that the unusual mechanical properties of chiral systems can be utilised in a variety of applications requiring both small and large extent of deformation. At this point, it is also worth to mention some of the more recent studies relating to chiral and anti-chiral honeycomb systems which were primarily focused on the connectivity within the structure [282] and the effect which the introduction of the disorder to the system has on its properties [283].

Rotating rigid unit systems

According to the currently accepted definition, rotating rigid unit systems (RUMs) consist of a set of perfectly rigid elements connected at vertices by means of point-like hinges. It is assumed that the shape of these units cannot be distorted during the process of deformation which manifests itself by a change in the angle of aperture between adjacent units. This in turn results in a rotation of rigid units.

In recent years it was proven that rotating rigid unit systems may exhibit auxetic behaviour, which result was first reported by Professor Ole Sigmund [284]. In his work, it was shown that periodic systems constructed both in two and three dimensions may lead to a wide range of Poisson's ratio. The model initially proposed by Sigmund consisted of two squares rotating in opposite directions, which was supposed to represent the behaviour of the auxetic structure. In the following years, a more simplified and hence more applicable approach was proposed by pioneers in the field of auxetic systems, namely Professors Joseph N. Grima and Kenneth E. Evans [202] as well as Professors Yoshihiro Ishibashi and Makoto Iwata [285]. In these models, it was assumed that the adjacent rigid units were connected at vertices by means of hinges. It

was also shown that the hinging process could be governed by a harmonic potential, which in practise could be realized throughout the use of springs attached to appropriate vertices of the structure.

The first studies on rotating rigid unit systems were focused on two-dimensional periodic systems having a simple polygon as an elementary rigid unit of the system which in turn was used to form a unit-cell of a theoretical crystal. One of the first models corresponding to such systems was based on squares [2]. This work turned out to be of great significance as it was shown that the investigated model is an isotropic structure with a Poisson's ratio of -1 which (as it was already mentioned) is the lowest possible value for isotropic materials. This result was soon followed by similar models addressing different types of polygons used as an elementary rigid unit. Some of the most studied examples of this approach are based on rectangles [3, 286, 287], triangles [288-292], parallelograms [202, 293, 294] and rhombi [287, 295, 296].

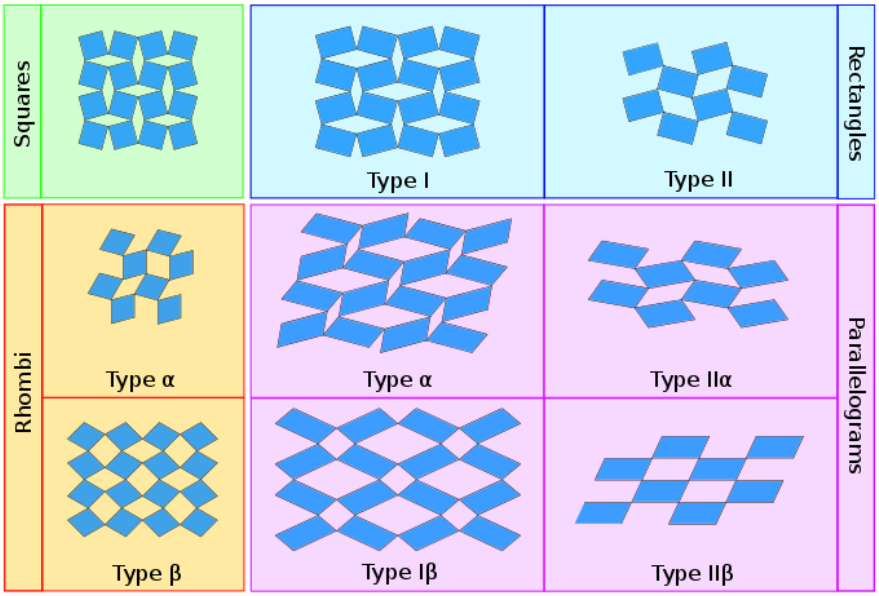

Figure 2-3 A diagram showing different possible connectivities of rotating rigid units systems constructed by means of different type of quadrilaterals, namely squares, rhombi, rectangles and parallelograms [Replicated from [297]].

Besides different geometries of individual units, another important aspect associated with rigid unit systems is their connectivity within the structure. Of particular importance is the work of Professor Joseph Grima [287], where it was shown that the particular way how the rigid elements are connected at vertices may significantly affect the mechanical properties of the investigated system. In other words, the same set of rigid units connected in a different manner may lead to different values of the Poisson's ratio. A very good example of this are systems constructed by means of rotating rigid rectangles referred to as Type I and Type II (see Figure 2-3). Mathematical models established to assess their mechanical properties show that Type I structures are anisotropic and may exhibit Poisson's ratios ranging between negative and positive values depending on the angle of aperture within the system. This is in sharp contrast to the Type II system found to be isotropic with a Poisson's ratio equal to -1 irrespective of the value of the angle between the rigid units. This study was later extended to other rotating rigid unit systems such as ones constructed from parallelograms and rhombi [293, 297] to deduce the effect of the various possible connectivites of the units constituting these networks. A similar approach concerning changes in the connectivity of the rotating rigid unit system (having a particular type of polygon as an elementary unit) in order to alter mechanical properties of the system, was later applied in the case of geometries such as parallelograms and rhombi [203, 293, 297]. It is also interesting to note that elementary rigid units having a very simple geometry may in general lead to a wide variety of connectivities. A good example are systems constructed from parallelograms, in which case the structure composed of such simple quadrilaterals can be connected in four different ways.

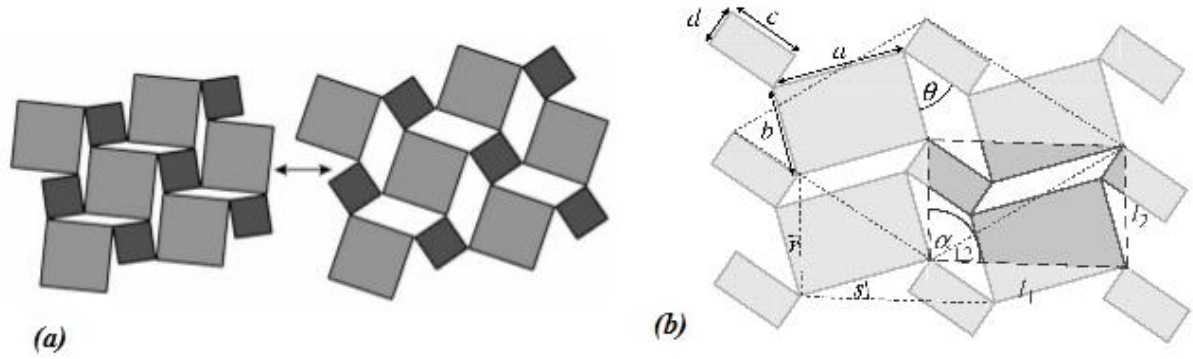

Figure 2-4 Panels show: (a) a system consisting of two types of differently-sized squares connected at vertices proposed by Grima *et al.* [2] [diagram adapted from [2]] (b) a system constituted by two types of differently-sized rigid rectangles connected at vertices proposed by Grima *et al.* [298] [Taken from [298]].

Another interesting direction of studies on rotating rigid unit systems relates to the use of differently-sized units within the same system. The first person to propose this concept was Professor Joseph Grima in his paper [2] published back in 2000. In his work it was shown that one may construct a system exhibiting negative Poisson's ratio upon connecting differently-sized squares at their vertices (see Figure 2-4(a)). A similar concept involving the use of two types of differently-sized rotating rectangles [298] was proposed in 2011 (see Figure 2-4 (b)) in which work it was reported that the investigated system exhibits an on-axis auxetic behaviour irrespective of the size and shape of rectangles. Moreover, upon changing the relative shape of rectangles one may change the mechanical properties (their magnitude) for loading in a particular direction. This work was of great significance as it showed that it is possible to alter the system in a way which would make it mimic the geometry of certain types of crystalline structures. This was not possible in the strongly idealised unimode rotating rigid systems having only one type of elementary unit constituting the system. Another approach aimed towards increasing the versatility of rigid unit systems was proposed by Professor Holger Mitschke. The main objective of his work [299-301] was to come up with different periodic systems exhibiting negative Poisson's ratio with such structures being constructed by means of two or more different types of rigid units (see Figure 2-5). Moreover, in his work it was shown how the solid

rigid units can be replaced by rigid rods forming an analogical shape, which approach may prove to be particularly useful in computational studies involving molecular dynamics.

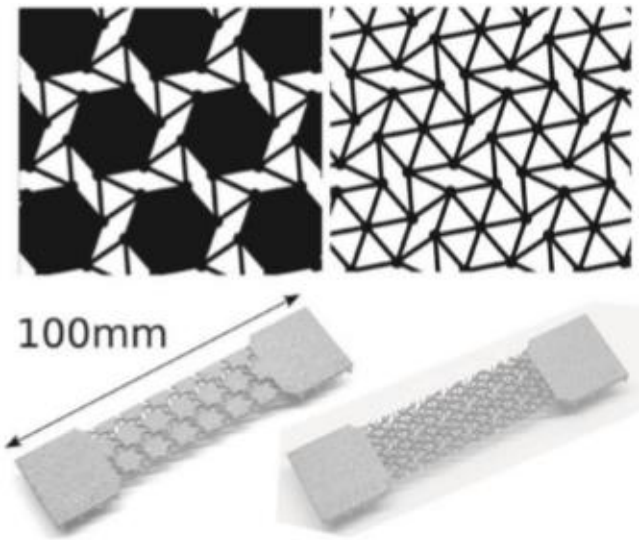

Figure 2-5 A diagram presenting the use of a few different types of polygons to form a periodic system capable to exhibit a negative Poisson's ratio [Adapted from [299]].

Even though the rotating rigid unit systems are usually associated with two-dimensional structures, it is also possible to design analogical structures in three dimensions. Some of the first models describing this concept were proposed by Alderson *et al.* [91, 214, 215, 302] with these studies being focused on the deformation of tetrahedral frameworks. In another work, Attard *et al.* [303] proposed a mechanical metamaterial composed of cubic rigid units (see Figure 2-6(a)) which was proven to have a potential to exhibit auxetic behaviour. This work may also serve as a blueprint showing that it is possible to implement the concept commonly used in two dimensions in order to design three-dimensional counterparts of these systems. It is also worth to highlight the fact that there is a number of papers [304, 305] where analogical systems are constructed by means of elastic materials. A good example of this approach is the work by Shen *et al.* [304]. In his study, a cellular three-dimensional material was investigated (see Figure 2-6(b)) which, despite the use of an elastic material, deforms primarily via rotation of its units (especially for relatively small deformations). It was also reported that even in the

case of very simple geometries used to produce a periodic three-dimensional structure, it is possible to model a system exhibiting negative Poisson's ratio in all three main directions. Another interesting approach associated with three-dimensional auxetic structures corresponds to the use of two-dimensional rotating rigid unit systems arranged in a non-planar conformation. A very good example of this concept is the work by Gatt *et al.* [306], where the system of rotating squares (analogical to the one proposed by Grima *et al.*) was folded into a tubular stent-like conformation.

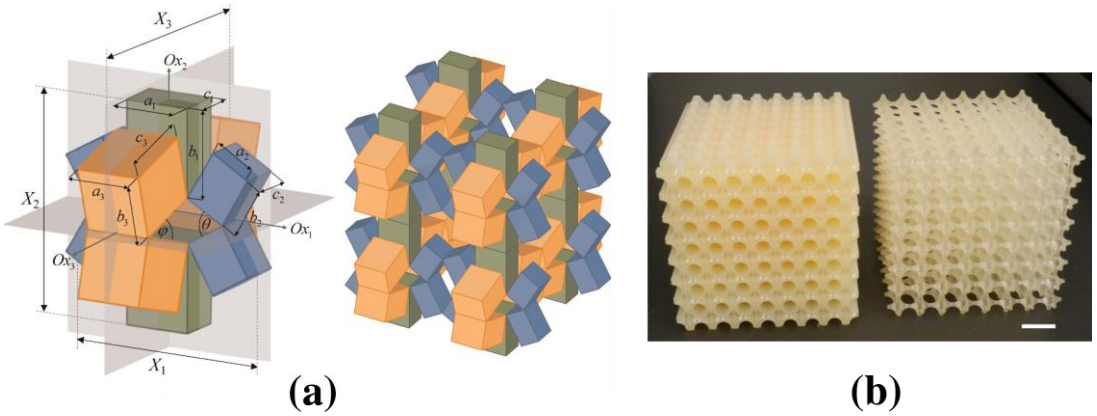

Figure 2-6 Panels show: (a) a model composed of rotating rigid unit cubes arranged in a 3D configuration [Taken from [303]] and (b) an experimental realisation of the three-dimensional cellular structure proposed by Shen *et al.* [304].

Despite their relative simplicity, over the years, systems constructed from rigid units connected at their vertices were proven to provide a reliable description of real (more complex) systems. It was also reported that these systems may mimic the behaviour of real systems with sizes ranging between nano and macro-scale, which makes them a perfect tool to simulate a large variety of materials used in industry.

One of the most common examples of this approach at micro-scale is associated with the use of RUMs as the most significant mechanism governing deformation of foams [291, 307]. This concept stems from the fact that in foam cells, in the vicinity of joints, one can observe a

significantly larger amount of material than is the case for ribs. Thus, the joints tend to be stiffer than the rest of the cell structure, and behave as quasi-rigid units during the deformation process. As a result, the ribs within the cells start to buckle as schematically shown in Figure 2-7. In this case, the behaviour of the system can be loosely described by means of a theoretical system of rotating triangles, which proves that even complex systems might be modelled by means of rigid units systems. A confirmation of this result (involving the use of 3D X-ray micro-tomography) was provided by McDonald *et al.* [163, 308].

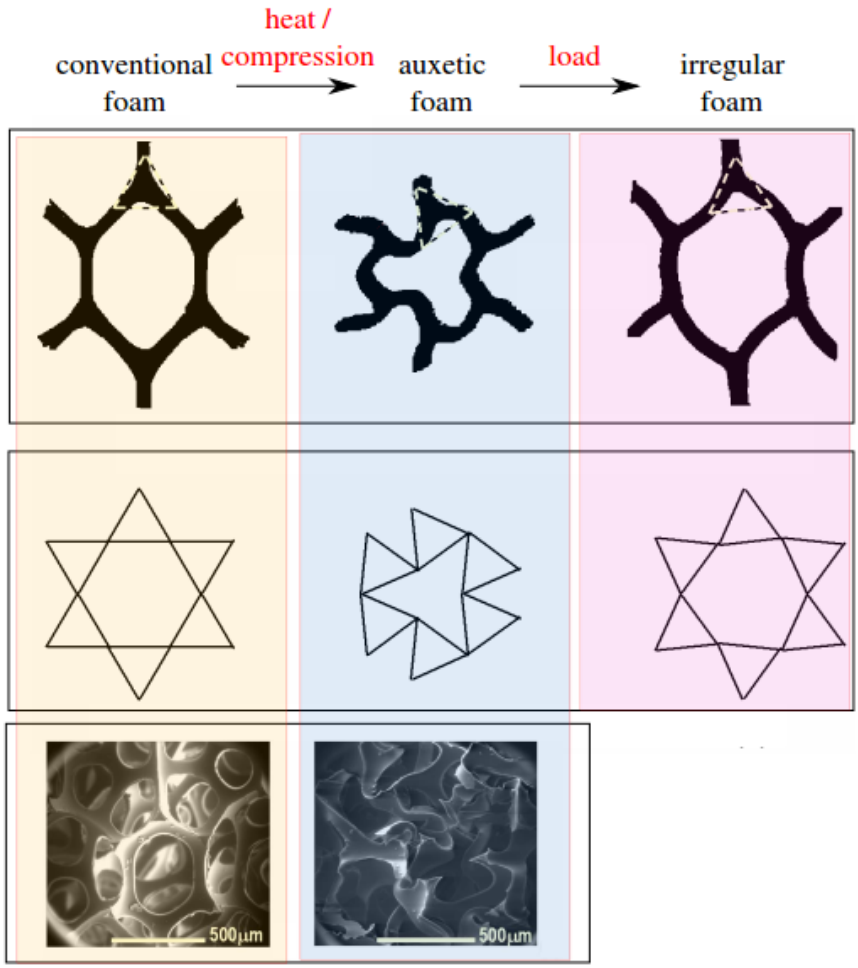

Figure 2-7 A diagram showing that a deformation of a foam might be modelled by means of rotating rigid units systems [Adapted from [307]].

As described in the section devoted to a general overview of auxetic systems, there is a large number of systems at the nano-scale [202-205, 209, 214-216, 309-316] which can exhibit

negative Poisson's ratio. As a matter of fact, it was also proven that the behaviour of a number of these systems can be represented by rotating rigid unit systems with some of the most studied examples being silicates, zeolites and various zeolite-based frameworks. Another interesting direction of studies relating to this concept is associated with the use of rigid units to model thermal expansion of these structures [46-51, 289, 317]. This was possible due to the fact that vibrations of respective units within molecules of crystalline structures tend to be highly symmetric which process resembles rotations of rotating rigid units with respect to a certain equilibrium angle.

In recent years, mostly due to rapid developments in 3D-printing and experimental techniques [9, 318, 319], a lot of attention was devoted to auxetic perforated materials [5, 9]. These macroscopic structures are often designed in a similar manner to rigid unit systems known from the literature. The main difference between theoretical rotating rigid unit and perforated systems is the fact that in the case of the latter class of materials, the units constituting the system cannot be connected by means of point-like hinges. Instead, the adjacent units are connected with each other by means of an additional amount of material which makes it more difficult for the units to rotate. Moreover, it was reported that the smaller the amount of material used to connect respective units, the easier it is for the system to deform [320]. It was also shown that upon decreasing the amount of material used to connect neighbouring units, a description of the system by means of theoretical rigid units becomes more reliable.

Last but not least it is also important to mention that similarly to systems at different scales described above, rotating rigid unit systems may also be used in order to mimic the deformation mechanism associated with other types of mechanical metamaterials (e.g. chirals, perforated materials etc.). This concept was thoroughly investigated by Professor Lim, who is one of the pioneers in the field of auxetic materials and related systems, in his recent work [321], where analogies between the deformation mechanism corresponding to different types of mechanical

metamaterials such as: rotating rigid units, perforated materials and chiral structures etc. were presented.

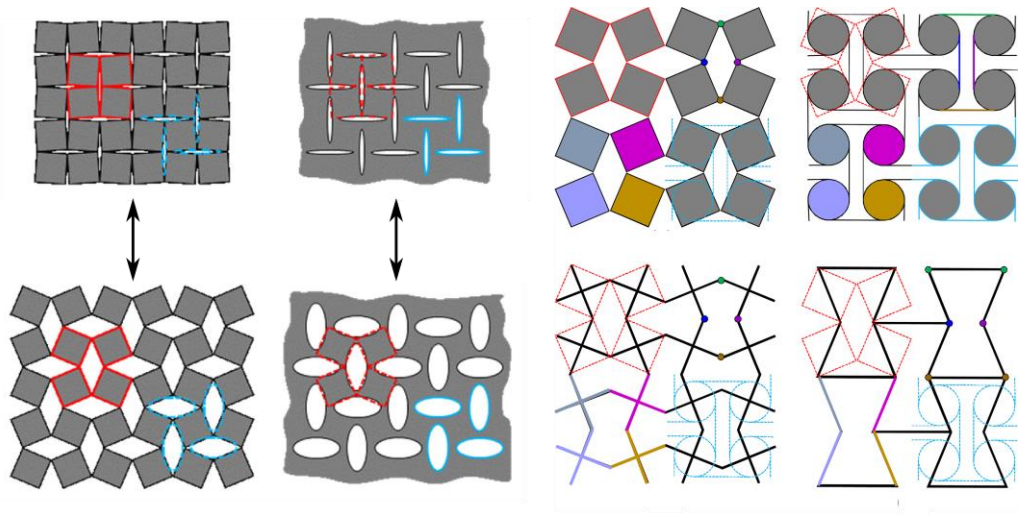

Figure 2-8 Graphical representation of different mechanical metamaterials corresponding to a common deformation mechanism [Taken from [321]].

Hierarchical systems

Over the years, the concept of hierarchy in nature has been investigated by numerous scientists. It is normally assumed that a given system is a hierarchical one if it consists of substructures having their own structure. This concept was first proposed by Professor Roderic Lakes in his famous paper published back in 1993 [322]. In his work, a convention for the way how the respective levels of the hierarchical system should be referred to was proposed (Level 0 corresponds to the most elementary unit constituting the system). Furthermore, according to recent studies, one may find examples of hierarchical systems occurring naturally in our environment. Some of the more studied examples of such structures are wood [323] (tree trunks, branches etc.), insect wings [324] (in particular dragonfly wings were investigated) and bones [325].

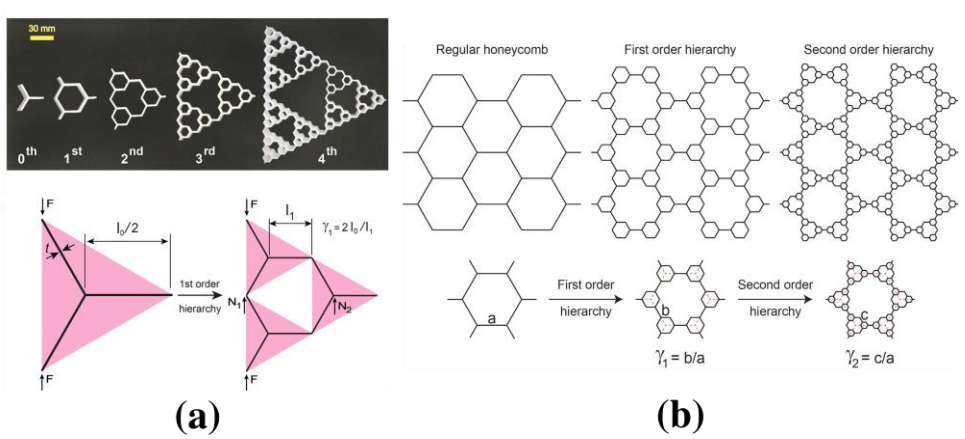

Figure 2-9 Hierarchical systems composed of honeycomb units forming elementary building blocks of the structure. Panels shown: (a) model proposed by Oftadeh *et al.* [Taken from [326]] and (b) model proposed by Mousanezhad *et al.* [Taken from [327]].

In the last couple of years, a lot of attention was devoted to two-dimensional hierarchical systems constructed by means of simple elementary units corresponding to known designs of non-hierarchical mechanical metamaterials. One of the first examples of such systems was proposed by Oftadeh *et al.* in his paper [326] published in 2014. In his work, the system composed of simple hexagonal units [326, 328] forming larger triangular motifs was discussed (see Figure 2-9(a)). It was shown that upon increasing the level of hierarchy such system may result in a fractal-like geometry (see Figure 2-9(a)). The process of increasing the hierarchy of the system was also reported to increase the effective elastic modulus of the structure without an increase in the density. A similar concept was published one year later by Mousanezhad *et al.* [327] for the system shown in Figure 2-9(b) where the considered structure could deform both via the rotation of subunits and buckling of the material. Another interesting work associated with hierarchical materials was the study published by Cho *et al.* [329]. In this work, it was shown that perforated materials can be used to design systems where the geometry of subunits resembles rigid units systems (see Figure 2-10(a)). It was also discussed that the use of hierarchy allows the fully-stretched system to achieve significantly larger area than would be the case for a similar system which does not utilise this concept. Another work where a similar structure was investigated was published by Gatt *et al.* [330]. In this work, it was shown

that one may design a hierarchical structure upon connecting rigid squares at vertices in a manner shown in Figure 2-10(b). This work also investigated different types of connectivities of subunits that can be used to construct the hierarchical system. All of the discussed structures were investigated numerically by means of Materials Studio software which led to the conclusion that such systems, similarly to unimode rotating squares, can exhibit auxetic behaviour. It was also proposed that hierarchical systems may be used in a variety of biomedical applications ranging from stents to skin grafts which utilise their enhanced mechanical properties.

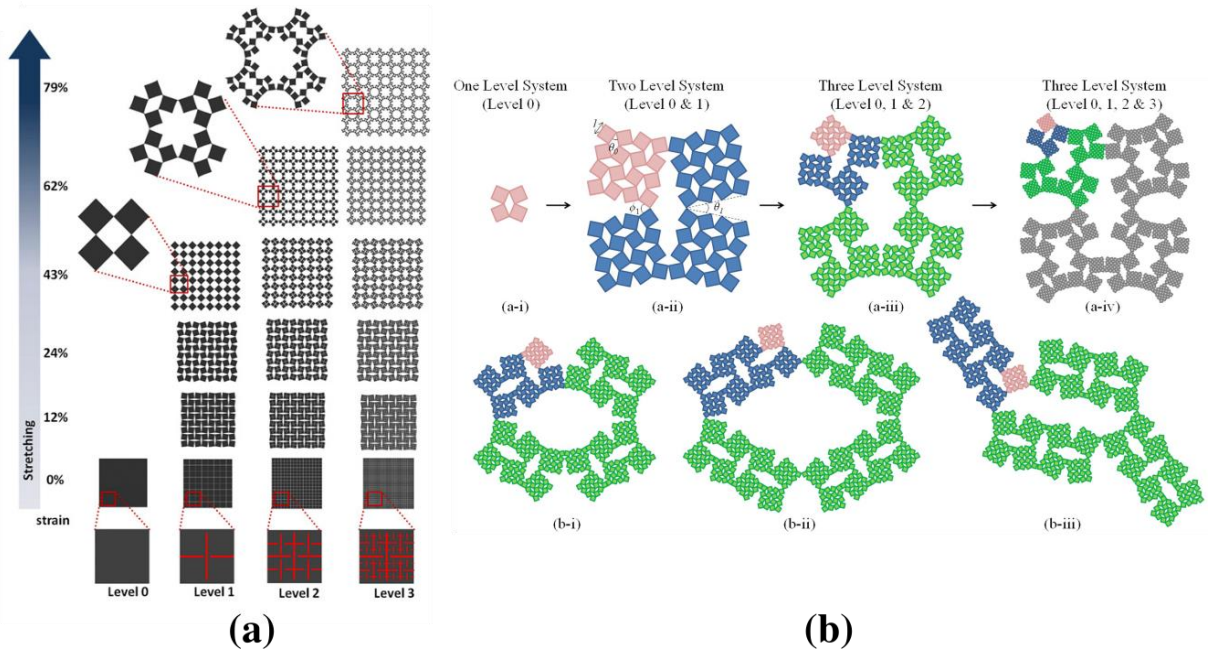

Figure 2-10 Panels show: (a) a diagram presenting a perforated fractal-cut model of the hierarchical mechanical metamaterial proposed by Cho *et al.* [Taken from [329]] and (b) different models proposed by Gatt *et al.* which present different ways of how elementary units consisting of rigid squares may form a hierarchical system [Taken from [330]]. On panel (b) different colours were used in order to highlight different levels of hierarchy within the structure.

The work of Cho *et al.* and Gatt *et al.* commenced a series of studies [320, 331-333] on similar systems to those shown in Figure 2-10(b) where similarly to the conclusions raised by the aforementioned authors it was confirmed that these systems can be expanded to a

particularly large extent while exhibiting negative Poisson's ratio. In addition to that, in the recent work by Seifi *et al.* [333], the possible extent of deformation of the discussed system was specified. Furthermore, in the paper published by Kunin *et al.* [320] it was reported that angles corresponding to respective levels of the hierarchical system are mutually independent. This means that based on a particular angle associated with a particular level of the structure it is not possible to determine the geometric configuration associated with the remaining levels. This observation is of great significance as it indicates that one cannot use a static approach in order to investigate the deformation process of analogical hierarchical systems. At this point, it is also worth to mention that these systems were investigated [320, 331-332] from the point of view of analysis of phonon dispersion graphs in order to evaluate their suitability for wave propagation. Last but not least it is important to mention the work published recently by Li *et al.* [334] where the potential of a novel hierarchical mechanical metamaterial composed of honeycomb-based unit cells to exhibit energy absorption and related properties was investigated. More specifically, depending on the level of hierarchy of the structure (see Figure 2-11(a)), it was shown that the system responds differently to a collision with an external body (see Figure 2-11(b)). This in turn, as reported by Li *et al.* [334] could lead to a design of acoustic dampers and tunable membrane filters.

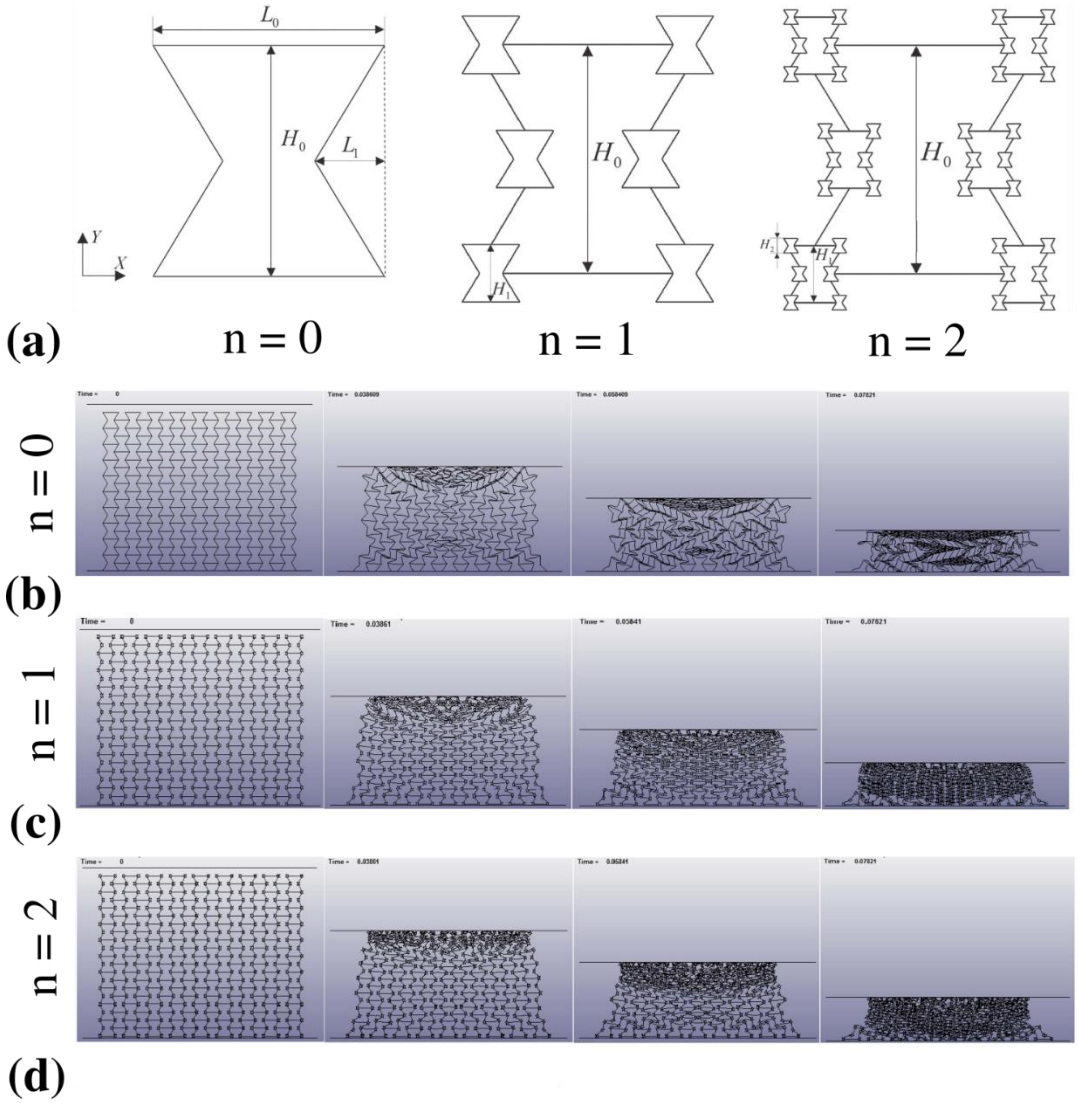

Figure 2-11 A hierarchical structure composed of elementary units in the form of re-entrant honeycombs. Panels show: (a) unit-cells corresponding to different levels of hierarchy, (b), (c) and (d) reaction of the hierarchical structure corresponding to different levels of hierarchy (n) upon being subjected to the collision with the external body [Taken from [334]].

2.1.2 Systems exhibiting negative compressibility

Even though compressibility is one of the most fundamental mechanical properties, the existence of materials exhibiting negative compressibility has not been reported until 1972. In this year, Gunton *et al.* published an article where it was stated that negative area compressibility can be observed in the case of the trigonal phase of arsenic [335]. This result

was soon reported to be incorrect. As explained in the following years by Morosin *et al.* [336], this incorrect result was caused by an inaccurate measurement. Soon afterwards, a number of papers were released where the presence of negative linear compressibility in the case of crystals such as cesium dihydrogen phosphate [337] and phase 5 of an orthorhombic paratellurite at high pressure (TeO_2) [338] was reported. Despite these studies, the person who is considered as a pioneer in the field is Prof. Ray H. Baughman who in 1998 published a famous work [72] where it was reported that rare crystal phases may exhibit both negative linear and area compressibility. The work of Prof. Baughman resulted in further studies by scientists from the field of material science on systems having a potential to exhibit negative compressibility in at least one direction (as discussed in the Introduction, in general materials cannot exhibit negative volumetric compressibility), with some examples being systems such as zinc dicyanoaurate [339], $KMn[Ag(CN)_2]_3$ [340] and methanol monohydrate [341].

Apart from studies on negative compressibility systems such as crystals and different chemical compounds, a new direction of studies in this field lies in the design of mechanical metamaterials to exhibit such a characteristic. This concept is of particular importance, as similarly as in the case of other mechanical properties, mechanical metamaterials may be tailor-made in order to exhibit a particular type of compressibility which makes them suitable to be used in industry. One of the most studied examples of these systems which have a potential to exhibit negative compressibility in at least one direction are wine-rack systems. These systems are based on the concept of rigid rods connected to each other with hinging being the mechanism governing their deformation. The first work where this concept was proposed was published by Weng *et al.* [342] (see Figure 2-12(a)), with this idea being further developed by Grima *et al.* [343]. Apart from deriving analytical expressions describing negative linear compressibility of the wine-rack system [344, 345], Grima *et al.* has also reported [343] this effect in the case of honeycombs (see Figure 2-12(b)). Furthermore, one year later he extended

this concept to the three-dimensional model of dodecahedron [261] (as shown in Figure 2-12(c)) which is an example of a cellular structure. Other three-dimensional cellular systems which were recently reported to exhibit negative linear and area compressibility and deform analogically to the wine-rack mechanism include the hexahedron (see Figure 2-12(d-i)) and the octahedron model [346] (see Figure 2-12(d-ii)). It is also worth to mention a recent work by Lim *et al.* [347] where two types of mechanical metamaterials deforming analogically through the wine-rack mechanism were reported to have a potential to exhibit negative area compressibility. One should also note that analogical behaviour to the wine-rack system can be also observed at the molecular level with one of the most recent examples being the work by Grima *et al.* [348].

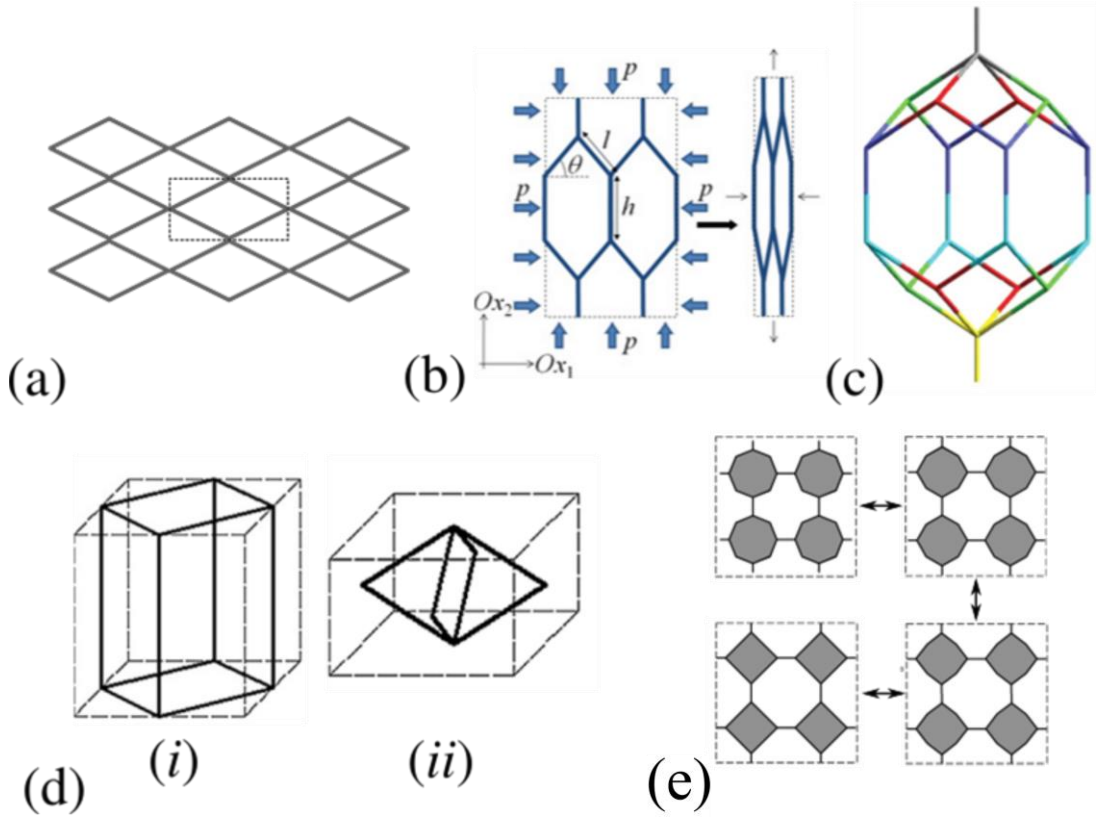

Figure 2-12 Panels show: (a) a conceptual representation of the wine-rack structure [Taken from [342]], (b) hexagonal structure exhibiting NLC [Taken from [343]], (c) a 3D model of dodecahedron [Taken from [261]], (d) cellular systems capable of exhibiting NLC [Adapted from [346]] and (e) novel system having a potential to exhibit NAC [Adapted from [347]].

Another important recent study is that by Qu *et al.* where the novel concept of mechanical metamaterials exhibiting negative effective compressibility is proposed [349]. This statement may seem to be confusing at first as in general materials cannot exhibit negative static volumetric compressibility with the justification being provided in the Introduction section of this thesis. On the other hand, one should distinguish between effective negative compressibility and negative compressibility as even though very similar, both of these quantities are different. Effective compressibility is defined as:

$$\beta_{V,eff} = -\frac{1}{V_{eff}}\left(\frac{\partial V_{eff}}{\partial p}\right)_T \qquad 2\text{-}1$$

where, p stands for the external hydrostatic pressure, T represents temperature and V_{eff} is the effective volume. This expression is almost identical to the definition of the static volumetric compressibility with the only difference being the fact that the volume V is replaced by V_{eff}. The difference between V and V_{eff} can be particularly visible in the case of porous materials where the size of pores can be too small to be visible with the naked eye. In such cases, it is possible that the material seemingly experiences a decrease in its perceived volume V_{eff} while at the same time the actual volume V corresponding to the constituent material is being decreased. In the situation described above, V_{eff} can assume negative values without contradicting the conservation of energy principle. This concept was proposed and validated numerically for a model shown in Figure 2-13. An additional confirmation was provided by these authors in their recent experimental study [350].

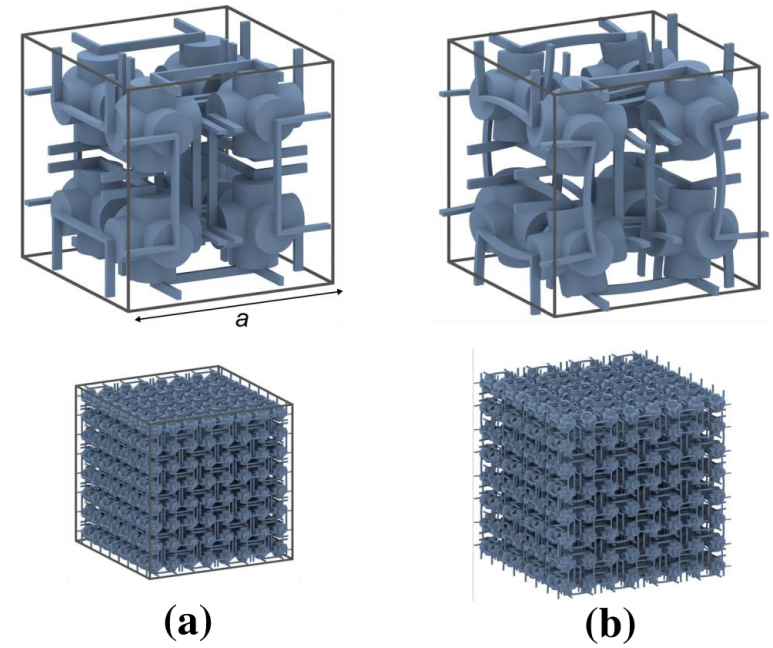

Figure 2-13 Panels show: (a) a unit-cell and the structure before an increase in the hydrostatic pressure and (b) the analogical system after an increase in the hydrostatic pressure [Taken from [349]].

Apart from systems deforming solely as a result of the hinging of connected perfectly rigid rods there are also other types of systems which can exhibit negative compressibility. One such example are truss-type systems composed of several types of materials which respond differently to a change in pressure. The first work utilizing this concept was published by Grima *et al*. [351]. In this work, it was shown that different Young's moduli of constituent materials may affect the compressibility exhibited by the system. This effect was investigated both for two (see Figure 2-14(a)) and three-dimensional models (see Figure 2-14(b)) being composed of a varying number of materials. Based on the presented results it was concluded that these system may exhibit both negative linear as well as area compressibility with the possibility of controlling the magnitude of both of these effects by means of appropriate parameters. In another work [76], Gatt *et al.* reported that it is also possible to use bimaterial constituents in order to design mechanical metamaterials exhibiting the discussed characteristic. Another class of systems with a propensity to exhibit negative compressibility and numerous other types of negative behaviour was proposed by Prof. Lakes and Prof. Wojciechowski in 2008. In their

work [75], it was first shown using a simple model composed of uniaxial pistons connected by springs that systems analogical to the structure presented in Figure 2-14(c) may exhibit negative compressibility as well as other types of unusual mechanical properties including negative thermal expansion. In the same work, it was also shown that this simple one-dimensional model can be extended in order to design a two-dimensional mechanical metamaterial exhibiting similar characteristics. In a more recent study [352], Hewage *et al.* used the concept proposed by Prof. Lakes and Prof. Wojciechowski to experimentally investigate properties of an analogical system for a variety of interactions between neighbouring units.

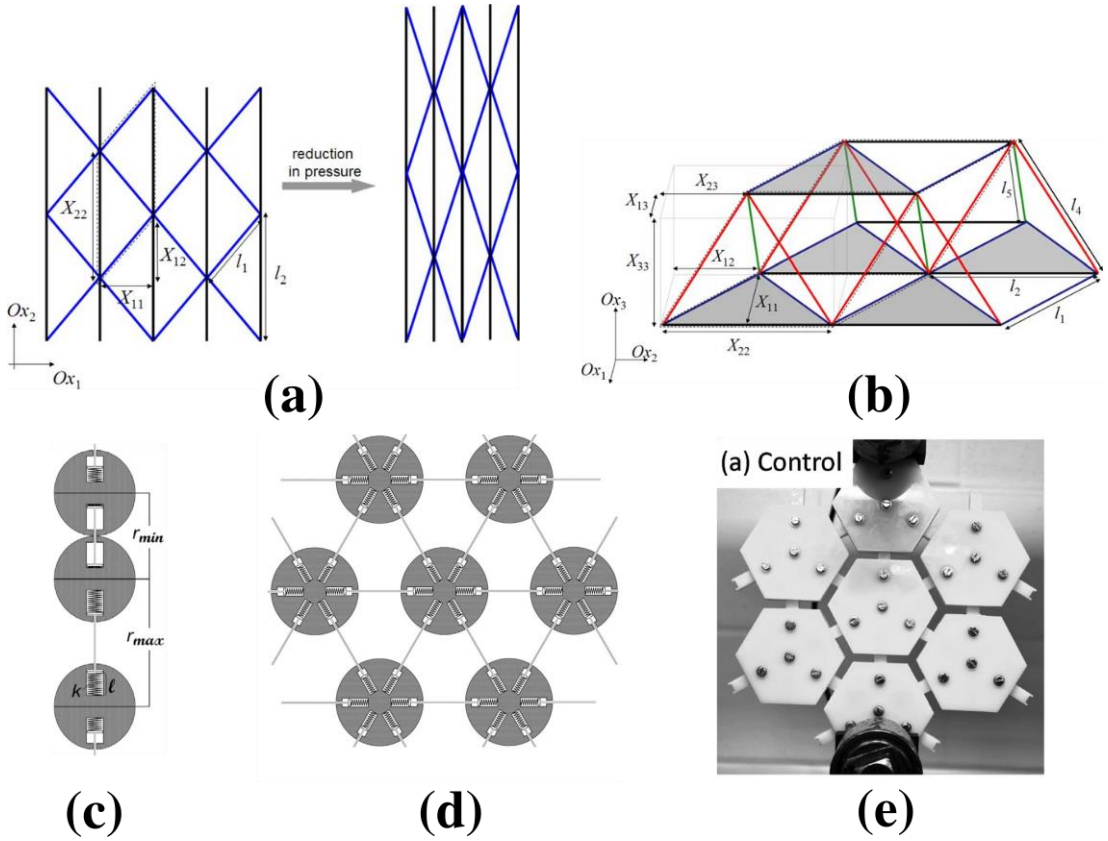

Figure 2-14 Different systems having a propensity to exhibit negative compressibility in at least one direction. Panels show: (a) a two-dimensional truss-type structure composed of two different materials [Taken from [351]], (b) an equivalent concept presented in 3D [Taken from [351]], (c) One dimensional model composed of pistons connected to each other by springs [Taken from [75] and [347]], (d) a two-dimensional model which is equivalent to the model shown on panel (c) [Taken from [75]] and (e) an experimental model working on a similar principle as the model shown on panel (d) [Taken from [352]].

In this thesis, it was already discussed that rotating rigid units systems may exhibit anomalous mechanical behaviour in the form of the negative Poisson's ratio. As it turns out, these systems if appropriately designed may also exhibit negative compressibility in at least one direction. The first example of this approach was reported by Grima *et al.* [290] where the system of generic rigid triangles connected at vertices was investigated (see Figure 2-15(a)). In the more recent study [353], it was also shown that negative compressibility is possible for different quadrilaterals connected to each other at vertices as shown in Figure 2-15(b) taking type I rotating rectangles as an example. It was also reported that the extent of NLC in such systems depends on geometric parameters describing a given structure.

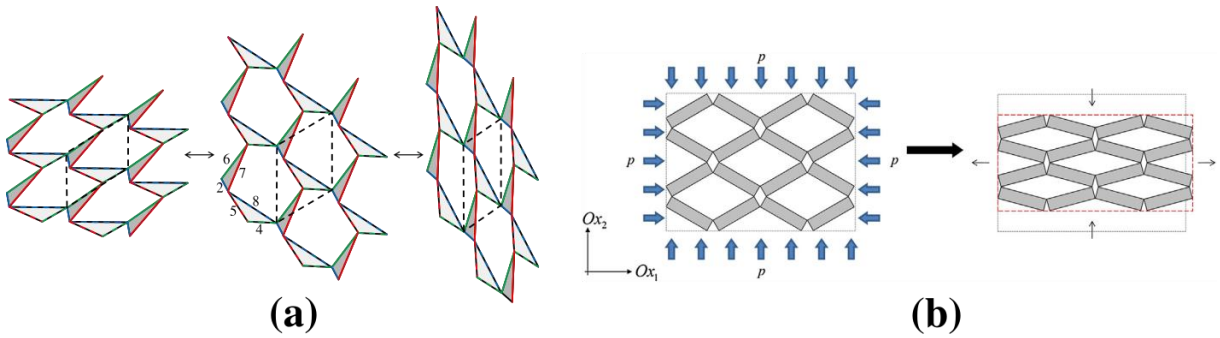

Figure 2-15 Different types of rotating rigid unit systems which are known to have a propensity to exhibit negative linear compressibility. Panels show: (a) generic rotating rigid triangles [Taken from [290]] and (b) Type *I* rotating rigid rectangles [Taken from [353]].

2.1.3 Systems exhibiting negative stiffness

Even though studies associated with systems exhibiting negative stiffness were started as early as 1957 [354] it had been many years until research in this area provided results which could be applied in industry. The mathematical formulation of negative tangent (incremental) stiffness was proposed several years later by Cenap Oran [355] whose research paved the way for a number of studies that pointed to several mechanisms associated with negative stiffness materials. One of the first studies in this field was commenced by Thompson *et al.* in 1979

[356] who proposed that systems of constrained buckled beams are unstable. Many years later, this concept was confirmed by Chan *et al.* [357] who also observed that such behaviour may lead to negative stiffness. This study was soon followed by that of Wang and Lakes [77] who showed that buckled beams (see Figure 2-16(a)) may use their stored energy to contribute to the deformation rather than oppose it. This in turn, as discussed by these authors, is a manifestation of negative stiffness. In their work, it was also observed that systems exhibiting negative stiffness are unstable and should one remove the constraints then they would try to assume one of the energetically favourable conformations. This mechanism is the origin of the discussed mechanical property. Also, as stated by Falk *et al.* [358], negative stiffness in elastic materials may be observed only if the energy plotted with respect to displacement has at least two local minima. Wang and Lakes also reported that it is possible to replace the buckled beam with pre-loaded connected springs in order to observe an analogical characteristic. In the following years, many scientists continued efforts associated with studies on pre-buckled beams having a propensity to exhibit negative stiffness. Most notably, in 2008 Yap *et al.* [78] showed that negative stiffness can be achieved in multiwalled carbon nanotubes (see Figure 2-16(b)). In this work, apart from verifying the results observed at the macroscopic level it was also suggested that these nanotubes can be used to design composites at the nano-scale which would have a potential to exhibit anomalous mechanical behaviour such as negative stiffness. Another interesting study was reported by Kashdan *et al.* [359] where it was shown that the concept of the constrained buckled beam may be modified by an addition of another spring (see Figure 2-16(c)). It is also important to mention the work by Coulais *et al.* [79] where the concept of the pre-buckled beam exhibiting negative stiffness was modified by the introduction of evenly-distributed apertures on the beam itself (see Figure 2-16(d)). Last but not least, the most recent contribution to the field of pre-buckled beam-like systems exhibiting negative stiffness was reported by Cortes *et al.* [360]. In this work, it was shown that a pre-buckled beam may be used

in order to design a piston-like subunit. It was also discussed what would happen with properties of such system should one insert it into a polymer matrix (see Figure 2-16(e)). A similar concept associated with honeycomb-like materials was also reported in [361, 362].

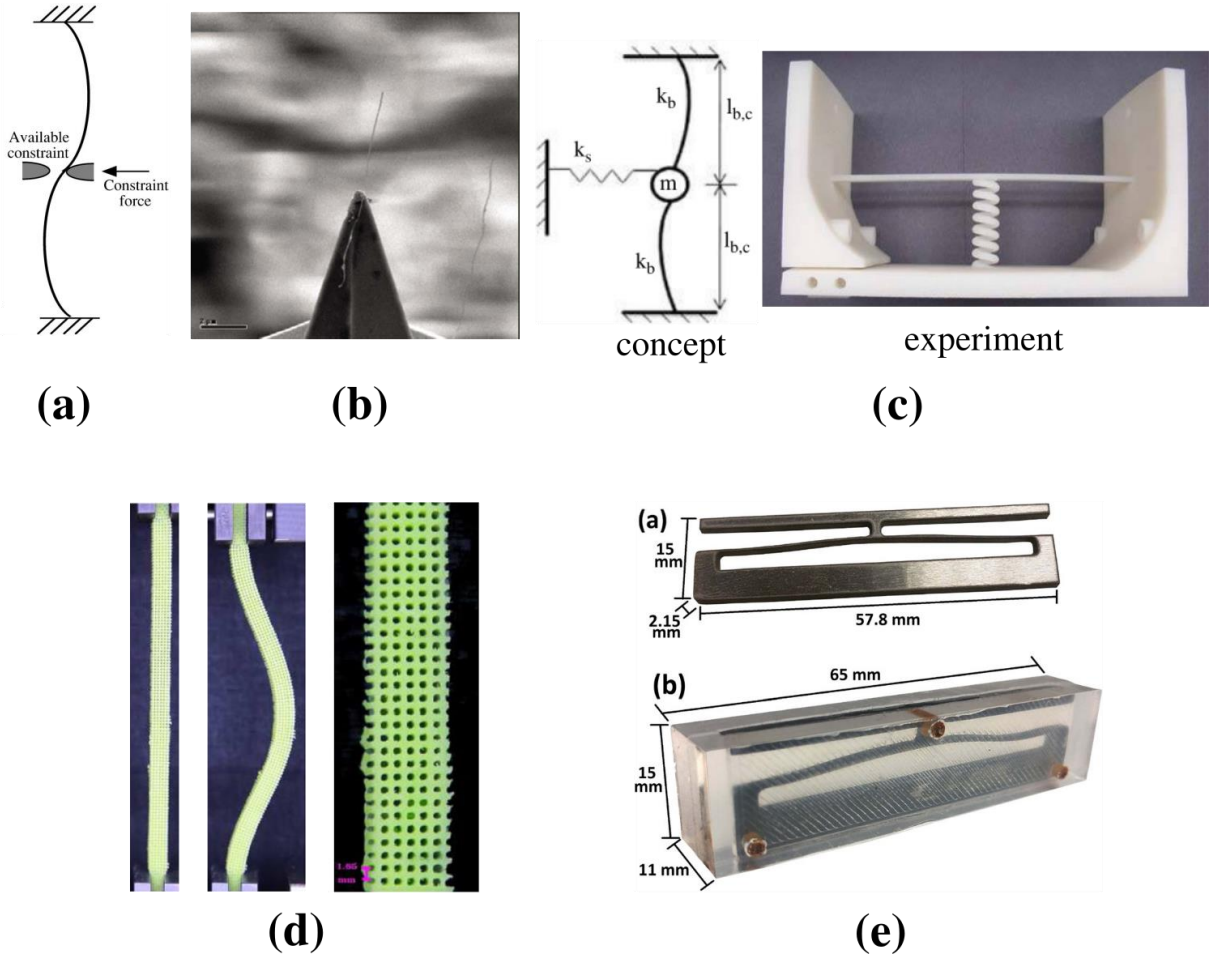

Figure 2-16 Panels show: (a) theoretical concept of the buckled beam [Taken from [77]], (b) carbon nanotube exhibiting analogical behaviour to the buckled beam [Taken from [78]], (c) a buckled beam with an additional spring [Taken from [359]], (d) a buckled beam with additional apertures [Taken from [79]] and (e) buckled beam forming a piston-like mechanism submerged into a polymer matrix [Taken from [360]] .

Another area of study where the use of the concept of negative stiffness has been of great significance are composites with negative stiffness inclusions. The pioneer in this field is Prof. Lakes and his group who in 2001 published an experimental paper [363] where it was shown that it is possible to achieve a stable positive stiffness composite upon inserting negative stiffness inclusions into a matrix despite the fact that such inclusions would be unstable if

considered separately. To achieve this effect, Lakes *et al.* inserted negative stiffness inclusions in the form of ferroelastic vanadium dioxide into a positive stiffness tin matrix. It was also reported that introducing such inclusions in the system makes it possible to increase the stiffness of the whole composite [364] with the extent of this effect being even greater than in the case of diamond inclusions. This in turn, as suggested by these authors, could make such materials suitable for applications such as superior vibration damping devices. A similar suggestion was also made by Lakes *et al.* in his following papers [365-368] which discussed extreme damping observed in composites with negative stiffness inclusions. In the same year, Wang e*t al.* [369] suggested that composites with negative stiffness inclusions may lead to anomalous coupled field properties such as piezoelectricity and negative thermal expansion. In 2007 Jaglinski *et al.* [370] went as far as to show experimentally that the effect of stiffening of the resultant composite may lead to a stiffness greater than that of diamond (it was also shown that a similar effect of stiffening may be achieved upon combining elements with negative and positive Poisson's ratio [371, 372]). This novel result (up to this point it has not been confirmed experimentally) was obtained for a composite composed of a metal matrix with barium-titanate inclusions (see Figure 2-17(a)). In the following years, the concept of stiffening of a composite as a result of the introduction of negative stiffness elements to the system was described and quantified by means of a theoretical model proposed by Drugan in 2007 [373]. Another interesting work [374] in this field was published by Kochmann *et al.* who showed that similar behaviour may be observed should one consider a negative stiffness cylinder with a positive stiffness coating (see Figure 2-17(b)). This concept was developed even further by these authors in their next study on this subject [375] where they showed that it is possible to achieve an arbitrarily large value of positive stiffness for the analogical system upon allowing it to rotate. A few years later, Dyskin *et al.* [376] proposed a concept of an elastic composite where isotropic negative stiffness inclusions having a cylindrical shape are inserted into an isotropic matrix

with a positive stiffness (see Figure 2-17(c)). In this work, it was shown that depending on the concentration of such inclusions within the matrix, the resultant composite may exhibit very different types of behaviour in terms of stiffness. More specifically, by means of the theoretical model, it was shown that if the number of cylindrical inclusions does not exceed a particular threshold value then the whole composite exhibits positive stiffness having its value enhanced in comparison to the stiffness of the matrix. On the other hand, if this threshold value is exceeded the contrary is observed, with the system exhibiting unstable behaviour corresponding to negative stiffness. At this point, it is also worth to mention that the studies described above were followed by a number of different research projects [377-380] associated with the use of negative stiffness inclusions in mechanical systems at different scales (see Figure 2-17(d) for an example of such system [379]).

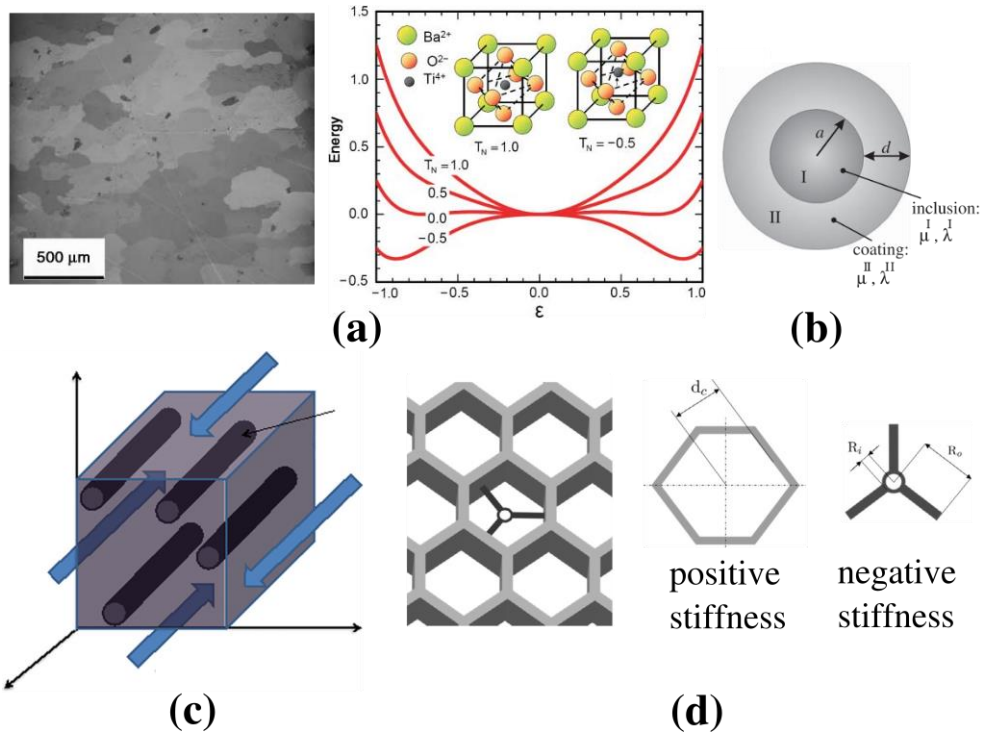

Figure 2-17 Panels show: (a) figure of the composite investigated by Jaglinski *et al.* [370], where black dots indicate negative stiffness inclusions and the remaining grey-scale background is a positive stiffness matrix [Taken from [370]], (b) cylindrical composite proposed by Kochmann *et al.* [Taken from [374]], (c) model investigated by Dyskin et al. [Taken from [376]] and (d) composite proposed by Chronopoulos et al. [Taken from [379]]).

Negative stiffness is a property which is particularly required in the case of vibration damping devices. As a result, there has been a large number of studies [381-387], where a variety of mechanical devices were reported to have a propensity to exhibit such a characteristic. From the point of view of this thesis, of particular interest are those devices which make use of magnetic interactions in order to induce a required type of stiffness as opposed to other types of physical interactions. As reported by Feldman [388], negative stiffness can also be achieved as a result of interaction of attracting magnets. Over the years, this concept has resulted in a number of studies where different configurations of magnets were used in vibration damping devices which exhibit the required properties. One of the prime examples of this approach is the work by Carrella *et al.* [381] (see Figure 2-18(a)) where the proposed damper was composed of three uniaxial magnets with an additional spring being the source of the positive stiffness. In this work it was shown that, depending on the ratio of the strength of magnets with respect to the stiffness constant associated with springs, such a structure may exhibit positive or negative stiffness. It was also reported that this system may undergo a transition from one type of stiffness to another during the process of mechanical deformation which corresponds to a change in the distance between respective magnets. A similar concept was reported one year later by Robertson *et al.* [389], with the difference being lack of springs in the design of the mechanism (see Figure 2-18(b)). In the same year, Ravaud *et al.* [390] showed that it is also possible to arrange magnets in a way shown in Figure 2-18(c) in order for the structure to exhibit negative stiffness (a similar more recent concept can be found in [391]). As reported by the authors of this work, such a configuration may also serve as a bearing in the case of devices which require near zero friction on their axis of rotation in order to operate. Some other more complex devices [392-394] were also proven to have a potential to exhibit negative stiffness in the following years. Amongst more recent studies in this field, it is worth to mention the work by Wu *et al.* [395] who in 2014 proposed a novel

concept concerning the magnetic "spring-like" mechanism which was reported to exhibit negative stiffness (see Figure 2-18(d)). One year later, Shi *et al.* [396, 397] managed to construct experimental prototypes of magnetic vibration damping devices which are based on some of the concepts proposed in previous years (see Figure 2-18(e)). According to his study, analytical predictions made in the past were indeed correct where the considered systems showed a propensity to exhibit negative stiffness.

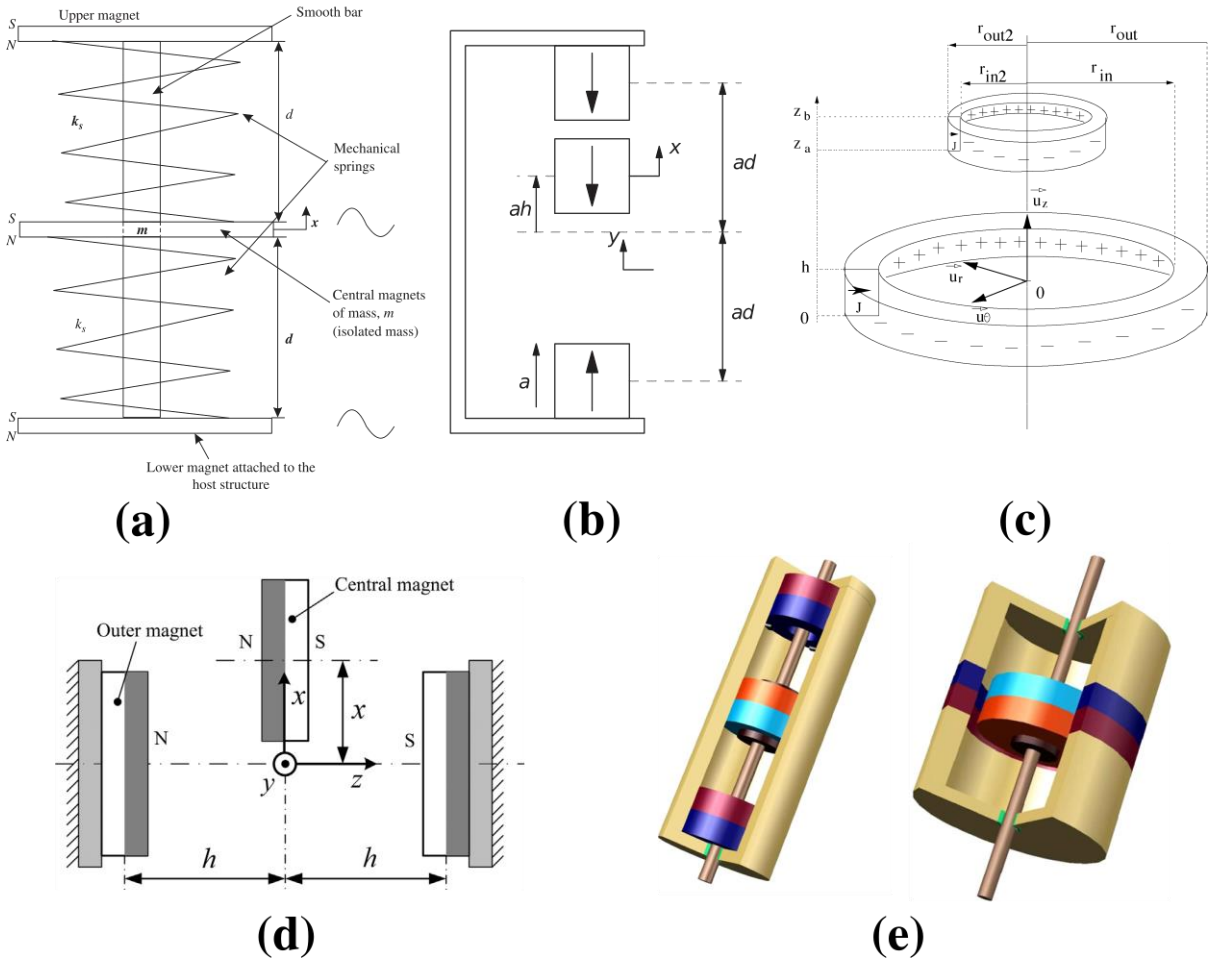

Figure 2-18 Panels show: (a) uniaxial attracting magnets with an additional spring offering positive stiffness to the system [Taken from [381]], (b) model composed of uniaxial magnets proposed by Robertson *et al.* [Taken from [389]], (c) concept corresponding to uniaxial magnetic rings proposed by Ravaud *et al.* [Taken from [390]], (d) structure acting as magnetic spring [Taken from [395]] and (e) examples of structures investigated experimentally by Shi *et al.* [Taken from [396]].

At this point it is also worth to mention the recent work published by Hewage *et al.* [352], where using an experimental prototype motivated by the concept proposed initially by Prof. Lakes and Prof. Wojciechowski [75], it was shown that it is possible to design complex mechanical metamaterials which can exhibit several unusual mechanical properties (including negative stiffness) at the same time. This indicates, that soon it may become possible to combine the benefits associated with negative stiffness and other unusual materials such as auxetics at the industrial scale in order propose novel applications which could lead to a potential breakthrough in the field of material engineering. As a matter of fact, even nowadays when negative stiffness devices do not normally exhibit several other anomalous properties, these systems are very useful in a number of everyday applications such as isolation of vehicle seat vibrations [398], isolation of vibrations in railroads [387] and minimisation of the seismic response of a building [399, 400].

2.2 Mechanical metamaterials and other systems with magnetic inclusions

As discussed in the former chapters, despite a significant number of conducted studies, materials exhibiting anomalous auxetic behaviour constitute a still relatively new branch of material science. One of the most recent directions of studies in this field is associated with materials having magnetic inclusions where the behaviour of the system can be influenced by internal magnetic interactions between inclusions or the interaction of inclusions with an external magnetic field. One of the first studies involving the concept of magnetic inclusions in auxetic systems was the work of Scarpa *et al.* [401] where the suitability of polyurethane foam for sound absorption was discussed. More specifically, it was shown that the potential of investigated foams to exhibit acoustic absorption properties becomes additionally enhanced by

the insertion of micro-sized carbonyl iron particles into the system in the presence of an external magnetic field. In another study conducted by this author [402], mechanical, acoustic and electromagnetic properties of polyurethane foams with magnetic inclusions were analysed experimentally. Among other results, in this work it was reported that as in conventional foams, the insertion of magnetic particles into the system results in an increase in the refractive index. Another work relating to electromagnetism in the case of mechanical metamaterials is the work published by Smith *et al.* [403] where electromagnetic properties of re-entrant dielectric honeycombs were discussed. More specifically, it was shown that the permittivity of the system changes upon varying the geometric parameters of the structure which as suggested by the authors, may prove to be useful in electromagnetic window applications.

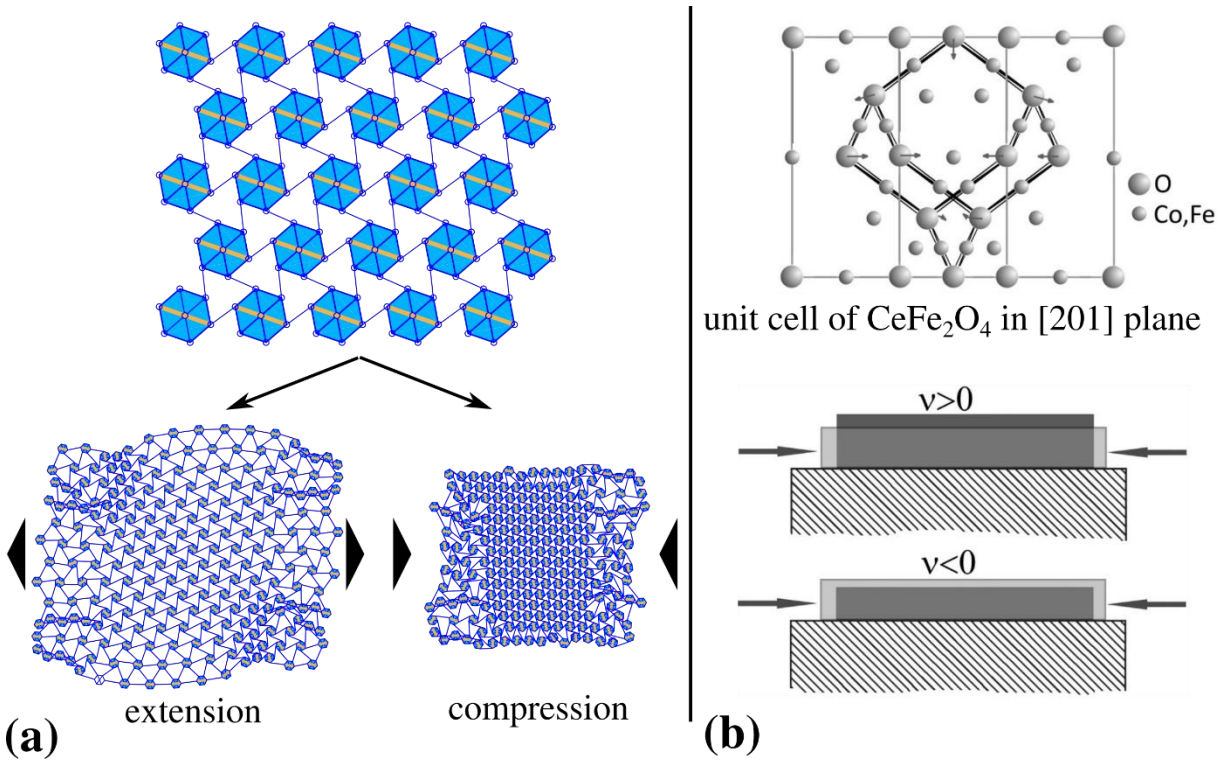

Figure 2-19 Systems of thin magnetic films having a potential to exhibit auxetic behaviour shown schematically in the case of (a) a theoretical work reported in [404] [Adapted from [404]] and (b) experimental work involving the use of $CoFe_2O_4$ [Taken from [123]].

The above studies conducted by the group led by Prof. Scarpa were soon followed by other researchers who shared the interest in the possibility of controlling / affecting the properties of a system by the use of magnetic inclusions. One such direction of studies was the work conducted by Prof. Dudek and Prof. Wojciechowski where the potential of ferrogels to exhibit auxetic behaviour was investigated by means of computer simulations (molecular dynamics simulations) [405]. In their work, the investigated structure was represented by a nonmagnetic polymer with magnetic grains having their motion governed by Landau-Lifshitz-Gilbert equation [482]. In the following study [404], these authors investigated mechanical properties of a thin magnetic film exposed to an external magnetic field. In this work, the structure consisted of hexagonal units with inclusions in the form of magnetic nanoparticles where the units were connected to each other by springs corresponding to chemical bonds (see Figure 2-19(a)). Amongst other results, the authors proved that such system may indeed exhibit auxetic behaviour. In the more recent experimental work on thin magnetic films, Valant *et al.* reported a negative Poisson's ratio equal to -0.85 for $CoFe_2O_4$ thin film subjected to a compressive axial strain (see Figure 2-19(b)) [123]. This result was explained based on the observation that the bonds in the unit cell of the investigated material form a honeycomb-like shape which is known to exhibit auxetic behaviour.

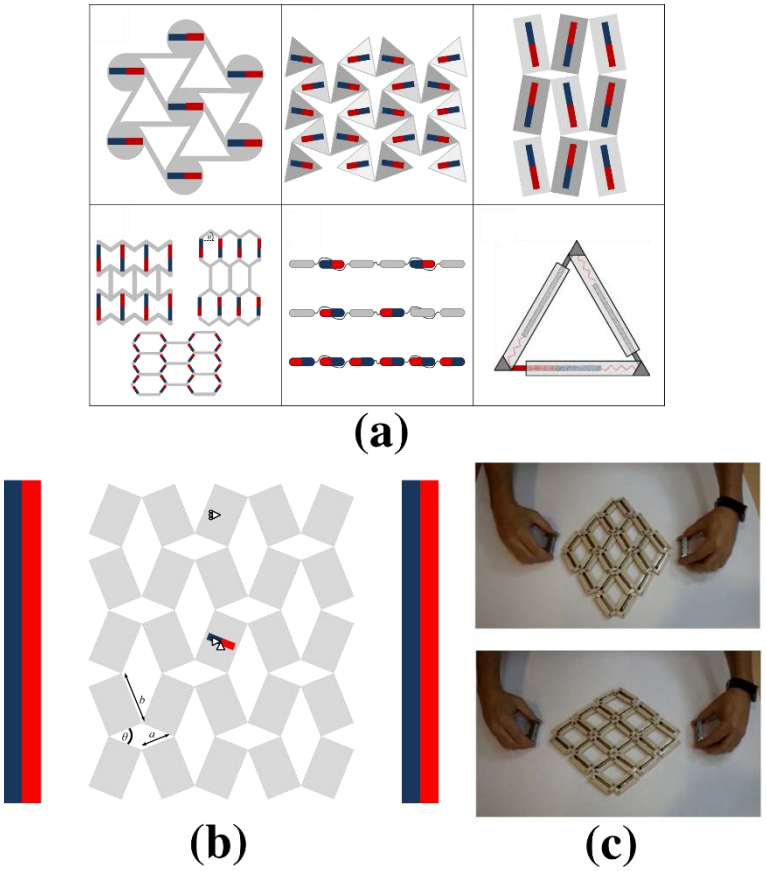

Figure 2-20 Panels show: (a) different examples of mechanical metamaterials which are potentially suitable to host magnetic inclusions, (b) the model investigated and (c) experimental realisation of the theoretical concept proposed on panel (b) [Adapted from [406]]

After the initial success of theoretical and experimental studies on systems at the nano and micro scale with magnetic inclusions, researchers working in the field of material science started working on projects where the magnetic inclusions could be utilised in macroscopic systems to control their motion. One of the first studies where such an attempt was made was the work by Prof. Grima *et al.* [406] where it was proposed that even at the macroscopic scale, one can place magnets on the structural units of the mechanical metamaterial in order to control its mechanical behaviour. This concept can be visualised with the help of a number of simple diagrams as shown in Figure 2-20(a). Furthermore, based on the theoretical model and the experiment, it was shown that one can indeed control the mechanical properties and the configuration of such systems through a variation in the external magnetic field which in the

case of this study was applied by means of magnets placed outside the system (see Figure 2-20 (b-c)). In the following years, it was reported that this approach can be also used in elastic materials with magnetic inclusions. In such systems, mechanical properties may be fined-tuned by the interplay between the elastic behaviour of the material and magnetic interactions between magnetic inclusions and the external magnetic field. One of the first conceptual papers reporting this effect was published by Singh *et al.* [407], where the magneto-elastic buckling of a beam was investigated. In this work, it was shown that the magnetic interaction between the magnet set at one end of the beam and the external magnet may overcome the elastic forces within the material so that the beam could be bended to an arbitrary extent (see Figure 2-21(a)). This work was soon followed by studies on more complex magneto-elastic systems such as the kagome lattice with magnetic inclusions in the work published by Schaeffer *at al.* [408] (see Figure 2-21(b)). In this work, amongst other results, it was shown that the discussed system can deform to a significant extent upon being subjected to an external magnetic field. It was also observed that the stiffness of the investigated lattice may be fine-tuned as a result of the deformation. In recent years, the concept of the deformation of magneto-elastic systems caused by the application of an external magnetic field was also applied to different cellular structures with the first example of this approach being the work by Tipton *et al.* [409] where it was proposed that the discussed effect is scalable and could potentially become an actuation mechanism for a change in the topology of a given structure. After a few years, a similar result was also reported by Harne *et al.* [410] in which work it was additionally shown that the magnetically-induced deformation of the magneto-elastic cellular system may lead to auxetic behaviour (see Figure 2-21(c)).

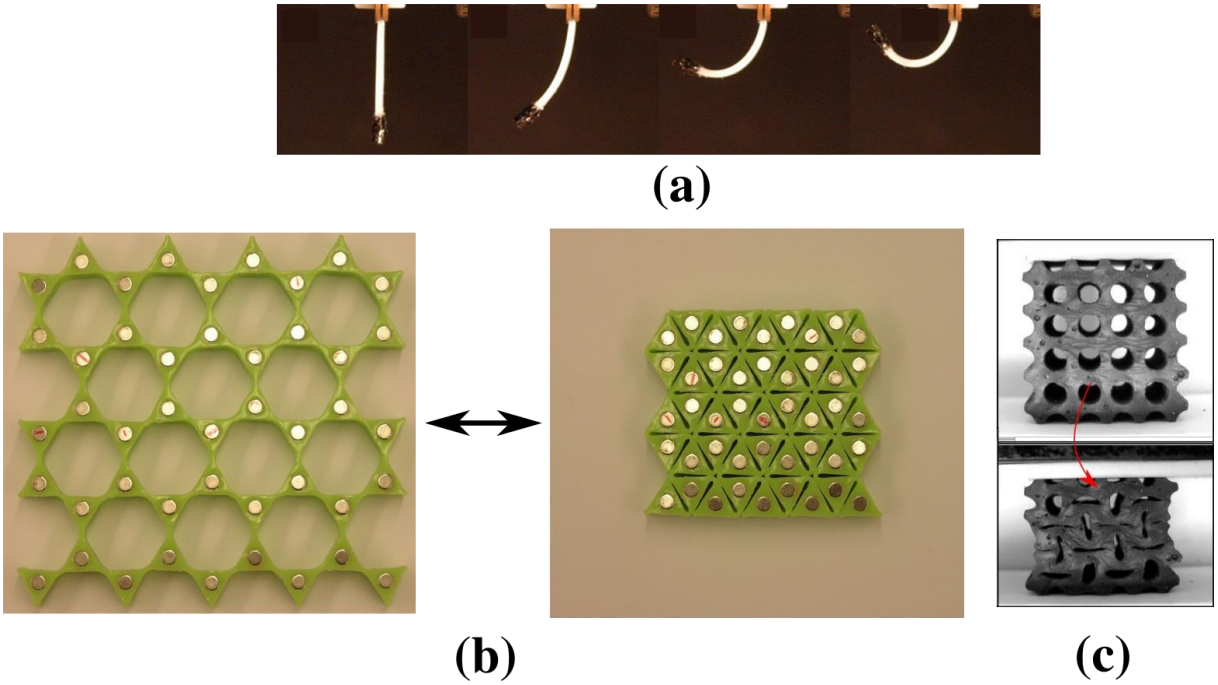

Figure 2-21 Panels show: (a) elastic Euler beam with a magnet at one of its ends which is being attracted by an external magnet [Taken from [407]], (b) kagome lattice with magnetic inclusions [Adapted from [408]] and (c) cellular structure with magnetic inclusions deformed by an external magnetic field [Adapted from [410]].

Having established that the deformation process of mechanical metamaterials with magnetic inclusions can be controlled via an external magnetic field, it is useful to consider different applications that make use of such systems. One branch of material science where these structures have been successfully used are studies on wave propagation phenomena in magneto-elastic mechanical metamaterials. A pioneer in this field is Prof. Ruzzene with his group who has proposed a number of theoretical models focusing on the control of wave propagation properties. One of the first papers where this phenomenon was thoroughly investigated is the work by Schaeffer *et al.* [411]. In this work, different multistable one and two-dimensional magneto-elastic lattices were investigated by means of dispersion diagrams and numerical simulations. In the case of each of the investigated systems, it was assumed that the structure is composed of axial and torsional springs with magnets represented by individual magnetic moments being located at intersections between respective springs (see Figure 2-22 for examples of such systems). Based on the obtained results, it was concluded that the band

gap formation is strongly affected by the choice of the investigated geometry. Upon minimizing the potential energy of the considered structures, it was also shown which types of stable configurations can be assumed by respective systems. A similar work devoted solely to the search for energetically-optimal configurations of one and two-dimensional magneto-elastic lattices was published a few months later by the same group [412]. It is also worth to note that in one of their recent studies, this group has also investigated wave propagation properties in magneto-elastic kagome lattices [408].

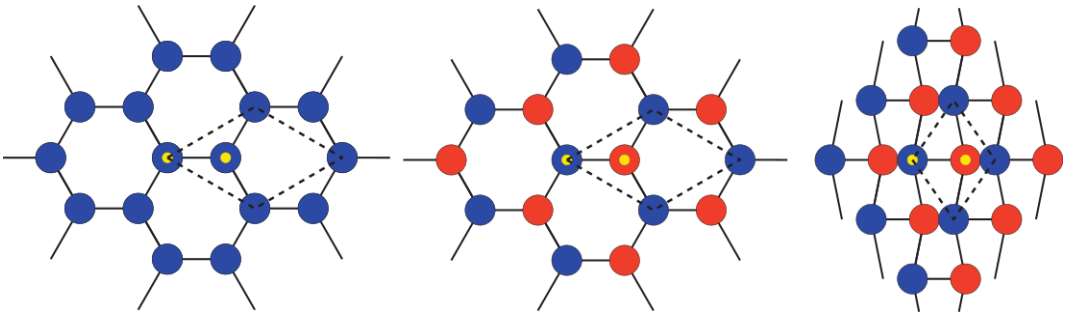

Figure 2-22 Different examples of magneto-elastic lattices with magnetic moments represented by blue or red points being oriented in the perpendicular direction to the plane of the figure [Taken from [412]].

The class of mechanical systems which perhaps finds the largest number of applications in the industry are vibration dampers with magnetic inclusions. As reported by Feldman *et al.* [413] and Carrella *et al.* [414], attracting magnets have a potential to exhibit negative stiffness. This mechanical property is in turn known to be essential in the case of materials used to construct devices meant for vibration isolation and vibration damping. One of the prime examples of this approach is the work by Shi *et al.* [396] where a set of three uniaxial magnets composes a device exhibiting negative stiffness (see Figure 2-23(a)). At this point it is also important to highlight the fact that it is possible to design more complex periodic mechanical metamaterial systems exhibiting this characteristic as a result of magnetic interaction between constituting elements with a good example being the work published by Hewage *et al.* (see Figure 2-23(b)) [352].

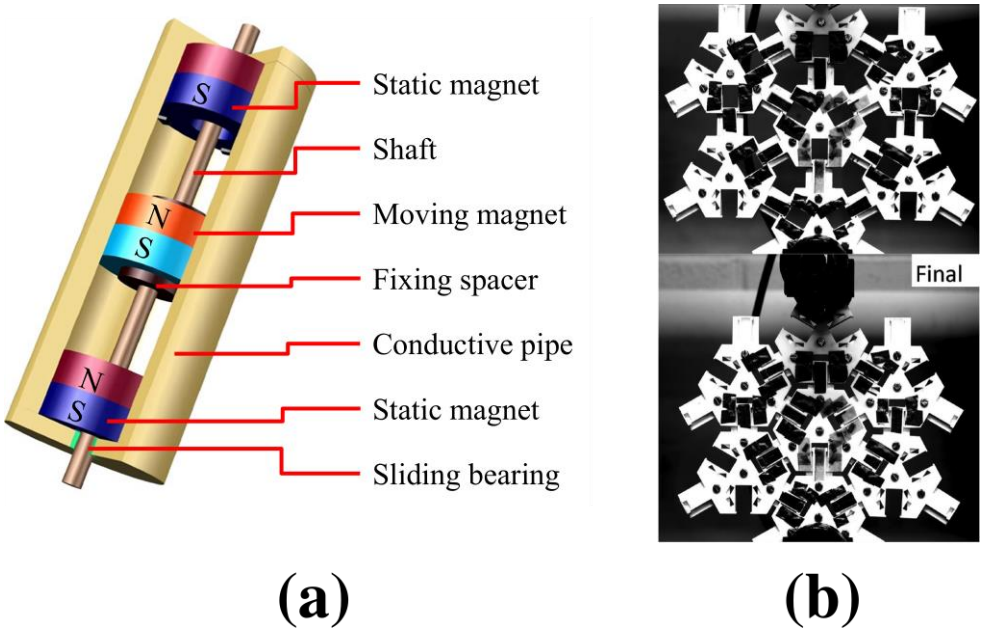

Figure 2-23 Panels show: (a) model of a magnetic vibration damper operating through the principle of negative stiffness [Taken from [396]] and (b) an experimental example of the mechanical metamaterial exhibiting negative stiffness [Taken from [352]].

3. Scope of this Work and Topics Addressed

As discussed in the preceding Literature Review, over the years, mechanical metamaterials have been proven to have a potential to exhibit unusual mechanical properties such as negative Poisson's ratio, negative stiffness, negative compressibility and negative thermal expansion. The possibility of achieving these anomalous properties has been the main focus of scientists working on mechanical metamaterials as such properties may be used in a variety of applications ranging from impact-resistant devices to sound-proofing and biomedical devices.

However, even though several forms of mechanical metamaterials have been thoroughly investigated from the point of view of achieving the above properties, the field is still expanding. It is likely that there are still a number of mechanisms which can result in unusual properties that have yet to be identified and / or studied further. For example, although there have been many developments on systems which incorporate within them some form of rotating rigid units, there are various aspects and properties that these systems may have which have never been investigated or their development is still in its infancy. These include the dynamic aspects associated with auxetic mechanisms, the behaviour of mechanical metamaterials with magnetic inclusions and other different physical phenomena which have not yet been investigated vis-à-vis the mechanical metamaterials.

In view of the above, this thesis will take as a starting point the classical 'rotating squares' concept and develop it so as to examine how some interesting effects can be achieved if one had to take a different approach at how these systems operate. In particular, through a dynamics approach, the thesis will first look at how the rotation of the subunits constituting rotating rigid units structures may in general lead to the overall rotational motion of the system. More specifically, the methodology is developed and applied on finite fragments of the rotating squares system with the scope of developing the theoretical framework to examine how rotating

squares systems may induce their own rotation. This is followed by a qualitative experimental verification of this phenomenon so as to confirm in a definite manner that this effect may be indeed observed in reality. The theory behind the concept is then further extended to examine how this effect can be enhanced and generalised through the use of systems where the squares are replaced with rectangles which can be considered as more general analogues of squares. Following this, using a similar dynamic approach the behaviour of a two-level hierarchical system composed of rotating squares is re-examined in an attempt to address an important unanswered question, more specifically why in real experimental scenarios the higher level of a hierarchical system tends to open up to a significantly greater extent than the lower levels of the system.

Even though all of the systems mentioned above make use of square/rectangle-like motifs, it does not mean that novel types of mechanical behaviour cannot be exhibited by other systems which have not yet been proposed. As a matter of fact, due to the possible versatility of mechanical metamaterials, one can expect that there is a plethora of such systems. Thus, this thesis will attempt to show that even though mechanical metamaterials have been extensively studied, it is still possible to design novel types of these systems with a potential to exhibit unusual mechanical behaviour. More specifically, an original design of a mechanical metamaterial composed of rigid triangles will be proposed and analysed in detail so as to assess its Poisson's ratio, compressibility and thermal expansion properties.

Following the above studies, this thesis will look at another aspect of mechanical metamaterials, namely the behaviour of mechanical metamaterials having their behaviour governed by magnetic interactions. In particular, mechanical metamaterials with magnetic inclusions will be studied through both theory and experiment in an attempt to show that the use of magnetic inclusions may enhance anomalous mechanical properties exhibited by the system as well as make it exhibit mechanical properties which would not be manifested without

the use of such inclusions. In particular, it will be shown that, at the macroscopic scale, it is possible to insert magnets / electromagnets into the mechanical metamaterials in order to make them exhibit a desired type of stiffness whose effect may be accompanied by other unusual mechanical properties related to the geometric design of the system. Using a theoretical model, it will be also shown that mechanical metamaterials with magnetic inclusions may exhibit novel physical phenomena which are not necessarily related to mechanical properties. More specifically, a hypothetical mechanical metamaterial with magnetic inclusions at the nanoscale will be used to examine how one may induce a magnetocaloric effect solely as a result of the mechanical deformation even though normally the presence of an external magnetic field would be necessary to observe this phenomenon. This is followed by an investigation on the rate of growth of magnetic domains in magneto-mechancial systems represented by the Ising model defined on the nonmagnetic mechanical system with magnetic inclusions and how this rate of growth depends on the rate at which the system is deformed.

4. Self-induced global rotation of mechanical metamaterials: Theory[1]

Highlights

- The concept of the self-induced global rotation of mechanical metamaterials is introduced;
- A model allowing to analyse the extent of the global rotation of the particular mechanical metamaterials, i.e. the rotating square system, is formulated and analysed;
- It is shown that extent of self-induced global rotation depends on the mass distribution and the number of units constituting the system;
- It is proposed and discussed that the mechanical deformation leading to the global rotation of the considered system could be induced upon incorporating magnetic inclusions into some of the units constituting the system.

4.1 Introduction

In the literature, there are several examples of systems which can induce their own global rotation as the result of the rotation of their components. One of the prime examples of this approach are spacecrafts where the attitude control (control over the orientation in space) is attained via the use of reaction wheels [415, 416]. Such reaction wheels can be described as rigid bodies having normally a cylindrical geometry which rotate in a particular direction in order to induce the rotation of the spacecraft in which they are located in the opposite direction

[1] The content of this chapter has already been published in the peer-reviewed journal AIP Advances: **K. K. Dudek**, R. Gatt, L. Mizzi, M. R. Dudek, D. Attard, J. N. Grima, Global rotation of mechanical metamaterials induced by their internal deformation *AIP Adv.* **7** 095121 (2017)

which effect can be explained by means of the angular momentum conservation principle. However, the fact that reaction wheels normally have a cylindrical geometry does not mean that one cannot consider the use of another geometry in order to observe a similar effect. In fact, it is even possible to consider the system analogous to the aforementioned reaction wheels which is not a rigid body. Such a system, apart from rotating as the result of the direct application of the torque to the structure by an external motor, may also induce its own global rotation via the rotation of its components.

A perfect candidate to design such a device is the use of mechanical metamaterials which are known to have a potential to deform via rotation of their subunits. As discussed in the previous chapters (Introduction and the Literature Review), over the years, mechanical metamaterials have been thoroughly investigated from the point of view of their potential to exhibit unusual thermo-mechanical behaviour with some of the most studied examples of such properties being negative Poisson's ratio, negative thermal expansion, negative compressibility and negative stiffness. In an attempt of designing mechanical metamaterials capable of exhibiting such properties, many separate directions of studies related to different classes of mechanical metamaterials have been commenced. These studies resulted in the rapid increase of the interest of scientists working in the field of materials science in these systems as well as provided a platform allowing to introduce some of the most interesting concepts reported in this field to different branches of the industry ranging from medicine to civil engineering. However, despite all of the progress made in the field of mechanical metamaterials there are still different aspects related to these systems which remain to be discovered. One such aspect is the effect which the rotation of subunits has on the global rotation of the whole system.

In view of this, in this chapter, the potential of mechanical metamaterials to induce their own global rotation was investigated for one of the most fundamental examples of such systems, i.e. the rotating square system. More specifically, in this chapter, the concept

corresponding to a potential of the rotating square system to induce its own global rotational motion is going to be discussed. This effect can be set into action through the use of magnetic inclusions. Another aspect which will be investigated is the effect which the number of subunits composing the structure and the mass distribution have on the extent of rotation of the whole system. This chapter also discusses how the novel concept reported here may lead to potentially new uses of mechanical metamaterials in applications such as telescopes employed in space and wind turbines.

4.2 Model

A model designed to induce and control its own rotational motion based on the two-dimensional rotating rigid squares mechanism will be presented in this section. This auxetic mechanism, which is one of the earliest systems studied with respect to its potential to exhibit a negative Poisson's ratio, consists of square units connected to each other at their corners through hinges (see Figure 4-1(a)). When the rotating squares structure is uniaxially stretched, the individual squares constituting the structure rotate relative to each other in order to attain a more open conformation, with every square rotating in the opposite direction to the one adjacent to it.

At this point, it is important to note that rigid units which in this work are referred to as squares, in reality represent cuboids connected in exactly the same manner as squares shown in Figure 4-1(a). This nomenclature is used in order not to confuse the discussed structure with the other well-known mechanical metamaterial which is often referred to as rotating cuboids system [303] which system corresponds to a completely different deformation mechanism.

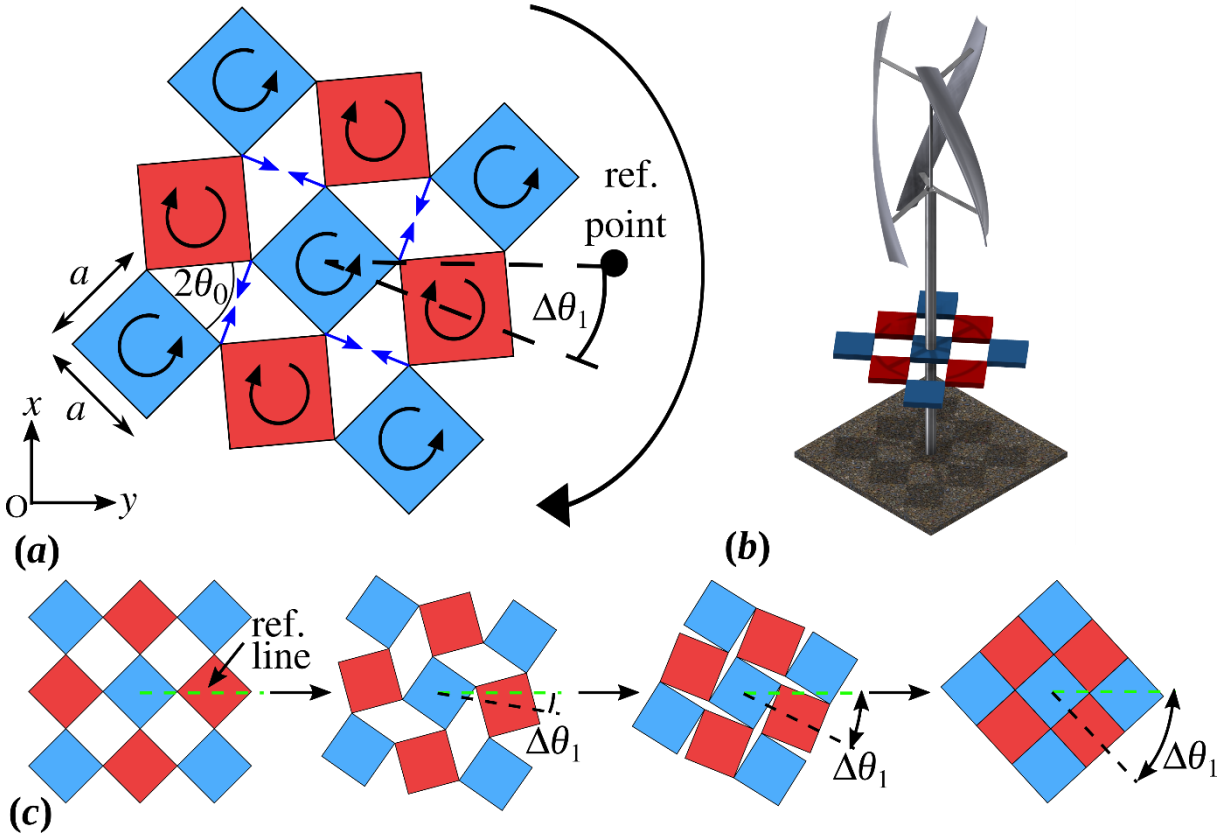

Figure 4-1 The panels show (a) the model of the discussed system with schematically drawn blue arrows indicating the positioning of linear actuators inducing a deformation of the system (black arrows indicate all types of rotations exhibited by the system), (b) a diagram presenting a possible connection of the discussed system with an external body, (c) diagrams depicting the concept of global rotation of the system in which the rotation of rigid units results with a decrease of the angle θ_0 and a change in the value of $\Delta\theta_1$. The change in the value of $\Delta\theta_1$ corresponds to the rotation of the structure with respect to its centre of mass.

In this chapter, a three-dimensional system whose cross-section may be described as a finite rotating rigid square system made up of $N_S \times N_S$ squares will be considered where the rigid units are connected at vertices acting as hinges. Deformation of the system is assumed to occur only through opening and closing of these hinges, with squares themselves remaining perfectly rigid. The cross-sectional dimensions of the rotating units, i.e. the lengths of their sides, are defined by the parameter *a*, while their thickness or depth is denoted by *z*. Consequently, their mass, *M*, may be defined in terms of these dimensions and the density of the rotating units, ρ, as: $M = \rho z a^2$.

It shall be assumed that a deformation which results in a relative rotation of respective rigid units in the way described above is achieved as a deformation induced internally within the structure, i.e. in a manner other than pulling of the system. This can be achieved, for example, *via* the use of a set of linear actuators embedded in a system in a way so that the opposite ends of diagonals of apertures formed between the adjacent units would be either brought closer or farther from each other (see Figure 4-1(a)). As a result of the action of such actuators (or some other alternative means to achieve the same net effect), the rigid units constituting the system will rotate. So as to avoid undue complexity, it will be further assumed that, throughout the process the rigid units are rotating with a constant angular acceleration ε_0 which results in a change in the angle between the adjacent units. This angle is denoted as $2\theta_0$ (see Figure 4-1(a)) which means that in terms of magnitude, all of the units rotate with the same angular velocity $\omega_0 = \frac{d\theta_0}{dt}$ which stems from the particular geometry of the system. It is also worth to note that the rigid units may rotate within the limits of geometric constraints of the system, i.e. as long as the condition $\theta_0 \in [0°, 90°]$ is satisfied. It should be also noted that it shall be assumed that the considered system is isolated which means that the effect of external forces on its behaviour will not be taken into consideration.

As mentioned above, it is assumed that the respective rigid units within the system rotate with an angular velocity changing accordingly with a constant angular acceleration. This process leads to the change in their angular momentum in time which results with a generation of a torque by each of the units. Since in a rotating square system each square rotates in the direction opposite to the one next to it, the net torque of a system made up of an even number of identical rotating units should be equal to zero, as the opposing rotations of the adjacent individual units comprising the system would cancel each other out. However, if N_S is an odd number, the number of squares rotating in one direction will be greater by one in comparison

to those rotating in the opposite direction. In view of this, systems considered in this work will only correspond to odd values of N_S as such systems have the potential to generate a larger overall torque than their even-numbered counterparts which would result with a greater extent of rotation. Another way of amplifying the net torque generated by the system corresponds to the differentiation of the mass of two sets of units rotating in the opposite directions, with squares in different sets being equally-sized but having a different density. The masses of these squares will be denoted by M_H and M_L respectively, where M_H and M_L correspond to units with larger (ρ_H) and lower density (ρ_L) respectively. The square at the centre of the system will always be assumed to have a mass of M_H and therefore the system will in all cases be made up of $\frac{N_S{}^2+1}{2}$ heavy rotating units and $\frac{N_S{}^2-1}{2}$ light rotating units. Furthermore, the extent of rotation of the whole system with respect to its centre of mass and an external global axis will be denoted by $\Delta\theta_1$, where initially the unrotated system has a θ_1 value of $0°$.

As it was mentioned above, the accelerated motion of respective heavy and light units results in a generation of the net torque τ_0 $\left(\tau_0 = \left|\overrightarrow{\tau_0}\right|\right)$, which quantity may be defined in the following manner:

$$\tau_0 = \frac{dL_H}{dt} - \frac{dL_L}{dt} + \frac{dL_{ob}}{dt} \qquad 4\text{-}1$$

where, L_H and L_L stand for a sum of angular momenta coming from all of the heavy and light units respectively. L_{ob} represents the magnitude of the angular momentum associated with an external body attached to the centre of the square located in the middle of the system (it is not related to L_H nor L_L). As shown in Figure 4-1, the centre of the square in the middle of the system also corresponds to the axis of rotation of the whole system. The third term in equation 4-1 has the same sign as the term corresponding to the rotation of heavy units, which stems

from the fact that the external body is attached to the heavy square. As a result, it must also rotate with the same angular velocity as heavy units which rotate with respect to their own centres (see Figure 4-1(a)). At this point, one should note that in the case when there is no external body attached to the system constituted by rigid squares, the last term in the above equation assumes the value of 0. Equation 4-1 may also be written down in a discrete form in terms of parameters corresponding to the mass distribution and geometry of the system [417].

Torque τ_0 contributes to the overall rotation of the system with respect to its centre of mass, which in turn is associated with the change in the angle θ_1. Taking all of this into consideration, an overall rotation of the discussed system, induced by the opening / closing of the rotating units, can be expressed through the rotational analog of Newton's equation of motion in the following manner:

$$-\tau_0 + \tau_{ext} = \frac{d}{dt}\left[\left(I_1 + I_{ob}\right)\frac{d\theta_1}{dt}\right] \qquad 4\text{-}2$$

where the negative sign in front of τ_0 arises due to Newton's third law for rotational motion as the magnitude of reaction torque has the same magnitude as torque τ_0 generated by individual units but the opposite orientation. Torque τ_{ext} is associated with any additional factors which may affect the overall rotational motion of the system, i.e. factors such as an additional motor located on the main axis of rotation which directly induces a rotation of the system, wind, air resistance etc. Assuming that there are not any additional factors contributing to the global rotation of the system, the term τ_{ext} would assume the value of 0. The moment of inertia I_1, corresponds to the rotation of all of the rigid units with respect to the centre of mass of the whole system and may be defined as follows (see Appendix I for the full derivation):

$$\begin{aligned} I_1 = {} & \frac{1}{12}a^2\left[\left(N_S{}^2 - 1\right)M_L + \left(N_S{}^2 + 1\right)M_H\right] + \\ & + \frac{1}{4}d^2\left(N_S{}^2 - 1\right)\left[\left(\frac{N_S{}^2}{3} - 1\right)M_L + \left(\frac{N_S{}^2}{3} + 1\right)M_H\right] \end{aligned} \qquad 4\text{-}3$$

where, d stands for the distance between centres of adjacent squares and can be expressed by means of the following equation: $d = \sqrt{2}a\sin\left(\frac{\pi}{4} + \theta_0\right)$.

From these expressions, it is possible to simulate the behaviour of such systems as a function of time by solving numerically the differential equation 4-2 as discussed below.

4.3 Simulation Details, Results and Discussion

In order to analyse the behaviour of the discussed system, equation 4-2 was solved numerically by means of the fourth-order Runge Kutta algorithm [418]. In this work, all of the results, summarised in Figure 4-2, were generated under the assumption that the auxetic system defined in the model section is being deformed from its fully-open to the fully-closed conformation, which corresponds to the change in the value of $2\theta_0$ from $90°$ to $0°$. These results clearly show that this phenomenon of the global rotation is indeed manifested by the systems considered in this study as evidenced by a nonzero value of $\Delta\theta_1$ which is being induced solely from a change in θ_0. Note that for the purpose of this work, it is being assumed that a system stops deforming when θ_0 reaches $0°$, i.e. it is being assumed that the rigid units are colliding in a fully inelastic manner.

The parameters used in order to generate these results, which were the same for all considered sets of results, were set to be the following: $\tau_{ext} = 0$ Nm, $a = 0.33$ m, $z = 0.02$ m, $\rho_H = 8000$ kg m^{-3}, $M_H = 17.78$ kg, $\rho_L = 2000$ kg m^{-3}, $M_L = 4.44$ kg, $I_{ob} = 0$ kg m^2, $\varepsilon_0 = -0.5$ rad s^{-2}, $\omega_0(t=0) = 0$ rad s^{-1}.

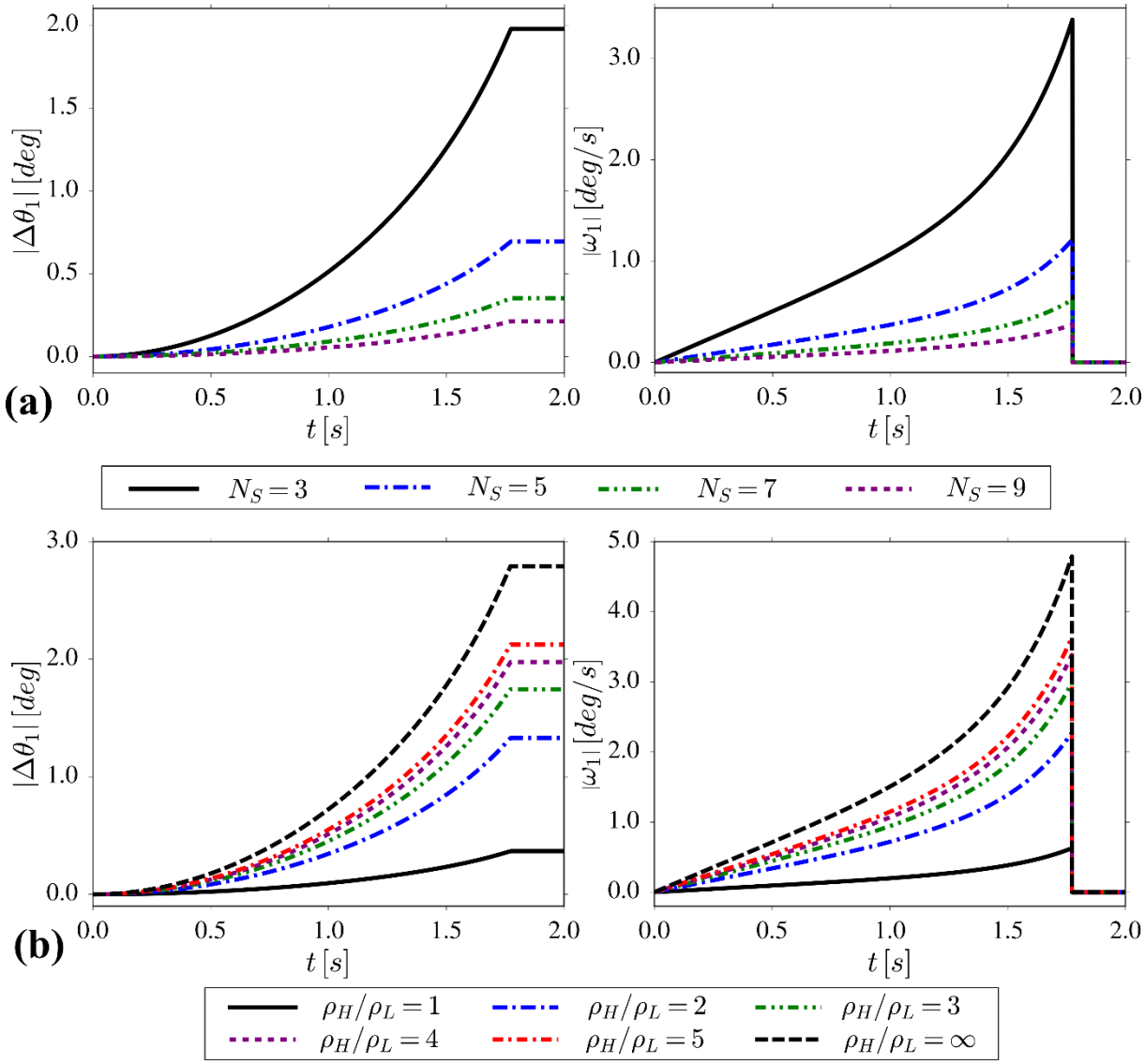

Figure 4-2 The panels show (a) comparison of the behaviour of systems consisting of a different number of rigid units and (b) the change in the behaviour of the system upon varying the magnitude of the ratio ρ_H/ρ_L associated with densities of heavy (ρ_H) and light (ρ_L) units for a system with a conserved mass. The point where the system stops exhibiting the global rotation, i.e. the values of $\Delta\theta_1$ do not change in time anymore, corresponds to the conformation of the system where $2\theta_0 = 0°$. In the case of the above graphs, *t* stands for the time corresponding to a deformation process.

Results shown in Figure 4-2(a) were generated in order to determine which value of N_S results with the maximum enhancement of the extent of rotation of the investigated system with respect to its centre of mass. In order to do that, the value of N_S was set to assume the respective values from the given set of odd numbers {3, 5, 7, 9} with the remaining parameters being set

to be the following: $a \in \{0.33, 0.20, 0.14, 0.11\}$ m, $\rho_H = 8000$ kg m^{-3}, $M_H = \{17.78, 6.40, 3.265, 1.975\}$ kg, $\rho_L = 2000$ kg m^{-3}, $M_L = \{4.44, 1.6, 0.816, 0.494\}$ kg. Note that the values of the length *a* where such that for all systems, all systems had the same area of 1m^2 when they were in their fully-closed conformation ($2\theta_0 = 0°$).

Furthermore, results shown in Figure 4-2(b) were generated in order to investigate a change in the behaviour of the system upon varying the magnitude of ρ_H / ρ_L ratio assuming that $N_S = 3$. In the case of all of the considered values of these ratios, the total mass of the system and dimensions of rigid units were kept constant. The remaining parameters used in order to generate these results were set as follows: $\rho_H / \rho_L \in \{1, 2, 3, 4, 5, \infty\}$, $\rho_H \in \{5333.33, 6857.14, 7578.95, 8000.0, 8275.86, 9600.0\}$ kg m^{-3}, $M_H \in \{11.852,\ 15.24,\ 16.84,\ 17.77,\ 18.39,\ 21.33\}$ kg, $\rho_L \in \{5333.33,\ 3428.57,\ 2526.32,\ 2000.0,\ 1655.17,\ 0.0\}$ kg m^{-3}, $M_L \in \{11.85, 7.62, 5.61, 4.44, 3.67, 0.0\}$ kg. Note that systems with sub-units having zero mass are obviously theoretical constructs as in reality, such units are not realisable.

As mentioned earlier, based on Figure 4-2, one may note that the rotation of respective rigid units may result with the global rotation of the whole system. Such behaviour is clearly manifested by nonzero values of $\Delta\theta_1$ and ω_1 on the graphs. This means that in order to induce the rotation of the system, there is no need for the external application of the force to the system which process would result with the generation of the torque. This stems from the fact that the torque contributing to the rotation of the system with respect to its centre of mass may be generated by the change in the angular velocity ω_0 of its constituents as explained in the model section.

Apart from the fact that the rotation of respective rigid units constituting the discussed system may result with its overall rotation, it is also interesting to consider an optimisation of

this effect. More specifically, it is interesting to check which parameters associated with the geometry and mass distribution within the system could enhance the extent of rotation of the investigated system.

As discussed previously in the model section, variation of the mass of the two sets of rotating units rotating in opposite directions also affects the torque experienced by the whole system when subjected to a linear deformation resulting in the rotation of the respective units. In Figure 4-2(b), results are shown for systems having the same total mass as well as a size and angular velocity of rigid units (associated with a constant value of ε_0), with different density ratios, ρ_H / ρ_L. It is evident from the plots that the larger the difference between the masses of the two sets of rotating units, the greater the extent of rotation of the system. However, while there is a large difference between plots of the angular velocity generated for systems where the ρ_H / ρ_L ratio is 1 and 2, the difference between systems corresponding to consecutive values of ρ_H / ρ_L decreases significantly, indicating that the effect of this parameter on the extent of rotation of the system tends to a constant for relatively large values. Another parameter that has a significant effect on the magnitude of the discussed effect, is the value of N_S. As shown in the plots in Figure 4-2(a), the maximum extent of rotation and the corresponding angular velocity were generated by the system with the smallest number of rotating units, i.e. $N_S = 3$. This is very convenient since it means that there is no need to design a structure with a large number of rotating units and hence, a large number of small actuators, which could make the system more prone to malfunctions and defects, in order to generate a large reaction torque.

At this point it is also important to highlight the fact that the discussed system may also influence the rate of rotation of the external system without being deformed, i.e. when the respective rigid units constituting the system are not rotating ($\omega_0 = 0$). This result, which is not normally observed in the case of other devices allowing to induce the rotation of the external

system such as reaction wheels, stems from the fact that even when the respective units stop rotating the new configuration of rotating squares varies from the initial one. This means that the whole system corresponds to a different moment of inertia. This in turn can make it either simpler or more difficult to rotate the system depending on the value of the moment of inertia.

All this is very significant, since these results show that the novel metamaterial-based device presented here, besides being an effective alternative method to attain the control over the rotation of the system, is also extremely versatile since it allows the fine-tuning of the extent of rotation of the system by varying a number of parameters. Moreover, the rotation of the entire system is induced through the application of tensile force on the sub-structure of the mechanical metamaterial rather than through a direct application of a torque to the rigid body. At this point it must be emphasized that the mathematical model presented in this work is merely one example of this new class of rotational motion controllers and in general one could use other mechanical metamaterials deforming via the rotation of its subunits [277, 320, 329].

Furthermore, it should be noted that although in this work it was tacitly assumed that the squares are made from a single material, it is possible to manufacture the structure in a manner where the added mass in the heavier units is imparted as a result of inclusions incorporated into such units. Whilst such inclusions could simply act as an entity to add weight, it is also possible to incorporate within the system more complex devices which may range from simple magnets to micro-electronic devices. Should one consider the use of inclusions being in the form of magnets or electromagnets, then apart from the obvious advantage of adding the extra mass to the system, one could also acquire the possibility of deforming the system as a result of interactions between such inclusions. For example, one can imagine the scenario where electromagnets having the identical orientation would be set at the centre of units corresponding to a larger mass while on the lighter units there would be no inclusions. Then as a result of their interactions, the distance between the adjacent inclusions would be either decreased or

increased which process corresponds to the mechanical deformation of the considered system. Also, as already discussed in this chapter, mechanical deformation of the system composed of units having a different mass which rotate in the opposite directions, leads to the global rotation of the entire system. Thus one can conclude that the use of magnetic inclusions could induce this effect in a controllable manner as the magnitude of interaction between the magnetic inclusions could be fine-tuned *via* the intensity of the current provided to respective electromagnets. It should be also noted that such a solution offers another advantage as it does not require the use of any additional devices which are not an integral part of the rigid units used to deform the structure.

Before concluding, it is important to highlight the potential applicability of these systems. As mentioned previously, the control over the rotational motion is one of the most important factors in attitude control (control over the orientation in space) of spacecraft. Moreover, these mechanical metamaterial-based systems could also be employed in concert with other systems to fine-tune the orientation of objects such as telescopes. Another potential use for these systems is in wind turbines (see Figure 4-1(b)). The efficacy of wind turbines for the production of energy depends strongly on the angular velocity of the system, with maximum efficiency being achieved if the optimal angular velocity is maintained at all times. However, in reality, shifting wind currents make this extremely difficult, and thus the discussed device could be implemented within the turbine in a manner such as that shown in Figure 4-1(b) in order to increase / decrease the moment of inertia depending on the strength of wind. This in turn would make it significantly simpler for rotating blades to maintain a particular value of the angular velocity of the wind turbine. Obviously there are still a number of additional aspects which should be considered prior to the practical large-scale implementation of the concept of the self-induced global rotation of mechanical metamaterials in industry. Amongst other things, it is essential to confirm experimentally that this phenomenon may indeed be observed in reality.

Also, since in this chapter the concept was developed only for rotating squares, it would be beneficial to assess whether other geometries may be more amenable to induce global rotation. These aspects will be discussed in the following chapters.

4.4 Conclusions

In this chapter, the novel concept corresponding to the global rotation of mechanical metamaterials induced by the rotation of their subunits was proposed. In order to investigate this effect, the theoretical model associated with a particular system, i.e. the rotating square system, was introduced. Through this model, it was confirmed that the phenomenon of the global rotation induced solely via a rotation of the subunits in the system is indeed being manifested and that the extent of the global rotation of the system depends on parameters associated with its mass distribution and geometry thus making it possible to fine-tune the extent of the discussed phenomenon. It was also shown that the concept proposed here may be employed in a number of practical applications. In particular, in this chapter the possibility of controlling the magnitude of the angular velocity of the external system such as a wind turbine upon changing the moment of inertia of the discussed structure which would be connected to the external body was discussed. All of these results suggest that the concept reported in this chapter might prove to be important in the case of potential applications such as telescopes employed in space and wind turbines where the control over the rotational motion is known to be of great significance.

5. Self-induced global rotation of mechanical metamaterials: Experimental verification of the concept[2]

HIGHLIGHT

- The theoretical concept corresponding to the possibility of inducing the global rotation of mechanical metamaterials solely as a result of the rotation of their subunits was confirmed using an experimental prototype corresponding to the rotating square system.

5.1 Introduction

In the previous chapter, the novel concept corresponding to the induction of the global rotation of mechanical metamaterials solely as a result of the rotation of their subunits was proposed. This concept was investigated through a theoretical model for the particular case of the rotating square system. In Chapter 4, it was also discussed that this concept may potentially prove to be useful in the case of applications such as wind turbines and spacecraft where the control over the rotational motion is very important. However, before attempting to optimise the system so as to maximise global rotation as a result of internal rotations, it would be useful to first experimentally verify whether the discussed effect can indeed be observed in reality. In view of this, in this chapter, the semi-qualitative results corresponding to the experimental prototype of the device analogous to the rotating square system discussed in the last chapter are going to be presented.

[2] The content of this chapter has been published in the peer-reviewd journal *Smart Materials and Structures*:
K. K. Dudek, K. W. Wojciechowski, M. R. Dudek, R. Gatt, L. Mizzi, J. N. Grima, Potential of mechanical metamaterials to induce their own global rotational motion *Smart Mater. Struct.* (2018) DOI: 10.1088/1361-665X/aabbf6

5.2 Experimental Model

5.2.1 General description

The prototype shown in Figure 5-1 was constructed in order to experimentally confirm the potential of mechanical metamaterials to induce their own rotational motion as the result of the rotation of their subunits. The considered system corresponds to the rotating square system composed of two different types of equally-sized square units having the linear dimension *a*, where in this case $a = 7$ cm. The entire structure consists of 3×3 such units which can rotate with respect to their centres which process corresponds to the deformation of the whole system. The out of plane thickness *z* of each of the units was the same and was approximately equal to 2 cm. The respective unis were produced by means of the 3D extrusion printer (equipped with ABS plastic) and connected to each other by means of cylindrical hinges which were supposed to ensure that the system would not buckle out-of-plane.

Figure 5-1 The experimental prototype used in order to investigate the potential of mechanical metamaterials to induce their own rotational motion as the result of the rotation of their subunits.

As discussed in the last chapter, it is possible to enhance the extent of the global rotation of the system upon increasing the mass of one class of units rotating in a specific direction with respect to remaining units rotating in the opposite directions. In view of this, in the case of the considered prototype, 5 units corresponding to the blue colour on Figure 5-1 were made heavier than the remaining four units associated with the red colour. More specifically, the mass of the heavy (M_H) and light (M_L) units was estimated to be in the vicinity of 121 g and 37 g respectively. In order to differentiate the mass of these two types of units, metal discs were inserted into the units corresponding to the mass M_H. These discs had an outer and inner diameter equal to approximately 4 cm and 9 mm respectively. This means that the mass distribution within the units constituting the discussed system was not uniform. It should be also highlighted that metal discs inserted into the aforementioned units were oriented in a way so that their faces were parallel to the base of each of the units and their centres corresponded to centres of units. This means that the axis of symmetry associated with the discussed units was not only passing through their geometric centres but it was also passing through their centre of mass. It should be also mentioned that as shown in Figure 5-1, the angle of aperture between adjacent rigid units was denoted as $2\theta_0$.

The discussed system was set on a bearing passing through the centre of mass of the entire system which in the case of this particular prototype was associated with the geometric centre of the heavy unit located in the middle of the structure. As a result, the entire system was free to rotate only with respect to its centre of mass which behaviour should be expected if one were to consider employment of such a system in space where the effect of external forces on its behaviour would be negligible.

5.2.2 Technique used in order to induce the deformation

As discussed in the previous chapter, in order to analyse the discussed phenomenon, a key aspect which need to be ensured is that the deformation of the discussed system should be solely as a result of internal rotations of the subunits i.e. the deformation must be induced internally within the structure. Ideally, such effect should be achieved through a mechanism where the action on the system can be applied in a repeatable and quantifiable manner for example through the use of actuators located appropriately within the system, or as discussed in the previous chapter through the use of electromagnetic inclusions. However, it is beyond the scope of this work to use such complex devices to induce the deformation when the same effect can be induced, albeit not in a fully-repeatable nor quantifiable manner, in a much simpler manner. In this particular case, in order to induce the deformation of the considered experimental prototype, rubber bands were attached to opposite vertices in one of the apertures within the structure (see Figure 5-1). The particular positioning of rubber bands results in the situation where the change in their extension leads to the rotation of respective rigid units constituting the system which as discussed in the last chapter, would be expected to lead to the global rotation of the system which stems from the conservation of the angular momentum principle. In order to release the system, the thread which was holding the system at rest (as it prevents vertices from moving further apart under the influence of the force applied by rubber bands) at the initial configuration corresponding to $2\theta_0 = 134.1° \pm 1.7°$ was being burned. At this point, it should be noted that as opposed to any other approach involving the use of the external body to hold the structure at the initial conformation, this particular technique allowing to release the system ensures that there is no external interference which could affect the investigated phenomenon. Furthermore, it should be mentioned that in the case of the considered prototype, upon releasing the system, the respective units start rotating up to the moment when the system

assumes the configuration associated with the angle $2\theta_0 = 22.3° \pm 1.6°$ at which point the units composing the structure collide.

5.2.3 Technique used in order to calculate the extent of the global rotation of the system

In order to analyse the behaviour of the prototype discussed in this work, the motion of the system was recorded by means of the camera capable of recording 240 frames per second. Such a large number of recorded frames in each second was required in order to ensure that all stages of the deformation could be analysed. Of particular importance was here the possibility of attaining the information about the configuration assumed by the system at the moment when the structure was released and when the rigid units collided for the first time respectively. This stems from the fact that pictures extracted from the recorded video which corresponded to these two particular stages of the deformation were used in order to calculate the total extent of the global rotation of the discussed system, i.e. $\Delta\theta_1$.

As mentioned in the above paragraph, two particular pictures were selected for a given experiment in order to calculate the extent of the global rotation exhibited by the considered experimental prototype. For each of those pictures, a number of easily distinguishable points such as centres of hinges or centres of rigid units were selected in order to check their coordinates by means of the appropriate graphical software (in the case of this work Inkscape™ [483]). Based on such coordinates, it was possible to define vectors describing the global orientation of the system. Subsequently, upon using vectors associated with the same two points within the structure at the different stage of the deformation, it was possible to calculate the angle between such vectors by means of the sine rule. At this point, it should be noted that in the case of pictures corresponding to the two aforementioned stages of the deformation, such angle between vectors could be interpreted as $\left|\Delta\theta_1\right|$. Furthermore, in order to determine the

extent of the global rotation exhibited by the system, the experiment was repeated ten times where each time the structure was released from approximately the same initial configuration corresponding to $2\theta_0 = 134.1° \pm 1.7°$. For each experiment, the above procedure corresponding to the measurement of $|\Delta\theta_1|$ was repeated 3-4 times for different pairs of points. This number was not exactly the same for all of the conducted experiments as some of the points on analysed pictures were too blurred to obtain a reliable reading.

5.3 Results and Discussion

A representative sample of the images recorded in the experiment are shown in Figure 5-2 where one can clearly observe that the system is indeed globally rotating as the internal components rotate thus confirming the potential of mechanical metamaterials to induce their global rotation as the result of the rotation of their subunits, which effect was predicted from theoretical studies presented in the previous chapter.

In fact, as shown in Figure 5-2(a), upon releasing the system, the respective units start rotating which process corresponds to the decrease in the value of $2\theta_0$. More specifically, heavy units rotate in the anticlockwise direction while light units rotate in the clockwise direction which behaviour is continued up to the moment when units collide. It is important to note that as individual units start rotating, the entire system starts rotating with respect to its centre of mass. Moreover, as expected based on theoretical predictions which are primarily based on the conservation of the angular momentum principle, the system rotates in the clockwise direction which is an opposite direction of rotation to that exhibited by heavy units.

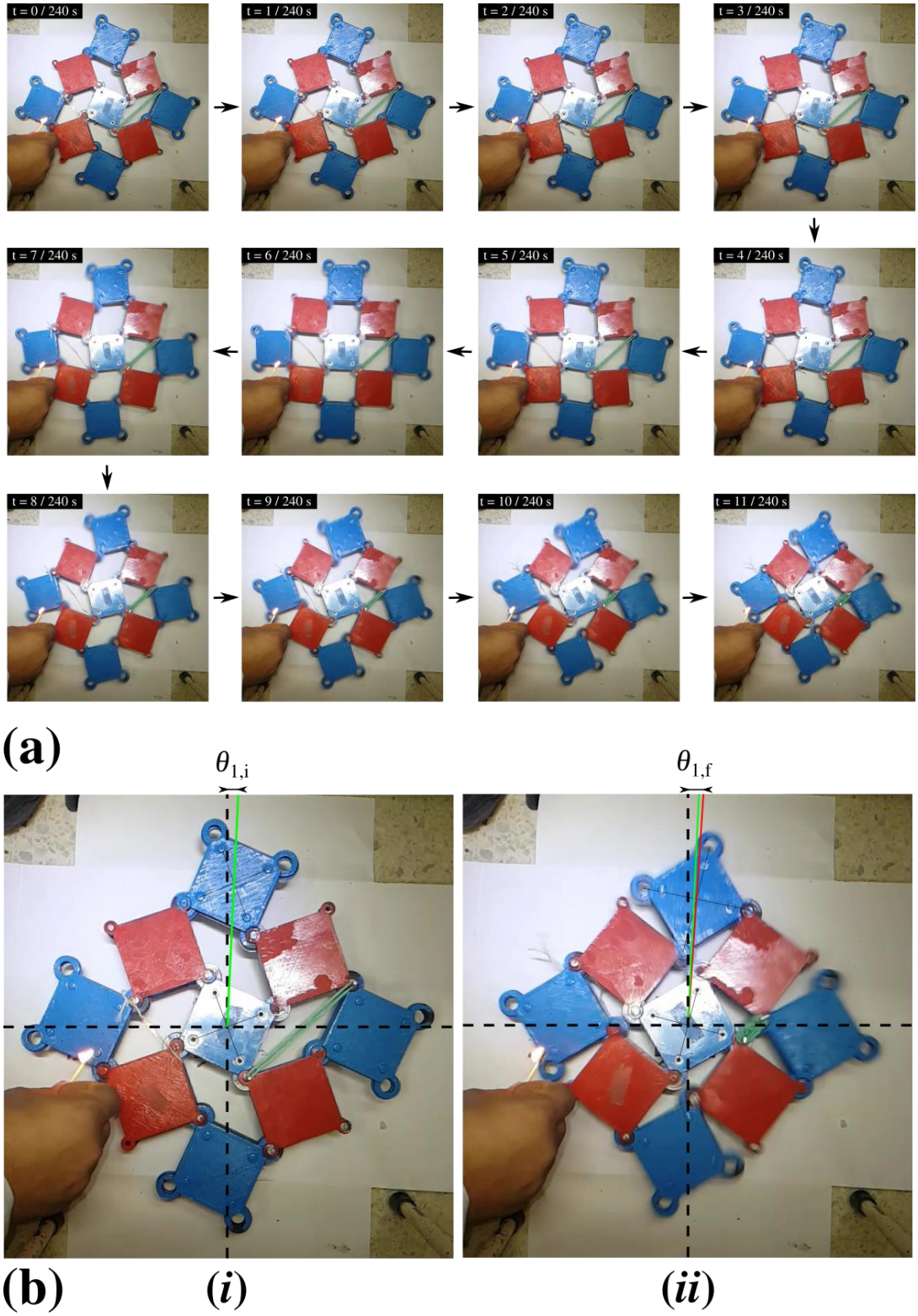

Figure 5-2 Panels show: (a) the evolution of the system in time from the moment when it was released to the moment when the rigid units collided for the first time and (b) pictures corresponding to (i) the initial configuration assumed by the system and (ii) the configuration assumed by the system at the moment when rigid units collided for the first time. In the case of panel (b), the auxiliary lines indicating the orientation of the system connect two particular points within the structure at different stages of the deformation.

As discussed in the Experimental Model section, the extent of the global rotation exhibited by the system may be calculated based on the configuration assumed by the system at two different stages of the deformation, i.e. at the moment when the system was released and when rigid units collided for the first time. An example of such configurations can be seen in Figure 5-2(b) where in order to better visualise the concept of the change in the orientation of the system, two auxiliary lines connecting the same two points within the structure were drawn for the considered stages of deformation. In the case of this work, such extent of the global rotation corresponding to $|\Delta\theta_1|$ was approximately equal to $0.97° \pm 0.24°$.

One should also highlight the fact that as discussed in the Experimental Model section, this experiment was repeated ten times where apart from rotating each time in the same direction, which is in agreement with theoretical predictions, the considered system exhibited the rotation of the very similar magnitude in the case of all of the conducted experiments thus giving more credibility to the obtained results.

As discussed in this and in the former chapter, due to the conservation of the angular momentum, the discussed system may induce its own global rotational motion as long as individual units are rotating. Assuming that before the process of deformation the entire system was at rest, this means had the collisions been perfectly inelastic (as it was assumed in the previous chapter), once the rigid units reach the locked configuration where they cannot rotate any further, the whole system would stop rotating as well. However, in reality very few collisions may be considered as perfectly inelastic in which case at the moment when units collide all of the kinetic energy would have to be converted into other types of energy such as heat etc. In view of this, in the case of the experimental prototype considered in this chapter, as the result of the elastic collision, the respective rigid units are expected to start rotating in the opposite direction to the direction in which they were rotating before the collision. Such recoil

effect could be prevented should one for example consider the use of appropriately located electromagnets preventing the structure from reopening. However, in the case of the discussed experiment, there is no mechanism preventing such behaviour other than rubber bands. In view of this, as may be seen in Figure 5-3 and Figure 5-4, after the initial collision, the structure starts reopening which process corresponds to the increase in the value of $2\theta_0$. In theory, if one were to consider a hypothetical system where there is no loss of the energy as the units collide and no friction, then after the collision the units would be expected to rotate backwards up to the moment when the system would assume the initial configuration. As a result, the entire system would act as the harmonic oscillator. Nonetheless, in the considered experiment, both friction and loss of the energy are not negligible which results in the system reopening to the smaller extent than the initial configuration after which point the units are brought back by the rubber bands to the locked conformation. As can be seen based on Figure 5-3 and Figure 5-4, such recoil effect occurred once more after the initial collision although the loss of the energy was so large that the extent of rotation of respective units can be assumed to be negligible. It should be also noted that at the end of such process the system remains at rest at the configuration which approximately corresponds to the minimum value of $2\theta_0$.

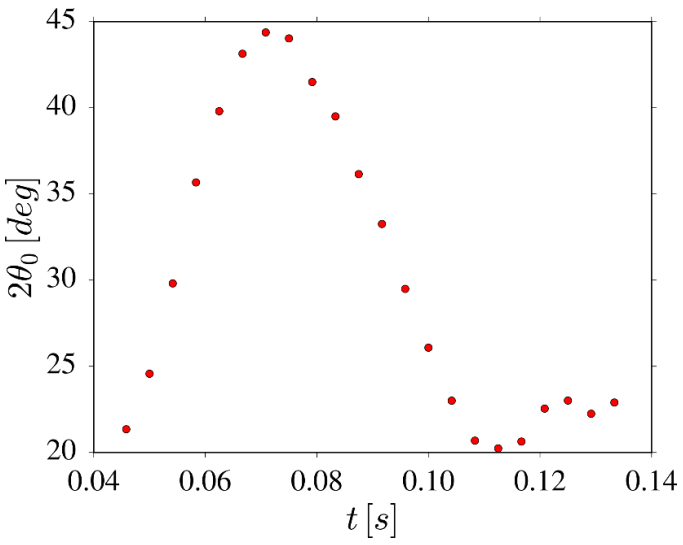

Figure 5-3 The variation in the angle $2\theta_0$ corresponding to the behaviour of of the system after the first collision between the rigid units.

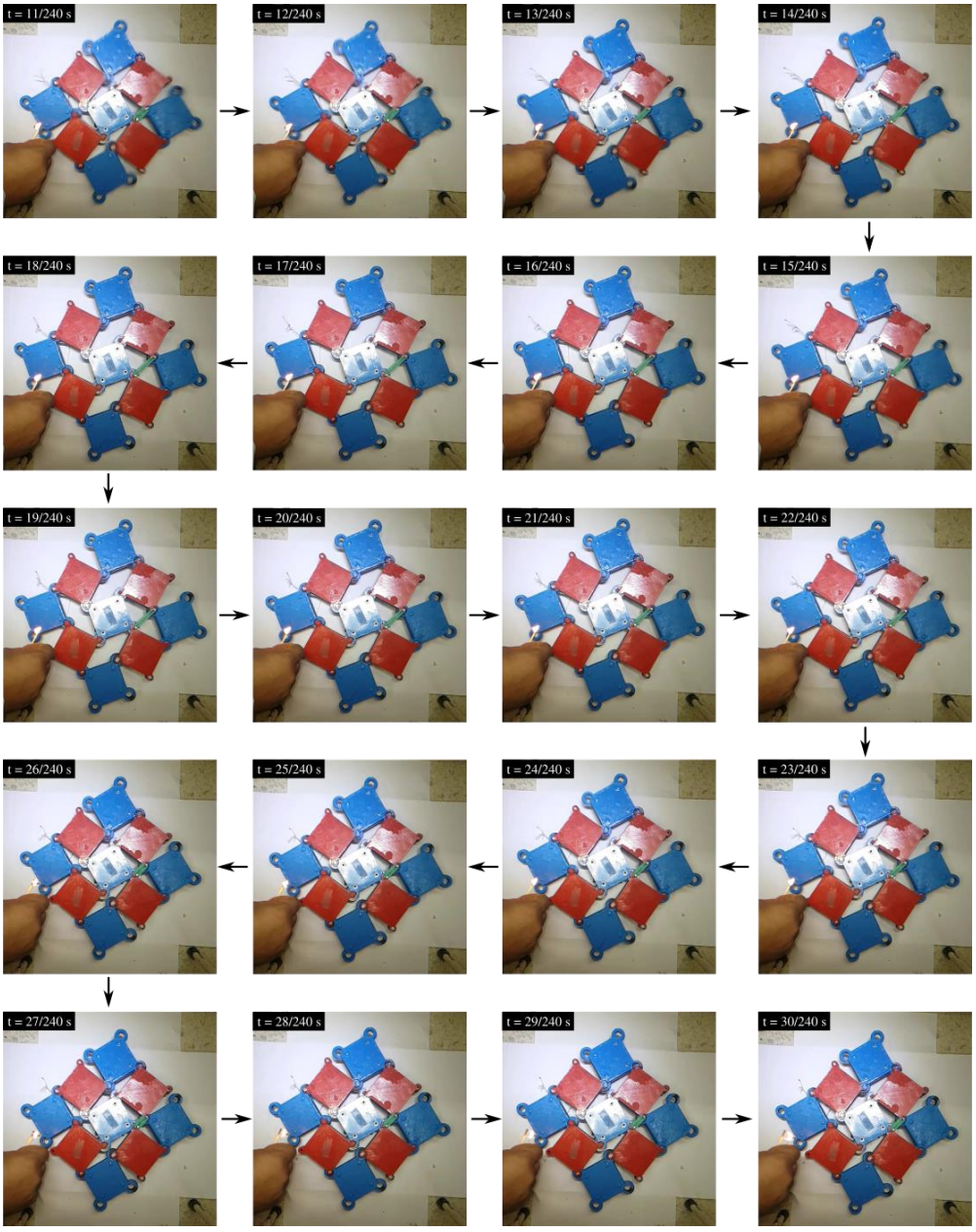

Figure 5-4 Behaviour of the system after the first collision between the rigid units.

Before concluding, it should be highlighted that all of the results reported in this chapter confirm theoretical predictions corresponding to the potential of mechanical metamaterials to induce their own rotational motion as the result of the rotation of their subunits. These results also indicate which type of the behaviour should be expected upon constructing the device meant to utilise this concept in reality. This in turn could encourage scientists to implement this concept in the case of applications such as wind turbines, telescopes employed in space etc. where the control over the rotational motion is of great importance. It should also be noted that

up to now, only a particular type of the mechanical metamaterial system, i.e. the rotating square system, was investigated from the point of view of its propensity to exhibit the discussed characteristic. However, this does not mean that it is the most suitable geometry to induce the global rotation of mechanical metamaterials. In view of this, before potentially considering the implementation of the discussed concept in the case of applications such as telescopes employed in space or wind turbines, it should be analysed whether there are other geometries which are more conducive to the discussed phenomenon.

5.4 Conclusions

In this chapter, the theoretical concept proposed in the last chapter corresponding to the potential of mechanical metamaterials to induce their own global rotational motion was confirmed experimentally. More specifically, through the use of the experimental prototype of the rotating square system composed of two different types of units, it was shown that as a result of the rotation of individual units constituting the system, the entire structure rotates in the direction opposite to the direction of rotation of heavy units. This in turn confirms theoretical predictions made for this system in the previous chapter. It was also discussed what type of behaviour of the system should be expected in the case of real life experimental realisations of the considered concept. One may note that such observations may help to assess the suitability of different prototypes utilising the considered concept in the case of specific applications.

6. Self-induced global rotation of mechanical metamaterials: different geometries[3]

HIGHLIGHTS

- A more generic version of the model proposed in the former chapters is presented where different rotating rectangular systems are analysed in order to assess their propensity to exhibit self-induced global rotation;
- It is shown that the use of rectangles permits control of the extent of the observed phenomenon where, for certain types of connectivity between rigid units of rotating rectangle systems, the variation in the aspect ratio of rigid rectangles constituting the system significantly affects the extent of the global rotation, whilst, for the other types of connectivity, the analogical change in the geometry of the rigid units does not affect the behaviour of the system;
- It is proposed that hypothetically one may design hinges of the rotating rigid unit system, possibly using electromagnets, in a way so that the considered phenomenon of the self-induced global rotation could be maintained after the point where upon reaching the final configuration the respective rigid units collide with each other.

6.1 Introduction

In the last two chapters, the novel concept corresponding to the potential of mechanical metamaterials to induce their own rotational motion solely as a result of the rotation of their subunits was proposed and studied through a theoretical model and experiment though the specific example of the rotating squares system. However, as noted earlier, whilst this was

[3] The content of this chapter has been published in the peer-reviewd journal *Smart Materials and Structures*:
K. K. Dudek, K. W. Wojciechowski, M. R. Dudek, R. Gatt, L. Mizzi, J. N. Grima, Potential of mechanical metamaterials to induce their own global rotational motion Smart Mater. Struct. (2018)

sufficient to prove the idea that rotating rigid unit mechanical metamaterials are suitable candidates to induce the global rotation as a result of its internal deformation, the particular geometry studies may not necessarily be the most suitable system to exhibit the discussed effect. In view of this, it would be interesting to analyse the propensity of different mechanical metamaterials to induce their own rotational motion in an attempt of determining the system which could exhibit the largest extent of rotation as it could enhance the efficiency of devices based on this concept in the case of potential applications.

Based on very promising results associated with systems composed of rigid squares, the natural candidate to further investigate the potential of mechanical metamaterials to induce their own rotational motion are rotating rigid rectangle systems. Structures composed of rectangular units not only allow for a simple comparison of the obtained results with those associated with squares but also offer a wide range of different geometric shapes which they can assume. This stems from the fact that the particular geometric configuration which can be assumed by these systems does not only depend on the aspect ratio of respective units, but as discussed in the Literature Review, it also depends on the connectivity between adjacent units. In view of this, in this chapter, the potential of different rotating rigid rectangle mechanical metamaterials to induce their global rotation as a result of the rotation of their subunits is going to be discussed in an attempt to generalise the work present in the earlier chapters.

6.2 Model

6.2.1 Considered systems

In this work, the systems which were chosen in order to evaluate their suitability to induce their own global rotation may be described as finite fragments from periodic rotating rigid rectangles [286, 287]. As discussed in [287], depending on the manner how the different rectangular units are connected, such systems, may be classified as either Type I or Type II (see

Figure 6-1(a) and Figure 6-1(b) respectively), where as illustrated in Figure 6-1, the symmetry is different as a result of the different types of pores present. More specifically, in Type I rotating rectangle system, there are always two types of pores assuming the shape of the rhombus having linear dimensions equal either to l_a or l_b where different pores assume alternate positions within the system. On the other hand, in the case of Type II rotating rectangle system, there is always only one type of pore which has the same linear dimensions as rectangles constituting the system, i.e. two sides having a length of l_a and l_b respectively. Despite the fact that in terms of geometry both systems consist of identical rigid units, the difference in the shape of pores of both of the considered systems leads to a very different deformation pattern of the entire structure. This in turn, results in a very different profile of mechanical properties with different Poisson's ratios. In fact, although both systems have the potential of exhibiting negative Poisson's ratios, the system characterised as Type II exhibits isotropic Poisson's ratio of -1 irrespective of the shape of the rectangles or the angles between them whilst in the case of the Type I system, the Poisson's ratio, which can be negative or positive, is anisotropic and dependent on both the shape of the rectangles and their relative orientation.

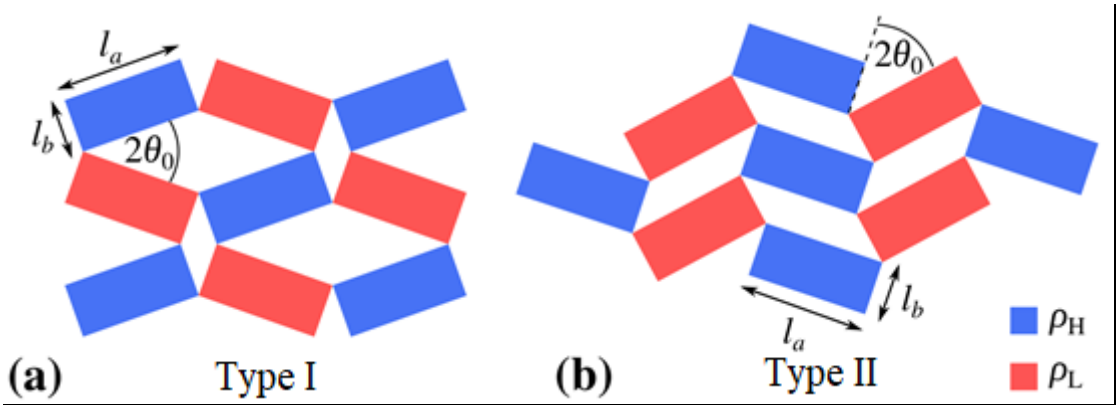

Figure 6-1 Panels show: (a) Type I and (b) Type II rotating rectangles systems investigated in this Chapter. Red and blue colours correspond to different densities of units rotating in the opposite directions in the case of each of the structures. Note that these systems have different symmetries and profile of pores which result from the different manner how the rectangles are connected together to form the network. In particular, in the Type I four $l_a \times l_b$ rectangles are connected in such a way that the empty spaces between the rectangles form rhombi of size $l_a \times l_a$ and $l_b \times l_b$ whilst the Type II network has parrallelogramic pores of the same size $l_a \times l_b$.

As shown in Figure 6-1, linear dimensions of rectangular units constituting both types of considered systems are denoted as l_a and l_b. The angle of aperture between adjacent rigid units is denoted as $2\theta_0$. Furthermore, similarly to the assumptions made in Chapter 4, it is assumed that the structure can deform only via the respective rotation of rigid units, during which process, dimensions of rectangular units remain constant. It should be also noted that such process of deformation corresponds to the change in the value of θ_0. Due to the particular geometry of considered systems, both in the case of Type I and Type II system, $2\theta_0$ may assume any value from the range $[0°,180°]$, where the minimum and the maximum value from this interval correspond to the geometric lockage of the structure at which point rigid units cannot rotate any further as they are touching their neighbours. It is also assumed that, as shown in Figure 6-1, both of the considered systems consist of 3×3 rigid units as such a system offers a number of practical advantages as discussed below.

In the case of rigid unit systems considered in this Chapter, rigid units may rotate in the clockwise or anticlockwise direction depending on their position within the system. As in the case of the rotating squares (see Chapter 4), a net torque resulting in a global rotation would arise if there is a difference in the magnitude of torques associated with both of these groups of rigid units. Such a difference in torque would arise if the total mass of the units which rotate in the clockwise direction is different from the total mass of the units rotating in the anticlockwise direction, or vice versa. This difference in mass may be brought about by using an odd number of equally heavy sub-units, or through the use of sub-units which would have the same in-plane size so as to fulfil the required geometric constraints for connectivity, but have different masses which could be brought about by using a different amount of material to manufacture the sub-units and/or using materials of different densities. In this present Chapter, it shall be assumed that all of the units are equally-sized and have a continuous mass distribution, where, in an

attempt to enhance the extent of the global rotation of the system, the five units rotating in a specific direction are made to be heavier than the other four remaining units rotating in the opposite direction by setting ρ_H, the density of the heavier units (shown in blue in Figure 6-1) to be larger than ρ_L, the density of the four lighter units (shown in red in Figure 6-1). Although in theory, there is no restriction on the materials that one may use to construct such systems, in this work, in order to make a reliable comparison of the potential of all of the discussed systems to induce their own rotational motion, it was assumed that the total mass *M* of all of the systems is the same and may be defined as follows: $M = \left(5\rho_H + 4\rho_L\right) l_a l_b l_z$, where l_z is the out-of-plane thickness of the system. It is also worth to note, that in the case of such systems, the centre of mass of the given structure always corresponds to the centre of the unit located in the middle of the system, which in this case is one of the heavier units (shown in blue). As before, it should also be noted that for both of the systems, the centre of mass of the whole structure corresponds to the centre of the heavy unit located in the middle of the system.

As discussed in Chapter 4, upon comparing structures having exactly the same size for a locked conformation $\left(\theta_0 = 0°\right)$ and being constructed by means of the same two types of materials corresponding to units rotating in the opposite directions, systems composed of 3×3 units are the most suitable to induce their own global rotation as a result of the rotation of their subunits. This stems from the fact that for such systems, heavy units constitute the largest possible percentage of the area of the entire system. One may note that upon increasing the number of units constituting such $N \times N$ lattices, the ratio of the area associated with heavy and light units would start approaching the value of 1/2. However, for $N = 3$, such ratio is equal to 5/9. Note that as discussed in Chapter 4, the aforementioned variation in weight can be achieved by having magnetic inclusions, in which case the aspects discussed in Chapter 4 also apply here.

6.2.2 Motion exhibited by the system

As it was discussed in Chapter 4, in order to investigate the potential of discussed systems to induce their global rotational motion with respect to the centre of mass as a result of the rotation of their subunits, it is assumed that they deform in the following manner:

- The system which is initially at rest is being deformed from the initial to the final configuration associated with $2\theta_0$ equal to $0°$ and $180°$ respectively;
- In terms of magnitude, all of the rigid units rotate at a given time with the same angular velocity ω_0 $\left(\omega_0 = |\vec{\omega}_0|\right)$ which condition stems from the geometry;
- It is assumed that in terms of magnitude, all of the rigid units constituting the system rotate with a constant angular acceleration ε_0 $\left(\varepsilon_0 = |\vec{\varepsilon}_0|\right)$;
- It is assumed that upon reaching the final configuration, irrespective of the type of the system and the mass of rigid units, the rigid units do not rotate backwards as a result of the collision, i.e. inelastic collision is assumed. It should also be noted, that in this chapter, the potential effect of the elastic collision between rigid units on the behaviour of the system is not taken into consideration. Hypothetically, one could achieve a similar effect through the use of magnets located on neighbouring rigid units which would prevent them from reopening after the collision;
- It is assumed that considered systems are isolated.

According to the above assumptions, all of the rigid units within the system rotate with a constant angular acceleration which means that in time they experience a change in the angular momentum which leads to the generation of the torque by each of the units. Thus, the net torque $\vec{\tau}_0$ associated with the rotation of all of the units within the system may be calculated as follows:

$$\vec{\tau}_0 = \frac{d\vec{L}_H}{dt} + \frac{d\vec{L}_L}{dt} \qquad 6\text{-}1$$

where, $\vec{L}_H$ ($\vec{L}_H = 5I_H\vec{\omega}_0$) and $\vec{L}_L$ ($\vec{L}_L = 4I_L\vec{\omega}_0$) stand for a sum of the angular momenta associated with all of the heavy and light units respectively (all of the angular momenta were calculated with respect to the centre of mass of the entire system). At this point, it should also be noted that due to a particular geometry of considered systems, the angular momentum of respective units depends solely on the angular velocity associated with the rotation of rigid units with respect to their centres and does not depend on their linear velocity (see Appendix I). One should also note that in general, one may design a variety of systems where the angular momentum associated with linear velocity of individual units would make a non-zero contribution to the net angular momentum corresponding to all of the subunits.

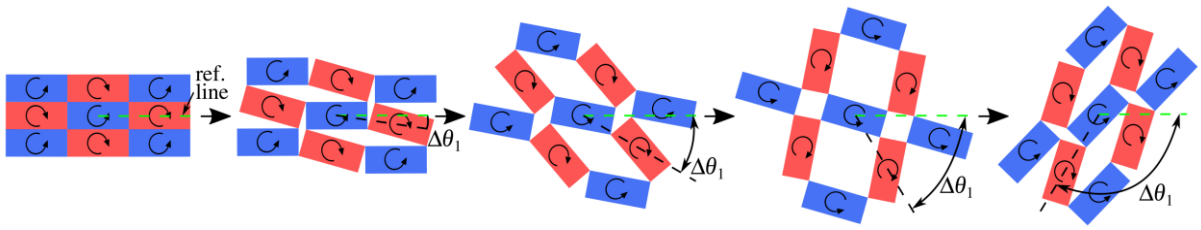

Figure 6-2 A diagram presenting the concept of the global rotation of the Type I rotating rectangle system induced by the rotation of its subunits.

As shown schematically in Figure 6-2, the resultant non-zero torque $\vec{\tau}_0$ associated with the rotation of individual units contributes to the rotation of the whole system with respect to its centre of mass as a result of the conservation of angular momentum principle. Similarly to the notation introduced in the preceding chapters, it is assumed that the extent of such global rotation corresponds to the change in the angle θ_1, which means that the extent of the global rotation can be denoted as $\Delta\theta_1$. In view of this, in order to investigate the rotation of the whole system with respect to its centre of mass, it is sufficient to solve the following equation of motion:

$$-\vec{\tau}_0 = \frac{d}{dt}\left[I_1 \frac{d\theta_1}{dt} \right] \qquad 6\text{-}2$$

where, I_1 stands for the moment of inertia associated with the rotation of the whole system with respect to its centre of mass. One should note that this quantity changes as the structure deforms, i.e. when the value of $2\theta_0$ is being changed. On the other hand, $\frac{d\theta_1}{dt}$ corresponds to the angular velocity associated with the rotation of the system with respect to its centre of mass (for the sake of the simplicity $\frac{d\theta_1}{dt}$ will be also referred to as ω_1). The negative sign on the left hand side of equation 6-2 is associated with the third Newton's law of motion. More specifically, the net torque $\vec{\tau}_0$ being the result of the rotation of respective units induces the rotation of the whole system through the application of a torque having the same magnitude as $\vec{\tau}_0$ but the opposite orientation.

6.2.3 Parameters

In order to analyse the propensity of considered systems to exhibit the discussed phenomenon, the respective parameters were set to be the following: $\rho_H = 8000\ \mathrm{kg\,m^{-3}}$, $\rho_L = 2000\ \mathrm{kg\,m^{-3}}$, l_a ={0.316, 0.707, 1.0, 3.162} m, l_b={0.316, 0.141, 0.1, 0.032} m, l_z=0.02 m and $\varepsilon = 400\ \mathrm{rad\,s^{-1}}$. Furthermore, in the case of each of the considered systems, equation 6-2 which describes the rotational motion of the whole system with respect to its centre of mass was solved numerically by means of the classical fourth-order Runge-Kutta method [418] where the time step was constant throughout the entire simulation and was set to be equal to 2×10^{-8} s.

6.3 Results and Discussion

The results of the calculations for the type I and type II rotating rectangles systems are summarised in Figure 6-3 which shows plots (against time) of (a-b) the angle of aperture $2\theta_0$ and (c-d) the extent of global rotation, $\Delta\theta_1$. These plots clearly show that all of the systems are capable of inducing their own global rotation the extent of which, for the Type I systems but not the Type II, can be fine-tuned by changing the aspect ratios of the rectangles.

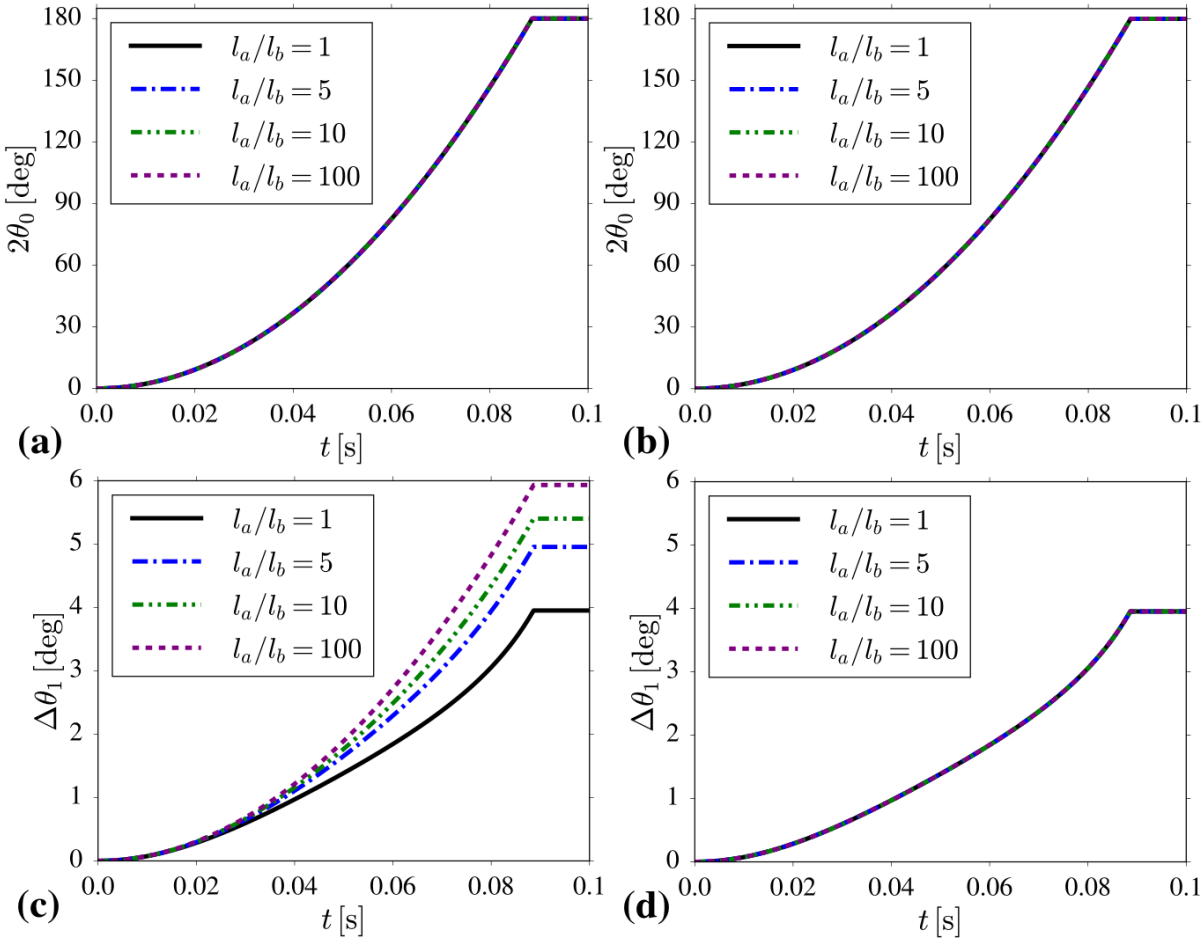

Figure 6-3 Panels (a) and (b) show the variation in the angle of aperture between rigid units $2\theta_0$ plotted with respect to time for Type I and Type II rotating rectangle systems composed of rectangular units associated with different values of the aspect ratio l_a / l_b. Panels (c) and (d) show the variation in the extent of the global rotation exhibited by Type I and Type II respectively for deformation process from panels (a) and (b).

Based on Figure 6-3(c), one may note that upon elongating the units corresponding to type I rotating rectangles system, i.e. upon increasing l_a / l_b ratio, the system may rotate to a greater extent than is the case for lower values of l_a / l_b. It is also evident that in the case of considerably large values of l_a / l_b, the relative change in the extent of rotation of the investigated system becomes negligible. This result suggests that in reality, there is no need to construct the system corresponding to extreme values of l_a / l_b in order to maximise the global rotation of the considered structure. Furthermore, according to Figure 6-3(d), type II rotating rectangles system exhibits a different behaviour than was the case for type I rotating rectangles systems. In this case, the extent of rotation of the whole system is not affected by the variation in the magnitude of l_a / l_b ratio. This result could prove to be useful in the case of applications concerning devices employed in space where the deformation of the structure would not have to lead to the undesired type of rotation of the whole system. On the other hand, should one be interested in inducing the maximal rotation of the system by means of rectangle-based system then it would be more plausible to consider the use of type I rotating rectangles system as it allows to induce the greater extent of rotation than type II rotating rectangles system for any value of l_a / l_b greater than 1. In other words, irrespective of the ratio of sides of its units, the Type II system always exhibits the same rotational behaviour. This in turn could allow to change the dimensions of the structure used to induce the rotation of the external body without altering its dynamics.

In order to better understand the results observed for both types of systems composed of rigid rectangles, one may analyse the variation in the moment of inertia of the whole system (I_1), which is an interesting result in its own accord, as well as moments of inertia of individual units which change accordingly to the aspect ratio of linear dimensions of rigid units. As stems from the parallel axes theorem, the moment of inertia I_1 depends on the distance of each of the

units constituting the system from its centre. This means that as the system deforms, this quantity would be expected to change which effect can be seen in the case of both of the considered systems in Figure 6-4(a-b). Furthermore, due to a different deformation pattern which is the result of a difference in the connectivity between rigid units in the investigated structures, the distances between the respective units and the centre of the system change very differently for both types of systems. Thus, the variation in I_1 is not the same in the case of both types of rotating rectangle systems. At the same time, the moment of inertia of individual rigid units (I_H and I_L) is not only the same for both systems (assuming the same aspect ratio of rigid units) but also remains constant throughout the process of deformation. At this point, one can note that in order to justify the results observed in Figure 6-3(c-d), one can use the principle of angular momentum conservation as well as the above information related to effect which the deformation of the considered systems has on their moment of inertia. This stems from the fact that at any point of the discussed process, the angular momentum of the whole system must be conserved, which in the case of the considered highly-symmetric systems leads to the following expression: $I_1\omega_1 = \left(5I_H - 4I_L\right)\omega_0$ (as mentioned in the model section, due to the particular geometry, the net angular momentum associated with the rigid units does not depend on their linear velocity). Based on this equation, one may conclude that in the case of the particular model considered in this work, in order for a system to exhibit a different type of behaviour for different types of rectangles composing the structure, the factor $\left(5I_H - 4I_L\right)/I_1$ must change for systems consisting of rectangles having different aspect ratio. As the matter of fact, based on Figure 6-4(c), one may note that this type of the variation in the aforementioned parameter can be observed for Type I rotating rectangles which explains why the extent of rotation of the whole system was changing for different types of rectangles. Conversely, in the case of systems where the global rotation does not depend on the ratio of linear dimensions of rigid units, the

factor $(5I_H - 4I_L)/I_1$ should assume the same values for a given value of $2\theta_0$ irrespective of the aspect ratio of rigid units. In fact, as shown in Figure 6-4(d), this very effect can be observed for Type II rotating rectangles which also explains the unusual behaviour observed in the case of this system. At this point, one should also note that in all of the considered cases, the moment of inertia I_1 changes symmetrically throughout the process of deformation as expected based on the geometry of considered systems.

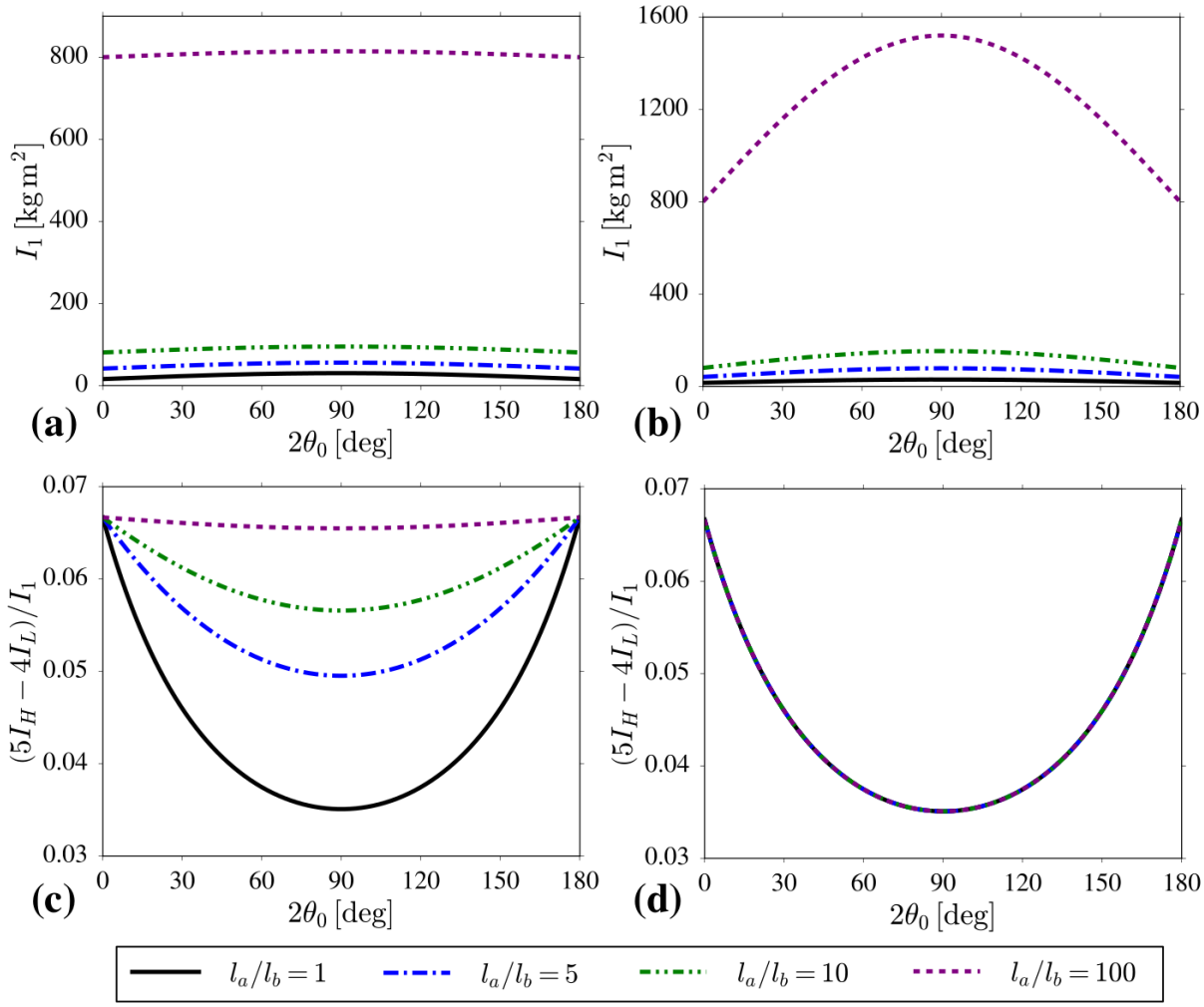

Figure 6-4 Panels (a) and (b) show the variation in I_1 for Type I and Type II rotating rectangle systems during the process of mechanical deformation. Panels (c) and (d) show the variation in the parameter $(5I_H - 4I_L)/I_1$ for Type I and Type II systems associated with different values of l_a/l_b ratio respectively.

As discussed above, based on the theoretical model it was shown that investigated systems may induce their own global rotation as a result of the rotation of their subunits. At the same time, it is important to note that for the sake of simplicity, the model used in order to describe the discussed phenomenon was relatively simple and does not apply to all possible scenarios where the similar concept could be applied. For example, in this chapter (and in Chapter 4 where the concept was first presented), it is assumed that all of the units are perfectly rigid which, amongst other things, means that the moment of inertia associated with the rotation of individual units with respect to their centres is constant. A more complex mathematical description could, in theory, be used, so as to consider systems composed of units which are not perfectly rigid and may change their shape throughout the process of deformation. In such cases, the variation in the shape of the units is expected to affect the extent of the global rotation. Another assumption made in this chapter corresponds to the lack of resistance between hinges connecting respective units (e.g. friction, use of a spring-like hinge, etc.) as well as to the lack of friction on the main axis of rotation passing through the centre of mass of the whole system. Any resistance between adjacent units would affect the magnitude of the generated torque if one was to use a particular force to deform the system. However, should one consider the use of actuators to deform the structure at a given rate irrespective of the resistance between units, then this effect would be made negligible. Also, should one attempt to implement the considered concept in conditions other than those in space, then it would be difficult to completely avoid the effect associated with certain resistance of the whole system to the rotational motion. Furthermore, due to the assumption that considered structures are isolated systems, the effect of external forces such as the gravitational force etc. is not taken into account where such forces could in general significantly affect the discussed phenomenon.

Before concluding, it should be noted that there are still various aspects of the concept being presented here which would benefit from further development. For example, with the present

design, mechanical metamaterials may only induce their own rotational motion as long as the rigid units constituting the given system are rotating. Once the system reaches the configuration corresponding to the maximal value of $2\theta_0$, the units must either cease to rotate or start rotating in the opposite direction which would result in the reversed direction of the global rotation. This limitation imposed by geometry may be overcome if the design is modified so that the units constituting the system would be physically able to continuously rotate in the same direction. Whilst this is not possible for systems where the connectivity of rigid units cannot be changed, one could consider the replacement of standard hinges with devices that may enable a change in the topology in order to be able continue the internal rotations of subunits and hence perpetuate the global rotational motion of the whole structure in a particular direction. For example, this could be achieved with the use of hinges having embedded electromagnetic components. A diagram presenting this concept upon taking the system of rotating squares (which is the special case of the Type I and Type II rectangles with $l_a = l_b$) as an example is shown in Figure 6-5. Based on this diagram, one can note than in the case of the fully-closed configuration of the considered system, the connectivity between the adjacent units is indistinguishable. This means that in theory, if one was to consider the hypothetical use of the electromagnet-based hinges, one could switch the electric current in a way so that at a given time it would run through specific 'vertices'. As a result, it would be possible to form an arbitrary type of the connectivity between 'vertices' of rigid units. This in turn would allow the system to undergo a transition in the connectivity of neighbouring units upon reaching the threshold configuration, hence it would be possible for respective units to continue their rotation in the same direction as was the case before reaching the 'locked' configuration.

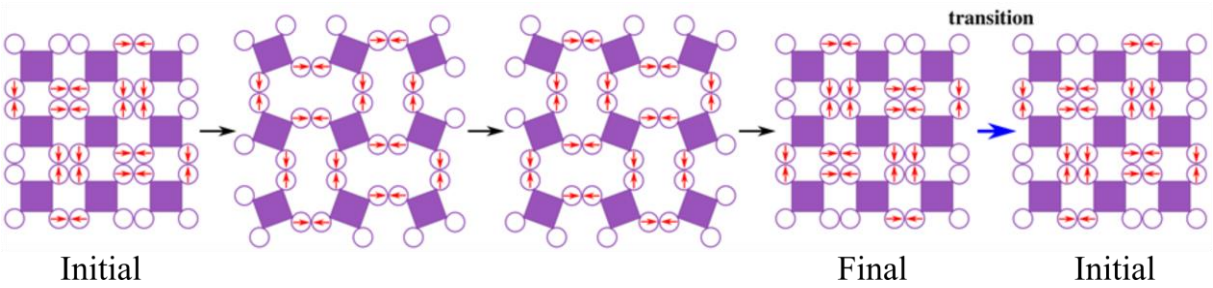

Figure 6-5 A diagram presenting the hypothetical concept of the deformation of the rotating square system having electromagnetic hinges connecting adjacent units at vertices. Those pairs of the vertices which form a hinge as a result of the mutual interaction (for example induced by electromagnets or other devices) are highlighted by means of the connected red arrows. It should also be noted that the concept of the global rotation is not shown in this diagram.

Finally it should be mentioned that all of the results discussed in this and in the preceding chapters, i.e. self-induced global rotation and self-induced variation of moment of inertia, besides being interesting from the theory point of view, may also be used in the case of a variety of applications where the control over the rotational motion of the system is of great importance. As discussed in the former chapters, some of the potential applications of these concepts include wind turbines, spacecraft, satellites and telescopes employed in space where the need for various attitude control devices is historically known (currently reaction wheels are used to control the rotation of such objects).

At this point, one should mention that one of the main motivations behind studying novel types of behaviour which might be exhibited by mechanical metamaterials (such as the aforementioned potential of mechanical metamaterials to induce their own global rotational motion) was to potentially introduce these system to novel branches of the industry which could lead to interesting applications. However, the fact that it is possible to propose novel concepts associated with the behaviour of mechanical metamaterials does not mean that the studies related to their better-known aspects such as the potential of these systems to exhibit unusual mechanical properties should be neglected. As the matter the fact, further studies on different anomalous mechanical properties which may be exhibited by mechanical metamaterials could

eventually lead to the application of some of the interesting concepts related to these system in the case of everyday materials in order to enhance their properties. One very interesting class of mechanical metamaterials where the studies on mechanical properties are still in their infancy and the results reported up to date indicate the potential of these systems to exhibit superior counter-intuitive mechanical properties are hierarchical mechanical metamaterials. In view of this, in the following chapter, the potential of these systems to exhibit unusual mechanical behaviour is going to be investigated.

6.4 Conclusions

In this chapter, it was shown that different mechanical metamaterials may induce their own rotational motion as a result of the rotation of their subunits. Upon analysing the propensity of considered systems to exhibit the discussed phenomenon it was also shown that different mechanical metamaterials may in general induce their global rotational motion to a varying extent depending on their geometric parameters. It was also discussed that in theory, one may construct the system similar to those discussed in this chapter where all of the units could indefinitely rotate in the same direction which would also make it possible for the entire system to rotate for an arbitrarily long period of time. All of the reported results could also be used in order to implement the discussed concept of the self-induced global rotation of mechanical metamaterials in the case of various applications such as spacecraft, satellites, telescopes employed in space and wind turbines.

7. Control over mechanical properties of hierarchical rotating rigid unit auxetics[4]

CHAPTER HIGHLIGHTS:

- In hierarchical systems composed of rigid units connected *via* hinges, both lower and higher levels of the hierarchical system may deform;
- Deformation pattern of the hierarchical system can be controlled *via* the resistance of hinges connecting rigid units to the rotational motion, i.e. systems with the same initial geometry having different resistance associated with the hinges will deform differently;
- A change in the Poisson's ratio need not be imparted through a change in the geometry of the system, as is normally the case, but may be also achieved through a change in the 'stiffness' of the hinges;
- It is proposed that the control over the resistance of hinges to the rotational motion which can lead to the behaviour discussed in this chapter can be achieved *via* the use of magnetic inclusions located on rigid units constituting the system.

7.1 Introduction

As discussed in the Literature Review, over the years, mechanical metamaterials have been extensively studied from the point of view of their potential to exhibit unusual mechanical properties such as negative Poisson's ratio. As the results of such studies, these systems were proven to be useful in the case of the variety of applications such as in the manufacture of

[4] The content of this chapter has already been published in the peer-reviewed journal *Scientific Reports*: **K. K. Dudek**, R. Gatt, L. Mizzi, M. R. Dudek, D. Attard, K. E. Evans, J. N. Grima, On the dynamics and control of mechanical properties of hierarchical rotating rigid unit auxetics *Sci. Rep.* **7** 46529 (2017)

impact resistant, sound-proofing and/or biomedical devices. In an attempt of introducing mechanical metamaterials to new sectors of industry, more properties of such metamaterials are being studied, such as the novel effect corresponding to the propensity of these systems to induce their own global rotational motion, which was proposed and analysed in the last three chapters of this thesis. However, the fact that it is worth to investigate novel aspects associated with mechanical metamaterials does not mean that the studies related to more fundamental aspects of design and mechanical properties of mechanical metamaterials are completed. As the matter of fact, now that systems exhibiting anomalous mechanical properties are starting to prove their usefulness in everyday applications (e.g. sports shoes, gloves and helmets [419]), it is even more important to intensify efforts aimed towards enhancing their properties in order to try to reach their full potential.

One very interesting class of mechanical metamaterials are hierarchical mechanical metamaterials. As discussed in detail in the Literature Review, the studies related to incorporating the concept of hierarchy in the case of these systems were commenced very recently with some of the first papers being published on the verge of the year 2014 and 2015 by Cho *et al.* [329] and Gatt *et al.* [330]. These studies were primarily focused on systems composed of rotating square motifs and different geometries which such systems can attain. In those studies, it was also reported that during the deformation process of such system, units corresponding to lower levels of hierarchy tend to open to a significantly lower extent than is the case for higher levels. However, this interesting observation was not followed by the proposal of any model nor other form of justification which would allow to explain the observed phenomenon. In view of this, in this chapter, an attempt is going to be made in order determine the mechanism leading to this particular type of behaviour. In order to do that, a particular two-level hierarchical mechanical metamaterial is going to be analysed through the dynamics approach meant to primarily qualitatively asses the behaviour of the considered system. By

means of the very simplified theoretical model, it is also going to be analysed whether it is possible to attain the control over the deformation and mechanical properties which may be exhibited for such system through the variation in certain parameters defining the structure.

7.2 Model

In this chapter, a model specifically designed to describe the dynamic behaviour and predict the mechanical properties of the hierarchical system shown in Figure 7-1(b) will be presented and discussed. This may be described as a finite two-level hierarchical system having four square-like units in the upper level (corresponding to Level 1 of the structure) each of which is made from four other squares (the Level 0) having a linear dimension of *l*. This system is a particular case of a more general two-level hierarchical system where each of the Level 1 building blocks consists of $2N_{0,x} \times 2N_{0,y}$ squares, where $N_{0,x}$ and $N_{0,y}$ stand for the number of Level 0 units in the two orthogonal directions associated with a Level 1 building block, see Figure 7-1(a). Note that if $N_{0,x} = N_{0,y} = N_0$, the Level 0 would approximately assume the shape of a square (as is the case in the this chapter) whilst if $N_{0,x} \neq N_{0,y}$, the Level 0 would assume the shape of a rectangle.

Variables θ_0 and θ_1 correspond to angles between the adjacent units of the zeroth and first level respectively. These quantities can in turn be used in order to determine the linear dimensions (L_x and L_y) of the discussed system (see Appendix III). It is also very important to note that the hierarchical systems considered in this study cannot be constructed for an arbitrary combination of θ_0 and θ_1. The possible values of these angles are given in Figure 7-1 (c).

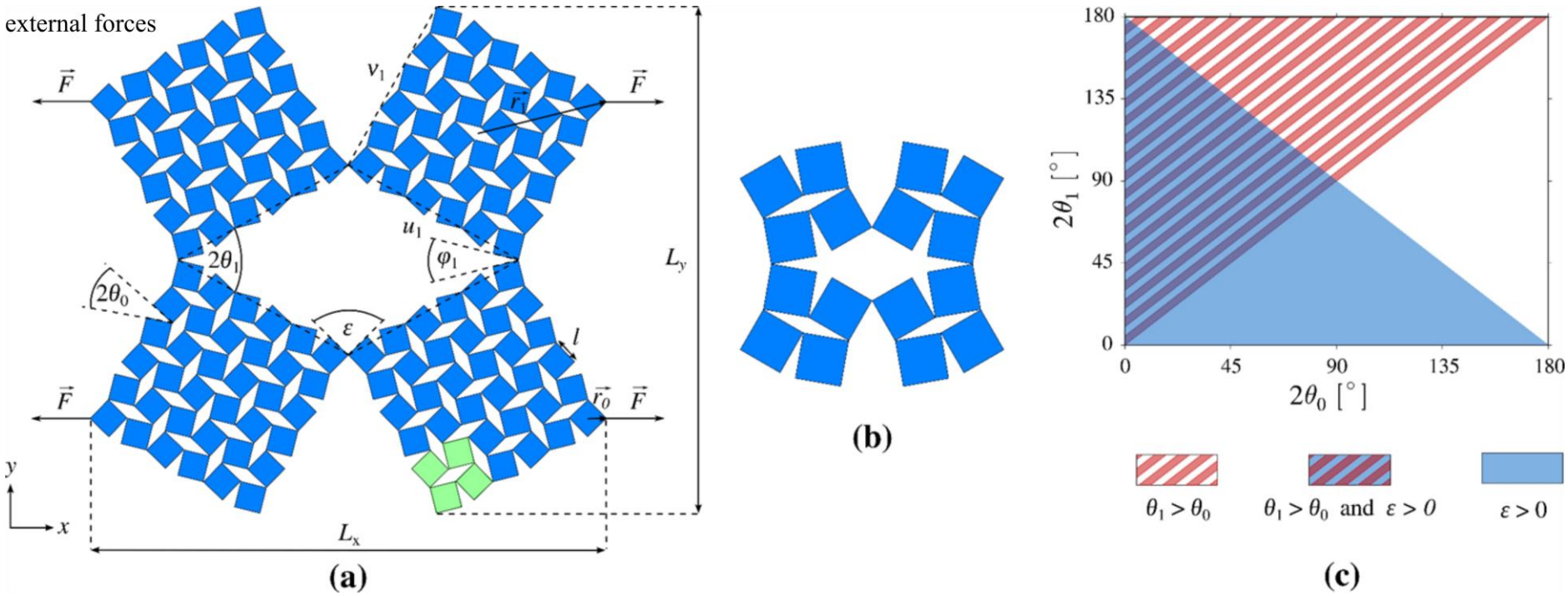

Figure 7-1 The panels in this figure present (a) the two-level hierarchical auxetic system with four square-like units corresponding to Level 1 of the structure, where each unit consists of $N_0 \times N_0$ (in the provided example $N_0 = 3$) Level 0 repeat units (bright green), (b) an example of the structure corresponding to $N_0 = 1$ and (c) the permissible angles for θ_0 and θ_1, which conditions ensure that the squares do not overlap with each other and the system retains the same connectivity. This is attained when conditions $\theta_1 > \theta_0$ and $\varepsilon = \pi - 2\theta_1 - 2\theta_0 > 0$ are satisfied.

This model operates under the assumption that the Level 0 rotating square units of the system are completely rigid and cannot distort or change shape in any way during deformation. The validity or otherwise of this assumption for a real physical system will depend on how the real system is constructed. For example, this model derived here is likely to be valid for systems constructed from stiff units (e.g. metal) connected through hinges, i.e. a system which is purposely constructed to satisfy these assumptions of the model. For small strains, the 'rigid units' assumption is also expected to be applicable to other systems, such as perforated systems as described in Cho *et al.* [329] and Grima *et al.* [420], where previous studies have shown that the smaller the 'connection' between the squares in relation to the size of the units (e.g. squares) themselves, the more valid the assumption is [420]. Furthermore, the Level 0 squares and Level 1 building blocks will be assumed to be connected together through hinges which permit relative rotation of two connected units. In order to further simplify the description of the very complex system discussed in this chapter, it is also going to be assumed that the variation in the moment of inertia of respective units / building blocks constituting the system is relatively small. The symmetry of the system, as well as its geometric constraints result in a system which only has few degrees of freedom. In particular, under the condition of uniaxial on-axis loading, all of the units constituting the *i*-th level of the system are geometrically constrained to rotate by the same angle, while the 0-th level squares remain rigid, i.e. they do not distort or change shape in any way. Under these conditions, for a given value of *l* (size of the length of a single square), the geometry of the whole system can be described through just two independent variables, angles θ_0 and θ_1. This means that it is sufficient to investigate the rotation of individual units in both levels in order to obtain a complete picture of the deformation mechanism of the considered structure, i.e. the dynamics of the system may be fully described through a set of equations which are the rotational analogues of Newton's equation of motion, which equations may be solved numerically. In other words, the deformation through time, of

the whole system may be established by solving the equations governing the changes in the angles θ_i at a given time, an approach which allows for perfect rigidity of the 0-th level rotating units and is highly efficient from a computational time point of view, as the number of equations which must be solved at a given time corresponds to the number of levels within the system and is nearly independent of the number of units constituting a given level. This stems from the fact that the number of rigid units corresponding to the *i*-th level is only a number parameter in the equation describing the dynamics of the angle θ_i, as will be discussed later in this paper.

In order to induce a deformation in the systems discussed in this work, a force $\vec{F}$ (the same in terms of magnitude) is applied on each of the leftmost and rightmost vertices of the system, as shown in Figure 7-1(a) (or topmost and bottommost, depending on the direction of loading).

At this point, it should be noted that even though in former chapters the resistance of hinges connecting the respective vertices of rigid units to the rotational motion was not taken into consideration as it would affect the discussed phenomenon only quantitatively, in general it does not have to be the case. As a matter of fact, there is a variety of systems where the resistance of hinges to the rotational motion may qualitatively affect the investigated behaviour. One such example is the system analysed in this chapter, where the resistance of the hinge to rotation may be defined in a number of ways depending on the way how the hinges within the considered system are constructed. A very well-known approach makes use of a harmonic potential in order to describe the hinging process, an approach which can mimic a number of realistic scenarios, including the behaviour at small strains of perforated and other similar systems corresponding to an analogical geometry.

In the considered model, based on a harmonic potential, it is assumed that resistance to rotation is solely due to a restoring force associated with hinges. In other words, apart from assuming that Newton's equations are adequate to describe the dynamics of the discussed

system, it is also being assumed that the system is just being uniaxially stretched and not being subjected to additional factors (magnetic field, medium viscosity etc.). The approach used here is expected to be valid only for certain macroscale systems present in a medium with relatively low viscosity which are not subjected to additional environmental factors such as gravitational force etc. At this point it is important to note that, in the case of this particular potential, even if all of the hinges within the system were the same, the restoring force corresponding to hinges from Level 0 and Level 1 may vary as angles θ_0 and θ_1 might be opened to a different extent with respect to equilibrium angles $2\theta_{0,eq}$ and $2\theta_{1,eq}$ respectively. In such a case, the resistance to rotation associated with individual hinges may be quantified in terms of torques as $2K_h\left[\left(\theta_1-\theta_0\right)-\left(\theta_{1,eq}-\theta_{0,eq}\right)\right]$ or $2K_h\left(\theta_0-\theta_{0,eq}\right)$ depending on the position within the system. In this case K_h stands for a stiffness constant associated with the harmonic potential resistance torque. Furthermore, based on Figure 7-1(b), one may note that for the considered structure there are always four hinges corresponding to Level 1 of the system and by extension to the torque $2K_h\left[\left(\theta_1-\theta_0\right)-\left(\theta_{1,eq}-\theta_{0,eq}\right)\right]$. However, in the case of Level 0 of the system, all of the hinges within the structure correspond to this level.

Under the assumptions made in this chapter, for a given level to keep expanding, the resultant resistance torque associated with this level has to be overcome by the torque corresponding to the force applied to the system at all times. This means, that in general, one can describe the motion of units constituting the *i*-th level of the structure by means of the of the following equation of motion:

$$I_i\frac{d^2\theta_i}{dt^2}=\tau_i\pm B_i \qquad 7\text{-}1$$

where, I_i stands for the collective moment of inertia of all of the units within the system and $\frac{d^2\theta_i}{dt^2}$ is the angular acceleration associated with the rate of change in the angle θ_i. The

remaining variables in the above equation, i.e. τ_i and B_i, stand for the magnitude of the torque induced by the application of the external forces (having a magnitude of *F*) to the leftmost and rigtmost vertices of the structure and the resistance torque associated with hinges. Upon follwing this general formulation, the deformation of the system can then be established through the rotation of the units found in each level, by means of the rotational analog of Newton's equation of motion:

$$I_1 \frac{d^2\theta_1}{dt^2} = 8r_1 F \sin\left(\sphericalangle\vec{r_1}, \vec{F}\right) \mp 8K_h\left[\left(\theta_1 - \theta_0\right) - \left(\theta_{1,eq} - \theta_{0,eq}\right)\right] \quad 7\text{-}2$$

$$I_0 \frac{d^2\theta_0}{dt^2} = 8r_0 F \sin\left(\sphericalangle\vec{r_0}, \vec{F}\right) \mp 8K_h\left[\left(\theta_1 - \theta_0\right) - \left(\theta_{1,eq} - \theta_{0,eq}\right)\right] \mp 2\left(n_i - 4\right)K_h\left(\theta_0 - \theta_{0,eq}\right) \quad 7\text{-}3$$

where, n_i, is the number of hinges corresponding to Level *i* of the system, r_i, is the distance between the vertex where the force is applied and the centre of mass of the Level *i* building block. Since in this study, a two-level system is being considered, and hence *i*=0,1. Here, I_0 corresponds to the rotation of individual squares with respect to their own centres and I_1 is associated with the rotation of the Level 1 building blocks with respect to their centres of mass. The information concerning the way how these quantities were calculated can be found in Appendix III.

The signs in equations 7-2 and 7-3, are set in a way so that the resultant resistance torque always opposes the rotational motion of units corresponding to the *i*-th level. Furthermore, the factor 8 in equations 7-2 and 7-3 is associated with the way the force is being applied to the system and the resulting reaction forces as described in [421].

It is important to note that the methodology developed here can be applied to various other analogous constructs including other hierarchical system composed of an arbitrary type of rotating rigid units. Furthermore, it is important to highlight the fact that although the model proposed above is based on a specific type of hinge in which the rotational motion is governed

by harmonic potential, the derived model can be used for an arbitrary potential or type of interaction. A very good example can be hinges where the rotational motion is governed by friction. In this case, one can assume that for a considered model, a resistance to rotation is solely due to friction from all the hinges in the system, which are identical to each other irrespective of their position within the system. In this case, the resistance to rotation may be quantified in terms of a friction torque $f = f_i$ $(i = 0,1)$ resulting from the friction caused by the rotational motion of the hinge, where the value of *f* remains constant regardless of changes in angular velocity and angle of aperture of the subunit. Under such assumptions, for a given level to start deforming, the resultant friction torque associated with this level has to be overcome by the torque corresponding to the force applied to the system. In this case, the Newton's equation of motion describing a rotational motion of the *i*-th level, can be written in an analogical manner as it was the case for the harmonic potential as follows:

$$I_i \frac{d^2\theta_i}{dt^2} = 8 r_i F \sin\left(\sphericalangle \vec{r_i}, \vec{F}\right) \mp n_i f \ . \qquad 7\text{-}4$$

Systems having hinges governed by friction, apart from being indisputably simple to describe mathematically, are a very good representation of macroscopic pin-jointed structures where the resistance to rotation of the hinge is associated with the friction governing the hinging process.

Calculation of the Poisson's ratio

In general, for loading in the *x* direction, the Poisson's ratio can be expressed as follows:

$$\nu_{xy} = -\frac{\varepsilon_{yy}}{\varepsilon_{xx}} \qquad 7\text{-}5$$

where ε_{xx} and ε_{yy} are the strains in the *x* and *y* directions respectively. In this work, the value of ν_{xy} at a given time was calculated using the following formula:

$$\nu_{xy,k+1} = -\frac{\varepsilon_{yy,k+1}}{\varepsilon_{xx,k+1}} = -\frac{L_{y,k+1} - L_{y,k}}{L_{y,k}} \Bigg/ \frac{L_{x,k+1} - L_{x,k}}{L_{x,k}} \qquad 7\text{-}6$$

Parameters

In order to investigate the deformation behaviour of the discussed system for loading in the *x*-direction, a structure consisting of $1\times1\left(N_0 \times N_0\right)$ Level 0 building blocks was used. The constants characterising this system were set as follows: F = 500 N, l = 0.05 m, $\rho = 3000\ \mathrm{kg\cdot m^{-2}}$ (area density of the material making up the Level 0 subunits), ω_1 and $\omega_0 = 0\ \mathrm{deg\cdot s^{-1}}$ (the initial angular velocity of the rotating units in the respective first and zeroth levels), $\Delta t = 10^{-7}$ s. In addition, the initial geometric parameters of the system were set as: $2\theta_1 = 20°$, $2\theta_0 = 10°$, which in the case of $N_0 = 1$ leads to, L_x = 0.248 m and L_y = 0.234 m. Furthermore, in order to show how the deformation of the system changes upon varying the value of K_h, K_h was set to be equal to {0.035, 0.174, 0.349, 0.698, 1.396, 2.093} $\mathrm{N\cdot m\cdot deg^{-1}}$. In the case of the structure constructed by means of hinges governed by friction, all of the parameters, with exception for *f*, were kept fixed. In the considered cases *f* assumed the values of {0.0, 0.5, 1.0, 1.5, 2.0, 2.5, 3.5} Nm.

7.3 Results and Discussion

Numerical solutions of the model presented above suggest that irrespective of the hinge being used, a tensile force results in the system deforming through a relative rotation of the constituent units where, for a given initial structure, the actual manner of deformation, and hence the Poisson's ratio, is dependent on the resistance to motion offered by the hinges. This means that if the magnitude of the resistance to rotational motion offered by the hinges could be controlled, then it would be possible to control the mechanical behaviour of the system without altering its geometry. Such control over the resistance to the rotational motion of the hinges can be achieved through the use of magnetic fields (which concept was first proposed by Grima *et al.* [406]) or thermal expansion of hinges. This is very significant as it is the first time that a change in the Poisson's ratio is not being imparted through a change in the geometry of the system, as is normally the case, but merely due to a change in the resistance associated with the hinges of the hierarchical system. This is clearly shown by the results plotted in for systems with the same initial geometry, set to l = 0.05 m, $N_0 = 1$, $2\theta_0 = 10°$ and $2\theta_1 = 20°$, having hinges which offer different resistance to motion. Here it is important to note that the changes in the mechanical properties of the hierarchical systems occur while the system is still deforming via the rotating mechanism. This is completely different from the effect observed in other auxetic systems such as hexagonal re-entrant honeycombs [15, 235, 236], where the mechanical properties depend on the interplay between the three main deformation mechanisms present in these systems, i.e. the stretching, hinging and flexing mechanisms. For such re-entrant systems one could alter the mechanical properties by changing the ratio of their respective stiffness constants. However in our case, there is no such interplay of mechanisms and the change in mechanical properties was obtained solely as a result of the relative rotations of Level 0 and Level 1elements.

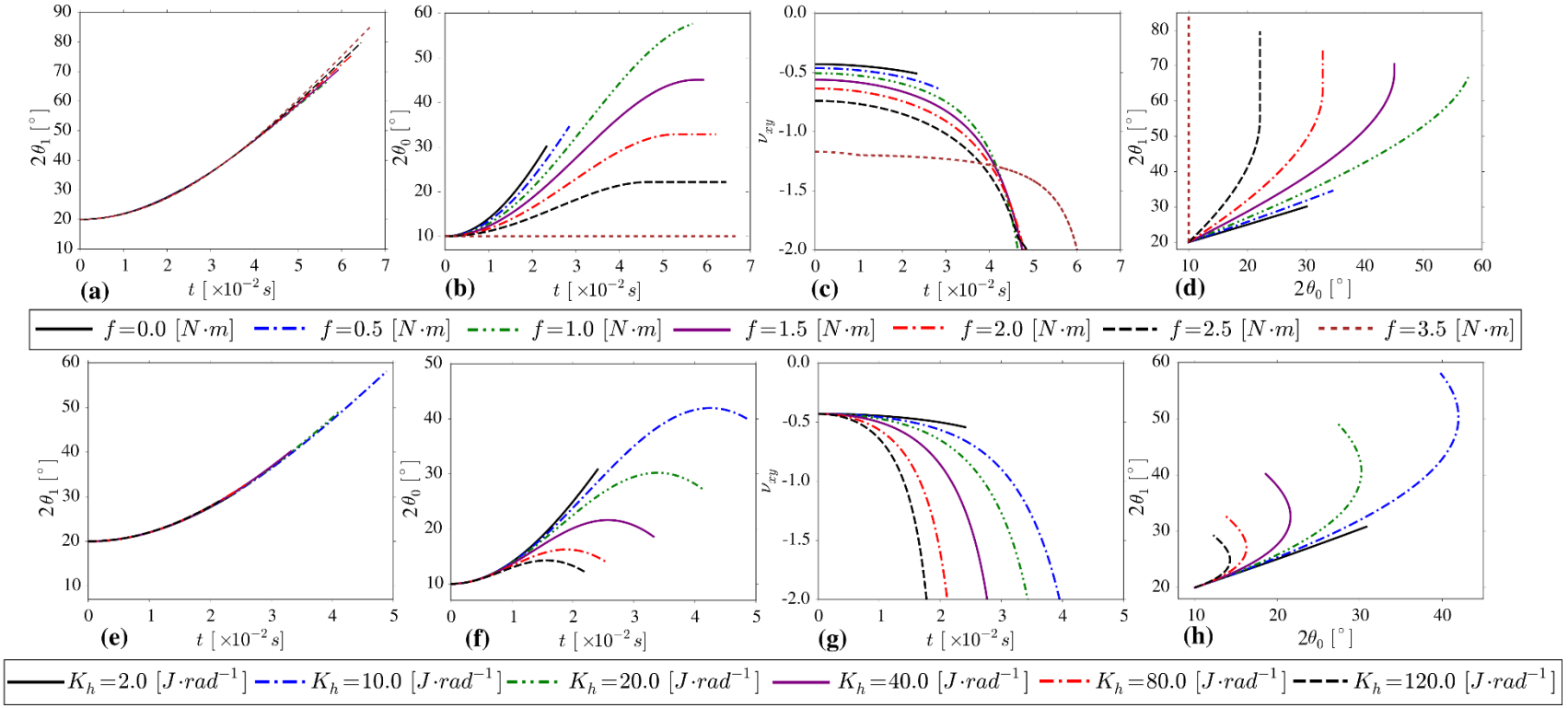

Figure 7-2 Plots showing the variation in (a) θ_1 (b) θ_0 and (c) Poisson's ratio ν_{xy} as a function of time *t* for loading in the *x* direction for systems with K_h values ranging from 0.035 $\mathrm{N \cdot m \cdot deg^{-1}}$ to 2.093 $\mathrm{N \cdot m \cdot deg^{-1}}$ and (d) the relation of θ_1 to θ_0 for a deforming structure having the motion of the hinges governed by harmonic potential. Similarly, plots (e), (f) and (g) show the variation in θ_1, θ_0 and ν_{xy} respectively as a function of time in the case of friction-based hinges corresponding to the value of *f* ranging between 0 $\mathrm{N \cdot m}$ and 3.5 $\mathrm{N \cdot m}$. (h) shows the relation of θ_1 to θ_0 for a deforming structure having the motion of the hinges governed by friction. In all cases considered, $N_0 = 1$ and *F*=500 N. It is important to note that in the case of (c) and (g), the scale in the y-axis (incremental Poisson's ratio) was arbitrarily stopped at -2, since this value of the Poisson's ratio tends to $-\infty$ upon approaching the maximum deformation. A cut-off value of -2 is appropriate in view of the fact that the part of the deformation which is not included in panels (c) and (g) is relatively small, as shown in Table 7-1. An analogical set of results, plotted with respect to applied strain, is provided in Appendix III.

f [Nm]	ν_{xy}	$\varepsilon_{x,\,final}$	$K_h\left[\mathrm{N\cdot m\cdot deg^{-1}}\right]$	ν_{xy}	$\varepsilon_{x,\,final}$
0.0	-0.508 at $\varepsilon_x = 0.157$	0.157	0.035	-0.543 at $\varepsilon_x = 0.162$	0.162
0.5	-0.640 at $\varepsilon_x = 0.194$	0.194	0.174	-2.0 at $\varepsilon_x = 0.253$	0.271
1.0	-2.0 at $\varepsilon_x = 0.289$	0.303	0.349	-2.0 at $\varepsilon_x = 0.199$	0.212
1.5	-2.0 at $\varepsilon_x = 0.273$	0.291	0.698	-2.0 at $\varepsilon_x = 0.134$	0.143
2.0	-2.0 at $\varepsilon_x = 0.246$	0.266	1.396	-2.0 at $\varepsilon_x = 0.181$	0.086
2.5	-2.0 at $\varepsilon_x = 0.211$	0.234	2.096	-2.0 at $\varepsilon_x = 0.057$	0.062
3.5	-2.0 at $\varepsilon_x = 0.183$	0.187	-	-	-

Table 7-1 Values of the strain (ε_x) corresponding to the minimum value of the Poisson's ratio presented in Figure 7-2 in comparison to the final value of the strain ($\varepsilon_{x,\,final}$) associated with the geometric lockage of the system.

K_h [J deg^{-1}]	**0.035**	**0.174**	**0.349**	**0.698**	**1.396**	**2.093**
$2\theta_{0,\,final} - 2\theta_{0,initial}$ [deg]	20.811	29.766	17.233	8.600	3.780	2.231
$2\theta_{1,\,final} - 2\theta_{1,initial}$ [deg]	10.812	38.101	29.261	20.175	12.661	9.302

Table 7-2 Difference between the final and initial value of the angle θ_i for particular values of K_h. In all of the considered cases, the system was subjected to a constant force having a magnitude F=500 N throughout the whole process of deformation, i.e. from $\theta_{i,initial}$ up to $\theta_{i,\,final}$, when the system goes to the locked conformation.

Figure 7-2 (a)-(d) show the results for systems where the resistance to motion is governed through a harmonic potential associated with every hinge within the system. These different structures have the same initial geometry but different values of a stiffness constant K_h ranging from $0.035\,\mathrm{N\cdot m\cdot deg^{-1}}$ to $2.093\,\mathrm{N\cdot m\cdot deg^{-1}}$. In all cases, the system was subjected to a constant force having a magnitude of 500 N until it was geometrically locked i.e. until the system could not continue to deform through rotations of the level 1 and / or level 0 quadrilaterals. A detailed analysis of these results indicates that in the case of the hierarchical

systems having relatively high values of K_h, Level 1 opens to a greater extent than Level 0 of the structure. This can be concluded from the fact that angle θ_1 opens to a greater extent than angle θ_0 as shown in Figure 7-2 and Table 7-2. This is in accordance with the numerical and experimental work conducted by Gatt *et al.* [330] and Tang *et al.* [331] concerning the deformation of hierarchical perforated materials. However this deformation behaviour is not observed for all systems with the equivalent initial geometric configuration. In fact, for systems having relatively low values of K_h, the opposite behaviour is observed, with the Level 0 squares opening to a greater extent than the larger Level 1 units. Therefore, these results suggest that the deformation behaviour depends on the magnitude of the K_h coefficient (or other parameter depending on the type of hinge). This is very important as it indicates that for a given initial conformation, the final loaded structure depends upon the value of the hinge resistance to the rotational motion coefficient, as indicated in Figure 7-2. It is also important to note that although θ_1 always increases, for relatively low values of K_h, referring to Figure 7-1(a) and Figure 7-2, angle φ_1 becomes smaller with time whilst for relatively large values of K_h this angle becomes increasingly larger. It is also important to note that the deformation behaviour (and hence mechanical properties) of this hierarchical system can also be controlled through the magnitude of the force applied. In particular, for a system having a constant resistance to rotational motion, an increase in the magnitude of the force results in level 0 quadrilaterals opening to a greater extent in comparison to level 1 quadrilaterals, without changing the structure itself i.e. without having to deconstruct and re-construct the structure with different hinges. Additional fine-tuning may also be achieved by applying a force which changes in magnitude with time (see Appendix III).

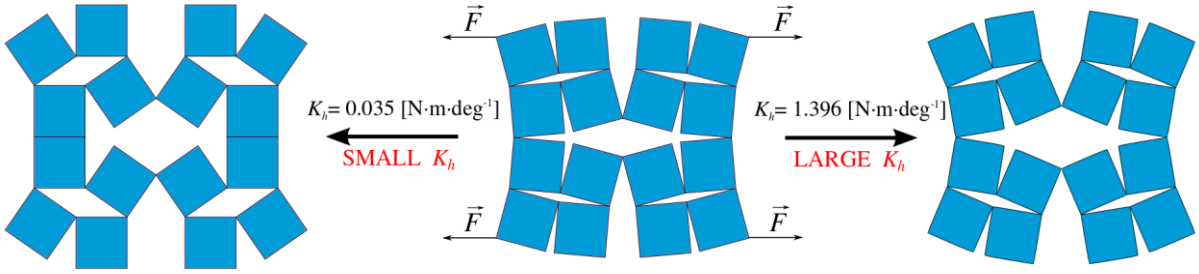

Figure 7-3 Diagrams showing the final state of the deformation of two systems, where the hinging process is governed by friction, with K_h values of $0.035\,\mathrm{N\cdot m\cdot deg^{-1}}$ and $1.396\,\mathrm{N\cdot m\cdot deg^{-1}}$.

This difference in the deformation mechanisms upon altering the K_h coefficient may be explained if one considers the number of hinges present within each level of the system. The deformation of the rotating units in the respective levels is governed by the ratio of the resultant friction torque in the zeroth and first level of system. For the hierarchical structure considered above, the total number of hinges present in Level 0 (n_0) is equal to 20 whilst the total number of hinges present in Level 1 (n_1), is equal to 4. Based on equations 7-2 and 7-3, the resultant resistance torque, which the system has to overcome in order to expand, depends on a number of hinges present within each level of the system. Hence, in the considered case of $N_0 = 1$, the corresponding resistance torque of the zeroth level of the structure is significantly larger than in the case of the first level, which stems from the fact that a number of hinges corresponding to Level 0 is five times greater than it is the case for Level 1. Thus for relatively large values of K_h, for example $K_h = 1.396\,\mathrm{N\cdot m\cdot deg^{-1}}$, the magnitude of the resultant resistance torque corresponding to Level 0 is relatively large when compared to that of the torque associated with the applied force. At the same time, Level 1 units are not as affected by the value of K_h (see Figure 7-2(a)) due to the fact that in this case, the resistance torque associated with only 4 hinges has to be overcome. This results in a greater deformation of the Level 1 units. However, in cases where the K_h constant assumes a relatively small value (such as in the case of

$K_h = 0.035\ \mathrm{N \cdot m \cdot deg^{-1}}$), the resultant resistance torque becomes insignificant in comparison to the one associated with an applied force and the distance r_i becomes the governing factor for the deformation of the system. This means that the Level 0 units deform to a greater extent in the case of a relatively small value of K_h. The effect which the value of K_h has on the deformation of the system is clearly shown in Figure 7-2(d) and Figure 7-3 where the final configuration of the system corresponding to both of the discussed values of K_h is presented. Based on Figure 7-2(b), one can note that Level 0 starts closing during the process of deformation. This result is associated with the fact that the resultant restoring force (for this level) is greater than in the case of Level 1 (number of hinges is greater for Level 0 than it is the case for Level 1), hence it is more prone to exceed the torque corresponding to the external force. In order to better understand the extent of deformation for each of the considered parameters, the analogical set of results plotted with respect to strain is provided in Appendix III.

The above results indicate that one may control the deformation behaviour of the system simply by changing the magnitude of the coefficient corresponding to the resistance to the rotational motion (such as K_h in the case of a harmonic potential). This also suggests that for any two-level hierarchical rotating squares geometry (assuming that both levels open at the same time), there is a specific value of K_h where the rate of angle opening of θ_0 and θ_1 is equal. Such a threshold value of K_h can be denoted as $K_{h,T}$. It can be obtained by means of equations 7-2 and 7-3, where by assuming that $\omega_1 = \omega_0$, the value of $K_{h,T}$ can be found once the condition $\frac{d^2\theta_0}{dt^2} = \frac{d^2\theta_1}{dt^2}$ is satisfied. It is also important to note that the value $K_{h,T}$, can be determined only for a given time since it varies as the angles change.

Figure 7-2(c), shows the change in the incremental Poisson's ratio with time for the hierarchical structure under consideration having different values of K_h. The incremental Poisson's ratio [422], also known as the Poisson's function [423] was used in this study as it gives a much better indication of changes in the lateral dimension of the system as a measure of applied stress (i.e. during the deformation) when compared to the engineering Poisson's ratio. From Figure 7-2(c), it is clear that the value of the Poisson's ratio at a particular time, depends on the value of K_h. This stems from the fact that the geometry of Level 1 units (defined by u_1 and υ_1 in Figure 7-1(a)) can be described as rectangles rather than as squares, with $u_1 = 0.1083$ m and $\upsilon_1 = 0.0996$ m. For relatively large values of K_h, θ_0 changes to a small extent, meaning that the dimensions of the Level 1 units remain roughly constant throughout the deformation of the hierarchical structure. It is well known that the Poisson's ratios of the rotating rectangles model is dependent on the dimensions of the rectangles and the angle between them, where the incremental Poisson's ratio exhibit an asymptote-like behaviour ($\nu_{xy} \to \pm\infty$) upon approaching the locking conformation, i.e. upon reaching the maximum applied strain in the loading direction. For relatively small values of K_h, (for example $K_h = 0.035\ \mathrm{N \cdot m \cdot deg^{-1}}$) θ_0 changes to a large extent, meaning that the dimensions of the Level 1 units change throughout the deformation of the hierarchical structure. This means that in this case, the Poisson's ratio of the hierarchical system will depend on the relative changes of θ_0 and θ_1. Furthermore, one may note that the initial value of the Poisson's ratio is the same for all the systems considered (governed by a harmonic potential) irrespective of the value of the stiffness constant. This effect can be explained by the fact that in the case of the harmonic potential, at the time equal to zero, the term corresponding to the restoring torque (see equations 7-2 and 7-3) assumes a value of zero as the hinges are in their equilibrium states.

At this point, it is important to note that the results presented above relate only to a hinge governed by the harmonic potential, but the findings that the deformation pathway and mechanical properties are affected by the properties of the hinges is a general result. As an example, a similar set of results was produced for structures in which the hinging process is governed by a friction rather than a harmonic potential. The values of *f* (associated with the friction of a hinge) for these structures were set in the range between $0\,\mathrm{N\cdot m}$ and $3.5\,\mathrm{N\cdot m}$, while the same geometric parameters considered for the hinges governed by harmonic potential were used. From the results obtained, see Figure 7-2(e)-(h), one can note that even though the deformation patterns are slightly different than it was the case for Figure 7-2 (a)-(d) (which stems from a different nature of the hinging process), both of the systems lead to the same conclusions as analogical trends can be observed in both sets of figures. For example, for relatively high values of *f*, Level 0 of the hierarchical system opens to a greater extent than Level 1 and, vice-versa, for relatively low values of *f*, Level 0 opens to a greater extent than Level 1 (see Table 7-3). Furthermore, in the case of the friction-based hinges, the initial Poisson's ratio is not the same for different values of *f*, which was not the case for the hinges governed by harmonic potential (see Figure 7-2 (c), (g)). This is due to the fact that the initial system varies for different values of *f* as a different resistance to motion has to be overcome from the beginning of the deformation. In fact, referring to Figure 7-4, it can be shown that for the hierarchical system having $f = 3.5\,\mathrm{Nm}$, the Poisson's ratio follows the same profile as the rigid rotating rectangles model proposed by Grima *et al.* [286]. This result also proves the suitability of this dynamics method to model systems based on rigid rotating units.

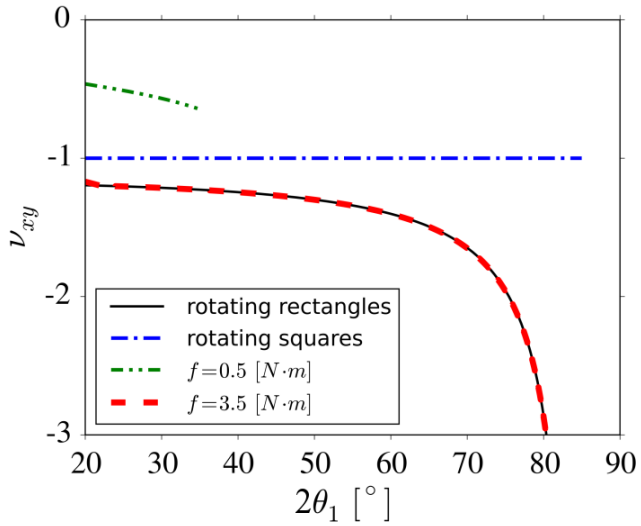

Figure 7-4 A plot showing a comparison of the Poisson's ratios obtained from the numerical solutions presented here for f = 0.5 Nm and f = 3.5 Nm with those calculated from analytical models for uni-level rotating rigid rectangle and square systems.

f [Nm]	**0.0**	**0.5**	**1.0**	**1.5**	**2.0**	**2.5**	**3.5**
$2\theta_{0,\,final} - 2\theta_{0,initial}$ [deg]	20.133	24.686	47.658	35.075	22.869	12.176	0.034
$2\theta_{1,\,final} - 2\theta_{1,initial}$ [deg]	10.134	14.688	46.793	50.492	55.351	59.799	65.182

Table 7-3 Difference between the final and initial value of the angle θ_i for particular values of f. In all of the considered cases, the system was subjected to a constant force having a magnitude F=500 N throughout the whole process of deformation, i.e. from $2\theta_{i,initial}$ up to $2\theta_{i,\,final}$, when the system goes to the locked conformation.

Also, although the results discussed here are specific to a particular geometry, the same trends in deformation and Poisson's ratios are expected to occur for other initial geometric conformations of the hierarchical system (see [424]). Furthermore, this result is expected to be valid for larger values of N_0. However, one may presume that as N_0 increases, Level 0 becomes increasingly rigid meaning that the Poisson's ratio would increasingly depend on the deformation of the Level 1 units. Moreover, as $N_0 \to \infty$, the geometry of Level 1 units resembles more closely that of a square and thus the Poisson's ratio of the system would approach -1 as expected for the rotating squares model [2].

All this is very significant, since the work presented here shows that it is possible to alter the deformation mechanism, and hence the mechanical properties of a hierarchical rotating rigid unit system simply by changing the resistance to rotational motion of all the hinges in an even manner. This property is not observed in currently known non-hierarchical rotating rigid unit systems and adds another element of versatility to this class of auxetic structures, which has already been shown through previous studies to possess the potential to exhibit a considerable range of mechanical properties through geometric variation alone [329-331]. This means that if, for example, one were to build a hierarchical system where the Level 0 squares are connected together through 'smart/intelligent' hinges with tuneable friction coefficients, one could achieve a considerable range of negative Poisson's ratio without altering the initial geometry of the system. Moreover, the examples discussed here only provide a glimpse of the true potential of these systems. A greater degree of versatility is envisaged if other geometries besides the rotating square motif are employed and if the number of hierarchical levels in the system is increased. This increased versatility could make these systems ideal for a number of niche applications such as smart filters, where the friction coefficients of 'intelligent' hinges may be customized according to the required pore sizes. This way, one filter may be used to filter a range of substances with different parameters, hence reducing material costs. Also, such a filter would be much easier to clean than a normal filter due to the adjustable pore size. Such systems with tunable porosity could also find applications in the design and manufacture of smart dressings as discussed elsewhere [330, 425].

Before concluding, it is important to highlight the fact that whenever there is an even number of units, as a result of the particular design, the considered hierarchical system cannot induce the effect discussed in former chapters, i.e. it cannot induce its global rotation as a result of the rotation of its subunits. However, should one for example change the mass distribution within the structure, so that units rotating in a specific direction would be heavier than units

rotating in the opposite direction, then in theory it should be possible to observe the effect of the self-induced global rotation. Nonetheless, in order for this phenomenon to be manifested, the structure should be deformed internally as opposed to the external application of forces to the system as is the case in this chapter. Such internal deformation could be induced through the appropriate use of actuators located between the adjacent units within the system. It could also be achieved through the use of magnets / electromagnets located on neighbouring rigid units which could change the angle of aperture between the rigid units as a result of mutual interaction. Both of these solutions make it possible to deform different levels of the hierarchical structure independently which effect, as discussed in this chapter, is very difficult to be achieved upon applying external forces to the system. In view of this, it may be expected that the internal deformation of the system allows for a greater control over the deformation pattern of the entire structure and hence it may prove to be useful in the case of applications where one wants the hierarchical structure to assume the particular configuration.

As mentioned in this chapter, in order to achieve the control over the resistance of respective hinges to the rotational motion, one can use the magnetic field which could be induced by magnets which would be appropriately inserted into the system. This means that magnetic inclusions inserted into mechanical metamaterial systems could be expected to affect their mechanical properties. As the matter of fact, as discussed in the Literature Review, there are already a few studies where it was shown that the use of magnetic inclusions could lead to the design of mechanical metamaterials exhibiting anomalous mechanical behaviour which otherwise would not be possible. Also, as recently reported [352], the use of magnetic inclusions may also lead to the design of mechanical metamaterials exhibiting several unusual mechanical properties at the same time which effect is very rarely observed in other classes of mechanical metamaterials. However, despite the potential of mechanical metamaterials with magnetic inclusions to exhibit enhanced unusual mechanical behaviour, the studies related to

this concept are still in their infancy. In view of this, in future chapters, the concept corresponding to the mechanical system with magnetic inclusions exhibiting a number of anomalous properties will be proposed.

Furthermore, up to this point of the thesis, all of the novel types of mechanical behaviour or unusual mechanical properties were exhibited by mechanical metamaterials composed of square/rectangle-like motifs having parallelogram-shaped pores. However, this does not mean that mechanical metamaterials exhibiting counterintuitive properties need to be necessarily built from rigid squares/rectangles. In fact, it has already been amply demonstrated that other motifs built from triangles, rods, etc. can also exhibit unusual mechanical behaviour, as discussed in Chapter 2. One may also argue that it is more than likely that many other new metamaterials constructs will be discovered in the future. The next chapter will look at one such novel motifs, namely simple systems which are built from rigid triangles connected at their vertices, where, like the rotating square/rectangle systems discussed so far, also have parallelogram-shaped pores.

7.4 Conclusions

In conclusion, through a dynamics approach, a simple model was designed to predict the Poisson's ratio and approximately quantify the relative rotations of the units at each hierarchical level for the hierarchical rotating rigid unit systems. It was shown that unlike unilevel systems, the Poisson's ratios and deformation patterns for a given applied load of such hierarchical structures may be altered solely by changing the relative resistance to the rotational motion of the hinges of the systems. This contrasts sharply with the behaviour of other auxetic systems where, unless the geometry of the system is altered, changes in the mechanical properties can only be attained through changes in the interplay of different deformation mechanisms. This is

very significant as it suggests that if one were to construct such a system through the use of hinges where the resistance to the rotational motion could be fine-tuned, then in theory it would possible to control relative deformations of the various hierarchical levels and hence the overall macroscopic and mechanical properties of the system.

8. Mechanical metamaterial composed of generic triangles with the potential to exhibit negative compressibility and negative thermal expansion[5]

HIGHLIGHTS

- Novel design of the mechanical metamaterial system composed of generic rigid triangles connected at vertices is proposed;
- The considered system has a propensity to exhibit negative linear compressibility in at least one direction irrespective of the stage of the mechanical deformation or the type of rigid units constituting the system;
- It is shown that apart from the negative linear compressibility, the proposed system may also exhibit negative thermal expansion.

8.1 Introduction

In this thesis, it was already shown that despite the fact that mechanical metamaterials have been thoroughly studied over the last two decades, it is still possible to propose novel concepts leading either to anomalous mechanical properties or to other types of interesting behaviour. It might be also noted that all of the novel systems discussed in this dissertation, which were capable of exhibiting unusual type of behaviour as the result of their geometry, consisted of rotating rigid square/rectangles motifs. However, this does not mean that it is not possible to propose other types of novel designs of mechanical metamaterials which could have the

[5] The content of this chapter has already been published in the peer-reviewed journal *Smart Materials and Structures*: **K. K. Dudek**, D. Attard, R. Caruana-Gauci, K. W. Wojciechowski, J. N. Grima, Unimode metamaterials exhibiting negative linear compressibility and negative thermal expansions *Smart Mater. Struct.* **25** 025009 (2016)

propensity to exhibit unusual characteristic. As the matter of fact, as discussed in the Literature Review, there is a plethora of novel mechanical metamaterials which in recent years were reported to have a potential of exhibiting unusual mechanical and other types of behaviour. In view of this, in this chapter, a novel type of such system, which was inspired by the work of Prof. Milton [426], will be proposed and analysed in order to assess its mechanical properties.

Milton proposed and generalised various periodic unimode structures (structures that have a single easy mode of deformation [427]) built from rigid bars and pivots [426, 428], including ones built from connected triangles which behave as rotating rigid units [426]. One such system can be described through a sub-structure composed of four triangles which are connected together. Milton regards this structure, which should not be confused with other triangular lattices and geometries which have been extensively studied [255, 288, 290, 300, 301, 429-431], as an expander since an application of a small strain in one direction may result in a considerable enhancement of the strain in the orthogonal direction [426]. In fact, it may be shown that such a structure may lead to very high positive Poisson's ratios in particular directions, which as discussed in this chapter may in turn give rise to NLC.

Milton's work has clearly confirmed that the systems he considers exhibit high expandability. However, generalised mathematical models describing the mechanical behaviour of these systems and similar ones have not yet been established in terms of geometry. In this respect, it would be useful to develop a model which can quantify not only the expandability and expected Poisson's ratios of such systems but also other thermo-mechanical properties, such as thermal expansion or compressibility properties, which could also be of interest.

In view of this, and the important role that the relative rotation of rigid units has in generating anomalous thermomechanical properties, this chapter will look into more general systems which could be potentially constructed from Milton's expander, with the aim of

formulating an analytical model which can predict the Poisson's ratios, compressibility properties and thermal expansion behaviour of such construct.

8.2 The model

Before examining the mechanical properties of these systems, it is useful to discuss their geometries, which are essentially generalisations and variations of Milton's expanders implemented as tessellations. One can establish a basic unit cell for such networks, consisting of two sets of two non-equivalent scalene triangles, as illustrated in Figure 8-1(a). In such a case the shape of the system is describable through seven independent geometric parameters, six of which relate to the shape of the triangles of dimensions of $a \times b \times c$ and $d \times e \times f$ and one which relates to the degree of aperture of the system, angle θ. If one assumes that the triangles are rigid constructs, then the shape and size of this system rely on only one degree of freedom, the angle of aperture, thus qualifying it as a unimode system.

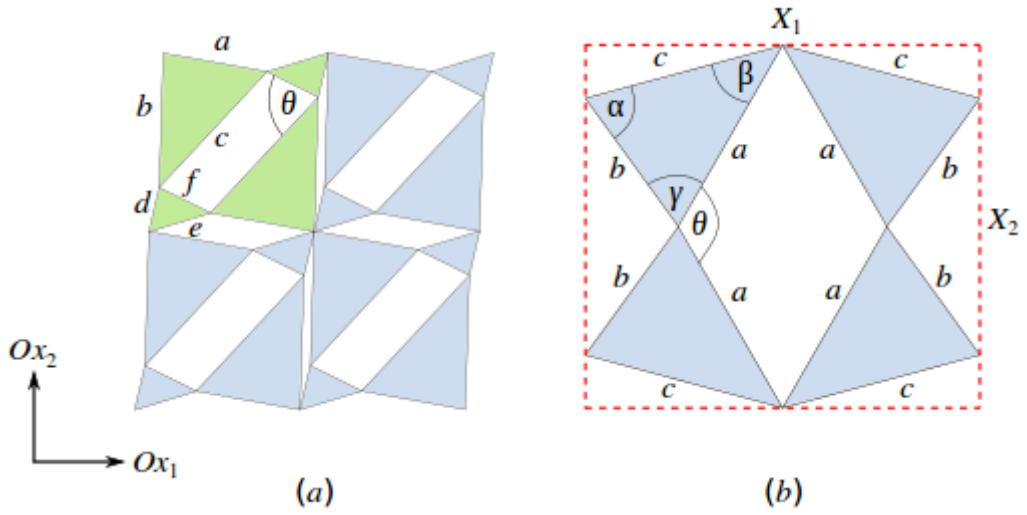

Figure 8-1 (a) A generalised structure based on Milton's expanders (b) the complement unit cell of a typical form of the systems studied here [Taken from [432]].

In this chapter, a simpler case is studied, where only one type of triangle making up the unit cell is considered. The sides of the triangle are denoted as *a*, *b* and *c* which subsequently define the interior angles of the triangle α, β and γ. The angle of aperture is defined by the

angle θ which is twice the angle subtended between the side of length *a* and the Ox_1 direction. The triangles are connected in such a manner that sides of the same length make up the perimeter of the resulting pores (see Figure 8-1(b)). Typically a triangle has all three vertices connected resulting in pores which are rhombic in shape. However there are some cases, in which the triangle has only two connections leaving a free vertex and as a consequence of this, a more complex pore shape is observed. The resulting unit cell always has two lines of symmetry.

For a given triangle the system may be connected together in a tessellatable manner in a number of ways, henceforth referred to as forms. As a result of the geometry, although the different forms are very similar to each other, it is not possible to move from one form to another without permitting overlap of the triangles which de facto means that systems would be constrained to exist in only one of these forms unless the system is dismantled and re-assembled. In other words, depending on the value of θ and the dimensions $a \times b \times c$, only one of the six forms is permissible, i.e. a form may only exist in a bound range of angles, whose limits are henceforth referred to as transition angles θ^*. The transition angles occur whenever one of the three pores in the unit cell assumes a fully closed position. Since each pore has two different closed configurations, a total of six transition angles occur. These transition angles for $0° \le \theta^* \le 360°$ are a function of the interior angles of the triangle and are given by;

$$\theta^* \in \{2\beta, 180° - 2\gamma, 180°, 180° + 2\beta, 360° - 2\gamma, 360°\} \qquad 8\text{-}1$$

Note that the order of occurrence of the transition angles is not always the same and is dependent on the parameters describing the shape of the triangle. As a consequence of this, it is a futile exercise to name the different forms occurring for a general case of $a \times b \times c$.

The dimensions of the unit cell (in this case a width and length of the unit cell respectively) are also a function of the parameters a, b, c and θ and can be expressed as:

$$X_1 = 2\left(\max\left[0, a\cos\left(\frac{\theta}{2}\right), b\cos\left(\gamma+\frac{\theta}{2}\right)\right] - \min\left[0, a\cos\left(\frac{\theta}{2}\right), b\cos\left(\gamma+\frac{\theta}{2}\right)\right]\right) \qquad 8\text{-}2$$

$$X_2 = 2\left(\max\left[0, a\sin\left(\frac{\theta}{2}\right), b\sin\left(\gamma+\frac{\theta}{2}\right)\right] - \min\left[0, a\sin\left(\frac{\theta}{2}\right), b\sin\left(\gamma+\frac{\theta}{2}\right)\right]\right) . \qquad 8\text{-}3$$

Equations describing linear dimensions were obtained by considering a single triangle from the unit cell, calculating the co-ordinates of each of its vertices when the side *a* is aligned horizontally and then performing a rotation transformation by an angle $(\theta/2)$ to get the co-ordinates of the triangle when the degree of aperture of the system is θ. By subtracting the minimum *X* and *Y* co-ordinates from the maximum co-ordinates one can find the dimensions of the unit cell (an example concerning the dimensions of the unit-cell can be found in Appendix IV).

8.2.1 Mechanical properties

Using the obtained expressions for the dimensions of the unit cell, following the methodology discussed elsewhere [202, 287, 288, 290, 430], one can then calculate the Poisson's ratio for each form using:

$$\nu_{12} = \frac{1}{\nu_{21}} = -\frac{\varepsilon_2}{\varepsilon_1} = -\frac{X_1}{X_2}\left(\frac{dX_2}{d\theta}\right)\left(\frac{dX_1}{d\theta}\right)^{-1} . \qquad 8\text{-}4$$

The Young's moduli, assuming a unit thickness *z* (where *z* is of the same order of magnitude of the parameters *a*, *b* and *c*), can be obtained using an energy approach. If the unit cell has an overall stiffness of K_h (which relates to the work required to change the angle of aperture) then the strain energy stored per unit cell, *U* is given by:

$$U = \frac{K_h}{2X_1X_2z}(d\theta)^2 . \qquad 8\text{-}5$$

The Young's modulus is related to the strain energy by:

$$E_i = \frac{2U}{\varepsilon_i^{\,2}} = K_h \frac{X_i^{\,2}}{X_1 X_2 z}\left(\frac{dX_i}{d\theta}\right)^{-2} \qquad \text{where } i = 1, 2 \,. \tag{8-6}$$

One may also write expressions for the linear compressibilities along the Ox_1 and Ox_2 directions [433] in terms of the Young's moduli and Poisson's ratios:

$$\beta_L\left[Ox_1\right] = \frac{1}{E_1} - \frac{\nu_{21}}{E_2} \tag{8-7}$$

$$\beta_L\left[Ox_2\right] = \frac{1}{E_2} - \frac{\nu_{12}}{E_1} \,. \tag{8-8}$$

The area compressibility can be found from the linear compressibilities through:

$$\beta_A = \beta_L\left[Ox_1\right] + \beta_L\left[Ox_2\right] \,. \tag{8-9}$$

8.2.2 Thermal properties

Apart from the mechanical properties of the model under consideration, one could also investigate the thermal expansion properties of the presented system, based on the work on RUMs (Rigid Unit Modes) which has already been done in the field of thermal expansion [434-437]. If the system is in a conformation having a maximum area when in its cold state (corresponding to the temperature in the vicinity of 0 K), where the angle between the units is $\theta = \theta_0$, then it is possible for it to exhibit a NTE (negative thermal expansion) upon heating as the units vibrate with an amplitude of $\Delta\theta$ about θ_0.

To simplify the analysis, based on previous work [434, 438], the following assumptions will be made, namely that (i) the units are rigid so that the only mode of deformation is through rotation; (ii) the rigid units behave as harmonic oscillators so that the thermal average of $\Delta\theta$ at a given temperature *T*, i.e. $\langle\Delta\theta\rangle_T$ is zero; (iii) the amplitude of oscillations is small so as to allow for small angle approximations for terms involving $\Delta\theta$.

For the sake of simplicity, systems constructed from isosceles triangles with $b = c > a$ shall be used as an example to illustrate this NTE effect. For such a case, as discussed in further detail in the discussion, the form which occurs in the range of $180° - 2\gamma < \theta < 2\beta$ is one of the most predominant forms and also has the maximum area for the system. For such a form, the unit cell dimensions can be expressed by means of the following equations:

$$X_1 = a\cos\left(\frac{\theta}{2}\right) - b\cos\left(\frac{\theta}{2}\right) \qquad \text{and} \qquad X_2 = b\sin\left(\gamma + \frac{\theta}{2}\right). \tag{8-10}$$

Thus the area of the unit-cell may be defined as a product of the above quantities, hence:

$$A(\theta) = X_1 \cdot X_2 = b\left[a\cos\left(\frac{\theta}{2}\right)\sin\left(\gamma + \frac{\theta}{2}\right) - b\cos\left(\gamma + \frac{\theta}{2}\right)\sin\left(\gamma + \frac{\theta}{2}\right)\right]. \tag{8-11}$$

From this equation it can be shown that the maximum area of the unit-cell occurs at $\theta_0 = \frac{\pi}{2}$ about which point it is also symmetric such that $A(\theta_0 + \Delta\theta) = A(\theta_0 - \Delta\theta)$. Subsequently, the area can be expressed in terms of the equilibrium angle θ_0 and its change $\Delta\theta$ as follows (see Appendix IV for the derivation):

$$\begin{aligned} A\left(\frac{\pi}{2} + \Delta\theta\right) &= b\left[\frac{a}{2}\sin\left(\gamma + \frac{\pi}{2} + \Delta\theta\right) + \frac{a}{2}\sin\gamma - \frac{b}{2}\sin\left(2\gamma + \frac{\pi}{2} + \Delta\theta\right)\right] \\ &= \frac{ba}{2}\left(\cos\gamma\cos\Delta\theta - \sin\gamma\sin\Delta\theta\right) + \frac{ba}{2}\sin\gamma \\ &\quad - \frac{b^2}{2}\left(\cos 2\gamma\cos\Delta\theta - \sin 2\gamma\sin\Delta\theta\right) \end{aligned} \tag{8-12}$$

Assuming the change in angle, $\Delta\theta$, is small, this equation can be further simplified, using the Taylor series $\left(\cos\Delta\theta \approx 1 - \frac{\left\langle \Delta\theta^2 \right\rangle_T}{2} \text{ and } \sin\Delta\theta \approx \Delta\theta \approx 0\right)$, so that the thermal average of the area can be expressed by:

$$\left\langle A \right\rangle_T = b\left[\frac{a}{2}\cos\gamma\left(1 - \frac{\left\langle \Delta\theta^2 \right\rangle_T}{2}\right) + \frac{a}{2}\sin\gamma - \frac{b}{2}\cos 2\gamma\left(1 - \frac{\left\langle \Delta\theta^2 \right\rangle_T}{2}\right)\right]. \tag{8-13}$$

In order to express $\left\langle \Delta\theta^2 \right\rangle_T$ in terms of the temperature *T* one could use the approach proposed in [434] which is based on the principle of the equipartition of the energy, which states

that every mode, of which there is only one in this case, is provided with the energy equal to $\frac{1}{2}k_BT$ where k_B is the Boltzmann constant (1.38×10^{-23} J K^{-1}). Thus:

$$\frac{1}{2}I\omega^2\left\langle\Delta\theta^2\right\rangle_T=\frac{1}{2}k_BT \qquad 8\text{-}14$$

where I is the moment of inertia of the rotating rigid units and ω is the frequency by which the units oscillate. This gives a thermal expansion coefficient α_A of:

$$\alpha_A=\frac{k_B\left(b\cos(2\gamma)-a\cos(\gamma)\right)}{2aI\omega^2\sin(\gamma)+a\left(2I\omega^2-k_BT\right)\cos(\gamma)-b\left(2I\omega^2-k_BT\right)\cos(2\gamma)}\ . \qquad 8\text{-}15$$

8.3 Results and Discussion

Plots for the dimensions and mechanical properties of three particular cases of triangles (equilateral, isosceles and scalene) are presented in Figure 8-2 and Figure 8-3. The plots are divided into regions corresponding to different forms of the triangles (diagrams representing these three types of triangles and their respective forms and transitions can be found in Appendix IV). It is evident that on changing the geometry of the triangle, the mechanical properties change accordingly. However, before discussing the actual mechanical properties of the systems, it is useful to first discuss the constructability or otherwise of these systems, i.e. the number of forms that such systems can have and the angle range over which these forms occur. This will be followed by a discussion of thermomechanical properties afforded by these systems.

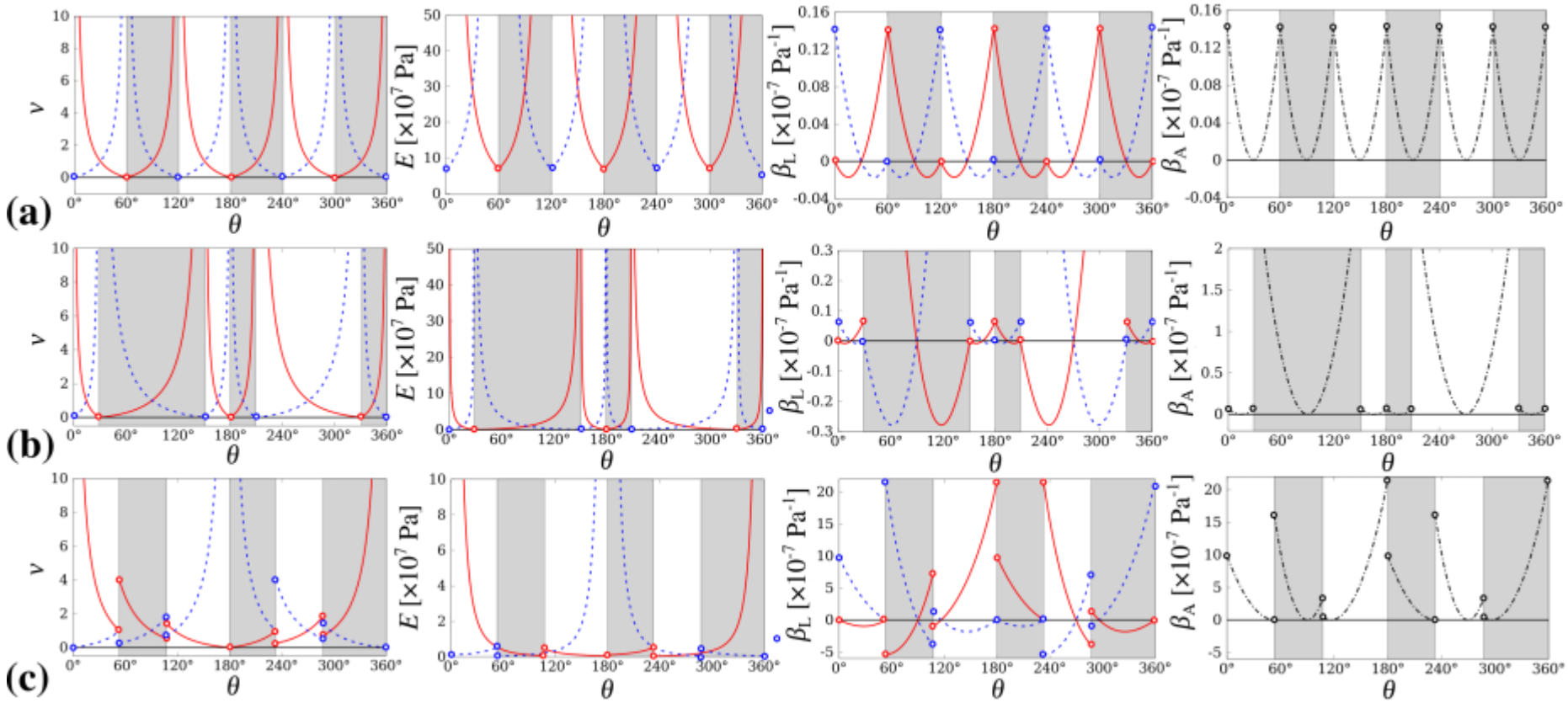

Figure 8-2 Variation in mechanical properties for three different types of systems. Panels show results for systems where the unit-cell is composed of (a) equilateral triangles having dimensions a = 1 nm, b = 1 nm and c = 1 nm, (b) isosceles triangles corresponding to dimensions a = 1 nm, b = 2 nm and c = 2 nm and (c) scalene triangles where a = 6 nm, b = 3 nm and c = 4 nm. Solid red and dashed blue lines indicate mechanical properties exhibited by the system in the Ox_1 and Ox_2 directions respectively. Different colours on of the background helps to make a distinction between different forms assumed by considered systems [Taken from [432]].

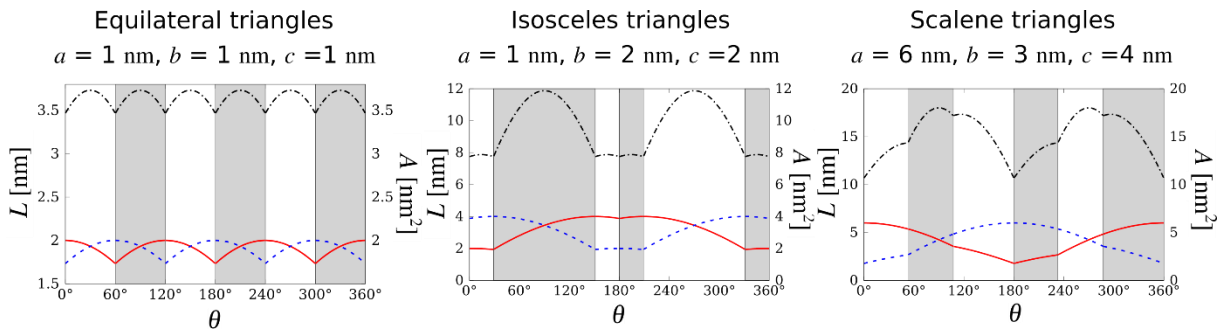

Figure 8-3 Variation in geometric dimensions of the unit-cell for three different types of systems. Solid red and dashed blue lines indicate mechanical properties exhibited by the system in the Ox_1 and Ox_2 directions respectively. The black dashed line represents the area of the unit-cell corresponding to a given system [Taken from [432]].

Looking at the constructability of these systems, it should be noted that the range of angles over which the different forms occur changes with the shape of the triangle, even though there are always six of such forms. For an equilateral triangle, all six forms will each have a range of 60°, whilst for an isosceles triangle, four forms will have the same extent of range and two forms will have the same extent of range, which range is different from the other four forms. On the other hand, a scalene triangle will have three pairs of forms where each pair has the same extent of range, which extent is different from that of other pairs. This pairing up of forms occurs since these forms are a $90°$ rotation of each other. Thus on considering all types of triangles, it becomes evident that the change in the extent of the ranges is related to the ratio of the sides of the triangles. On increasing the disparity of the sides (and hence changing their ratio), the extent of the ranges changes accordingly. This can be observed, especially for isosceles triangles, from figures Figure 8-2, Figure 8-3 and Figure 8-4. This kind of behaviour is reflected in all the mechanical properties of the systems. It must be mentioned that if one were to increase the sides of the triangle in such a manner so as to keep the same ratio, the

extent of the ranges will remain unchanged but the magnitude of the mechanical properties is affected except for the Poisson's ratio since this is scale independent.

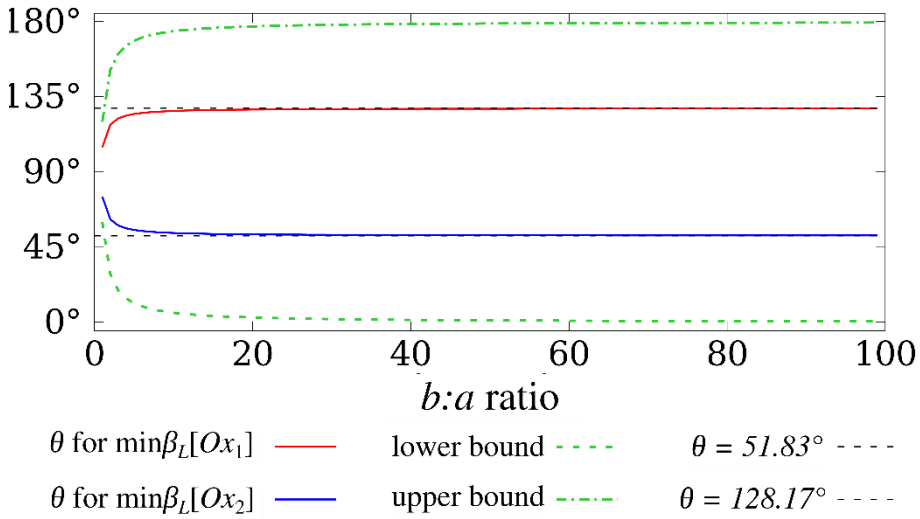

Figure 8-4 Variation of the range of angles in which NLC is exhibited for a particular form on changing the *b*:*a* ratio of an isosceles triangle.

In terms of the mechanical properties, a look at the plots shown in Figure 8-2 will reveal that the mechanical properties afforded by the systems are highly dependent on the form in which the system exists, with a marked discontinuity in the mechanical properties between one region and the next. This is because at the transition angles, the forms are in a locked conformation and hence the mechanical properties at that particular angle cannot be defined. This is in contrast to the behaviour of the unit cell dimensions which are characterised by a continuous transition from one form to the next. This implies that at the transition angles, both forms have the same dimensions.

On examining the Poisson's ratio for all three different types of triangles presented, it is evident that the Poisson's ratio is positive for all values of θ and can have large values, i.e. there is no auxetic behaviour. These large values tend to occur when the derivative of the dimension along which the system is being loaded tends to zero. In the case of the equilateral and isosceles triangles, such behaviour is observed at the vicinity of each transition angle. A similar behaviour is also observed for the Young's moduli.

It is also evident from the plots in Figure 8-2 and Figure 8-3 that all the systems considered exhibit NLC. In fact, for the whole range of θ-values the systems exhibit NLC along Ox_1 or Ox_2 but never in both directions simultaneously. This ensures that the area compressibility β_A is never negative, so that on application of a hydrostatic pressure, the area of the system always decreases, resulting in densification of the system, even though one dimension may increase in size. Thus the 2D equivalent of the bulk modulus of these systems is always positive. It is interesting to note that the total range over which NLC is observed along the Ox_1 direction is equal to that over which NLC is observed along the Ox_2 direction. In other words, NLC is observed in the Ox_1 and Ox_2 over a total range of almost $180°$ for each direction (except for values at the transition angles, at which values, compressibility is undefined).

On further examination of the plots, it can be observed that for each form, the range in which NLC occurs is bound. The bounds correspond to the instance where the unit cell of that form has a maximum area and by the instance when the form is fully opened in one of its major axis which occurs at the transition angle. When the area of a form is close to its maximum, applying a hydrostatic pressure causes it to decrease. Since the Poisson's ratio of the system is positive for all angles, then on application of a hydrostatic pressure, one of the unit cell dimension increases in length exhibiting NLC whilst the other unit cell dimension decreases in length, exhibiting positive linear compressibility. This effect is observed until the unit cell dimension which is increasing in length achieves a fully extended position, at which point the transition angle would have been reached.

Another way of describing the range in which NLC is observed is through the Poisson's ratios. It can be shown that in cases where deformation occurs through a unimode hinging mechanism, as in the systems described here, typically, the Poisson's ratio fulfils the relation $\nu_{12} = (\nu_{21})^{-1}$. In such cases, it follows from equations 8-4 and 8-6 that the occurrence of NLC

along Ox_1 direction (equation 8-7) can be expressed by the requirement that the strains along the Ox_1 and Ox_2 directions, ε_1 and ε_2 respectively, must satisfy the condition $\varepsilon_1^2 + \varepsilon_1\varepsilon_2 < 0$, i.e. $\varepsilon_1\varepsilon_2 < 0$ and $|\varepsilon_1\varepsilon_2| > \varepsilon_1^2$. This condition is satisfied whenever $|\varepsilon_2| > |\varepsilon_1|$ and the Poisson's ratios are positive (see Appendix IV for a detailed derivation). Thus, when $\nu_{12} > 1$, $\beta_L[Ox_1] < 0$. In a more general manner, this means that whenever one of the Poisson's ratios for loading in one direction is greater than +1 (and hence larger than the Poisson's ratio for loading along the other direction because of their inverse relation), NLC is observed in that direction.

It should also be mentioned here that the magnitude of NLC is affected by the shape and size of the triangles. Considering an isosceles triangle (b=c) for the sake of simplicity (but similar arguments may also hold for scalene triangles), on increasing the sides but keeping the same aspect ratio, the magnitude of the compressibilities increases accordingly, while the range over which NLC is exhibited for a particular form remains unchanged. On the other hand, if the b:a ratio of the isosceles triangles increases from 1, NLC values become more negative and one of the forms becomes increasingly more predominant. In the limit that this ratio approaches infinity, when virtually only one form is possible, the triangles become flattened to a line, and geometry wise, the structure becomes similar to a wine-rack. As illustrated in Figure 8-4, on increasing the b:a ratio, the angles at which the most NLC values occur tend to that of 128.17° or 51.83° (corresponding to $\beta_L[Ox_1]$ and $\beta_L[Ox_2]$ respectively) which angles are identical to that at which the wine-rack-type mechanism exhibits minimum (most negative) linear compressibility [439]. These angles do not seem to have any particular geometrical significance but are obtained on solving for the minimum compressibilities. In fact, in the particular cases where $b > a$, the form with the widest extent of range and which exhibits the most negative values for linear compressibility has the cell parameters:

$$X_1 = 2a\cos\left(\frac{\theta}{2}\right) - 2b\cos\left(\gamma + \frac{\theta}{2}\right) \qquad 8\text{-}16$$

$$X_2 = 2b\sin\left(\gamma + \frac{\theta}{2}\right) . \qquad 8\text{-}17$$

In the limit that $b \gg a$, $\gamma \to 90°$ and hence the above equations may be expressed by:

$$X_1 \approx 2b\sin\left(\frac{\theta}{2}\right) \qquad \text{and} \qquad \mathrm{X}_2 \approx 2\mathrm{bsin}\left(\gamma + \frac{\theta}{2}\right) \qquad 8\text{-}18$$

which equations correspond to that of the wine-rack-like [439] structure after recognising the differences in orientation.

In terms of the thermal expansion properties, the equations derived above, particularly equation 8-15 suggests that the system presented here may also exhibit NTE, that is, it decreases in size along one or more directions on the application of heat. From the plots of the unit-cell parameters (see Figure 8-2) it is evident that at certain angles of aperture the unit-cell has a maximum area. If on heating, the system oscillates about a point of maximum area configuration via a 'RUM', as discussed in various works [434-436] its area will decrease. This is of particular significance as it suggests that the presented system may exhibit both NLC (Negative Linear Compressibility) and NTE.

Moreover, as evident from equation 8-15, the magnitude of the coefficient of thermal expansion is dependent on the shape of the isosceles triangles, i.e. on the ratio of the side dimensions. This is illustrated more clearly in Figure 8-5 which shows how the coefficient of thermal expansion for a system of isosceles triangles vibrating about an equilibrium angle of 90° (which angle, as illustrated in Figure 8-3, is a point of maximum area) changes with the shape of the isosceles triangles. In the cases considered the temperature was set to be equal to T = 293 K and the value of $I\omega^2$ was set to be equal to $75k_BT$. In general the dimensions of the triangular units could be assigned arbitrary values in the nano-scale. In these cases the value of *a* was kept constant at 0.5 nm whilst the lengths of sides *b* and *c* were increased up to 50 nm in

steps of 0.001 nm. The plot in Figure 8-5 suggests that, in this case, the magnitude of NTE increases as the triangles become more slender, as was the case for the compressibility. Here, it should be highlighted that the plot only represents one of the six forms in which the system can exist. There may be other forms which also give rise to NTE, albeit to a different extent, as is clear from the plot of area against θ in Figure 8-3, where for any type of triangle, more than one area maximum occur.

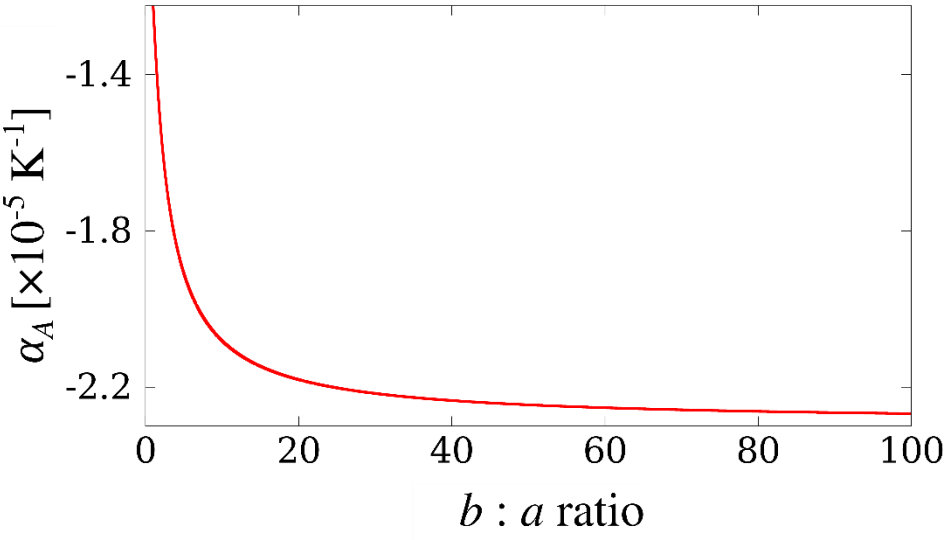

Figure 8-5 Variation of the thermal expansion coefficient with the aspect ratio of isosceles triangles for systems where $b = c > a = 1$ having a form that exists for $180° - 2\gamma < \theta < 2\beta$ and vibrating about an equilibrium angle of $90°$. The temperature was set to be equal to T = 293 K and the value of $I\omega^2$ was set to be equal to $75k_BT$. The provided results were generated by means of the expression for the area thermal expansion coefficient α_A, which expression was derived based on the procedure proposed by Welche *et al.* [434].

All this is very significant because the system studied here can be used as a blueprint to design materials that not only have NLC but also NTE concurrently. Also significant is the finding made through this work that although networks constructed from rotating rigid triangles are usually closely associated with auxeticity, this may not always be the case as clearly illustrated by the systems considered here which instead can exhibit giant positive Poisson's ratio properties which are conducive to NLC. This highlights the versatility of these systems which when designed in a specific geometric conformation have the potential to exhibit tailored

negative properties. Possible applications for systems which exhibit NLC include their use in high pressure environments and as sensitive interferometric pressure sensors [433]. NTE materials are sought for their use in obtaining composites with tailored coefficients of thermal expansion. Such composites could be used in a variety of ways ranging from dental fillings [440] to solar arrays in telescopes [441] and other applications which involve large fluctuations in temperature that could lead to thermal cracking.

Before concluding one should mention that although a prima facie both equations describing the compressibility and thermal expansion of the systems seem to be only dependent on the ratios of the sides of the triangles, the NLC and NTE effects described here are likely to manifest themselves only if the system is at a molecular scale. For the thermal expansion analysis described here to apply, the structural features must be small enough for thermal vibrational motion to be present. One would not expect such thermal vibrations, and hence such a mechanism, to occur on a macro-scale structure. Similarly, the mechanism responsible for NLC in the model presented here is such that the hydrostatic pressure is only exerted on the outside of the system, that is, the fluid particles exerting the hydrostatic pressure on the system should not permeate through the system (as discussed in [439]). Thus it may be difficult for such a mechanism to operate at a macroscale, however, it may manifest itself at a nano level, providing the material has the necessary geometric features which allow this mechanism to occur, which ideally is also the only mechanism of deformation. Other modes of deformation acting concurrently with the hinging mechanism may in fact diminish the effect of NLC where it exists [439], although, they may themselves cause NLC in particular directions to be exhibited over a larger range of angles.

8.4 Future perspectives

In this chapter, it was shown that despite thorough studies on mechanical metamaterials, it is still possible to design novel systems with the potential to exhibit anomalous mechanical

behaviour. In order to do that, a particular mechanical metamaterial system composed or rigid triangles connected at vertices was investigated in terms of its propensity to exhibit unusual mechanical behaviour such as negative linear compressibility and negative thermal expansion. However, the fact that such system has a potential to exhibit unusual mechanical properties does not mean that it cannot manifest other type of behaviour which is discussed in this thesis.

For example, in theory, as shown schematically in Figure 8-6(a), one could consider the use of the mechanical metamaterial consisting of rigid triangles in order to induce its global rotation as a result of the rotation of its subunits. This stems from the fact that the only condition required in order to observe the discussed phenomenon is a non-zero net angular momentum associated with the motion of subunits which effect similarly as was the case for rigid squares could be achieved for example by the variation in the mass of units rotating in opposite directions.

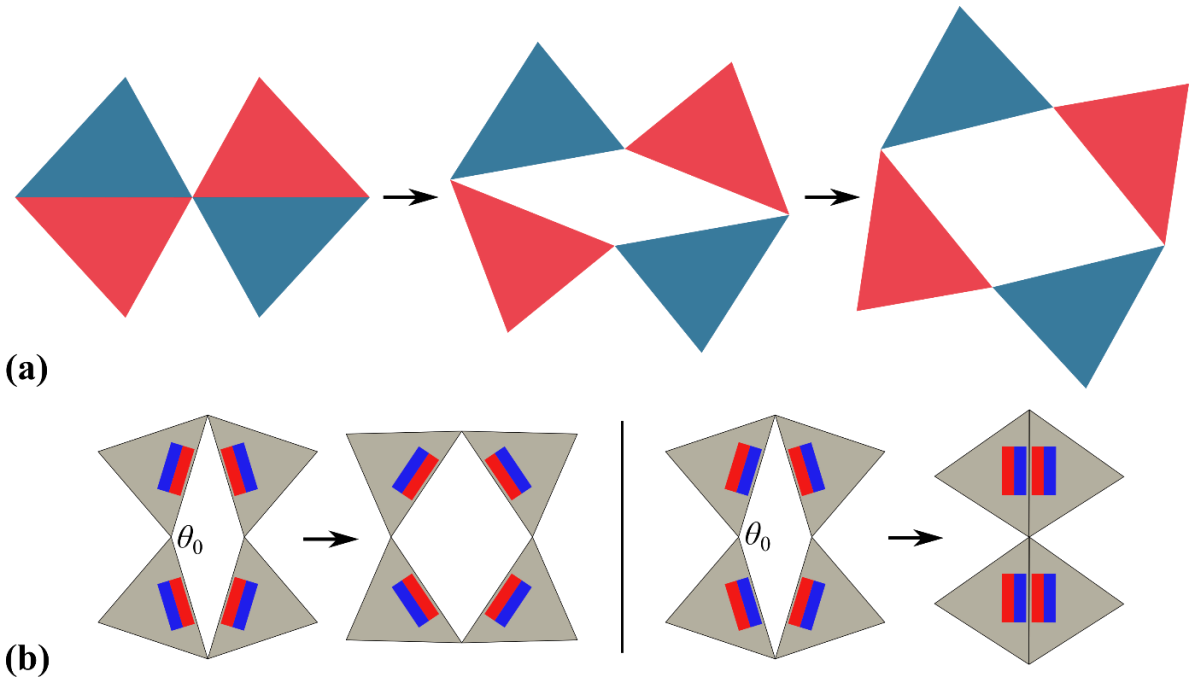

Figure 8-6 Panels show: (a) a visualisation of the hypothetical concept related to the self-induced global rotation of mechanical metamaterials composed of triangle motifs having different masses and (b) expected behaviour of the rotating rigid triangle systems with magnetic inclusions. In the case of diagrams shown on panel (b), the blue and red colour were used in order to indicate the north and south pole of magnets.

It is also possible to consider the use of magnetic inclusions in such systems in order to change the way how they deform which concept is shown schematically in Figure 8-6(b). Depending on the position and orientation of magnetic inclusions within the system, one could also expect that it would be possible to control the stiffness exhibited by the structure. One can also note that the behaviour of such system can be controlled solely as a result of magnetic interactions between magnetic inclusions which concept may lead to a design of programmable magneto-mechanical systems. For example, shown schematically in Figure 8-6(b) are the same mechanical systems with two different conformations of magnets. The system on the left has the magnets impregnated within it in a manner where the adjacent magnets tend to repel each other with the result that the system would prefer to adopt a conformation where the angle θ_0 tends to decrease. On the other hand, the system on the right hand side has the magnets inserted into the structure in a different manner with the result that the system would prefer to increase the angle θ_0. This shows that metamaterials with magnetic inclusions merit to be further studied in view of the properties they may achieve as a result of magnetic interactions. In view of this, the next chapters will look more closely at systems with magnetic inclusions.

8.5 Conclusions

In this chapter, it was shown that mechanical metamaterials composed of rigid triangles have a potential to exhibit negative linear compressibility in at least one direction irrespective of the type of the system or stage of a deformation. This stems from the high positive Poisson's ratio which is always exhibited by this system in the considered directions. As a matter of fact, it was even shown that there is a link between the negative compressibility and the value of the Poisson's ratio, i.e. whenever the value of the Poisson's ratio exceeds one then the system exhibits negative compressibility in this particular direction. Furthermore, upon analysing the

results presented in this chapter, it was also clear that the extent of investigated mechanical properties changes depending on the particular geometry of the system. Another interesting result reported in this chapter is associated with the propensity of the discussed system to exhibit negative thermal expansion. Finally, the potential of the proposed model to utilise some of the other concepts which are studied in this thesis was also discussed which hopefully will lead to the further interest of the scientific community in this system as well as in mechanical metamaterials in general.

9. Mechanical metamaterials with magnetic inclusions with the potential to exhibit both negative stiffness and auxetic behaviour simultaneously[6]

HIGHLIGHTS

- It is shown both by means of the theoretical model and experimental testing that magnetic inclusions can be used to alter the stiffness, where, depending on the orientation of magnets within the system, the considered mechanical metamaterial with magnetic inclusions may exhibit either positive or negative stiffness;
- The discussed magneto-mechanical system (metamaterial) is capable of exhibiting two different anomalous mechanical properties, i.e. negative stiffness and negative Poisson's ratio, at the same time;
- It is shown that the magnitude of the stiffness exhibited by the system may be controlled via the variation in the magnetic moment of magnets (which would not change the Poisson's ratio) or the change in the geometric parameters (which could change the Poisson's ratio).

9.1 Introduction

As discussed in the earlier chapters and literature review, scientists working in the field of materials science are becoming increasingly more interested in the concept of mechanical

[6] The content of this chapter is currently under review in the peer-reviewed journal Proceedings of the Royal Society A: **K. K. Dudek**, R. Gatt, M. R. Dudek, J. N. Grima, Negative and positive stiffness in auxetic magneto-mechanical metamaterials *Proc. Royal Soc. A* (2018)

metamaterials with magnetic inclusions [401, 406, 411, 442, 443]. This stems from the fact that, for example, as mentioned at the end of the last chapter, the use of magnetic inclusions may not only further enhance mechanical properties exhibited by the system but also potentially lead to the control over them. Some of the most promising studies related to this concept correspond to the possibility of incorporating magnetic inclusions into the system in a way resulting in the structure exhibiting negative stiffness which property as discussed in the Introduction and in the Literature review is highly desired due to potential applications where it can be implemented (variety of vibration damping devices etc.).

Despite the fact that it is known that negative stiffness can be exhibited by attracting magnets, which concept was confirmed both through theory and experimental studies [381, 413, 444], scientists working in the field of mechanical metamaterials have been primarily focused on the potential of mechanical metamaterials to exhibit negative stiffness as the result of their geometry. However, as shown in the recent work by Hewage *et al.* [352], the use magnetic inclusions may allow mechanical metamaterials to exhibit several anomalous characteristics at the same time. More specifically, it was shown that a particular mechanical metamaterial may simultaneously exhibit negative Poisson's ratio and negative stiffness. Studies on such systems are very important as they may lead to the implementation of mechanical metamaterials with magnetic inclusions in novel branches of the industry where the use of materials exhibiting several anomalous properties at the same time would be required.

In this chapter, the particular mechanical metamaterial system [445] which is historically known to exhibit negative Poisson's ratio, will be investigated from the point of view of its potential to exhibit negative stiffness after the insertion of magnetic inclusions in the form of magnets into it. Based both on theoretical studies and the experimental results, the effect of the orientation of magnets within the system on its stability and mechanical properties will be analysed. In this chapter, it will be also discussed that the use of magnetic inclusions may lead

to the negative stiffness in the case of otherwise conventional systems exhibiting positive stiffness.

9.2 Concept

The mechanical system investigated in this work corresponds to the mechanical metamaterial composed of "arrow head" units which was proposed by Larsen and Sigmund *et al.* [445]. This system is historically known to have a propensity to exhibit negative Poisson's ratio in the case when it deforms solely via the hinging of rigid bars having a length of l_a and l_b (see Figure 1-2) which constitute the structure. In the case of this work, for all of the considered cases $l_a > l_b$. Furthermore, as shown in Figure 9-1, the angle between ligaments corresponding to lengths l_a and l_b is denoted by θ, where it may be noted that the angle θ is the only parameter describing the configuration assumed by the system, hence the entire process of the mechanical deformation can be discussed in terms of the variation in this parameter. As the matter of fact, it might be even shown that for such system deforming solely as the result of hinging of rigid bars, the in-plane Poisson's ratio corresponding to loading in the vertical direction may be defined as follows:

$$\nu_{yx} = \frac{\left(l_a - l_b \cos\theta\right)\left(l_b - l_a \cos\theta\right)}{l_a l_b \sin^2\theta} \qquad 9\text{-}1$$

where for a particular system it will only depend on the variation in θ.

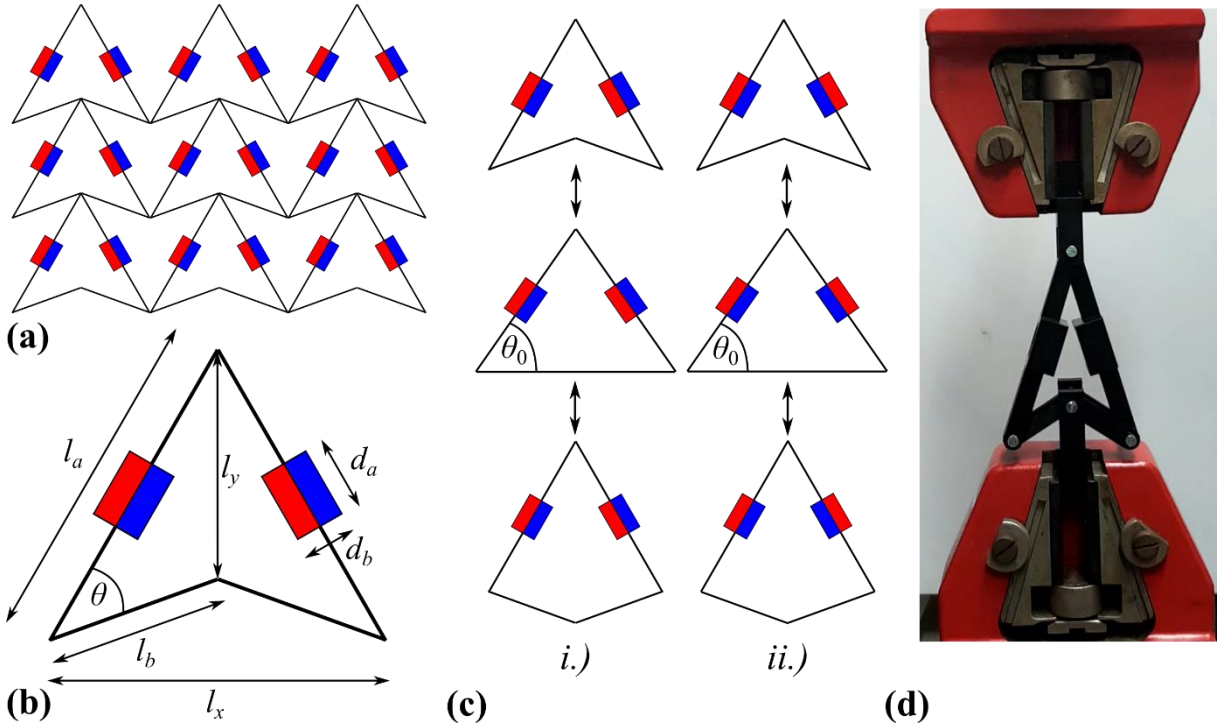

Figure 9-1 Panels show: (a) the considered system composed of a number of arrowhead units with magnetic inclusions, (b) a single unit of the system, (c)(i) stages of the mechanical deformation in the system with attracting magnets in each unit (ii) stages of the mechanical deformation in the system with attracting magnets in each unit and (d) experimental prototype used in order to investigate mechanical properties of the considered system.

As shown in Figure 9-1(b), within each unit of the considered mechanical system, there are magnetic inclusions in the form of magnets corresponding to linear dimensions d_a and d_b. These magnetic inclusions are located in the middle of bars having a length of l_a with their orientation being such that the magnetic dipole moment $\vec{\mu}$ associated with each of the magnets is always orthogonal to the bar on which the given magnet is located. It is assumed that all of the magnets within the system are identical and that there is no other source of the magnetic field within the system. It is also assumed that the rigid bars constituting the system are made of the non-magnetic material as otherwise the interaction between magnets and rigid bars should be taken into consideration.

Due to the particular geometry of the considered system, upon being extended in the vertical direction from the configuration corresponding to the angle $\theta_{\min}$ to the threshold

configuration associated with the angle θ_0, the system shown in Figure 9-1 would deform in a way resulting in the increase in the separation distance between magnets within a given unit. Upon assuming that magnets within the system are oriented as shown in Figure 9-1(a) and Figure 9-1(c-i), then their interaction offering the resistance to the vertical deformation of the system assumes the maximum value at the initial configuration associated with $\theta = \theta_{\min}$. This means that as the distance between neighbouring magnets increases as the result of vertical pulling, the strength of interaction between magnets decreases which in turn decreases the resistance which must be overcome in order to deform the system. In other words, throughout the deformation from the configuration corresponding to $\theta = \theta_{\min}$ to the threshold configuration $\left(\theta = \theta_0\right)$, it becomes increasingly simpler do deform the system. After surpassing the threshold configuration in an attempt to extend the system to the final configuration associated with the angle $\theta = \theta_{\max}$, the distance between the magnets starts decreasing and hence the magnitude of interaction between magnets increases. However, upon surpassing the threshold conformation, the interaction between attracting magnets promotes the deformation of the system in the vertical direction. In view of this, throughout the entire process of mechanical deformation from the configuration corresponding to the angle $\theta = \theta_{\min}$ to the configuration associated with the angle $\theta = \theta_{\max}$, it becomes increasingly simpler to overcome the resistance offered by the magnets and deform the system. According to the definition provided in this thesis, such anomalous behaviour is an indication of the negative stiffness (negative tangent / incremental stiffness). In terms of the force F $\left(F = \left|\vec{F}\right|\right)$ which should be applied to the topmost and bottommost part of the structure (see Figure 9-1(d)) in order to induce the vertical extension of the system at the constant rate, its magnitude would initially assume large positive values (in the vicinity of $\theta = \theta_{\min}$) in order to keep decreasing up to the end of the deformation process

where the system assumes the conformation corresponding to $\theta = \theta_{\max}$. Conversely, upon changing the orientation of magnets within the system so that within each of the units they would be repelling each other (see Figure 9-1(c-ii)), the opposite behaviour should be expected with the system exhibiting positive stiffness throughout the whole process of deformation as a result of magnetic interaction between magnets.

At this point, it is also important to note that the analogical behaviour of the system would be observed should the deformation process be reversed. This means that for example in the case of the system with attracting magnets within the unit, the system would also exhibit negative stiffness upon being deformed from the configuration corresponding to $\theta = \theta_{\max}$ to the configuration associated with $\theta = \theta_{\min}$.

9.3 Simulations

In order to investigate the considered system by means of the theoretical model, it is assumed that rigid bars constituting the system are highly idealised and apart from being perfectly rigid they also do not offer any resistance to the hinging process, which is the only mechanism corresponding to the deformation of the structure. It is also assumed that magnets inserted into the system are uniformly magnetised and have a magnetic dipole moment $\vec{\mu}$. Due to the fact that in this work, that size of magnets is not expected to be negligible in comparison to the distance between neighbouring magnets, it is assumed that each magnet can be represented by an array of $N_a \times N_b$ magnetic dipoles having a magnitude $\left|\vec{\mu}_{\text{int}}\right|$ which can be defined as follows [406]:

$$\left|\vec{\mu}_{\text{int}}\right| = \frac{1}{N}\left|\vec{\mu}\right| \qquad 9\text{-}2$$

where, *N* represents the number of magnetic dipoles constituting a given magnet $\left(N = N_a \times N_b\right)$. In the case of this chapter, quantities N_a and N_b were set to be equal to 20 and 10 respectively. The separation distances between respective magnetic dipoles are defined in the following manner:

$$s_a = \frac{d_a}{N_a - 1} \qquad \text{and} \qquad s_b = \frac{d_b}{N_b - 1} \ . \tag{9-3}$$

In order to analyse stability of the considered system at a particular configuration, it is first necessary to calculate its magnetic potential energy. To calculate such energy for individual magnets, one must determine the energy of interaction of individual magnetic dipoles located on the considered magnet with all of the magnetic dipoles associated with remaining magnets within the system. As shown in the literature [406, 446], the potential energy of an arbitrary *i*-th magnetic dipole interacting with the *j*-th magnetic dipole located on an arbitrary neighbouring magnet, can be defined as shown below:

$$U_{i,j}^{MAG} = -\left(\vec{\mu}_i \cdot \vec{B}_j\right) \tag{9-4}$$

where, $\vec{B}_j$ represents the magnetic field associated with the aforementioned *j*-th magnetic dipole measured at the point where the *i*-th magnetic dipole is located $\left(\left|\vec{\mu}_i\right| = \left|\vec{\mu}_j\right| = \left|\vec{\mu}_{\text{int}}\right|\right)$. Such magnetic field can be defined as follows [406, 446]:

$$\vec{B}_j = \frac{\mu_0}{4\pi}\left(\frac{3\left[\vec{\mu}_j \cdot \vec{r}\right]\vec{r}}{\left|\vec{r}\right|^5} - \frac{\vec{\mu}_j}{\left|\vec{r}\right|^3}\right) \tag{9-5}$$

where, $\vec{r}$ is the position vector pointing from the *j*-th magnetic dipole to the *i*-th magnetic dipole on the considered magnet. This also means that $\left|\vec{r}\right|$ stands for a distance between the two magnetic dipoles. At this point, it should be noted that due to the particular geometry of the system, the only possible difference between vectors $\vec{\mu}_i$ and $\vec{\mu}_j$ corresponding to the *i*-th and *j*-th magnetic dipole respectively is the sign. It should also be highlighted that in this work, the

interactions of magnetic dipoles located on the same magnet with each other are not taken into consideration.

Based on equations 9-4 and 9-5, and upon taking all of the dipole-dipole interactions for each of the magnetic dipoles from the considered magnet into consideration, it is possible to write down the expression corresponding to the total magnetic potential energy of the single magnet within the discussed system U^{MAG} in the following manner:

$$U^{MAG} = \sum_{neighbours} \left(\sum_{i=1}^{N} \sum_{j=1}^{N} U_{i,j}^{MAG} \right). \qquad 9\text{-}6$$

The first sum in the above equation corresponds to a number of neighbours of a single magnet. It should be noted that in the particular case when the system would consist of only one arrowhead unit (see Figure 9-1(b-d)), the first summation would disappear as there would be only one magnet apart from the magnet for which the energy would be calculated. One can also consider whether for a hypothetical very large or infinite system it is necessary to calculate the energy of a particular magnet based on all of the magnets within the system. As shown in equation 9-5, the magnitude of the magnetic field corresponding to the interaction between any two magnets decreases proportionally to their separation distance raised to the power of -3. This means that very distant magnets would make a negligible contribution to the energy of the given magnet. Thus, in order to obtain a reliable information regarding the magnetic potential energy associated with a single magnet, it should be sufficient to calculate the magnitude of the interaction of the considered magnets with those of its neighbours which make a significant contribution to its energy. The extent of such neighbourhood can be established by means of the appropriate convergence test (see Appendix V).

In order to investigate mechanical properties and stability of the discussed system, the considered structure was deformed from the initial to the final configuration corresponding to angles $\theta = \theta_{\min}$ and $\theta = \theta_{\max}$ respectively. At one point of such process corresponding to the

vertical extension, the system assumes the threshold triangle-like conformation where the separation distance between the magnets within the same unit assumes the maximum value. This means that at this stage of the process, the magnetic interaction between adjacent magnets is the weakest and one should expect the extremum in the energy profile (both for attracting and repelling magnets) to be observed. At this point, it should be also noted that in the case of the discussed theoretical model, it is also possible to calculate the stiffness exhibited by the system throughout the deformation. In order to do that, one may assume that the change in the energy of the system to undergo a transition from one configuration to another corresponds to the work *W* which must be done in order to extend the structure by a certain distance *dy* in the vertical direction. In view of this, the vertical force *F* required to extend the system can be determined based on these two quantities.

9.4 Construction of the Prototype and Experimental Testing

Apart from theoretical studies, the concept corresponding to the possibility of achieving negative stiffness in the discussed magneto-mechanical system was also confirmed experimentally. In order to do that, an experimental prototype consisting of a single unit (see Figure 9-1) having linear dimensions $l_a = 10$ cm and $l_b = 3.5$ cm was constructed by means of the 3D extrusion printer (using ABS plastic). The magnets which were inserted into the system were cylindrical neodymium magnets corresponding to the estimated magnetic dipole moment of $|\vec{\mu}| = 1.656$ Am^2. Each of those magnets had a radius of 1 cm $(d_a = 2$ cm$)$ and the out-of-plane thickness equal to 1 cm $(d_b = 1$ cm$)$. In order to investigate the potential of the discussed system to exhibit different types of stiffness, analogically to the concept shown schematically in Figure 9-1(c), two scenarios were analysed where the facing magnets were either attracting or repelling each other depending on the change in the orientation of one of them. It should also be noted that in the case of the experiment, the considered magnets were shifted inwards the

unit by 5 mm in the orthogonal direction to the linear dimension of rigid bars having a length of l_a.

In order to investigate the stiffness exhibited by the experimental prototype, the deformation of the considered system was induced by means of the Testometric universal loading machine (M350-20CT) equipped with a 1000 N load cell. More specifically, the considered prototype was subjected to the vertical displacement at a constant rate of 1 cm / min. It should be also noted that before recording any of the results, the force and displacement measured by the loading machine were zeroed at the moment when the system was assuming a threshold configuration corresponding to $\theta = \theta_0$.

In order to analyse properties of the experimental prototype, the system was deformed from the initial configuration corresponding to the angle $\theta_{\min} \approx 32.6°$ (see Figure 9-2(a-i)) to the final configuration associated with the angle $\theta_{\max} \approx 117°$ (see Figure 9-2(a-iii)).

9.5 Results and Discussion

Based on Figure 9-2(a), one can clearly see that as the system is being pulled in the vertical direction at the range of θ between $\theta_{\min}$ and θ_0, the structure expands in the horizontal direction which behaviour is an indication of the negative Poisson's ratio. This observation is also in accordance with the predictions made by Larsen and Sigmund *et al.* [445]. However, upon surpassing the threshold configuration, the system starts exhibiting positive Poisson's ratio as its horizontal dimension is decreasing. The variation in the value of the Poisson's ratio can be seen in Figure 9-2(b). It is also important to note that the force *F* recorded by the load cell during the experiment is plotted with respect to the vertical displacement in Figure 9-2(c). The stiffness corresponding to this experiment is presented in Figure 9-2(d).

As shown in Figure 9-2(c), as expected based on theoretical predictions, the force measured by the load cell for the system with attracting magnets was decreasing throughout the entire process of mechanical deformation corresponding to the change in θ from $\theta_{\min}$ to $\theta_{\max}$. Such behaviour, as already discussed in this chapter and in the Introduction of the thesis, is an indication of the negative stiffness. As the matter of fact, the negative values of the stiffness corresponding to this system are shown in Figure 9-2(d). Conversely, in the case of the system with repelling magnets, the opposite behaviour of the system can be observed, i.e. the force *F* is continuously increasing throughout the entire process of deformation. This in turn, as shown in Figure 9-2(d), leads to the positive stiffness which result is in accordance with predictions made in this chapter. As already mentioned in the thesis, it is very unusual to design mechanical metamaterials which can exhibit numerous anomalous mechanical properties at the same time. As shown while discussing the results from Figure 9-2(b), irrespective of the orientation of magnets, the considered system exhibits negative Poisson's ratio at the range of θ between $\theta_{\min}$ and θ_0 (Poisson's ratio would be the same even for the system without magnets as it depends solely on the geometry). This stems from the fact that throughout this part of the process of deformation, the horizontal dimension of the structure increases up the point when the system reaches the threshold configuration. However, as the system is further extended in the vertical direction, it starts exhibiting positive Poisson's ratio $\left(\theta \in \langle \theta_0, \theta_{\max} \rangle\right)$. It should also be noted that, as discussed in the above paragraph, the stiffness exhibited by the system varies significantly depending on the orientation of magnets within the system. In particular, it was shown that in the case of the structure with attracting magnets inserted into it, the negative stiffness can be exhibited at the range of θ between $\theta_{\min}$ and $\theta_{\max}$ (entire deformation). Thus, it may be concluded that the considered system with magnets oriented in a way as shown in Figure 9-1(c-i), may exhibit highly unusual negative Poisson's ratio and negative stiffness at

the same time while being deformed from the initial ($\theta = \theta_{\min}$) to the threshold configuration ($\theta = \theta_0$).

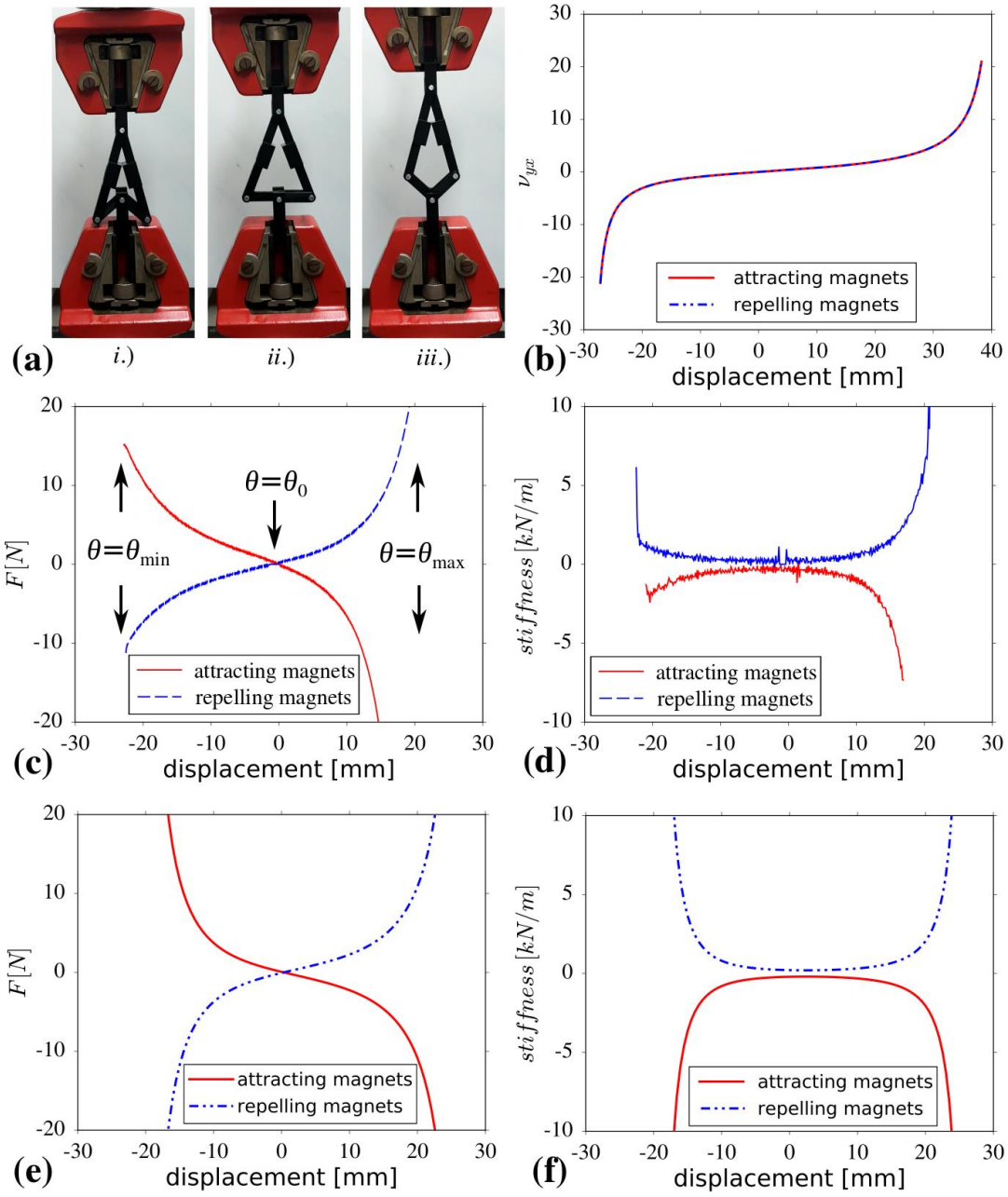

Figure 9-2 Panels show: (a) different stages of the deformation of the experimental prototype associated with: (i) initial, (ii) threshold and (iii) final configuration, (b) Poisson's ratio exhibited by the system for loading in the vertical direction, (c) force recorded by the tensile loader throughout the entire process of deformation of the experimental prototype, (d) stiffness exhibited by the prototype with attracting and repelling magnets, (e) theoretical results corresponding to the force required to deform the system analogical to the experimental prototype and (f) stiffness exhibited by the system according to the theoretical model.

As shown in Figure 9-2(e-f), the experimental results obtained in this work were also analysed by means of the theoretical model where all of the parameters were set in a way to closely resemble the experimental prototype in order to compare both sets of results. Based on generated results, one may note that the theoretical model leads to the same conclusions regarding the mechanical properties of the considered system. It may also be noted that in terms of the magnitude, there is a very good agreement between both sets of results which increases the credibility of the reported results. Of course, despite the fact that theoretical and experimental results reported in this work are very similar, they are not exactly the same as is normally the case upon comparing theoretical model to the experiment. One source of a small discrepancy between both sets of results could be the fact that due to a very strong interaction at small distances, the magnets in the experimental prototype were not perfectly aligned with the rigid bars having a length of l_a. In addition to that, it should be noted that the standard analytical expression used in order to calculate the magnetic field between any two magnetic dipole moments is expected to provide only approximated results especially with this approximation being less accurate for configurations where the distance between the magnets was relatively small.

Apart from results generated for systems composed of a single structural unit with two magnets (see Figure 9-1(b)), it is also possible to consider more complex systems with a large number of units (see Figure 9-1(a)). More specifically, in the case of this chapter a hypothetical large system was taken into consideration where the neighbourhood of each of the magnets similarly to infinite systems could be assumed to be the same for each of the magnets (see Model section). Furthermore, with the help of the appropriate convergence test (see Appendix V), the energy per magnet in such system was calculated in order to discuss the stability of the structure and later determine its stiffness.

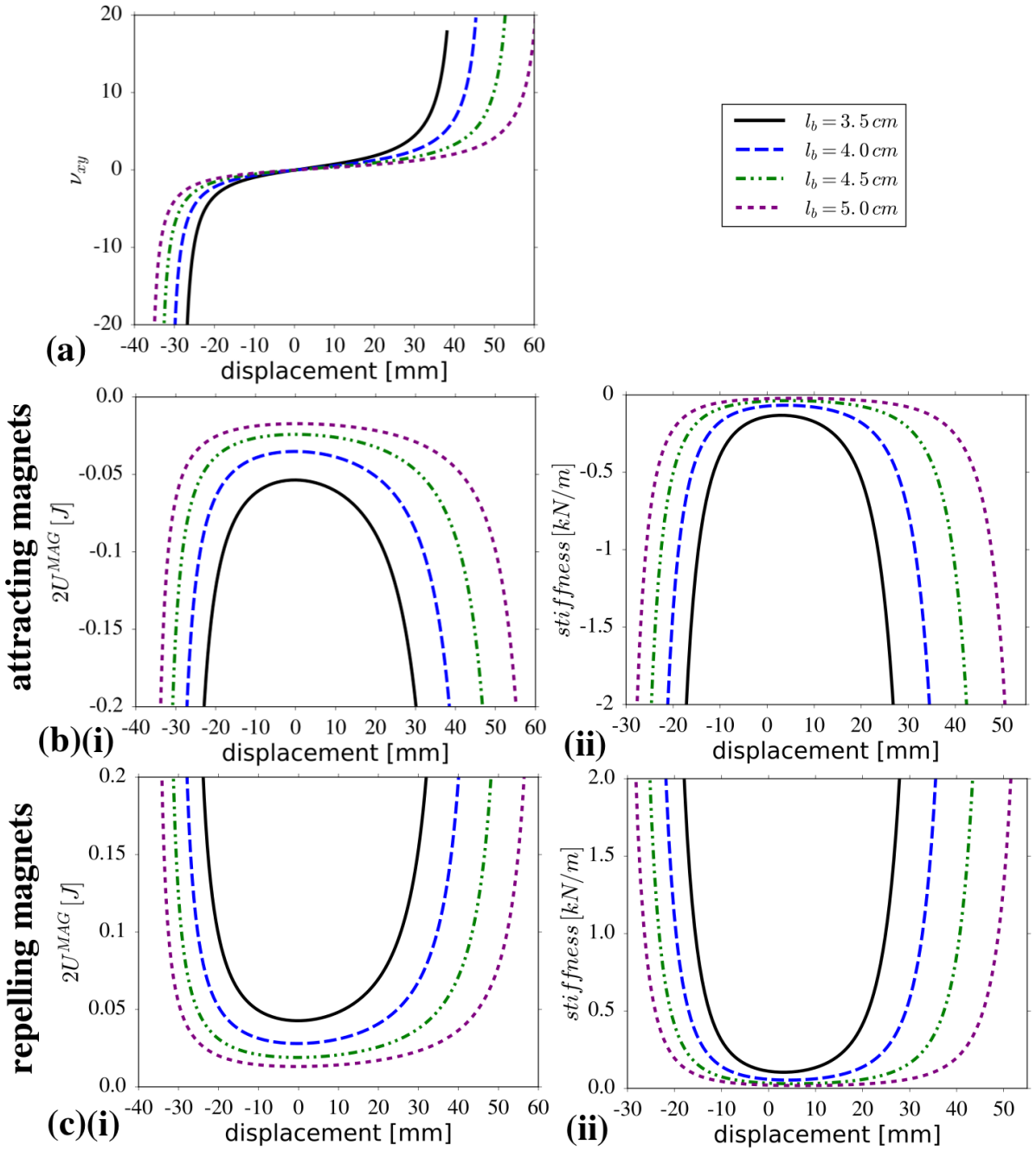

Figure 9-3 Panels show: (a) the variation in the Poisson's ratio in the loading direction for systems corresponding to a different value of l_b, (b) variation in the (i) magnetic potential energy per unit and (ii) stiffness of the system with attracting magnets for structures corresponding to different values of l_b and (c) graphs analogical to those from panel (b) but generated for systems with repelling magnets.

As shown in Figure 9-3(b-i), the magnetic potential energy of the system per structural unit with magnets oriented as in Figure 1-2(a), resembles the reversed parabola with the maximum at the threshold configuration where $\theta = \theta_0$. The extremum at this particular configuration is

associated with the fact that it corresponds to the largest possible distance between the magnets within each of the units. This particular energy profile also indicates that such system is unstable which behaviour as shown in Figure 9-3(b-ii) is an indication of the negative stiffness. Thus, should one set the system in a way so that at a given moment it would assume the threshold configuration, then in an attempt of reaching a more energetically favourable configuration, the system would want to assume the conformation corresponding to $\theta = \theta_{\min}$ or $\theta = \theta_{\max}$. However, should one change the orientation of one magnet in each of the structural units (see Figure 9-1(c-ii)), then a very different behaviour of the system in terms of its stability would be observed. Based on Figure 9-3(c-i), one may note that the profile of the energy of the system per structural unit resembles a parabola with a minimum corresponding to the threshold configuration ($\theta = \theta_0$). This means that the system would not want to leave this particular conformation as it is the most favourable from the energy point of view. This in turn indicates that the system is stable which behaviour is also normally expected to lead to the positive stiffness which as shown in Figure 9-3(c-ii) was also the case for the considered model.

Another interesting aspect of the discussed system which remains to be discussed is the effect which the geometry of the structure has on its behaviour. In view of this, in this chapter, the behaviour of the considered model was analysed for different values of l_b which quantity stands for a length of some of the ligaments within structural units (see Figure 9-1(b)). Based on Figure 9-3(a), one can note that the values of the Poisson's ratio exhibited by the system throughout the process of deformation are strongly affected by the variation in l_b. This should be expected as the Poisson's ratio depends solely on the geometry of the system. One can also note that in terms of the absolute magnitude, the lower the values of l_b, the larger the values of the Poisson's ratio for analogical values of the vertical displacement. Based on remaining panels in Figure 9-3, it can be concluded that the variation in the geometric parameter l_b does

significantly affect the energy of the system and it stiffness. More specifically, it may be noted that in terms of the absolute magnitude, irrespective of the stage of the deformation, the lower the values of l_b the larger the energy and stiffness of the system. This result may be easily understood should one realise that for small values of l_b, magnets are being brought closer to each other and hence the energy associated with their magnetic interaction is being increased. The stronger interaction between magnets makes it also more difficult (or conversely simpler) to deform the system which results in the increase in the magnitude of the stiffness.

Apart from the effect which the geometry of the system has on its behaviour, it is also possible to investigate the effect which the strength of magnets has on the energy and mechanical properties exhibited by the system. This can be achieved through the analysis of results corresponding to exactly the same systems in terms of their geometry but corresponding to different values of μ. As shown in Figure 9-4(a), the Poisson's ratio exhibited by considered systems is not affected by a type of the magnets inserted into the structure. However, according to the remaining panels from Figure 9-4, it may be noted that both the energy and the stiffness are significantly affected by the variation in μ. More specifically, as should be expected, one can see that the stronger the magnets the larger the absolute values of the energy and stiffness exhibited by the system. It should be also emphasised that the variation in μ does not change any of the trends exhibited by considered systems. At this point, it should be mentioned that in reality, the variation in the value of μ could be achieved upon replacing magnets with electromagnets in which case the strength of their interaction could be controlled by the intensity of the provided current. This in turn means that one could conveniently fine-tune the magnitude of the stiffness exhibited by the system. By changing the direction of the current, it could be also possible to change the stiffness of the system from positive to negative and *vice-versa* without the necessity of reconstructing the structure.

As discussed above, the possibility of replacing magnets with electromagnets in the case of the considered system would potentially make it possible to conveniently change the stiffness of the structure from positive to negative and *vice-versa* as well as to fine-tune its magnitude. It should be also emphasised that the potential of such system to exhibit a versatile stiffness could also be utilised together with the effect of auxetic behaviour which was also reported in this chapter as one of the characteristics of this system. Such control over the type of the stiffness exhibited by the system as well as the potential to exhibit other types of anomalous mechanical behaviour may lead to the proposal of novel types of applications where such versatility would be essential. One could for example consider the use of devices based on this concept as smart filtration devices where the size of the pore could be controlled by the electric current. It could also be potentially applied in the case of a variety of protective and vibration damping devices where both negative Poisson's ratio and negative stiffness are historically known to be of great importance.

Apart from considering mechanical metamaterials at the macroscale where such systems are normally investigated from the point of view of their mechanical properties, it would be also very interesting to consider such systems with magnetic inclusions at significantly lower scales such as the nano- or microscale. This stems from the fact that due to the relative ease with which mechanical metamaterials can be deformed, these systems could be considered as very interesting candidates to investigate different physical phenomena where the variation in the distance between magnetic inclusions is significant from the point of view of the exhibited effect. In view of this, in the following chapter, the propensity of the particular mechanical metamaterial system to enhance unusual physical phenomena at the nanoscale as the result of its deformation will be discussed.

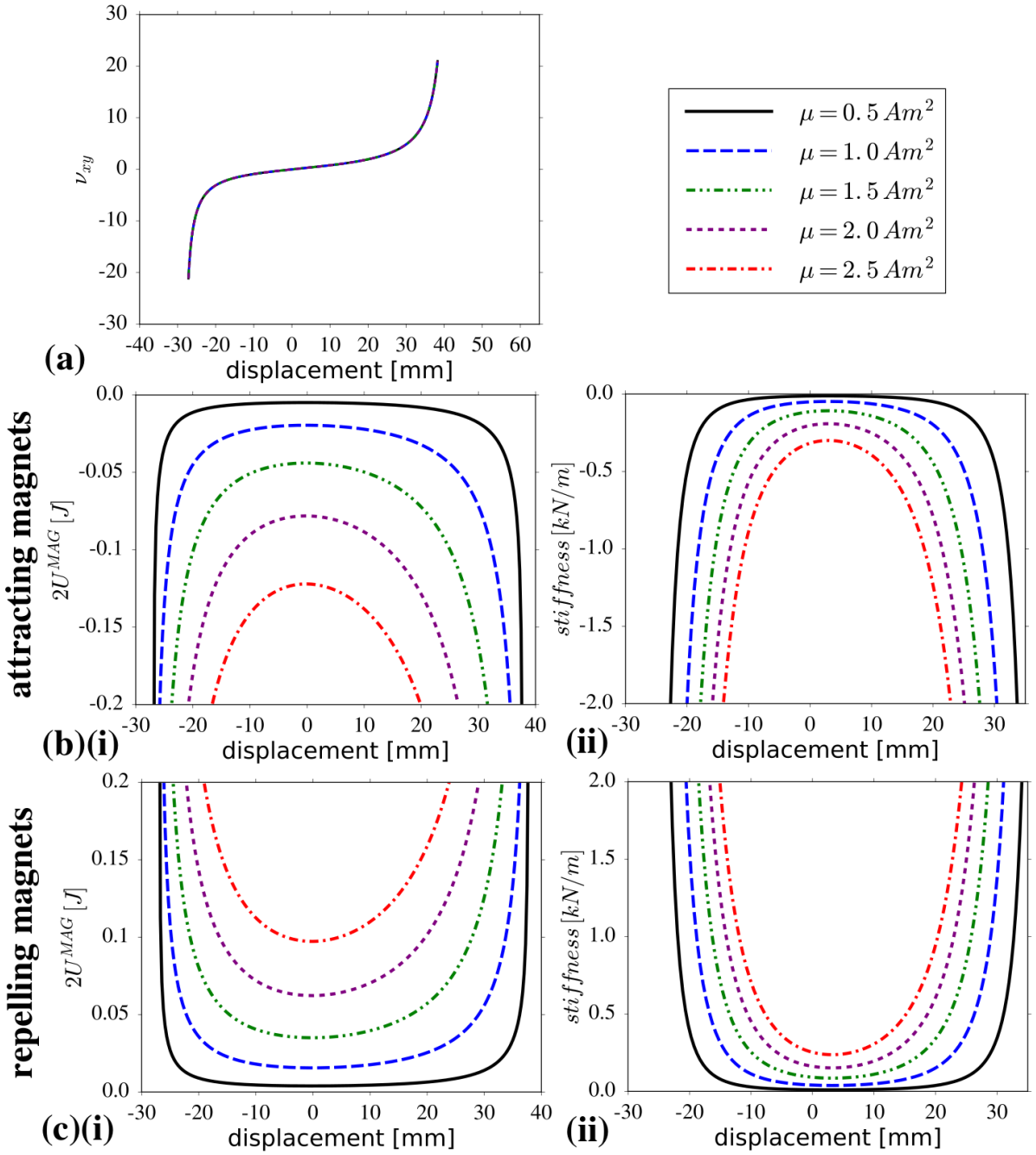

Figure 9-4 Panels show: (a) the variation in the Poisson's ratio in the loading direction for system with magnets corresponding to different values of μ, (b) variation in (i) magnetic potential energy per unit and (ii) stiffness of the system with attracting magnets for structures corresponding to different values of μ and (c) results analogical to those shown on panel (b) but generated for systems with repelling magnets within structural units.

9.6 Conclusions

In this chapter, the particular mechanical metamaterial with magnetic inclusions was proven to be capable of exhibiting both negative Poisson's ratio and negative stiffness at the same time. This highly unusual behaviour was analysed both by means of the theoretical model and experiment where both of these approaches were shown to lead to analogical results. It was also shown that different orientation of magnets within the structure may change the stiffness of the system from positive (repelling magnets) to negative (attracting magnets) and vice versa. Such variation in the orientation of magnets was also reported to lead to a different behaviour of the system in terms of its stability. All of these results indicate that the investigated system may prove to be useful upon designing novel vibration damping devices where apart from normally desired negative stiffness one could further enhance the properties of the system by the manifestation of the auxetic behaviour.

10. Potential of mechanical metamaterials with magnetic inclusions to exhibit magnetocaloric effect[7]

HIGHLIGHTS

- The potential of rotating square system with magnetic inclusions to exhibit magnetocaloric effect was investigated though a model where the system was represented by means of the Ising model (ferromagnetic interactions) defined on the square lattice as such approach allows to determine the exact expression for entropy of the system by means of the famous Onsager's solution. It is also discussed that the considered model may represent an array of magnetic particles arranged on the square lattice where Ising spins represent magnetic moments of individual particles;
- It was shown that this particular magneto-mechanical system may induce the magnetocaloric effect solely as a result of the mechanical deformation and without the presence of an external magnetic field;
- The magnitude of the magnetocaloric effect induced for the considered system during the isothermal process can be very large even in the vicinity of the room temperature.

10.1 Motivation

As discussed in the last chapter, apart from investigating the potential of macroscopic mechanical metamaterials with magnetic inclusions to exhibit anomalous mechanical behaviour, it would be also interesting to consider such systems at the nano-scale. This stems from the fact that as a result of the deformation of these systems it would be possible to change

[7] The content of this chapter has already been published in the peer-reviewed journal *Smart Materials and Structures*: M. R. Dudek, K. W. Wojciechowski, J. N. Grima, R. Caruana-Gauci, **K. K. Dudek**, Colossal magnetocaloric effect in magneto-auxetic systems *Smart Mater. Struct.* **24** 085027 (2015)

the magnitude of magnetic interaction between magnetic particles inserted into the mechanical structure. This in turn could prove to be useful in the case of different physical phenomena under the assumption that the system would consist of a large number of densly-packed magnetic nanoparticles where such change could be significant. One very interesting effect which could be expected to be affected by the variation in the distance between magnetic inclusions and is historically-known to be an intrinsic property of all of the magnetic systems subjected to a change in the magnetic field is the magnetocaloric effect. This phenomenon, which is explained and discussed in relation to the already existing studies in the following section, corresponds to the change in the temperature of the magnetic system as the result of the external stimuli and has been proven to be useful in the case of magnetic refrigeration techniques. More specifically, this effect is normally induced as a result of the change in the externally applied magnetic field or originates from the movement of the magnetic system in the magnetic field. However, one could also consider the possibility of inducing the analogical effect as a result of mechanical deformation of the magneto-mechanical system which concept despite being initially proposed [447, 448] has not been thoroughly investigated and many of its aspects still remain to be discovered. In view of this, the possibility of designing a hypothetical mechanical metamaterial with magnetic inclusions which would be capable to exhibit a strong magnetocaloric effect without the presence of the external magnetic field is going to be investigated in this chapter. It should be also noted that for a majority of magnetic materials, unless a very strong magnetic field is applied, the magnetocaloric effect induced by the application of the external magnetic field is very weak in the vicinity of the room temperature. Thus it would be interesting to analyse the propensity of mechanical metamaterials with magnetic inclusions at the wide range of temperatures including the room temperature where the considered effect could prove to be the most important from the point of view of potential applications.

10.2 Introduction

The magnetocaloric effect (MCE) is a phenomenon related to the heating of a magnetic material upon the application of a magnetic field, and conversely, its cooling after the removal of a magnetic field. MCE was first discovered in iron by Warburg in 1881 [449] and since then, a vast number of studies have been carried out on this phenomenon [450, 451]. MCE is an intrinsic property of magnetic materials but it is usually too weak to be used in everyday magnetic cooling applications operating at around room temperature. Some of the exceptions which correspond to systems where MCE under similar conditions can be significant include gadolinium (Gd), which has a critical temperature of $T_c = 294K$, various compounds based on manganites, and related compounds of rare earth metals [451]. It should also be noted that a significant progress associated with the proposal of new MCE materials has been noted since the discovery of giant MCE in $Gd_5(Si_2Ge_2)$ by Pecharsky and Gschneidner [452] which study encouraged other scientists to investigate the considered phenomenon.

As discussed above, the magnetocaloric effect for an arbitrary magnetic system is normally induced through the change in the external magnetic field or the movement of such system at the constant magnetic field. However, it does not mean that it is not possible to induce this effect by means of other techniques. In this thesis, it was already discussed that the mechanical deformation of the mechanical system with magnetic inclusions results in the change in the distance between respective magnetic inclusions which in turn affects the strength of their interaction. Thus, this process, which is very similar to the change in the external magnetic field, may be also expected to affect or even possibly induce the magnetocaloric effect in the case of mechanical systems with magnetic inclusions. As the matter of fact, despite being in its infancy and lacking more thorough analysis which could lead to potential applications, the

concept of inducing the magnetocaloric effect at the zero external magnetic field [451] as well as the possibility of affecting the magnetocaloric effect as a result of the mechanical deformation of the magnetic system [447, 448] have already been proposed. In particular, Tishin and Spichin introduced the concept of an elastocaloric effect which arises by changing the external pressure at a constant (or zero) magnetic field [451]. This study was followed by Mosca *et al.* who showed that strain can tune MCE related to the magneto-structural phase transition in MnAs [448]. In their work, it was also shown that the critical temperature of the strained epilayers of MnAs depends on the mean strain ε as $T_c = T_0\left(1+2\kappa\varepsilon\right)$ for some adjustable parameters T_0 and κ. Among some of the more recent studies related to this concept it is also worth to mention the work by Paes and Mosca [447] where the effect of an applied mechanical stress on galfenol was discussed and it was shown that magnetostriction and magnetoelastic interactions can be responsible for auxeticity in galfenol.

At this point, it is worth to mention that the recent trend which may be observed in the field of research related to the magnetocaloric effect indicates that scientists are increasingly more interested in finding novel materials capable to exhibiting a desired type of the magnetocaloric effect instead of fine-tuning the currently known solutions. In particular, single-domain magnetic nanoparticles have been found to be promising candidates to design such materials which stems from their potential to exhibit superparamagnetic behaviour above the blocking temperature T_b, their large area for heat exchange as well as the possibility of placing them into another host material which material can be non-magnetic [453]. In the system composed of such particles, each magnetic nanoparticle acts as a single superspin which can interact with the surrounding superspins through dipolar interactions [453]. In the relatively dense ensemble of magnetic nanoparticles they can show collective behaviour typical for spin-glass or superferromagnetic systems [453-456]. In particular, in the work by Petracic *et al.* [453] , where

thin layers of $Co_{80}Fe_{20}$ nanoparticles which are embedded in a diamagnetic Al_2O_3 matrix were investigated, it was shown that when the nominal thickness of the nanoparticles concentration exceeds the value of 1.1 nm, superferromagnetic ordering can be observed (such creation of magnetic domains is analogous to the behaviour observed in ferromagnets). In view of this, it would be very interesting to design a novel systems conducive to the magnetocaloric effect which could allow for interactions of single domain magnetic inclusions.

In this chapter, in view of the studies mentioned above, an attempt is made to investigate the possibility of inducing the magnetocaloric effect in the case of the particular hypothetical mechanical metamaterial system with magnetic inclusions without the presence of the external magnetic field. It will also be analysed whether the mechanically-driven magnetocaloric effect which is expected to be observed for the considered system may assume significant values at temperatures in the vicinity of the room temperature. Should it be the case, this result could prove to be important in the case of potential applications such as magnetic refrigerators which would ideally be able to operate at the room temperature. Note that for the sake of simplicity the considered magneto-auxetic system is going to be referred to as MAS in the remaining part of this chapter.

10.3 Concept

In this chapter, the possibility of inducing the magnetocaloric effect solely as a result of the mechanical deformation by the considered magneto-mechanical system is going to be investigated in the case of the isothermal process without the presence of the external magnetic field. In the case of such process, the magnetocaloric effect is manifested by the change in the magnetic entropy of the system. Upon representing magnetic inclusions within the considered system by means of the Ising model defined on a square lattice, the change in the magnetic entropy for such system can be determined by means of the famous Onsager's solution [457-

459]. More specifically, through the use of this solution, one may find the entropy of the system at a given configuration (particular arrangement of Ising spins in space governed by mechanical deformation). Thus, upon calculating the entropy of the system at two different configurations, it is possible to calculate the change in the magnetic entropy (a difference between entropies corresponding to the system at two different geometric configurations) corresponding to the deformation of the system from one configuration to another as discussed in more detail in the following sections of this chapter.

10.4 Model

The considered system corresponds to the non-magnetic matrix in a form of the rotating square system where at the centre of each of the rigid units there is a magnetic inclusion located. This model is inspired by the novel work by Grima *et al.* [406] where, as discussed in the Literature Review, a similar system with magnetic inclusions in the form of permanent magnets located at the centre of respective rectangular units was considered. In this chapter, it is assumed that the considered non-magnetic matrix consists of $N \times N$ identical perfectly rigid square-like units connected at vertices with each of the units having the linear dimension *a*. The angle of aperture between the adjacent rigid units is denoted as 2θ. Furthermore, all of the magnetic inclusions in the system are represented by means of the Ising model defined on the square lattice which means that the considered system is assumed to be the microscopic spin 1/2 system which can exhibit phase transitions. In such system, magnetic moments are represented by Ising spins $s_{ij} = \pm 1$ which are located at the centre of mass $\vec{r}_{ij}$ of the squares (*i*, *j*) where $i, j = 1, 2, ..., N$. A schematic representation of a MAS consisting of 3×3 square units is presented in Figure 4-2. It should be noted that for the considered system, the centres of mass of the squares create a two-dimensional square lattice where $L_x = L_y = L = Na\left[\cos\theta + \sin\theta\right]$.

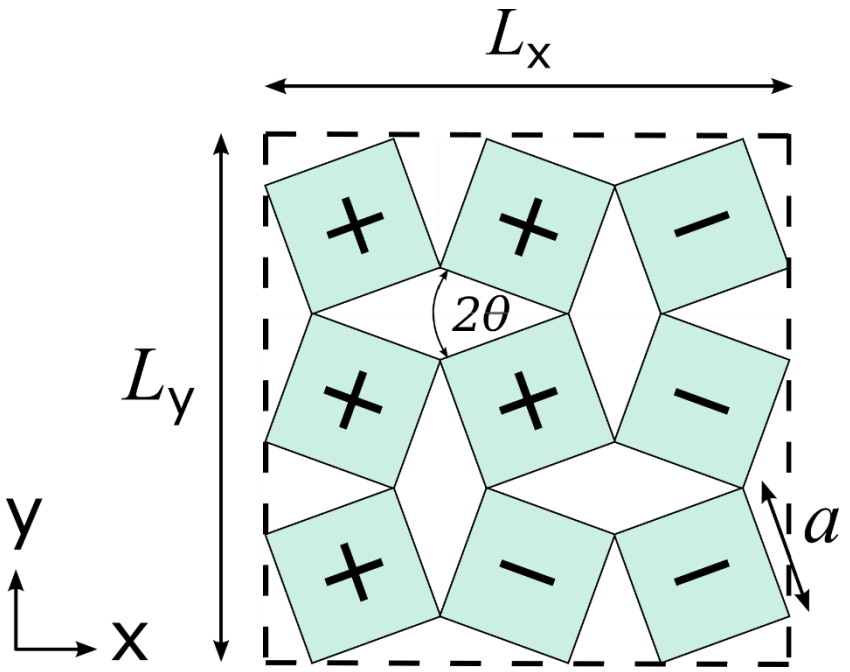

Figure 10-1 Magneto-auxetic system of 3×3 squares of dimension $a\times a$ with the exemplary configuration of Ising spins $s=\pm1$ denoted by "+" and "-" respectively, located at centre of mass of the squares. L_x and L_y denote linear dimensions of the system in the *x* and *y* directions respectively.

In general, the nearest-neighbour Ising model Hamiltonian [460] is used to describe magnetic interactions between Ising spins in the following manner:

$$H_{exact}^{IM} = -\sum_{\langle ij,kl\rangle} J_{ij,kl} s_{ij} s_{kl} - \mu_B H \sum_{i,j=1}^{N} s_{i,j} \qquad 10\text{-}1$$

where the angular brackets denote summation over the nearest-neighbour lattice pairs, *H* is the external magnetic field measured in Teslas, μ_B is the Bohr magneton (constant corresponding to the magnetic moment of an electron), $J_{ij,kl}$ is the coupling constant which depends on the distance $r_{ij,kl}$ between the nearest-neighbour sites (*i*, *j*) and (*k*, *l*). In this chapter, it is assumed that $J_{ij,kl} = J_0 / r_{ij,kl}^3$ and $J_0 > 0$ (ferromagnetic interaction). It should also be noted that, for the considered system (see Figure 10-1), the distance between centres of adjacent rigid units can be expressed as follows: $r_{ij,kl} = a\sqrt{2}\sin\left(\theta + \frac{\pi}{4}\right)$. Furthermore, as a result of the mechanical

deformation of the considered auxetic system, the symmetry of the magnetic Hamiltonian is not being changed because the centres of mass of the rotating squares are represented by a square lattice for an arbitrary value of θ which is permitted by the geometry of the system, i.e. $\theta \in [0, \pi]$ rad.

In a closed thermodynamic system of localized magnetic moments, the total entropy *S* depends on temperature *T*, pressure *p*, and external magnetic field *H*. In view of this, the full differential of the entropy can be written as:

$$dS = \left(\frac{\partial S}{\partial T}\right)_{p,H} dT + \left(\frac{\partial S}{\partial p}\right)_{T,H} dp + \left(\frac{\partial S}{\partial H}\right)_{T,p} dH \ . \qquad 10\text{-}2$$

It should be noted that the magnetocaloric phenomenon investigated in this chapter is represented by the isobaric-isothermal process ($dp = 0$, $dT = 0$) which leads to the following expression:

$$dS = \left(\frac{\partial S}{\partial H}\right)_{T,p} dH \ . \qquad 10\text{-}3$$

It is also important to highlight the fact that the magnetocaloric effect can be expressed in two different ways:

(i) by the temperature increase $\Delta T = T_f - T_i > 0$ of the magnetic material after a change in the magnetic field $\Delta H = H_f - H_i > 0$, from the initial value H_i to the final value H_f. In this case, the magnetic field is applied adiabatically through a thermodynamically reversible process;

(ii) by the decrease of the magnetic part S_M of the total entropy S after the magnetic field H_f ($H_f > H_i$) is applied isothermally to the system at temperature *T*, that is:

$$\Delta S_M = S_M\left(T, H_f\right) - S_M\left(T, H_i\right) < 0 \ . \qquad 10\text{-}4$$

In view of the latter approach leading to the magnetocaloric effect, it may be noted that there is another possibility of obtaining the change in entropy (see equation 10-2) which is possible through the isothermal process at constant magnetic field ($dT = 0$, $dH = 0$):

$$dS = \left(\frac{\partial S}{\partial p}\right)_{T,H} dp \ . \qquad 10\text{-}5$$

As reported by Tishin *et al.* [451], an example of such process can be the elastocaloric effect. In the case of the considered magneto-mechanical system, the infinitesimally small uniaxial stress $d\sigma_i$ for loading in the direction *i* (e.g. *x* or *y*) substitutes the infinitesimally small isotropic pressure change *dp* in equation 10-5. The stress $d\sigma_i$ can be expressed in terms of Young's modulus E_i and the strain ε_i for loading in the direction *i*, i.e., $d\sigma_i = E_i d\varepsilon_i$. In the particular case of the considered system which is shown in Figure 10-1, $d\varepsilon_i$ in the above expression assumes the same value for loading in the *x* and *y* direction, i.e. $d\varepsilon_i = \frac{dL_x}{L_x} = \frac{dL_y}{L_y} = \frac{dL}{L}$, where $dL = a\left[\cos\theta - \sin\theta\right]d\theta$. Thus, the full differential of the entropy from equation 10-5 can be expressed as follows:

$$dS = \left(\frac{\partial S}{\partial \theta}\right)_{T,H} d\theta \ . \qquad 10\text{-}6$$

A more general process is also possible if the external magnetic field was to be changed from the initial value H_i to the final value H_f $\left(H_i < H_f\right)$ concurrently to an applied strain. In the case of this chapter, the entropy decrease ΔS_M being the result of the magnetocaloric effect during the isothermal process is given by:

$$\Delta S_M = S_M\left(T, H_f, \theta_f\right) - S_M\left(T, H_i, \theta_i\right) < 0 \qquad 10\text{-}7$$

where θ_i and θ_f represent the initial and final values of θ for which the distance between the magnetic moments decreases.

In this chapter, in order to be close to the experimental values concerning materials with an MCE (Magneto Caloric Effect) near room temperature [451], the value of J_0 in the Hamiltonian expressed by equation 4-2 is chosen to be equal to 0.01116 eV. This value is such that $T_c = 293.9\ \mathrm{K}$ for $\theta = 90°$ and $T_c = 103.9\ \mathrm{K}$ for $\theta = 45°$, where T_c stands for the critical temperature. As mentioned before, the isothermal magnetic entropy change ΔS_M after the mechanical deformation $\Delta\theta = \theta_f - \theta_i$ can be easily determined with the help of the well-known Onsager solution [457-459] for the two-dimensional Ising model defined on the square lattice at zero magnetic field $(H = 0)$. In such the case, in order to determine the extent of the observed magnetocaloric effect, the entropy per site $s_M = \frac{S_M}{k_B}$ is calculated as $s_M = \beta\left(u - F\left(T,0\right)\right)$ (see Appendix VII for the implementation). Based on the above expression, one may note that in order to find the reduced entropy for a given configuration of the considered system, it is first necessary to determine its free energy per site *u* and the free energy per site reduced by temperature f. As shown in the literature [458], for the Ising model, these quantities may be expressed as follows: $u = -\frac{\partial f}{\partial \beta}$ and $f = \beta F\left(T,0\right)$ (see Appendix VI for the explicit form). At this point, it must be noted that in this chapter, the rotating squares system is used in order to have the exact Onsager solution for the Ising model, however there are other rotating rigid units or other mechanical systems which can be effectively used as a non-magnetic matrix. This means that even though, in general, one can use an arbitrary geometry to construct the system capable of inducing the discussed phenomenon, the extent of this effect could not be estimated for such systems by means of the exact analytical expressions known from the literature. It

should also be noted that should one try to apply the considered approach to real systems which have the analogical geometry, it would be valid only in the case of systems composed of a very large number of magnetic inclusions forming a particular square lattice and would not be expected to work for other systems.

It should also be noted that in the considered model, $T_c = T_c^{sq} / \left(a\sqrt{2} \sin\left(\theta + \frac{\pi}{4} \right) \right)^3$ where T_c^{sq} is the critical temperature for the Ising model defined on the square lattice with the unit lattice constant. This means that throughout the process of the mechanical deformation (followed by the change in θ) the critical temperature of the system T_c changes accordingly. Hence, there is a direct analogy between the considered model and the model proposed by Bean and Rodbell [461] where the dependence of the critical temperature on strain [448] was assumed.

10.5 Results and Discussion

In Figure 10-2, the dependence of $\Delta s_M = \frac{\Delta S_M}{k_B}$ per site on temperature is shown for different values of θ_i and θ_f (corresponding to a different extent of the mechanical deformation) with no presence of the external magnetic field. The characteristic feature of the plotted magnetic entropy difference Δs_M is that the concavity of this function changes (point of inflection) at temperatures corresponding to the critical temperature associated with the initial ($\theta = \theta_i$) and final ($\theta = \theta_f$) configuration of the considered system subjected to the mechanical deformation.

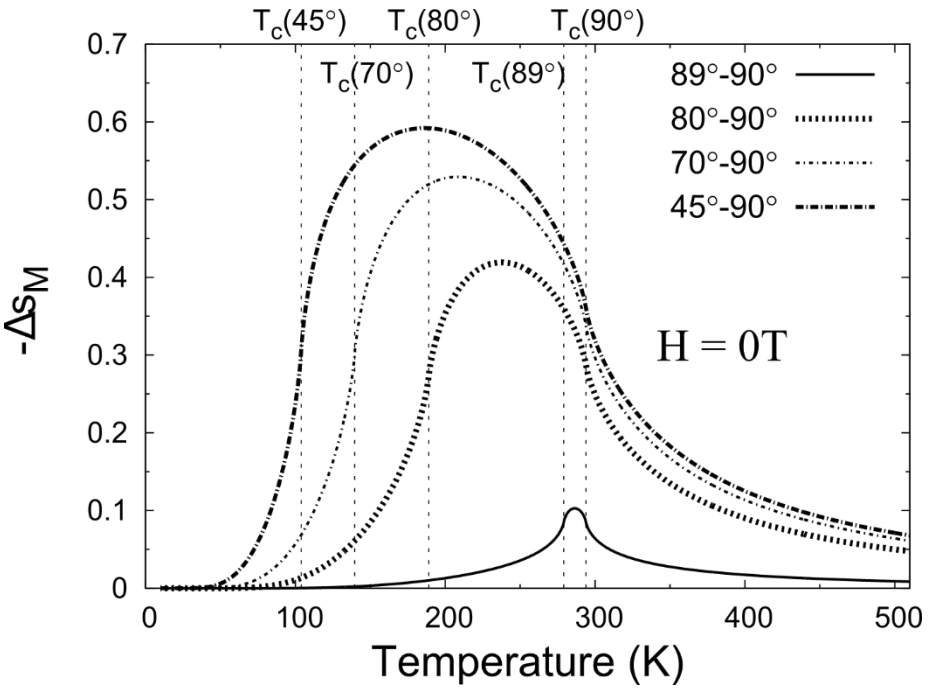

Figure 10-2 Temperature dependence of the isothermal entropy change Δs_M for MAS deformed from θ_i to θ_f at zero magnetic field. The plots representing deformations $89° \to 90°$, $80° \to 90°$, $70° \to 90°$, $45° \to 90°$ are shown (units in degrees). The vertical lines indicate location of T_c for a given value of θ_i and θ_f.

In the case of a spin 1/2 model taken into consideration, the maximum value of the reduced magnetic entropy $-\Delta s_M$ cannot exceed the value of $\log(2) \approx 0.693$ as for the Ising model (see Appendix VI for a detailed description corresponding to the calculation of $-\Delta s_M$). As can be seen in Figure 10-2, the largest value of the change in magnetic entropy is observed for the deformation from $\theta_i = 45°$ to $\theta_f = 90°$ where it is about 85% of the maximum possible value. This stems from the fact that for such system, during the process of deformation, the separation distance between the neighbouring Ising spins is changed from the maximum to the minimum distance which can be achieved for the considered system. Also, as shown in Figure 10-2, upon reducing the extent of mechanical deformation, the values corresponding to the change in the reduced magnetic entropy assume increasingly lower values (in terms of the absolute magnitude). However, it may be noted that even in the case of the relatively small deformation

by 1° from $\theta_i = 89^\circ$ to $\theta_f = 90^\circ$ (or equivalently from $\theta_i = 1^\circ$ to $\theta_f = 0^\circ$), the observed variation in $-\Delta s_M$ corresponds approximately to 15% of the maximum entropy. It should also be noted that even in the vicinity of the room temperature, the change in the reduced magnetic entropy is relatively close to the maximum value of $-\Delta s_M$ exhibited by each of the considered types of deformation. This in turn indicates that one could expect to observe a strong mechanically-driven magnetocaloric effect in the case of applications involving the use of this concept at temperatures in the vicinity of the room temperature.

In order to compare the obtained results with the results known from literature, one can hypothetically assume that Ising spins are replaced with some atoms. If for example Gd atoms (where the total angular momentum of an atom is equal to $7/2$) were substituted for the Ising "atoms", then, the maximum change in the magnetic entropy cannot exceed the value of $\log(8) \approx 2.079$. After the multiplication of this number with the gas constant $\left(R = 8.314 \text{ J mol}^{-1} \text{ K}^{-1}\right)$ for Gd atoms, this maximum value of the change in the magnetic entropy would correspond to $17.3 \text{ J mol}^{-1} \text{ K}$ or $110.02 \text{ J kg}^{-1} \text{ K}$ [451]. In view of this, in the case of the results shown in this chapter, the entropy change by 15% of the maximum entropy value would result in $16.50 \text{ J kg}^{-1} \text{ K}$. This value is more than three times larger than the maximum entropy change for Gd after an application of the external magnetic field of $2\text{T}\left(H_i = 0\text{T}, H_f = 2\text{T}\right)$ and it is of the same order of magnitude as in $Gd_5(Si_2Ge_2)$ for the same parameters (refer to figure 4 in the paper by Pecharsky and Gschneidner [452]). This means that solely mechanically-driven magnetocaloric effect which was observed for the considered hypothetical system can be very strong and as mentioned above, it may also exhibit large values in the vicinity of the room temperature.

In view of the very promising results discussed above, the question arises whether other currently known MCE (Magneto Caloric Effect) materials offer a similar level of expandability as the considered system which is clearly the reason behind the extent of the observed phenomenon. Due to a particular design of the non-magnetic matrix, the linear dimension L of the discussed system can increase up to 41% under a uniaxial strain applied in the x or y direction while the corresponding increase in area could reach up to 100% of the initial value. It may also be mentioned that for the hypothetical three-dimensional equivalent of the considered auxetic system, the volume could increase up to approximately 180%. This enormous expandability can be compared to present MCE materials where often only a small volume expansion $\Delta V/V < 0.1\%$ is observed at T_C due to a magnetoelastic transition. However, there are several materials known to lead to MCE which can deform to a relatively large extent. One such example can be intermetallic compound MnAs, which has a first-order phase transition, where the volume expansion can be of the order of 2% [462]. Another example can be samarium where in the case of the phase transition from fcc to dhcp after an application of a pressure of 7×10^8 Pa at room temperature [451], a volume decrease of approximately 8% can observed. Thus, upon comparing the volume changes of the already known MCE materials with that of the considered system it may be noted that the discussed model expands to a significantly larger extent than is the case for other materials which are known to exhibit MCE. This also indicates that the use of mechanical metamaterials with magnetic inclusions which systems are known from their capability to significantly change the distance between their constituents as a result of mechanical deformation could lead to a further progress related to the studies on MCE.

In order to better visualise the extent of MCE in the considered system, one could substitute the Ising spins found at the nodes of the lattice with magnetic moments of single-domain magnetic nanoparticles of Fe_3O_4. This, as mentioned in the introduction of this chapter, is one

of the most promising approaches related to the MCE materials. For such system, the magnetic moment per f.u. (formula unit) of the compound Fe_3O_4 is equal to $\mu/\text{f.u.} = 4.33\mu_B$ [463]. Thus, if for example the magnetic nanoparticles were considered to have a dimension of 5 nm, then the magnetic moment of nanoparticles could be estimated as $\mu \approx 3831\mu_B$. Moreover, if the centre-to-centre distance between two adjacent magnetic moments (or superspins as they may be also referred to [453]) is defined as *d*, then the potential energy of the superspin–superspin interaction can be determined as a function of *d*. Thus, assuming that *d* = 5 nm (i.e. the nanoparticles are touching each other) the interaction potential energy between two superspins can be estimated as: $E/k_B \approx 73\text{K}$ (see Appendix VI for more details). Furthermore, upon considering the four-nearest-neighbours interaction approach (i.e. the given superspin interacts with its four nearest neighbours as is normally the case for the Ising model) for *d* = 5 nm, then the total value of dipolar interaction energy is equal is approximately equal to: $E/k_B \approx 293\text{K}$. On the other hand, if the distance *d* was set to equal to 10 nm, the value of the energy including the four-nearest-neighbours interaction drastically would decrease drastically to the level of: $E/k_B \approx 37\text{K}$. This result clearly indicates that a change in energy occurs on changing the distance between the magnetic nanoparticles and that it can be significant at room temperature. It should also be noted that as already discussed, an analogical change in the separation distance between magnetic nonoparticles arises when modifying the geometry of the considered system.

Before concluding, one can note that the magnetic entropy in the Ising system depends on the orientation of Ising spins and the distribution of spins having the same orientation within the system, where as shown in this chapter the orientation of spins may be expected to change as a result of the mechanical deformation. Furthermore, it should also be noted that in this chapter, only specific configurations of the system were taken into consideration in order to calculate their entropy, i.e. two configurations represented by specific angles θ associated with

initial and final configuration of the deformed system. However, it would be also very interesting to investigate the evolution of magnetic domains in the magneto-mechanical systems and the effect which the rate of the mechanical deformation could have on their evolution.

10.6 Conclusions

In this chapter, the rotating square system with magnetic inclusions located at centres of respective units was modelled by means of the Ising model defined on the square lattice where the distance between the Ising spins can be changed as the result of the variation in the angle θ. Through the use of the exact Onsager's solution for the square lattice, it was shown that such a system, upon undergoing the transition from one configuration corresponding to a particular value of θ_i to another configuration $\left(\theta_f\right)$, may experience a significant change in the magnetic entropy during the isothermal process which result is an indication of the magnetocaloric effect (MCE). It was also shown that extent of this phenomenon may be very large at room temperature even without the presence of the external magnetic field which stimulus could potentially further enhance the magnitude of the discussed phenomenon. In view of this, the proposed concept corresponding to the use of mechanical metamaterials to induce a mechanically-driven magnetocaloric effect may prove to be useful in the case of rapidly developing magnetic refrigeration techniques where the possibility of inducing this effect in the vicinity of the room temperature is of great importance.

11. Magnetic domain evolution in magneto-auxetic systems[8]

HIGHLIGHTS

- Through the use of simulations involving the use of the Monte Carlo Metropolis algorithm, it was shown than one may control the evolution of magnetic domains in the considered magneto-mechanical system (which system similarly to the last chapter is represented by means of the Ising model) upon changing the rate at which the system is deformed;
- It was shown that the average size of magnetic domains within the system (r) does not increase in time (t) proportionally to the factor $t^{1/2}$, which is normally expected for the Ising system where the distance between the Ising spins is constant;
- The energy of the system corresponding to Ising spins located at boundaries of magnetic domains can be controlled via the variation in the rate of deformation of the system.

11.1 Motivation

In the last chapter, the Ising model defined on the lattice corresponding to the rotating square system was used in order to investigate the potential of such system with magnetic inclusions to induce the magnetocaloric effect. To asses its suitability the exhibit the aforementioned phenomenon, the entropy S was calculated with the help of the Helmholtz's free energy, $F = U - TS$, for different configurations of the system subjected to mechanical deformation at the constant temperature T, where U represents internal energy. As discussed in the previous chapter, the change ΔS between the entropies calculated for different

[8] The content of this chapter has already been published in the peer-reviewed journal Physics Status Solidi – Rapid Research Letters: **K. K. Dudek**, W. Wolak, M. R. Dudek, R. Caruana-Gauci, R. Gatt, K. W. Wojciechowski, J. N. Grima, Programmable magnetic domain evolution in magnetic auxetic systems *Phys. Status Solidi RRL* **11** 1700122 (2017)

configurations at a given value of *T* can be interpreted as the extent of the magnetocaloric effect in the case of the isothermal process. However, in the case of the procedure employed in the case of the last chapter, only the initial and final configuration of the system were taken into consideration in order to investigate the discussed physical phenomenon. Thus, it would be very interesting to analyse the evolution of clusters of magnetic moments having the same orientation throughout the whole process of mechanical deformation corresponding to the change in the distance between Ising spins. It would be also interesting to investigate the effect which the rate of such mechanical deformation has on the behaviour of the system. In view of this, in this chapter, both of these aspects related to the magnetic domain evolution in magneto-mechanical systems as going to be analysed.

11.2 Introduction

Over the years, the Ising model [464] has been proven to be a great tool in order to investigate a wide range of physical phenomena. In particular, based on the famous Onsager solution [465-466] for the two-dimensional square lattice at zero magnetic field, this model allowed to gain a fundamental understanding of critical phenomena. It also led to numerous discoveries in areas such as social physics [467], modelling of neural networks [468] and economy [469]. The interest of scientists in this particular technique resulted in numerous studies in which it was shown that in the systems modelled with the Ising model, the mean size of magnetic domains (after a temperature quench of the system from a disordered to an ordered phase) increases in time accordingly to a particular power law. More specifically, it changes proportionally to the evolution time raised to the power of 1/2 or 1/3 for systems with a non-conserved [470, 471] or conserved [472, 473] order parameter respectively. A detailed mathematical description of different laws governing a domain growth in various systems can be found in papers by Bray [474] and Rutenberg [475]. At this point, it is important to note that the results discussed above were obtained for systems in which the distances between the

neighbouring spins within the system were fixed. These rules regarding the rate of growth of domains in magnetic systems do not have to apply to systems in which the distances between the neighbouring spins change in time. In fact, over the years, numerous attempts [476, 477] have been made to analyse various physical phenomena associated with the deformed Ising model (e.g. compressed) with one of the most promising studies being the work of Cirillo *et al.* [478] where it was shown that the above characteristics are not valid for the Ising model subjected to a shear flow. This also suggests that if one was to be able to control the distance between the neighbouring Ising spins then it might be possible to observe a completely new type of evolution of magnetic domains in time.

As discussed in this thesis, mechanical metamaterials are a class of systems which as already discussed in this thesis may exhibit unusual behaviour upon being subjected to a mechanical deformation. These systems may be used to conveniently change the distance between the elements constituting the structure in a rather unusual pattern which would not be possible for conventional systems. Some of the most studied mechanical metamaterials are rotating rigid unit systems with one of the prime examples being 'rotating squares system' with a Poisson's ratio of -1. This particular system deforms in a highly symmetric manner which permits specific distances within the model, e.g. the distances between the centres of all of the neighbouring units, to change by exactly the same amount. This in turn makes this system to be a perfect candidate to alter the geometry of the Ising model throughout the process of simulation.

11.3 Model

In this chapter, the two-dimensional model based on a set of $N_x \times N_x$ rigid squares connected at vertices is going to be discussed (see Figure 11-1). It is assumed that each square has a side length of *a*. The angle between the adjacent units is denoted as 2θ and due to

geometric constraints its value lies within the interval between $0°$ and $180°$. Furthermore, in order to analyse the evolution of magnetic domains in time in such system, it is assumed that located at the centre of each square there is an Ising spin (see Figure 11-1). These spins assume one of the two possible orientations, i.e. either "up" or "down" which states correspond to values 1 and -1 respectively. One may note that Ising spins in such system form a square lattice with the distance *d* separating each pair of neighbouring spins which also means that *d* stands for a distance between the centres of adjacent squares.

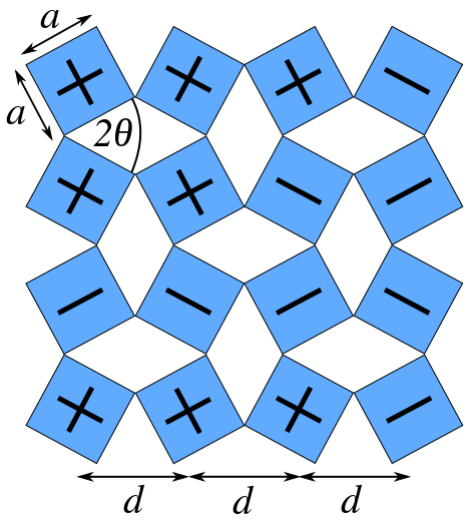

Figure 11-1 The model represented by a set of rigid squares connected at vertices. In this case, signs "+" and "-" located at the centre of each unit, correspond to opposite orientations of magnetic moments within the system. In this diagram, the number of squares was set in a way allowing to conveniently visualise the introduced variables.

Evolution of magnetic domains (collection of spins having the same orientation) is going to be investigated through the use of the well-known Metropolis algorithm [479] (with periodic boundary conditions imposed on the discussed system) in which case the energy of interaction between the neighbouring spins may be defined in the following manner (see Appendix VIII):

$$H = -J\sum_{\langle i,j\rangle}^{N_p}\sigma_i\sigma_j \qquad 11\text{-}1$$

where, *J* is the coupling constant, the angular brackets denote summation over the N_p nearest-neighbour square pairs with Ising spins σ_i and σ_j. Similarly as in the previous chapter, the

value of J depends on a distance *d* as shown in the following equation: $J = J_0 / d^3$ [480]. At this point one may also note that the value of *d* depends on the extent of the angle 2θ and may be expressed as follows:

$$d = a\sqrt{2}\sin\left(\frac{\pi}{4} + \theta\right) \qquad 11\text{-}2$$

It means that the energy of interaction between the adjacent magnetic moments changes accordingly to the value of the angle θ. It also means that the critical temperature T_c changes with the value of θ which stems from the fact that this particular quantity depends on $J = J(\theta)$. Thus, analogically to the last chapter, the value of T_c is given by:

$$T_c(\theta) = \frac{2.269 J_0}{k_B}\left(a\sqrt{2}\sin\left(\frac{\pi}{4} + \theta\right)\right)^{-3} . \qquad 11\text{-}3$$

In order to ensure that the initial state of the system resembles the situation which one would expect in reality, the fully-closed system $(2\theta = 0°)$ is initially subjected to the relatively high temperature T_h (significantly above the value of $T_c(\theta)$) for a duration of $N_{initial}$ Monte Carlo steps. After this pre-heating procedure, the evolution of magnetic domains in the system is investigated in the case of a deformation process corresponding to the change in the value of 2θ angle from $0°$ to $180°$ at a certain temperature *T*. At this point, one should note that a change in the value of the angle 2θ from $0°$ to $90°$ (maximal distance between adjacent spins) corresponds to an increase in the distance between the neighbouring spins by 41% which is associated with a significant change in the magnitude of *J*.

In order to analyse the evolution of magnetic domains, the discussed system was mechanically deformed at a temperature of $T = 77.35\ \mathrm{K}$ with the angle 2θ being changed from $0°$ to $180°$. The value of *T* was chosen in a way which for different values of θ results in it being both greater and lower than the value of T_c (see equation 11-3) throughout the

deformation process. More specifically, the value of T/T_c is equal to 2.142 and 0.963 in the case of 2θ assuming the value of $0°$ and $90°$ respectively. The process of deformation of the discussed system was investigated for different rates of opening of the angle 2θ, i.e. ω={0.5, 1.0, 10, 100}$°/MCs$ ($°/MCs$ - degree per Monte Carlo step). The remaining parameters defined in this Model section were set to be the following: $N_x \times N_x = 500 \times 500$, a = 18.475 nm, T_h = 800 K, $N_{initial} = 5$ and $J_0 = 50.42$ eV nm^3. At this point it is worth to note that before the pre-heating procedure, which procedure took place before the beginning of the deformation, the orientation of spins within the system was selected randomly. Furthermore, in order to ensure high quality of the generated results, each set of results was averaged 10 times.

11.4 Results and Discussion

Based on Figure 11-2(a), one can note that throughout the process of mechanical deformation, the change in size of magnetic domains (represented by means of the correlation length *r*) does not follow the well-known power law corresponding to Ising systems with a non-conserved order parameter, i.e. is not proportional to the time raised to the power of 1/2. Instead, the correlation length of the deformed system exhibits a more complex behaviour with two local extrema being observed. More specifically, at the range of θ between $0°$ and $30°$ the value of *r* increases in order to subsequently start decreasing upon surpassing the configuration corresponding to $2\theta = 30°$. This trend is continued up to the point where the local minimum of *r* is reached, i.e. around $90° - 100°$. During the remaining part of the mechanical deformation of the discussed system the angle 2θ is being changed from $90°$ to $180°$ (this process corresponds to a decrease of the distance between the adjacent spins) which results with an increase of the magnitude of the correlation length. This novel behaviour can be easily understood if one was to analyse the evolution of magnetic domains in time in the case of the analogical system in which the distance between the adjacent units does not change throughout

the simulation, i.e. $\theta = const.$ (see Figure 11-2(b)). From Figure 11-2(b), one can note that in the case of these systems, the lower the distance between the neighbouring units the larger the value of *r* throughout the simulation. On the other hand, the model discussed in this work is deformed in a way so that the value of 2θ changes from $0°$ to $180°$. This in turn means that the value of *d* increases at the interval between $0°$ and $90°$ and analogically decreases at the interval between $90°$ and $180°$. In view of this, one may imagine that the evolution of domains in the system in which the value of 2θ is being changed throughout the simulation can be approximately visualised as the function connecting different points at the consecutive time steps from functions corresponding to systems in which the distance between the neighbouring spins remains constant. In other words, according to Figure 10-2(b), the process discussed in this work can be approximated by the procedure in which we "move" in time from the line corresponding to $0°$ to the line corresponding to $90°$ (in the case of systems where the distance between spins is fixed) and then back from $90°$ to $0°$. Furthermore, in the case of Figure 11-2(b), the plots associated with relatively small values of θ correspond to the situation where $T < T_C$. In such cases the emergence of the formerly discussed power law is expected ($r \sim t^{\alpha}$, where $\alpha = 1/2$), which trend may be easily observed taking the system corresponding to $2\theta = 0°$ as an example. In this particular case, the exponent α associated with the system is equal to 0.49913 $\pm$ 0.00098.

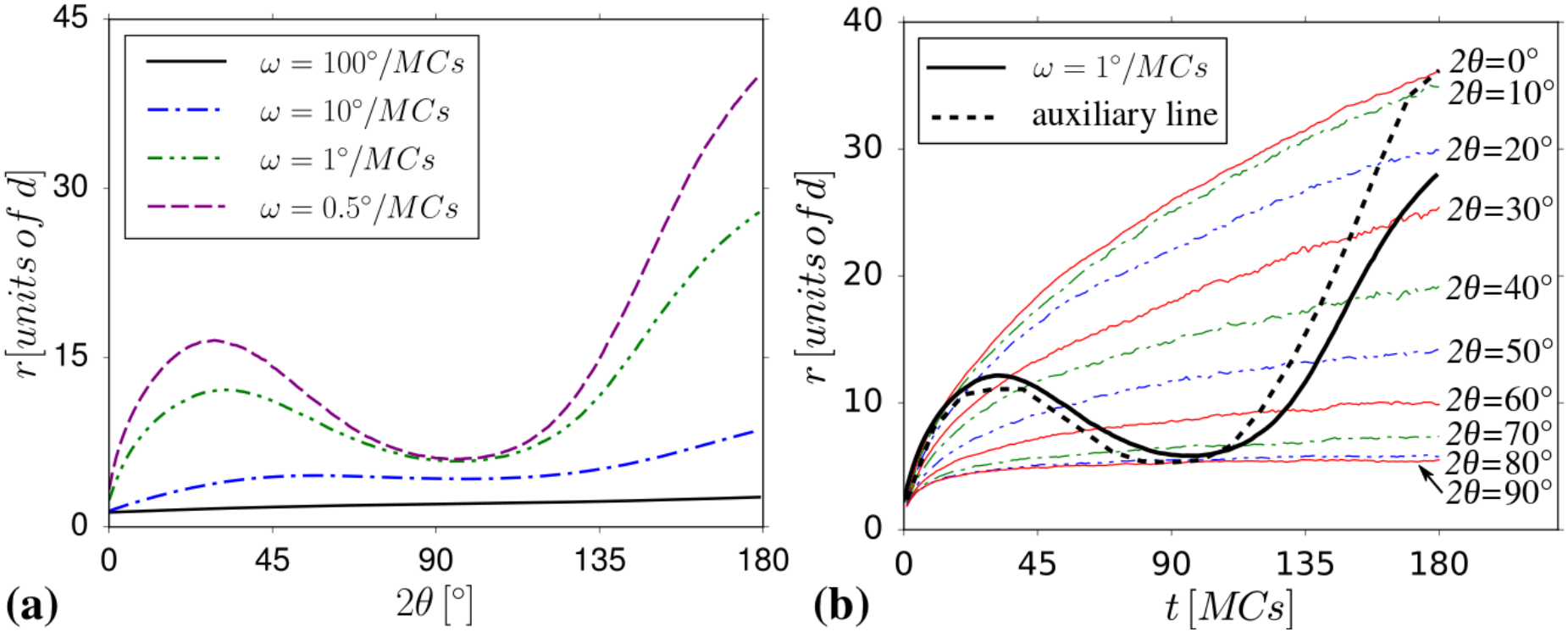

Figure 11-2 The panels present (a) the change in the correlation length r during the deformation process for different values of ω and (b) the comparison of the evolution of the system corresponding to $\omega = 1°/MCs$ to the behaviour of systems in which the distance between the neighbouring spins is not being changed throughout the simulation, i.e. the simulation takes place for a fixed value of θ. The correlation length r is expressed in terms of the distance d (see equation 11-2).

Another interesting result corresponds to the effect which the rate of opening of the angle 2θ has on the evolution of magnetic domains in the discussed system. As shown in Figure 10-2(a), a variation in the magnitude of the angular velocity ω allows to control the growth of domains within the system. In particular, it may be noted that the lower the magnitude of ω, the larger the value of *r* (average size of magnetic domains). Based on Figure 11-2(a) one can also see that there is a certain threshold value of ω below which value the system does exhibit the characteristics described above. In the case of results presented in Figure 11-2 (a) such threshold value would may be found in the vicinity of $\omega = 10° / MCs$. Above this value, magnetic domains do not have enough time to evolve during the deformation process which leads to significantly lower values of *r*. Moreover, in the case of relatively high values of ω, the local minimum of the function of *r*, which might be observed in the vicinity of $90°$, disappears. A clear difference between the evolution of domain in systems deformed with relatively high and relatively low value of ω is visualised in Figure 11-3.

It is also possible to analyse the change in energy during the deformation of the discussed system. In particular, the change in the energy *E* associated with spins at the boundaries of respective domains. Based on Figure 11-4, one can note that the change in ω results with qualitatively different results in terms of the energy *E* for systems corresponding to relatively large and small values of ω.

In this chapter, in order to generate the results discussed above, we consider the use of magnetic rigid units constituting the system of rotating squares. In reality, the behaviour of such theoretical structure could be represented by a non-magnetic system of rotating squares with magnetic nanoparticles embedded at the centre of each unit as discussed in the former chapter. Furthermore, in order to ensure that the discussed results could be obtained in reality, all of the parameters used in this work were set in a way so that the system behaves as if magnetic nanoparticles of the size of 10 nm were embedded on top of non-magnetic units.

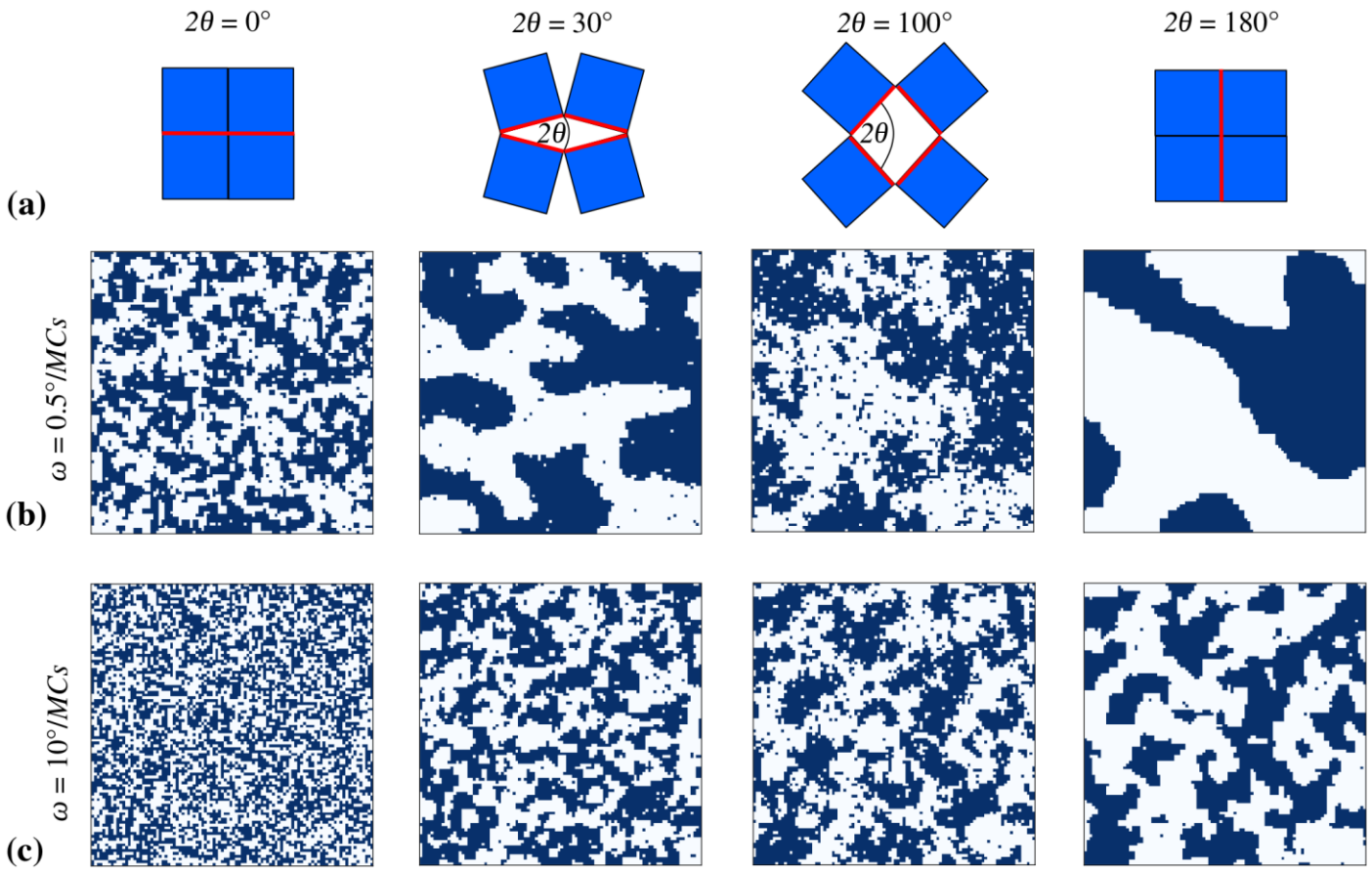

Figure 11-3 The panels present (a) diagrams visualising the configuration of the magnetic auxetic system corresponding to a particular value of the angle θ (red lines are used in order to highlight edges forming the aperture of the unit-cell), (b) evolution of magnetic domains for a system in which the angle θ is being changed with the constant angular velocity $\omega = 0.5°/MCs$ (relatively low value of ω) and (c) visualisation of the evolution of magnetic domains in the system corresponding to $\omega = 10°/MCs$ (relatively high value of ω). In order to better visualise the domains in the system on panels (b) and (c), only a fragment (100×100 units) of the larger square lattice considered in this work was selected.

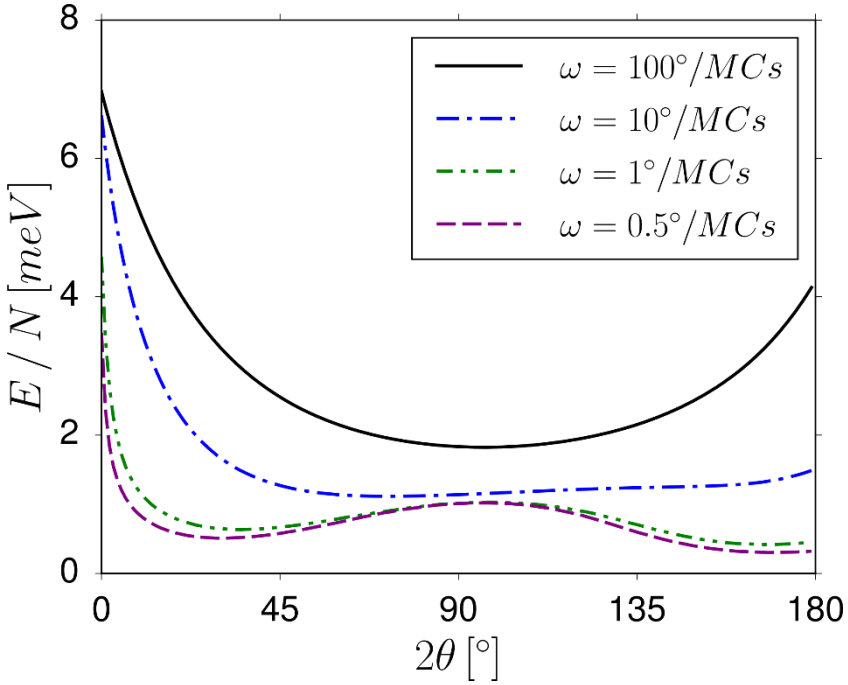

Figure 11-4 Energy of spins at the domain boundary per spin for different values of ω.

All of this is very important as it is shown that it is possible to control the evolution of domains upon changing the magnitude of the angular velocity ω. It is also shown that the variation in the value of ω leads to very different results in terms of the energy *E*. This control over the change in the value of the energy throughout the process of deformation may be used in order to control the magnitude of the mechanically-driven magnetocaloric effect as shown in the last chapter. This in turn would allow to increase or decrease the value of temperature of the system in a controllable manner without the presence of the external magnetic field. This result could prove to be very important for scientists working on novel techniques associated with magnetic refrigeration particularly in view of the recent wide interest in magnetic metamaterials and other systems. It is also hoped that this work may contribute to the further discussion concerning the use of the Ising model in the case of hierarchical systems which could possibly lead to novel applications of such systems.

At this point, it should be highlighted that even though in the case of this chapter a particular type of the non-magnetic matrix was chosen, magnetic inclusions could also be

inserted into a different mechanical system in order to analyse the effect of the magnetic domain evolution. However, for an arbitrary system there would not be any analytical expression allowing to determine the value of the critical temperaure corresponding to a given system. It should also be noted that the considered effect of the magnetic domain evolution can only be analysed in the case of large systems. This means that the behaviour of the hypothetical magneto-mechanical system which is discussed in this chapter is not expected to be observed in the case of real relatively large systems which despite the analogical geometry do not consist of a large number of magnetic inclusions.

11.5 Conclusions

In conclusion, in this chapter, it was shown that the evolution of magnetic domains in the Ising model associated with the magnetic system of rotating squares does not follow a well-known power law which is valid for systems in which the distance between the neighbouring units remains constant throughout the simulation. It was also shown that the evolution of magnetic domains can be controlled upon altering the magnitude of the angular velocity of rigid units constituting the system. Another result obtained through this study shows that upon changing the value of the angular velocity of rigid units, it is possible to control the energy of the system. It should also be noted that all of the discussed results could potentially prove to be useful in the case of applications related to the magnetic refrigeration.

12. General Discussion, Conclusions and Future Perspective

As said by Albert Einstein, “To raise new questions, new possibilities, to regard old problems from a new angle, requires creative imagination and marks real advance in science”. This famous quote suggests that sometimes in order to make a true contribution to science it is necessary to think “out of the box” and approach some of the problems from a new angle. Inspired by this approach, in this thesis an attempt was made to investigate some aspects of mechanical metamaterials which have never been studied or studies related to them are still in their infancy and should be further developed before proving to be useful in practise.

Over the years, mechanical metamaterials have been extensively investigated from the point of view of their capability to exhibit unusual mechanical properties such as negative Poisson’s ratio, negative thermal expansion, negative compressibility and negative stiffness. Thanks to their potential to exhibit such anomalous mechanical behaviour, these systems were found to be suitable for a variety of applications in different branches of industry. As discussed in the Literature Review, studies related to mechanical metamaterials have been primarily focused on the design of new types of such systems which could exhibit counterintuitive mechanical behaviour. As a result of these studies, over the years, many new classes of mechanical metamaterials have been proposed with some of the most studied examples being rotating rigid unit systems, perforated systems, re-entrant and chiral honeycomb structures as well as foams. One of the reasons behind the existence of numerous systems could be the fact that in the majority of cases, new systems have been proposed and analysed analytically and experimentally in an attempt to achieve novel behaviour. However, in theory, novel behaviour can also be obtained from already known systems by appropriately modifying them without the need to actually design a completely new geometry. For example, it might be possible to achieve unusual mechanical properties simply by using different materials to construct the system. However, the use of different constituent materials does not ensure that the resultant

structure would exhibit significantly different unusual mechanical properties than the original system composed of a single material. One may also expect that for such a system, it would be difficult to observe a novel mechanical behaviour which is not observed for its mono-material counterpart. Nevertheless, a new type of mechanical behaviour could be manifested should it be assumed that some of the constituents in a newly constructed system can interact with each other. It would be particularly interesting if one were to consider a system where constituents can interact with each other without the need of being physically connected with each other. One type of interaction which is known to satisfy this condition is magnetic interaction between magnetic entities where, in this work, this type of interaction between constituents was achieved through the introduction of magnetic inclusions to the mechanical metamaterial. Consequently, one can expect that the resultant magneto-mechanical system may possess superior mechanical properties in comparison to its non-magnetic mono-material counterpart where, as discussed in the Literature Review, the resultant structure may even exhibit anomalous mechanical behaviour which cannot be observed for a similar system without magnetic inclusions. At the same time, it is very important to highlight the fact that the concept based on the use of magnetic inclusions in the case of mechanical metamaterials is still relatively new and the research related to this topic is in its infancy. In addition to this, one should also note that as discussed in this thesis, the novel type of mechanical behaviour observed for already known mechanical metamaterials does not have to be induced by the use of magnetic inclusions and in general one could consider the use of a variety of different approaches such as the variation in the mass distribution of the system. In view of the above, this thesis focused primarily on the potential of already proposed mechanical metamaterials to exhibit novel types of mechanical behaviour or counterintuitive mechanical properties as a result of modifications made to historically-known mechanical metamaterials composed of a single material.

One of many interesting aspects related to the possible behaviour which can be exhibited by mechanical metamaterials which still remains to be explored corresponds to the capability of these systems to induce their own global rotation as a result of the rotation of their subunits. One of the possible reasons why this effect has not been yet studied by scientists working in this field might be the fact that normally in order to investigate mechanical metamaterials, these systems are being constrained which makes it impossible for the system to exhibit the discussed phenomenon. In view of this, in this thesis, the possibility of achieving this effect was investigated for a particular type of a mechanical metamaterial system composed of square-like rigid units which was free to rotate with respect to its centre of mass. More specifically, in Chapter 4 of the thesis, this novel concept was analysed through a theoretical model describing the dynamics of deformation of such a system for which the results suggest that the considered effect can be not only observed but its extent may also be controlled via the variation in the mass distribution.

In order to verify the possibility of achieving the self-induced global rotation of mechanical metamaterials in practise, in Chapter 5, an analogical system was also investigated through the use of an experimental prototype which study led to similar conclusions suggested by the theoretical predictions. More specifically, it was shown that as expected based on the conservation of angular momentum principle, the rotation of individual units constituting the system results in the rotation of the entire structure in the opposite direction to the rotation of heavy units. In this chapter, the behaviour of the system after the collision between the rigid units was also described which makes it easier to predict the behaviour of devices based on the proposed concept in reality. In the chapter following these results, i.e. in Chapter 6, it was shown that even though mechanical systems composed of rigid square-like units show great promise to induce their global rotation as a result of mechanical deformation, it is not the only geometry which might be conducive to this phenomenon. In view of this, to gain a better

understanding of the effect of the variation in geometry on the behaviour of the system, the aforementioned model was replaced with a similar system composed of rectangular units as it is significantly more versatile in terms of its geometry. More specifically, in this chapter, it was shown that depending on their connectivity, upon being subjected to mechanical deformation, different rotating rectangle systems exhibit a very different extent of global rotation which, for some of these systems, also depends on the aspect ratio of the structural units. However, despite these differences, it should be highlighted that nonetheless this phenomenon was observed in all of the considered systems. In view of this, it should be mentioned that all of the reported results relating to the ability of mechanical metamaterials to exhibit the discussed characteristics indicate that this concept may prove to be useful in a variety of applications. One type of such applications could be wind turbines where the ease with which these mechanical systems can be deformed could be used to fine-tune the moment of inertia of the entire wind turbine. This in turn, would allow the control of the reaction of the wind turbine to the wind having a particular strength, thus allowing increase in the efficiency of the device. Another broad class of applications where the considered concept of self-induced global rotation of mechanical metamaterials could be utilised relates to devices employed in space such as satellites, spacecraft or telescopes. Due to the fact that in space there is no medium to interact with, the only way for such systems to induce their own rotation is to change their mass (e.g. through gas jets) or change the angular momentum of one or more of their components, which process would lead to a change in the angular momentum of the entire system in a way that the angular momentum of the whole system would be conserved. The concept proposed in this work utilises the latter approach where through the rotation of subunits, one can induce and control the rotation of the whole system employed in space. However, it should be noted that before implementing the considered concept in industry one should conduct studies related to the fault control and cost analysis which are beyond the scope of this thesis.

As discussed in this thesis, even though novel types of behaviour which can be exhibited by mechanical metamaterials might be attractive enough to introduce them to new branches of industry, the research related to these systems is still primarily focused on the possibility of obtaining anomalous mechanical properties. In particular, in recent years, the scientific community working in this field devoted a lot of attention to the possibility of enhancing anomalous mechanical properties of mechanical metamaterials so that these systems could be even more efficient in various applications. One class of mechanical metamaterials which was recently reported to exhibit such a characteristic are hierarchical mechanical metamaterials, where it was shown that the resultant negative Poisson's ratio can assume lower values than would be the case for analogical systems which do not incorporate the concept of hierarchy. In those studies, it was also reported that lower levels of such multi-level systems tend to open up to a significantly lower extent than higher levels which do not allow the systems to achieve their full potential. In order to address this observation, in Chapter 7 of the thesis, a particular two-level hierarchical system composed of rigid squares connected at vertices was investigated through a dynamics approach. For this system, it was shown that the deformation pattern exhibited by the structure depends on the magnitude of the resistance of respective units to the rotational motion, which in turn is related to the number of hinges associated with each of the levels. Thus, as shown in this chapter, upon changing the magnitude of such resistance it is possible to open both levels of the considered system to a different extent, which also leads to a different value of the Poisson's ratio. This result is interesting as it shows that the exact same system (at least in terms of geometry), can deform differently and exhibit different mechanical properties solely as a result of the variation in the resistance of hinges connecting the structural units to rotational motion. However, this does not mean that a similar or greater level of control over the deformation pattern cannot be achieved by means of a different approach. As a matter of fact, as discussed in Chapter 7, even though the deformation of the considered hierarchical

system was induced through the application of external forces to the structure, it does not mean that one cannot deform it through the use of internal forces which could for example be applied by means of actuators or magnets / electromagnets appropriately located on adjacent rigid units. It should also be noted that the latter approach would be expected to make it possible to open a given level of the hierarchical structure to an arbitrary extent irrespective of the deformation of other levels.

One can note that in Chapters 4-7 of the thesis, novel mechanical behaviour, such as the self-induced global rotation of mechanical metamaterials, and unusual mechanical properties were reported for systems composed of square/rectangle-like motifs. However, this does not mean that one cannot propose novel mechanical systems capable of exhibiting such counter-intuitive behaviour. As a matter of fact, in view of the versatility that mechanical metamaterials afford, one can expect that there is a plethora of such systems which still remain to be discovered. As discussed in Chapter 8, an example of such a system is a mechanical metamaterial composed of generic rigid triangles connected at vertices. In this thesis it was shown that irrespective of the stage of the deformation and the shape of the structural units, such a system has the potential to exhibit negative linear compressibility in at least one direction. It was also reported that the considered system exhibits this particular characteristic whenever it also assumes a positive Poisson's ratio that exceeds the value of one for loading in the same direction. In addition to negative linear compressibility, this novel mechanical metamaterial was also reported to have a propensity to exhibit negative thermal expansion. It should also be highlighted that even though this system can exhibit anomalous mechanical properties solely as a result of its geometric design, its properties can be further enhanced and controlled through the use of magnetic inclusions. This in turn could allow the design of a device based on a such concept in a way which would make it act as a smart filtration device.

Deformation of mechanical metamaterials can in general be controlled or influenced through a variety of different techniques. One of the most common approaches to affect deformation in such systems is through the use of hinge-like elements whose deformation is governed by a harmonic potential, which normally would cause a given system to assume a particular conformation. However, such an approach does not provide a true control over the deformation of the given system. In addition to this, once such a system is produced, it is very difficult to change its properties. It seems that the most promising concept that provides a solution to both of these problems, thereby allowing one to acquire the desired level of control over the behaviour of the system, relies on the use of magnetic inclusions. This stems from the fact that, through mutual interactions, such inclusions may control the behaviour of the structure at any stage of the deformation. It should also be noted that as reported in the literature (see Literature Review), interactions between magnetic inclusions may also lead to anomalous mechanical properties which would be no longer observed upon removing such inclusions from the structure. Nonetheless, despite their great potential, studies related to mechanical metamaterials with magnetic inclusions are still in their infancy.

In view of the above, in Chapter 9 of this thesis, in an attempt to gain a better understanding of the behaviour of these systems, the potential of a particular mechanical metamaterial with magnetic inclusions in the form of magnets was investigated vis-à-vis its ability to exhibit unusual mechanical behaviour. More specifically, through a theoretical model as well as experimental testing, it was shown that the considered system may exhibit either positive or negative stiffness depending solely on the orientation of magnets within the system, where it should be noted that results generated by means of both of the techniques were in a very good agreement. In this chapter, it was also shown that a system composed of arrowhead structural units may also exhibit other unusual mechanical properties. More specifically, it was shown that throughout a significant part of the deformation process, the discussed system is capable

of exhibiting both negative Poisson's ratio and negative stiffness at the same of time, where the magnitude of these effects could be fine-tuned via the variation in geometric parameters defining the geometry of the structure. All of these results indicate that apart from smart filtration devices, the considered concept could prove to be useful in a variety of vibration damping devices where negative stiffness is normally required. These results also suggest that it may be possible to propose novel types of applications where materials exhibiting several anomalous mechanical properties simultaneously would be essential.

As discussed in Chapter 10 of the thesis, the concept of mechanical metamaterials with magnetic inclusions could also be used in order to investigate physical phenomena which are not directly related to mechanical properties. An example of a very interesting physical effect which is an intrinsic property of magnetic systems is the magnetocaloric effect, which is normally observed in the presence of an external magnetic field. However, in the literature there are a few studies which suggest that in addition to the variation in the magnetic field, this effect could also be achieved as a result of a deformation of the magnetic system (for example as a result of a compression of the system with magnetic inclusions). In order to investigate the possibility of observing such phenomenon for magneto-mechanical systems, a particular hypothetical system was considered where magnetic inclusions were set at the centres of respective units in a rotating square system at a constant temperature. This means that irrespective of the stage of the mechanical deformation of such a system, magnetic inclusions would always form a square lattice. Thus, as discussed in Chapter 10, the extent of the magnetocaloric effect for the considered system could be calculated as a change in the magnetic entropy upon deforming the system from one configuration to another. In view of this, in order to determine the possibility of generating the magnetocaloric effect (and its magnitude) for different ranges of mechanical deformation, the considered system was approximated by means of the Ising model without the presence of an external magnetic field. Furthermore, through the

use of this model, the entropy assumed by the system for each of the configurations was determined by means of the famous Onsager's solution. The generated results clearly indicate that the discussed phenomenon can indeed occur without the external magnetic field and that its magnitude can be large even at room temperature. In this chapter, it was also shown that the extent of the magnetocaloric effect can be controlled by adjusting the range of the mechanical deformation corresponding to the change in the distance between the magnetic inclusions.

In addition to the possibility of inducing the magnetocaloric effect, it could be also very interesting to analyse the process of magnetic domain evolution throughout the deformation of the magneto-mechanical system. In view of this, in Chapter 11, this phenomenon was simulated for a system analogical to that of Chapter 10 by means of the Monte Carlo Metropolis algorithm. According to the generated results, it may be concluded that the rate at which such magneto-mechanical systems are deformed affects the way how magnetic domains are evolving. It should be also noted that the variation in the mean size of magnetic domains in such systems subjected to mechanical deformation does not follow a well-known power law which normally characterises the evolution of magnetic domains in the Ising model. This result could encourage scientists working on critical phenomena to investigate such physical processes in systems subjected to mechanical deformation as they clearly show a potential to exhibit very interesting behaviour. Furthermore, keeping in mind the results proposed in chapters 10 and 11, it might be also possible that hypothetical mechanical metamaterial systems with magnetic inclusions constructed at the nanoscale may potentially be used to design magnetic refrigerators. In order to make such devices available to the general public, they should be able to operate at room temperature which normally is very difficult to achieve. However, as discussed in Chapter 10, the extent of the magnetocaloric effect for the considered system can assume large values at room temperature which makes it to be a very interesting candidate to further investigate its potential from the point of view of its applicability in the industry.

It is worth mentioning that the results presented and discussed in this thesis were generated by means of different approaches depending on the type of the investigated phenomenon. More specifically, in chapters 4-7, the dynamic behaviour of particular rotating rigid unit systems composed or square-like motifs was analysed by means of theoretical models where their evolution in time was described by means of appropriate equations of motion. Such approach was very convenient because of its relative simplicity. Also, unlike some other techniques, it made the obtained results easily reproducible for researchers who may want to further develop some of the ideas proposed in this thesis. However, it should be emphasised that should one consider a different set of assumptions than those made in the aforementioned chapters, then it might be necessary to consider the use of other methods. Furthermore, in chapters 8, 9 and 10, some of the standard theoretical models which are commonly used in the considered fields of science were used in order to analyse concepts proposed in these chapters. Such approach apart from being very reliable, also allows for a simple assessment of limitations of each of the considered theoretical models as in a majority of cases they have been already discussed in the literature. In chapter 11, in order to analyse the evolution of the Ising model defined in a way allowing to represent a particular magneto-mechanical system, the Monte Carlo Metropolis algorithm was used which is a standard tool used to minimise the free energy of the considered system. This approach is well-known to correctly describe the evolution of a variety of systems including magnetic inclusions which can be represented by the Ising model as is the case in this thesis. It should also be mentioned that in the case of chapters 5 and 9, the results obtained through the use of theoretical models were additionally verified by experiments involving the use of prototypes constructed by a 3D extrusion printer.

At this point, it should be noted that all of the concepts proposed in this thesis were discussed for two-dimensional systems. However, this does not mean that these concepts cannot be observed in three dimensional mechanical metamaterials. As discussed in the literature (see

Literature Review), planar mechanical metamaterials such as rotating square systems have their three-dimensional counterparts which are capable of exhibiting unusual mechanical properties in three dimensions as is the case for the rotating cuboid system [303]. It has also been already reported that two-dimensional planar mechanical metamaterials can be arranged into three-dimensional tubular configurations to utilise their unusual properties in applications such as stents etc. It is also worth to mention that one can design the considered systems in a way so that they would be capable of deforming from a planar to non-planar conformation and *vice-versa*. Such behaviour could for example be achieved as a result of magnetic interactions between magnetic inclusions implemented within the system.

Another aspect related to systems considered in this thesis which could benefit from being further investigated is the subject of order and disorder within the structure. All of the considered systems were designed in a manner so that one could distinguish a particular element within each of the structures which could be tessellated in order to reproduce the entire system. This means that all of these systems were ordered. However, this does not mean that it is not possible to design similar constructs incorporating the concept of disorder. As a matter of fact, in general, the behaviour of such systems would be expected to be different from their ordered counterparts which means that such systems could potentially exhibit very interesting behaviour. One could for example consider studies related to stiffness exhibited by disordered systems with magnetic inclusions where the emergence of regions of particularly large or small positive/negative stiffness could be expected.

At this point, it is important to mention that the majority of results discussed in this thesis, especially those related to the self-induced global rotation of mechanical metamaterials and the possibility of inducing either negative or positive stiffness in magneto-mechanical systems, are seemingly scale independent. This stems from the fact that such phenomena are expected to be observed as long as the considered systems can be constructed, which in theory does not depend

significantly on the scale of the system. However, one should note that upon decreasing the size of such systems, so that they would be in the vicinity of the nanoscale, their behaviour would no longer be governed by classical mechanics and instead one should consider the use of quantum mechanics to describe them. On the other hand, the magnetocaloric effect for the considered hypothetical magneto-mechanical systems would be observed only at the nanoscale as it requires a very large number of densely packed interacting magnetic particles to be manifested.

Finally, it can be concluded that despite numerous studies related to mechanical metamaterials, there are still many aspects of these systems which are worth being investigated. For example, despite the fact that all of the unusual effects discussed in this thesis were obtained for structures based mostly on historically-known mechanical metamaterials, it is still possible to propose novel designs of mechanical metamaterials which are capable of exhibiting anomalous mechanical and other types of behaviour with or without magnetic inclusions enhancing their properties. It is also important to note that concepts discussed in this thesis are not limited to particular geometries and in general they may be expected to be applicable for a variety of systems. In view of this, it is hoped that concepts discussed in this thesis will contribute to further studies related to mechanical metamaterials and will hopefully one day lead to their implementation in novel applications improving the standard of our lives. It is also worth to mention that some of the concepts reported in this thesis have already been followed by other researchers with one of the examples being the results from Chapter 8. More specifically, in his recent work [292], Zhou *et al.* studied the potential of the system composed of generic rigid triangles to exhibit negative linear compressibility for which a concept of a similar model was proposed in an aforementioned chapter in this thesis.

13. References

[1] J. N. Grima and R. Caruana-Gauci, “Mechanical metamaterials: Materials that push back”, *Nat. Mater.*, vol. 11, pp. 565-566, 2012.

[2] J. N. Grima and K. E. Evans, “Auxetic behavior from rotating squares”, *J. Mater. Sci. Lett.*, vol. 19, pp. 1563-1565, 2000.

[3] J. N. Grima, A. Alderson and K. E. Evans, “Negative Poisson’s ratio from rotating rectangles”, *Comput. Methods Sci. Technol.*, vol. 10, pp. 137-145, 2004.

[4] J. N. Grima, E. Manicaro and D. Attard, “Auxetic behaviour from connected different-sized squares and rectangles”, *Proc. R. Soc. London A Math. Phys. Eng. Sci.*, vol. 467, 2010.

[5] R. Bailey and R. Hicks, “Behaviour of perforated plates under plane stress”, *Arch. J. Mech. Eng. Sci.*, Vols. 1-23, pp. 143-165, 1960.

[6] J. Porowski and W. J. O’Donnell, “Effective Plastic Constants for Perforated Materials”, *J. Press. Vessel Technol.*, vol. 96, p. 234, 1974.

[7] W. J. O’Donnell, “Effective Elastic Constants for the Bending of Thin Perforated Plates With Triangular and Square Penetration Patterns”, *J. Eng. Ind.*, vol. 95, p. 121, 1973.

[8] M. Forskitt, J. R. Moon and P. A. Brook, “Elastic properties of plates perforated by elliptical holes”, *Appl. Math. Model.*, vol. 15, pp. 182-190, 1991.

[9] K. Bertoldi, P. M. Reis, S. Willshaw and T. Mullin, “Negative Poisson’s Ratio Behavior Induced by an Elastic Instability”, *Adv. Mater.,* vol. 22, p. 361–366, 2010.

[10] T. Mullin, S. Deschanel, K. Bertoldi and M. C. Boyce, “Pattern Transformation Triggered by Deformation”, *Phys. Rev. Lett.,* vol. 99, p. 84301, 2007.

[11] K. Bertoldi, M. C. Boyce, S. Deschanel, S. M. Prange and T. Mullin, “Mechanics of deformation-triggered pattern transformations and superelastic behavior in periodic elastomeric structures”, *J. Mech. Phys. Solids,* vol. 56, pp. 2642-2668, 2008.

[12] J. Li *et al.*, “Switching periodic membranes via pattern transformation and shape memory effect”, *Soft Matter,* vol. 8, p. 10322, 2012.

[13] R. Gatt, New structures and materials exhibiting negative Poisson’s ratios and negative compressibility, University of Malta: Ph.D. thesis, 2010.

[14] F. K. Abd El-Sayed, R. Jones and I. W. Burgess, “A theoretical approach to the deformation of honeycomb based composite materials”, *Composites,* vol. 10, pp. 209-214, 1979.

[15] L. J. Gibson, M. F. Ashby, G. S. Schajer and C. I. Robertson, “The Mechanics of Two-Dimensional Cellular Materials”, *Proc. R. Soc. London A Math. Phys. Eng. Sci.,* vol. 382, 1982.

[16] M. A. Grediac, “finite element study of the transverse shear in honeycomb cores”, *Int. J. Solids Struct.,* vol. 30, pp. 1777-1788, 1993.

[17] F. Scarpa, P. Panayiotou and G. Tomlinson, “Numerical and experimental uniaxial loading on in-plane auxetic honeycombs”, *J. Strain Anal. Eng. Des.,* vol. 35, pp. 383-388, 2000.

[18] F. Scarpa and G. Tomlinson, “Theoretical Characteristics of the vibration of sandwich plates with in-plane negative Poisson’s ratio values”, *J. Sound Vib.,* vol. 230, pp. 45-67, 2000.

[19] J. P. M. Whitty, A. Alderson, P. Myler and B. Kandola, “Towards the design of sandwich panel composites with enhanced mechanical and thermal properties by variation of the in-plane Poisson’s ratios”, *COMPOS. PART A-APPL. S.,* vol. 34, pp. 525-534, 2003.

[20] M. Ruzzene and F. Scarpa, “Control of Wave Propagation in Sandwich Beams with Auxetic Core”, *J. Intell. Mater. Syst. Struct.,* vol. 14, pp. 443-453, 2003.

[21] M. Ruzzene, L. Mazzarella, P. Tsopelas and F. Scarpa, “Wave Propagation in Sandwich Plates with Periodic Auxetic Core”, *J. Intell. Mater. Syst. Struct.,* vol. 13, pp. 587-597, 2002.

[22] A. Alderson *et al.*, “Modelling of the mechanical and mass transport properties of auxetic molecular sieves: an idealised organic (polymeric honeycomb) host–guest system”, *Mol. Simul.,* vol. 31, pp. 897-905, 2005.

[23] D. Li, J. Yin, L. Dong and R. S. Lakes, “Strong re-entrant cellular structures with negative Poisson’s ratio”, *J. Mater. Sci.,* vol. 53, pp. 3493-3499, 2018.

[24] K. W. Wojciechowski, “Two-dimensional isotropic system with a negative Poisson ratio”, *Phys. Lett. A,* vol. 137, pp. 60-64, 1989.

[25] R. S. Lakes, “Deformation mechanisms in negative Poisson’s ratio materials – Structural aspects”, *J. Mater. Sci.,* vol. 26, pp. 2287-2292, 1991.

[26] D. Prall and R. S. Lakes, “Properties of a chiral honeycomb with a Poisson’s ratio of -1”, *INT. J. MECH. SCI.,* vol. 39, pp. 305-314, 1997.

[27] O. Sigmund, S. Torquato and I. A. Aksay, “On the design of 1-3 piezo-composites using topology optimisation”, *J. MATER. RES.,* vol. 13, pp. 1038-1048, 1998.

[28] O. Sigmund and S. Torquato, “Design of smart composite materials using topology optimization”, *Smart Mater. Struct.,* vol. 8, pp. 365-379, 1999.

[29] A. Alderson, K. L. Alderson, G. Chirima, N. Ravirala and K. M. Zied, “The in-plane linear elastic constants and out-of-plane bending of 3-connected ligament and cylinder-ligament honeycombs”, *Composite Science and Technology,* vol. 70, pp. 1034-1041, 2010.

[30] X. Ren, J. Shen, P. Tran, T. D. Ngo and Y. Min Xie, “Design and characterisation of a tuneable 3D buckling-induced auxetic metamaterial”, *Mater. Des.,* vol. 139, pp. 336-342, 2018.

[31] R. S. Lakes and K. Elms, “Indentability of Conventional and Negative Poisson’s Ratio Foams”, *J. Compos. Mater.,* vol. 27, p. 1193–1202, 1993.

[32] N. Chan and K. E. Evans, “Indentation Resilience of Conventional and Auxetic Foams”, *J. Cell. Plast.,* vol. 34, pp. 231-260, 1998.

[33] Y. Scarpa, J. R. Yates, L. G. Ciffo and S. Patsias, “Dynamic crushing of auxetic open-cell polyurethane foam”, *Proc. Inst. Mech. Eng. Part C J. Mech. Eng. Sci.*, vol. 216, pp. 1153-1156, 2002.

[34] A. V. Shalaev, W. Cai, U. K. Chettiar, H.-. K. Yuan, A. K. Sarychev, V. P. Drachev and A. V. Kildishev, “Negative index of refraction in optical metamaterials”, *Optics letters*, vol. 30, pp. 3356-3358, 2005.

[35] C. M. Soukoulis, S. Linden and M. Wegener, “Negative Refractive Index at Optical Wavelengths”, *Science*, vol. 315, pp. 47-49, 2007.

[36] R. A. Shelby, D. R. Smith and S. Schultz, “Experimental Verification of a Negative Index of Refraction”, *Science*, vol. 292, pp. 77-79, 2001.

[37] V. M. Shalaev, “Optical negative-index metamaterials”, *Nat. Photonics*, vol. 1, pp. 41-48, 2007.

[38] D. R. Smith, J. B. Pendry and M. C. K. Wiltshire, “Metamaterials and Negative Refractive Index”, *Science*, vol. 305, pp. 788-792, 2004.

[39] K. E. Evans, I. J. Hutchinson and S. C. Rogers, “Molecular network design.,” *Nature*, vol. 353, p. 124, 1991.

[40] B. M. Lempiere, “Poisson’s ratio in orthotropic materials.”, *AIAA J.*, vol. 6, p. 2226–2227, 1968.

[41] K. W. Wojciechowski, “Remarks on ‘Poisson Ratio beyond the Limits of the Elasticity Theory’”, *J. Phys. Soc. Japan*, vol. 72, pp. 1819-1820, 2003.

[42] A. Branka, D. Heyes and K. Wojciechowski, “Auxeticity of cubic materials”, *Phys. Status Solidi B,* vol. 246, pp. 2063-2071, 2009.

[43] R. V. Goldstein, V. A. Gorodtsov and D. S. Lisovenko, “Classification of cubic auxetics”, *Phys. Status Solidi B,* vol. 250, pp. 2038-2043, 2013.

[44] C. Jasiukiewicz, T. Paszkiewicz and S. Wolski, “Auxetic properties and anisotropy of elastic material constants of 2D crystalline media”, *Phys. Status Solidi B,* vol. 245, p. 562, 2008.

[45] T. Paszkiewicz and S. Wolski, “Anisotropic properties of mechanical characteristics and auxeticity of cubic crystalline media”, *Phys. Status Solidi B,* vol. 244, p. 966–977, 2007.

[46] A. K. A. Pryde *et al.*, “Simulation studies of at high pressure”, *J. Phys. Condens. Matter,* vol. 10, pp. 8417-8428, 1998.

[47] M. A. White, Physical properties of materials, CRC Press, 2012.

[48] T. A. Mary, J. S. O. Evans, T. Vogt and A. W. Sleight, “Negative thermal expansion from 0.3 to 1050 kelvin in ZrW2O8”, *Science,* vol. 272, pp. 90-92, 1996.

[49] T. G. Amos and A. W. Sleight, “Negative Thermal Expansion in Orthorhombic NbOPO4”, *J. Solid State Chem.,* vol. 160, pp. 230-238, 2001.

[50] J. Tao and A. Sleight, “The role of rigid unit modes in negative thermal expansion”, *J. Solid State Chem.,* vol. 173, pp. 442-448, 2003.

[51] C. P. Romao *et al.*, "Thermal, vibrational, and thermoelastic properties of $Y_2Mo_3O_{12}$ and their relations to negative thermal expansion", *Phys. Rev. B,* vol. 90, p. 24305, 2014.

[52] R. Lakes, "Cellular solids with tunable positive or negative thermal expansion of unbounded magnitude", *Appl. Phys. Lett.,* vol. 90, p. 221905, 2007.

[53] J. N. Grima, P. S. Farrugia, R. Gatt and V. Zammit, "A system with adjustable positive or negative thermal expansion", *Proc. R. Soc. London A Math. Phys. Eng. Sci.,* vol. 463, 2007.

[54] A. L. Goodwin, "Colossal Positive and Negative Thermal Expansion in the Framework Material $Ag_3[Co(CN)_6]$", *Science,* vol. 319, pp. 794-797, 2008.

[55] A. Fedorova, L. Michelsen and M. Scheffler, "Polymer-derived ceramic tapes with small and negative thermal expansion coefficients", *J. Eur. Ceram. Soc.,* vol. 38, pp. 719-725, 2018.

[56] L. Wu, B. Li and J. Zhou, "Enhanced thermal expansion by micro-displacement amplifying mechanical metamaterial", *MRS Advances,* 2018.

[57] T.-C. Lim, "Negative thermal expansion structures constructed from positive thermal expansion trusses", *Journal of Materials Science,* vol. 47, p. 368–373, 2012.

[58] J. Qu, M. Kadic, A. Naber and M. Wegener, "Micro-Structured Two-Component 3D Metamaterials with Negative Thermal-Expansion Coefficient from Positive Constituents", *Sci. Rep.,* vol. 7, p. 40643 , 2017.

[59] K. Takenaka, Y. Okamoto, T. Shinoda, N. Katayama and Y. Sakai, “Colossal negative thermal expansion in reduced layered ruthenate”, *Nat. Commun.*, vol. 8, p. 14102, 2017.

[60] B. Singh *et al.*, “Role of phonons in negative thermal expansion and high pressure phase transitions in β-eucryptite: An ab-initio lattice dynamics and inelastic neutron scattering study”, *J. Appl. Phys.*, vol. 121, p. 085106, 2017.

[61] J. F. Nye, Physical Properties of Crystals, Clarendon Press, 1957.

[62] R. Gatt and J. N. Grima, “Negative compressibility”, *Phys. status solidi - Rapid Res. Lett.*, vol. 2, pp. 236-238, 2008.

[63] O. M. Yaghi, H. Li, M. Eddaoudi and M. O'Keeffe, “Design and synthesis of an exceptionally stable and highly porous metal-organic framework”, *Nature*, vol. 402, pp. 276-279, 1999.

[64] W. Zhou, H. Wu, T. Yildirim, J. R. Simpson and A. R. H. Walker, “Origin of the exceptional negative thermal expansion in metal-organic framework-5 Zn4O(1 , 4 - benzenedicarboxylate)3”, *Phys. Rev. B*, vol. 78, p. 54114, 2008.

[65] L. H. N. Rimmer, “Framework flexibility and the negative thermal expansion mechanism of copper(I) oxide Cu2O”, *Phys. Rev. B*, vol. 89, p. 214115, 2014.

[66] A. Schneemann *et al.*, “Flexible metal-organic frameworks”, *Chem. Soc. Rev.*, vol. 43, pp. 6062-6096, 2014.

[67] C. P. Romao, K. J. Miller, M. B. Johnson, J. W. Zwanziger, B. A. Marinkovic and M. A. White, “Thermal, vibrational, and thermoelastic properties of Y2Mo3O12 and their relations to negative thermal expansion”, *Phys. Rev. B,* vol. 90, p. 024305, 2014.

[68] J. S. O. Evans, T. A. Mary and A. W. Sleight, “Negative Thermal Expansion in Sc2(WO4)3”, *J. Solid State Chem.,* vol. 137, pp. 148-160, 1998.

[69] J. S. O. Evans, “Negative thermal expansion materials?”, *J. Chem. Soc. Dalt. Trans.,* p. 3317–3326, 1999.

[70] R. Mittal, S. L. Chaplot, H. Schober and T. A. Mary, “Origin of negative thermal expansion in cubic ZrW 2 O 8”, *Neutron News,* vol. 13, pp. 33-35, 2002.

[71] S. Allen and J. S. O. Evans, “Negative thermal expansion and oxygen disorder in cubic ZrMo2O8”, *Phys. Rev. B,* vol. 68, p. 134101, 2003.

[72] R. H. Baughman, S. Stafstrom, C. Cui and S. O. Dantas, “Materials with Negative Compressibilities in One or More Dimensions”, *Science,* vol. 279, pp. 1522-1524, 1998.

[73] B. Moore, T. Jaglinski, D. S. Stone and R. S. Lakes, “Negative incremental bulk modulus in foams”, *Philos. Mag. Lett.,* vol. 86, pp. 651-659, 2006.

[74] B. Moore, T. Jaglinski, D. S. Stone and R. S. Lakes, “On the Bulk Modulus of Open Cell Foams”, *Cell. Polym.,* vol. 26, pp. 1-10, 2007.

[75] R. Lakes and K. W. Wojciechowski, “Negative compressibility, negative Poisson’s ratio, and stability”, *Phys. Status Solidi B,* vol. 245, pp. 545-551, 2008.

[76] R. Gatt and J. N. Grima, “Negative compressibility”, *Phys. Status Solidi RRL,* vol. 2, pp. 236-238, 2008.

[77] Y. C. Wang and R. S. Lakes, “Extreme stiffness systems due to negative stiffness elements”, *Am. J. Phys.,* vol. 72, pp. 40-50, 2004.

[78] H. W. Yap, R. S. Lakes and R. W. Carpick, “Negative stiffness and enhanced damping of individual multiwalled carbon nanotubes”, *Phys. Rev. B,* vol. 77, p. 045423, 2008.

[79] C. Coulais, J. T. B. Overvelde, L. A. Lubbers, K. Bertoldi and M. van Hecke, “Discontinuous Buckling of Wide Beams and Metabeams”, *Phys. Rev. Lett.,* vol. 115, p. 044301, 2015.

[80] X. Shi, S. Zhu and B. F. Spencer Jr., “Experimental Study on Passive Negative Stiffness Damper for Cable Vibration Mitigation”, *Journal of Engineering Mechanics,* vol. 143, 2017.

[81] N. Attary, M. Symans and S. Nagarajaiah, “Development of a rotation-based negative stiffness device for seismic protection of structures”, *J. Vib. Control,* vol. 23, pp. 853-867, 2017.

[82] G. Dong, X. Zhang, S. Xie, B. Yan and Y. Luo, “Simulated and experimental studies on a high-static-low-dynamic stiffness isolator using magnetic negative stiffness spring”, *Mech. Syst. Signal Process.,* vol. 86, pp. 188-203, 2017.

[83] W. J. Drugan, “Wave propagation in elastic and damped structures with stabilized negative-stiffness components”, *J. Mech. Phy. Solids,* vol. 106, pp. 34-45, 2017.

[84] J. Zhao, X. Li, Y. Wang, W. Wang, B. Zhang and X. Gai, “Membrane acoustic metamaterial absorbers with magnetic negative stiffness”, *J. Acoust. Soc. Am.,* vol. 141, p. 840, 2017.

[85] B. M. Goldsberry and M. R. Haberman, “Negative stiffness honeycombs as tunable elastic metamaterials”, *J. Appl. Phys.,* vol. 123, p. 091711, 2018.

[86] W. Voigt, Lehrbuch der Kristallphysik, publisher: Elsevier, Leipzig 1928.

[87] G. Simmons and F. Birch, “Elastic Constants of Pyrite.”, *J. Appl. Phys.,* vol. 34, p. 2736, 1963.

[88] N. Benbattouche *et al.*, “The dependences of the elastic stiffness moduli and the Poisson ratio of natural iron pyrites FeS 2 upon pressure and temperature.”, *J. Phys. D. Appl. Phys.,* vol. 22, pp. 670-675, 1989.

[89] Y. Li, “The anisotropic behavior of Poisson’s ratio, Young’s modulus, and shear modulus in hexagonal materials.”, *Phys. Status Solidi,* vol. 38, pp. 171-175, 1976.

[90] D. Berlincourt and H. Jaffe, “Elastic and Piezoelectric Coefficients of Single-Crystal Barium Titanate.”, *Phys. Rev.,* vol. 111, pp. 143-148, 1958.

[91] A. Alderson *et al.*, “Deformation mechanisms leading to auxetic behaviour in the α-cristobalite and α-quartz structures of both silica and germania.”, *J. Phys. Condens. Matter,* vol. 21, p. 25401, 2009.

[92] E. Kittinger, J. Tichy and E. Bertagnolli, “Example of a Negative Effective Poisson’s Ratio.”, *Phys. Rev. Lett.,* vol. 47, pp. 712-714, 1981.

[93] F. Milstein and K. Huang, “Existence of a negative Poisson ratio in fcc crystals.”, *Phys. Rev. B,* vol. 19, pp. 2030-2033, 1979.

[94] R. H. Baughman, J. M. Shacklette, A. A. Zakhidov and S. Stafström, “Negative Poisson’s ratios as a common feature of cubic metals.”, *Nature,* vol. 392, pp. 362-365, 1998.

[95] D. T. Ho *et al.*, “Negative Poisson’s ratios in metal nanoplates.”, *Nat. Commun.,* vol. 5, pp. 1038-1040, 2014.

[96] D. J. Gunton and G. A. Saunders, “The Young’s modulus and Poisson’s ratio of arsenic, antimony and bismuth.”, *J. Mater. Sci.,* vol. 7, pp. 1061-1068, 1972.

[97] A. Yeganeh-Haeri, D. J. Weidner and J. B. Parise, “Elasticity of αcristobalite: A silicon dioxide with a negative Poisson’s ratio.”, *Science,* vol. 257, pp. 650-652, 1992.

[98] F. Homand-Etienne and R. Houpert, “Thermally induced microcracking in granites: characterization and analysis.”, *Int. J. Rock Mech. Min. Sci.,* vol. 26, pp. 125-134, 1989.

[99] M. Peura *et al.*, “Negative Poisson Ratio of Crystalline Cellulose in Kraft Cooked Norway Spruce.”, *Biomacromolecules,* vol. 7, pp. 1521-1528, 2006.

[100] K. Nakamura, M. Wada, S. Kuga and T. Okano, “Poisson’s ratio of cellulose I? and cellulose II.”, *J. Polym. Sci. Part B Polym. Phys.,* vol. 42, pp. 1206-1211, 2004.

[101] Y. T. Yao, A. Alderson and K. L. Alderson, “Towards auxetic nanofibres: Molecular modelling of auxetic behaviour in cellulose II.”, in *Behav. Mech. Multifunct. Mater. Compos. Proc. SPIE 8342,* 2012.

[102] D. R. Veronda and R. A. Westmann, “Mechanical characterization of skin—Finite deformations.”, *J. Biomech.,* vol. 3, pp. 111-124, 1970.

[103] C. Lees, J. F. V. Vincent and J. E. Hillerton, “Poisson’s Ratio in Skin.”, *Biomed. Mater. Eng.,* vol. 1, pp. 19-23, 1991.

[104] F. Song, J. Zhou, X. Xu, Y. Xu and Y. Bai, “Effect of a Negative Poisson Ratio in the Tension of Ceramics”, *Phys. Rev. Lett.,* vol. 100, p. 245502, 2008.

[105] J. L. Williams and J. L. Lewis, “Properties and an Anisotropic Model of Cancellous Bone From the Proximal Tibial Epiphysis.”, *J. Biomech. Eng.,* vol. 104, p. 50, 1982.

[106] C. E. Renson and M. Braden, “Experimental determination of the rigidity modulus, poisson’s ratio and elastic limit in shear of human dentine.”, *Arch. Oral Biol.,* vol. 20, p. 43, 1975.

[107] C. F. Schmidt, K. Svoboda, N. Lei, I. B. Petsche, L. E. Berman, C. R. Safinya and G. Grest, “Existence of a flat phase in red cell membrane skeletons.”, *Science,* vol. 259, pp. 952-955, 1993.

[108] X. Chen and G. W. Brodland, “Mechanical determinants of epithelium thickness in early-stage embryos.”, *J. Mech. Behav. Biomed. Mater.,* vol. 2, pp. 494-501, 2009.

[109] L. H. Timmins *et al.*, “Structural inhomogeneity and fiber orientation in the inner arterial media.”, *Am. J. Physiol. Heart Circ. Physiol.,* vol. 298, pp. H1537-45, 2010.

[110] K. Patten and T. Wess, “Suprafibrillar structures of collagen, evidence for local organization and auxetic behaviour in architectures.”, *J. Biophys. Chem.,* vol. 4, pp. 103-109, 2013.

[111] S. Pagliara *et al.*, “Auxetic nuclei in embryonic stem cells exiting pluripotency.”, *Nat. Mater.*, vol. 13, pp. 638-44, 2014.

[112] S. P. Tokmakova, “Stereographic projections of Poisson’s ratio in auxetic crystals.”, *Phys. status solidi*, vol. 242, pp. 721-729, 2005.

[113] J. N. Grima *et al.*, “Tailoring Graphene to Achieve Negative Poisson’s Ratio Properties.”, *Adv. Mater.*, vol. 27, pp. 1455-1459, 2015.

[114] N. Aouni and L. Wheeler, “Auxeticity of Calcite and Aragonite polymorphs of CaCO 3 and crystals of similar structure.”, *Phys. status solidi*, vol. 245, pp. 2454-2462, 2008.

[115] J.-. W. Jiang *et al.*, “Negative poisson’s ratio in single-layer black phosphorus”, *Nat. Commun.*, vol. 5, p. 126–128, 2014.

[116] J. W. Jiang *et al.*, “A Stillinger–Weber potential for single-layered black phosphorus, and the importance of cross-pucker interactions for a negative Poisson’s ratio and edge stress-induced bending”, *Nanoscale*, vol. 7, p. 6059–6068, 2015.

[117] J.-. W. Jiang *et al.*, “Thermal conduction in single-layer black phosphorus: highly anisotropic?”, *Nanotechnology*, vol. 26, p. 55701, 2015.

[118] M. Rovati, “On the negative Poisson’s ratio of an orthorhombic alloy”, *Scr. Mater.*, vol. 48, pp. 235-240, 2003.

[119] R. A. Kellogg, A. M. Russell, T. A. Lograsso, A. B. Flatau, A. E. Clark and M. Wun-Fogle, “Mechanical properties of magnetostrictive iron-gallium alloys in Smart Structures and Materials”, *Active Materials: Behaviour and Mechanics* , pp. 534-543, 2003.

[120] R. A. Kellogg *et al.*, “Tensile properties of magnetostrictive iron–gallium alloys”, *Acta Mater.*, vol. 52, pp. 5043-5050, 2004.

[121] G. Petculescu, K. B. Hathaway, T. A. Lograsso, M. Wun-Fogle and A. E. Clark, “Magnetic field dependence of galfenol elastic properties”, *J. Appl. Phys.*, vol. 97, p. 10M315, 2005.

[122] H. M. Schurter and A. B. Flatau, “Elastic properties and auxetic behavior of Galfenol for a range of compositions in Magnetostrictive Materials I”, *Proc. SPIE*, 2008.

[123] M. Valant, A.-K. Axelsson, F. Aguesse and N. M. Alford, “Molecular Auxetic Behavior of Epitaxial Co-Ferrite Spinel Thin Film”, *Adv. Funct. Mater.*, vol. 20, pp. 644-647, 2010.

[124] Y. Zhang, R. Wu, H. M. Schurter and A. B. Flatau, “Understanding of large auxetic properties of iron-gallium and iron-aluminum alloys”, *J. Appl. Phys.*, vol. 108, p. 23513, 2010.

[125] D. Li, T. Jaglinski, D. S. Stone and R. S. Lakes, “Temperature insensitive negative Poisson’s ratios in isotropic alloys near a morphotropic phase boundary”, *Appl. Phys. Lett.*, vol. 101, p. 251903, 2012.

[126] X. F. Wang, T. E. Jones, W. Li and Y. C. Zhou, “Extreme Poisson’s ratios and their electronic origin in B2 CsCl-type AB intermetallic compounds”, *Phys. Rev. B*, vol. 85, p. 134108, 2012.

[127] T.-. C. Lim, “On simultaneous positive and negative Poisson's ratio laminates”, *Phys. Status Solidi B*, vol. 244, pp. 910-918, 2007.

[128] T.-. C. Lim, “Mixed auxeticity of auxetic sandwich structures”, *Phys. Status Solidi B,* vol. 249, pp. 1366-1372, 2012.

[129] R. Lakes, “Foam Structures with a Negative Poisson’s Ratio”, *Science,* vol. 235, pp. 1038-40, 1987.

[130] E. A. Friis, R. S. Lakes and J. B. Park, “Negative Poisson’s ratio polymeric and metallic foams”, *J. Mater. Sci.,* vol. 23, pp. 4406-4414, 1988.

[131] C. P. Chen and R. S. Lakes, “Micromechanical Analysis of Dynamic Behavior of Conventional and Negative Poisson’s Ratio Foams”, *J. Eng. Mater. Technol.,* vol. 118, p. 285, 1996.

[132] N. Chan and K. E. Evans, “The Mechanical Properties of Conventional and Auxetic Foams. Part I: Compression and Tension”, *J. Cell. Plast.,* vol. 35, pp. 130-165, 1999.

[133] N. Chan and K. E. Evans, “The Mechanical Properties of Conventional and Auxetic Foams. Part II: Shear”, *J. Cell. Plast.,* vol. 35, pp. 166-183, 1999.

[134] A. Bezazi and F. Scarpa, “Mechanical behaviour of conventional and negative Poisson’s ratio thermoplastic polyurethane foams under compressive cyclic loading”, *Int. J. Fatigue,* vol. 29, pp. 922-930, 2007.

[135] A. Bezazi and F. Scarpa, “Tensile fatigue of conventional and negative Poisson’s ratio open cell PU foams”, *Int. J. Fatigue,* vol. 31, pp. 488-494, 2009.

[136] A. Bezazi, W. Boukharouba and F. Scarpa, “Mechanical properties of auxetic carbon/epoxy composites: static and cyclic fatigue behaviour”, *Phys. status solidi,* vol. 246, pp. 2102-2110, 2009.

[137] T. C. Lim, A. Alderson and K. L. Alderson, “Experimental studies on the impact properties of auxetic materials”, *Phys. Status Solidi B,* vol. 251, pp. 307-313, 2014.

[138] F. Scarpa, J. Giacomin, Y. Zhang and P. Pastorino, “Mechanical performance of auxetic polyurethane foam for antivibration glove applications”, *Cell. Polym.,* vol. 24, pp. 1-16, 2005.

[139] J. B. Choi and R. Lakes, “Analysis of elastic modulus of conventional foams and of re-entrant foam materials with a negative Poisson’s ratio”, *Int. J. Mech. Sci.,* vol. 37, pp. 51-59, 1995.

[140] J. Giacomin, F. Scarpa, A. Bezazi and W. Bullough, “Dynamic behavior and damping capacity of auxetic foam pads”, in *Proceedings of Smart Structures and Materials Conference*, San Diego, 2006.

[141] P. Pastorino *et al.*, “Strain rate dependence of stiffness and Poisson’s ratio of auxetic open cell PU foams”, *Phys. status solidi,* vol. 244, pp. 955-965, 2007.

[142] M. Ramirez *et al.*, “Enhancement of Young’s moduli and auxetic windows in laminates with isotropic constituents”, *Int. J. Eng. Sci.,* vol. 58, pp. 95-114, 2012.

[143] A. Lowe *et al.*, “Negative Poisson’s Ratio Foam as Seat Cushion Material”, *Cell. Polym.,* vol. 19, pp. 157-167, 2000.

[144] T-. C. Lim, “Auxeticity of Concentric Auxetic-Conventional Foam Rods with High Modulus Interface Adhesive”, *Materials,* vol. 11, p. 223, 2018.

[145] E. O. Martz, T. Lee, R. S. Goel, V. K. Park and R. Lakes, “Re-entrant transformation methods in closed cell foams”, *Cellular Polymers,* vol. 15, pp. 229-249, 1996.

[146] N. Chan and K. E. Evans, “Fabrication methods for auxetic foams”, *J. Mater. Sci.,* vol. 32, pp. 5945-5953, 1997.

[147] B. Brandel and R. S. Lakes, “Negative Poisson’s ratio polyethylene foams”, *J. Mater. Sci.,* vol. 36, pp. 5885-5893, 2001.

[148] A. M. Strek, “Production and study of polyether auxetic foam”, *Mech. Control,* vol. 29, pp. 78-87, 2010.

[149] M. Bianchi, F. Scarpa, M. Banse and C. W. Smith, “Novel generation of auxetic open cell foams for curved and arbitrary shapes”, *Acta Mater.,* vol. 59, pp. 686-691, 2011.

[150] M. Bianchi, S. Frontoni, F. Scarpa and C. W. Smith, “Density change during the manufacturing process of PU-PE open cell auxetic foams”, *Phys. Status Solidi B,* vol. 248, pp. 30-38, 2011.

[151] K. Alderson, A. Alderson, N. Ravirala, V. Simkins and P. Davies, “Manufacture and characterisation of thin flat and curved auxetic foam sheets”, *Phys. status solidi B,* vol. 249, pp. 1315-1321, 2012.

[152] A. Alderson and K. L. Alderson, “Developments in Auxetic Foams”, in *International Conference and 7 th International Workshop on Auxetics and Related Systems,* 2010.

[153] A. Alderson, K. L. Alderson, K. E. Evans, J. N. Grima, M. R. Williams and P. J. Davies, “ Modelling the deformation mechanisms, structure-property relationships and applications of auxetic nanomaterials”, *Phys. Status Solidi B,* vol. 242, pp. 499-508 , 2005.

[154] J. N. Grima, D. Attard and R. Gatt, “On foams exhibiting negative Poisson’s ratio: New manufacturing methods for making auxetic foams and for their re-conversion to

conventional foams", in *6 th International Workshop on Auxetics and Related Systems and 6 th Annual AuxetNet Young Researchers Forum*, 2009.

[155] K. E. Evans, M. A. Nkansah and I. J. Hutchinson, "Auxetic foams: Modelling negative Poisson's ratios", *Acta Metall. Mater.*, vol. 42, pp. 1289-1294, 1994.

[156] N. Chan and K. E. Evans, "Microscopic examination of the microstructure and deformation of conventional and auxetic foams", *J. Mater. Sci.*, vol. 32, pp. 5725-5736, 1997.

[157] D. W. Overaker, A. M. Cuitino and N. A. Langrana, "Effects of morphology and orientation on the behavior of two-dimensional hexagonal foams and application in a re-entrant foam anchor model", *Mech. Mater.*, vol. 29, pp. 43-52, 1998.

[158] V. Shulmeister, M. W. D. Van der Burg, E. Van der Giessen and R. Marissen, "A numerical study of large deformations of low-density elastomeric open-cell foams", *Mech. Mater.*, vol. 30, pp. 125-140, 1998.

[159] J. N. Grima, R. Gatt, N. Ravirala, A. Alderson and K. E. Evans, "Negative Poisson's ratios in cellular foam materials", *Mater. Sci. Eng. A*, vol. 423, pp. 214-218, 2006.

[160] M. Doyoyo and J. Wan Hu, "Plastic failure analysis of an auxetic foam or inverted strut lattice under longitudinal and shear loads", *J. Mech. Phys. Solids*, vol. 54, pp. 1479-1492, 2006.

[161] N. Gaspar, C. W. Smith, E. A. Miller, G. T. Seidler and K. E. Evans, "Quantitative analysis of the microscale of auxetic foams", *Phys. status solidi B*, vol. 242, pp. 550-560, 2005.

[162] F. Cadamagnani, S. Frontoni, M. Bianchi and F. Scarpa, “Compressive uniaxial properties of auxetic open cell PU based foams”, *Phys. status solidi B,* vol. 246, pp. 2118-2123, 2009.

[163] S. A. McDonald, N. Ravirala, P. J. Withers and A. Alderson, “In situ three-dimensional X-ray microtomography of an auxetic foam under tension”, *Scr. Mater.,* vol. 60, pp. 232-235, 2009.

[164] Z.-. X. Lu, Q. Liu and Z.-. Y. Yang, “Predictions of Young’s modulus and negative Poisson’s ratio of auxetic foams”, *Phys. status solidi B,* vol. 248, pp. 167-174, 2011.

[165] R. Panowicz and D. Miedzinska, “Numerical and experimental research on polyisocyanurate foam”, *Comput. Mater. Sci.,* vol. 64, pp. 126-129, 2012.

[166] A. A. Pozniak *et al.*, “Computer simulations of auxetic foams in two dimensions”, *Smart Mater. Struct.,* vol. 22, p. 84009, 2013.

[167] B. D. Caddock *et al.*, “Microporous materials with negative Poisson’s ratios. I. Microstructure and mechanical properties.”, *J. Phys. D. Appl. Phys.,* vol. 22, pp. 1877-1882, 1989.

[168] K. E. Evans, “Microporous materials with negative Poisson’s ratios. II. Mechanisms and interpretation.”, *J. Phys. D. Appl. Phys.,* vol. 22, p. 13, 1989.

[169] K. L. Alderson and K. E. Evans, “Strain-dependent behaviour of microporous polyethylene with a negative Poisson’s ratio”, *J. Mater. Sci.,* vol. 28, pp. 4092-4098, 1993.

[170] K. L. Alderson, A. Alderson, R. S. Webber and K. E. Evans, “Evidence for Uniaxial Drawing in the Fibrillated Microstructure of Auxetic Microporous Polymers”, *J. Mater. Sci. Lett.,* vol. 17, pp. 1415-1419, 1998.

[171] A. P. Pickles, R. S. Webber, K. L. Alderson, P. J. Neale and K. E. Evans, “The effect of the processing parameters on the fabrication of auxetic polyethylene”, *J. Mater. Sci.,* vol. 30, pp. 4059-4068, 1995.

[172] K. L. Alderson, R. S. Webber and K. E. Evans, “Microstructural evolution in the processing of auxetic microporous polymers”, *Phys. status solidi B,* vol. 244, pp. 828-841, 2007.

[173] N. Ravirala, A. Alderson, K. L. Alderson and P. J. Davies, “Auxetic polypropylene films”, *Polym. Eng. Sci.,* vol. 45, pp. 517-528, 2005.

[174] N. Ravirala, K. L. Alderson, P. J. Davies, V. R. Simkins and A. Alderson, “Negative Poisson’s Ratio Polyester Fibers”, *Text. Res. J.,* vol. 76, pp. 540-546, 2006.

[175] G. T. Chirima, K. M. Zied, N. Ravirala, K. L. Alderson and A. Alderson, “Numerical and analytical modelling of multi-layer adhesive-film interface systems”, *Phys. status solidi B,* vol. 246, pp. 2072-2082, 2009.

[176] K. E. Evans, “Auxetic polymers: a new range of materials”, *Endeavour,* vol. 15, pp. 170-174, 1991.

[177] K. L. Alderson, A. P. Pickles, P. J. Neale and K. E. Evans, “Auxetic polyethylene: The effect of a negative poisson’s ratio on hardness”, *Acta Metall. Mater.,* vol. 42, pp. 2261-2266, 1994.

[178] M. Franke and R. Magerle, “Locally Auxetic Behavior of Elastomeric Polypropylene on the 100 nm Length Scale”, *ACS Nano,* vol. 5, pp. 4886-4891, 2011.

[179] J. Baker, A. Douglass and A. Griffin, “Trimeric Liquid-Crystals - Model Compounds for Auxetic Polumers”, *Abstr. Pap. Am. Chem. Soc.,* vol. 210, p. 146, 1995.

[180] P. Liu, C. He and A. Griffin, “Liquid crystalline polymers as potential auxetic materials: Influence of transverse rods on the polymer mesophase”, *Abstr. Pap. Am. Chem. Soc.,* vol. 216, p. 108, 1998.

[181] C. He, P. Liu and A. Griffin, “Toward negative Poisson ratio polymers through molecular design”, *Macromolecules,* vol. 31, pp. 3145-3147, 1998.

[182] C. He, P. Liu, A. C. Griffin, C. W. Smith and K. E. Evans, “Morphology and Deformation Behaviour of a Liquid Crystalline Polymer Containing Laterally Attached Pentaphenyl Rods”, *Macromol. Chem. Phys.,* vol. 206, pp. 233-239, 2005.

[183] C. He, P. Liu, P. J. McMullan and A. C. Griffin, “Toward molecular auxetics: Main chain liquid crystalline polymers consisting of laterally attached para-quaterphenyls”, *Phys. status solidi B,* vol. 242, pp. 576-584, 2005.

[184] C. Li, X. Xie and S. Cao, “Synthesis and characterization of liquid crystalline copolyesters containing horizontal and lateral rods in main chain”, *Polym. Adv. Technol.,* vol. 13, pp. 178-187, 2002.

[185] S. Dey *et al.*, “Soft Elasticity in Main Chain Liquid Crystal Elastomers”, *Crystals,* vol. 3, pp. 363-390, 2013.

[186] R. H. Baughman and D. S. Galvao, “Crystalline networks with unusual predicted mechanical and thermal properties”, *Nature,* vol. 365, pp. 735-737, 1993.

[187] R. Baughman, D. Galvao, C. Cui and S. Dantas, “Hinged and chiral polydiacetylene carbon crystals”, *Chem. Phys. Lett.,* vol. 269, pp. 356-364, 1997.

[188] M. A. Nkansah *et al.*, “Modelling the mechanical properties of an auxetic molecular network”, *Model. Simul. Mater. Sci. Eng.,* vol. 2, pp. 337-352, 1994.

[189] J. N. Grima and K. E. Evans, “Self-expanding molecular networks”, *Chem. Comm.,* pp. 1531-1532 , 2000.

[190] J. N. Grima *et al.*, “On the mechanical properties and auxetic potential of various organic networked polymers”, *Mol. Simul.,* vol. 34, pp. 1149-1158, 2008.

[191] X. Wen, C. W. Garland, T. Hwa, M. Kardar, E. Kokufuta, Y. Li, M. Orkisz and T. Tanaka, “Crumpled and collapsed conformation in graphite oxide membranes”, *Nature,* vol. 355, pp. 426-428, 1992.

[192] N. Pour, L. Itzhaki, B. Hoz, E. Altus, H. Basch and S. Hoz, “Auxetics at the Molecular Level: A Negative Poisson’s Ratio in Molecular Rods”, *Angew. Chemie,* vol. 118, pp. 6127-6129, 2006.

[193] N. Pour, E. Altus, H. Basch and S. Hoz, “The Origin of the Auxetic Effect in Prismanes: Bowtie Structure and the Mechanical Properties of Biprismanes”, *J. Phys. Chem. C,* vol. 113, pp. 3467-3470, 2009.

[194] L. J. Hall, V. R. Coluci, D. S. Galvao, M. E. Kozlov, S. O. Dantas and R. H. Baughman, “Sign Change of Poisson's Ratio for Carbon Nanotube Sheets”, *Science,* vol. 320, pp. 504-507, 2008.

[195] Y. T. Yao, A. Alderson and K. L. Alderson, “Can nanotubes display auxetic behaviour?”, *Phys. status solidi B,* vol. 245, pp. 2373-2382, 2008.

[196] L. Chen, C. Liu, J. Wang, W. Zhang, C. Hu and S. Fan, “Auxetic materials with large negative Poisson’s ratios based on highly oriented carbon nanotube structures”, *Appl. Phys. Lett.,* vol. 94, p. 253111, 2009.

[197] F. Scarpa, S. Adhikari and A. Srikantha Phani, “Effective elastic mechanical properties of single layer graphene sheets”, *Nanotechnology,* vol. 20, p. 65709, 2009.

[198] F. L. Braghin and N. Hasselmann, “Thermal fluctuations of free-standing graphene”, *Phys. Rev. B,* vol. 82, p. 35407, 2010.

[199] E. Cadelano, P. L. Palla, S. Giordano and L. Colombo, “Elastic properties of hydrogenated graphene”, *Phys. Rev. B,* vol. 82, p. 235414, 2010.

[200] S. Sihn, V. Varshney, A. K. Roy and B. L. Farmer, “Prediction of 3D elastic moduli and Poisson’s ratios of pillared graphene nanostructures”, *Carbon,* vol. 50, pp. 603-611, 2012.

[201] P. Koskinen, “Graphene cardboard: From ripples to tunable metamaterial”, *Appl. Phys. Lett.,* vol. 104, p. 101902, 2014.

[202] J. N. Grima, R. Jackson, A. Alderson and K. E. Evans, “ Do zeolites have negative Poisson’s ratios?”, *Adv. Mater.,* vol. 12, pp. 1912-1928, 2000.

[203] J. N. Grima, New auxetic materials Ph.D Thesis, University of Exeter, Exeter, UK, 2000.

[204] C. Sanchez-Valle, S. V. Sinogeikin, Z. A. D. Lethbridge, R. I. Walton, C. W. Smith, K. E. Evans and J. D. Bass, "Brillouin scattering study on the single-crystal elastic properties of natrolite and analcime zeolites", *J. Appl. Phys.,* vol. 98, p. 053508, 2005.

[205] Z. A. D. Lethbridge, J. J. Williams, R. I. Walton, C. W. Smith, R. M. Hooper and K. E. Evans, " Direct, static measurement of single-crystal Young's moduli of the zeolite natrolite: Comparison with dynamic studies and simulations", *Acta Mater.,* vol. 54, pp. 2533-2545, 2006.

[206] C. W. Smith, K. E. Evans, Z. A. D. Lethbridge and R. I. Walton, " An analytical model for producing negative Poisson's ratios and its application in explaining off-axis elastic properties of the NAT-type zeolites", *Acta Mater.,* vol. 55, pp. 5697-5707, 2007.

[207] J. J. Williams, C. W. Smith, K. E. Evans, Z. A. D. Lethbridge and R. I. Walton, " Off-axis elastic properties and the effect of extraframework species on structural flexibility of the NATtype zeolites: Simulations of structure and elastic properties", *Chem. Mater.,* vol. 19, pp. 2423-2434 , 2007.

[208] J. N. Grima, R. Gatt, V. Zammit, J. J. Williams, A. Alderson and R. I. Walton, " Natrolite: A zeolite with negative Poisson's ratios", *J. Appl. Phys.,* vol. 101, p. 86102, 2007.

[209] J. N. Grima, V. Zammit, R. Gatt, A. Alderson and K. E. Evans, "Auxetic behaviour from rotating semi-rigid units", *Phys. Status Solidi B,* vol. 224, pp. 866-882, 2007.

[210] J. N. Grima, R. Gatt and E. Chetcuti, “On the behaviour of natrolite under hydrostatic pressure”, *J. Non-Cryst. Solids,* vol. 356, pp. 1881-1887, 2010.

[211] A. Kremleva, T. Vogt and N. Rosch, “ Monovalent cationexchanged natrolites and their behaviour under pressure. A computational study”, *J. Phys. Chem. C,* vol. 117, pp. 19020-19030, 2013.

[212] E. D. Manga, H. Blasco, P. Da-Costa, M. Drobek, A. Ayral, E. Le Clezio, G. Despaux, B. Coasne and A. Julbe, “ Effect of gas adsorption on acoustic wave propagation in MFI zeolite membrane materials: Experiment and molecular simulation”, *Langmuir,* vol. 30, pp. 10336-10343, 2014.

[213] M. Siddorn, F. X. Coudert, K. E. Evans and A. A. Marmier, “A systematic typology for negative Poisson’s ratio materials and the prediction of complete auxeticity in pure silica zeolite JST”, *Phys. Chem. Chem. Phys.,* vol. 17, p. 17927, 2015.

[214] A. Alderson and K. E. Evans, “ Molecular origin of auxetic behaviour in tetrahedral framework silicates”, *Phys. Rev. Lett.,* vol. 89, p. 225503, 2002.

[215] A. Alderson, K. L. Alderson, K. E. Evans, J. N. Grima, M. R. Williams and P. J. Davies, “Molecular modelling of the deformation mechanisms acting in auxetic silica”, *CMST,* vol. 10, pp. 117-126, 2004.

[216] A. Alderson, K. L. Alderson, K. E. Evans, J. N. Grima and M. Williams, “ Modelling of negative Poisson’s ratio nanomaterials: Deformation mechanisms, structure-property relationships and applications”, *J. METASTAB. NANOCRYST.,* vol. 23, pp. 55-58, 2005.

[217] R. Gatt, L. Mizzi, K. M. Azzopardi and J. N. Grima, “ A force-field based analysis of the deformation in α-cristobalit”, *Phys. Status Solidi B,* vol. 5, p. 8395, 2015.

[218] F. Nazare and A. Alderson, “ Models for the prediction of Poisson’s ratio in the α-cristobalite tetrahedral framework”, *Phys. Status Solidi B,* vol. 252, pp. 1465-1478, 2015.

[219] K. W. Wojciechowski, A. C. Branka and M. Parrinello, “ Monte Carlo study of the phase diagram of a two dimensional system of hard cyclic hexamers”, *Mol. Phys.,* vol. 53, pp. 1541-1545, 1984.

[220] K. W. Wojciechowski, “ Constant thermodynamic tension Monte Carlo studies of elastic properties of a two-dimensional system of hard cyclic hexamers”, *Mol. Phys.,* vol. 61, pp. 1247-1258, 1987.

[221] K. W. Wojciechowski and A. C. Branka, “Negative Poisson ratio in a two-dimensional "isotropic" solid”, *Phys. Lett. A,* vol. 40, pp. 7222-7225, 1989.

[222] K. W. Wojciechowski and A. C. Branka, “ Auxetics: Materials and models with negative Poisson’s ratios”, *MOLECUL. PHYS. REP.,* vol. 6, p. 71, 1994.

[223] K. V. Tretiakov and K. W. Wojciechowski, “ Orientational phase transition between hexagonal solids in planar systems of hard cyclic pentamers and heptamers”, *J. PHYS.-CONDENS. MAT.,* vol. 14, pp. 1261-1273, 2002.

[224] K. V. Tretiakov and K. W. Wojciechowski, “Monte Carlo simulation of two-dimensional hard body systems with extreme values of the Poisson’s ratio”, *Phys. Status Solidi B,* vol. 242, pp. 730-741 , 2005.

[225] K. V. Tretiakov and K. W. Wojciechowski, “Elastic properties of the degenerate crystalline phase of two-dimensional hard dimers”, *J. NON.-CRYST. SOLIDS,* vol. 352, pp. 4221-4228 , 2006.

[226] K. V. Tretiakov and K. W. Wojciechowski, “Poisson’s ratio of simple planar "isotropic" solids in two dimensions”, *Phys. Status Solidi B,* vol. 244, pp. 1038-1046, 2007.

[227] J. W. Narojczyk and K. W. Wojciechowski, “ Elastic properties of two-dimensional soft polydisperse trimers at zero temperature”, *Phys. Status Solidi B,* vol. 244, pp. 943-954, 2007.

[228] J. W. Narojczyk, A. Alderson, A. R. Imre, F. Scarpa and K. W. Wojciechowski, “ Negative Poisson’s ratio behaviour in the planar model of asymmetric trimers at zero temperature”, *J. NON.-CRYST. SOLIDS,* vol. 354, pp. 4242-4248 , 2008.

[229] J. W. Narojczyk and K. W. Wojciechowski, “ Elasticity of periodic and aperiodic structures of polydisperse dimers in two dimensions at zero temperature”, *Phys. Status Solidi B,* vol. 245, pp. 2453-2468 , 2008.

[230] J. W. Narojczyk and K. W. Wojciechowski, “ Elastic properties of degenerate f.c.c. crystal of polydisperse soft dimers at zero temperature”, *J. NON.-CRYST. SOLIDS,* vol. 256, pp. 2026-2032 , 2010.

[231] J. W. Narojczyk, P. M. Piglowski, K. W. Wojciechowski and K. V. Tretiakov, “ Elastic properties of mono and polydisperse two dimensional crystals of hard core repulsive Yukawa particles”, *Phys. Status Solidi B,* p. 1508–1513, 2015.

[232] K. V. Tretiakov, P. M. Piglowski, K. Hyzorek and K. W. Wojciechowski, “Enhanced auxeticity in Yukawa systems due to introduction of nanochannels in-direction”, *Smart Mater. Struct.,* vol. 25, p. 054007, 2016.

[233] A. el-Sayed, F. K. Jones and I. W. Burgess, “A theoretical approach to the deformation of honeycomb based composite materials”, *Composites,* vol. 10, pp. 209-214, 1979.

[234] L. J. Gibson, M. F. Ashby, G. S. Schajer and C. I. Robertson, “The mechanics of two-dimensional cellular materials”, *Proc. Royal Soc. A,* vol. 382, pp. 25-42, 2008.

[235] I. G. Masters and K. E. Evans, “Models for the elastic deformation of honeycombs”, *Comp. Struct.,* vol. 35, pp. 404-422, 1996.

[236] K. E. Evans, A. Alderson and F. R. Christian, “Auxetic twodimensional polymer networks: An example of tailoring geometry for specific mechanical properties”, *J. Chem. Soc. Faraday Trans.,* vol. 91, pp. 2671-2680, 1995.

[237] L. J. Gibson and M. F. Ashby, Cellular solids structure and properties, Cambridge University Press, 1997.

[238] K. E. Evans, “Design of doubly-curved sandwich panels with honeycomb cores”, *Comp. Struct.,* vol. 17, pp. 95-111, 1991.

[239] F. Scarpa and G. Tomlinson, “Theoretical characteristics of the vibration of sandwich plates with in-plane negative Poisson’s ratio values”, *J. Sound Vib.,* vol. 230, pp. 45-67, 2000.

[240] F. Scarpa, F. C. Smith, B. Chambers and G. Burriesci, “Mechanical and electromagnetic behaviour of auxetic honeycomb structure”, *The Aeronautical Journal,* vol. 107, pp. 175-183, 2002.

[241] D. H. Chen and S. Ozaki, “Analysis of in-plane elastic modulus for a hexagonal honeycomb core: Effect of core height and proposed analytical method”, *Comp. Struct.,* vol. 88, pp. 17-25, 2009.

[242] M. A. Grediac, “A finite element study of the transverse shear in honeycomb cores”, *International Journal of Solids and Structures,* vol. 30, pp. 1777-1788, 1993.

[243] F. Scarpa, P. Panayiotou and G. Tomlinson, “Numerical and experimental uniaxial loading on in-plane auxetic honeycombs”, *J. STRAIN ANAL. ENG.,* vol. 35, pp. 383-388, 2000.

[244] J. Ju and J. D. Summers, “Hyperelastic constitutive modeling of hexagonal honeycombs subjected to in-plane shear loading”, *J. ENG. MATER.-T. ASME,* vol. 133, p. 011005, 2010.

[245] J. Ju and J. D. Summers, “Compliant hexagonal periodic lattice structures having both high shear strength and high shear strain”, *Materials and Design,* vol. 32, pp. 512-524, 2011.

[246] J. Ju, J. D. Summers, J. Ziegert and G. Fadel, “Design of honeycombs for modulus and yield strain in shear”, *J. ENG. MATER.-T. ASME,* vol. 134, p. 011002, 2011.

[247] A. Bezazi, F. Scarpa and C. Remillat, “A novel centresymmetric honeycomb composite structure”, *Compos. Struct.,* vol. 71, pp. 356-364, 2005.

[248] J. S. Huang and F. M. Chang, “Effects of curved cell edges on the stiffness and strength of two-dimensional cellular solids”, *Compos. Struct.,* vol. 69, pp. 183-191, 2005.

[249] M. Y. Yang, J. S. Huang and J. W. Hu, “Elastic buckling of hexagonal honeycombs with dual imperfections”, *Compos. Struct.,* vol. 82, pp. 326-335, 2008.

[250] C. Lira, P. Innocenti and F. Scarpa, “Transverse elastic shear of auxetic multi re-entrant honeycombs”, *Compos. Struct.,* vol. 90, pp. 314-322, 2009.

[251] L. Mizzi, D. Attard, A. Casha, J. N. Grima and R. Gatt, “On the suitability of hexagonal honeycombs as stent geometries”, *Phys. Status Solidi B,* vol. 251, pp. 328-337, 2014.

[252] H. Ohtaki, G. Hu, Y. Nagasaka and S. Kotosaka, “Analysis of negative Poisson’s ratios of re-entrant honeycombs”, *JSME. INT. J. A-MECH. M.,* vol. 47, pp. 113-121, 2004.

[253] H. Wan, H. Ohtaki, S. Kotosaka and G. M. Hu, “A study of negative Poisson’s ratios in auxetic honeycombs based on a large deflection model”, *European Journal of Mechanics A - Solids,* pp. 95-106, 2004.

[254] F. R. Attenborough, The modelling of auxetic polymers, Ph.D Thesis, United Kingdom: University of Liverpool, 1997.

[255] U. D. Larsen, O. Sigmund and S. Bouwstra, “Design and fabrication of compliant micromechanics and structures with negative Poisson’s ratio”, *J. MICROELECTROMECH. S.,* vol. 6, pp. 99-106, 1997.

[256] A. T. Crumm and J. W. Halloran, “Negative Poisson’s ratio structures produced from zirconia and nickel using coextrusion”, *J. Mater. Sci,* vol. 42, pp. 1336-1342, 2007.

[257] J. X. Qiao and C. Q. Chen, “Impact resistance of uniform and functionally graded auxetic double arrowhead honeycombs”, *INT. J. IMPACT. ENG.,* vol. 83, pp. 47-58, 2015.

[258] A. Rafsanjani, A. Akbarzadeh and D. Pasini, “Snapping mechanical metamaterials under tension”, *Adv. Mater.,* vol. 27, pp. 5931-5935, 2015.

[259] A. Spagnoli, R. Brighenti, M. Lanfranchi and F. Soncini, “On the auxetic behaviour of metamaterials with re-entrant cell structures”, *PROCEDIA ENGINEER.,* vol. 109, pp. 410-417, 2015.

[260] K. E. Evans, M. A. Nkansah and I. J. Hutchinson, “Auxetic foams: Modelling negative Poisson’s ratios”, *ACTA METALL. MATER.,* vol. 42, pp. 1289-1294, 1994.

[261] J. N. Grima, R. Caruana-Gauci, D. Attard and R. Gatt, “Three-dimensional cellular structures with negative Poisson's ratio and negative compressibility properties”, *Proc. Royal Soc. A,* vol. 468, p. 3121, 2012.

[262] J. Schwerdtfeger, F. Schury, M. Stingl, F. Wein, R. F. Singer and C. Komer, “Mechanical characterisation of a periodic auxetic”, *Phys. Status Solidi B,* vol. 249, pp. 1347-1352, 2012.

[263] S. Krodel, T. Delpero, A. Bergamini, P. Ermanni and D. M. Kochmann, “3D auxetic microlattices with independently controllable acoustic band gaps and quasi-static elastic moduli”, *ADV. ENG. MATER.,* vol. 16, pp. 357-363, 2014.

[264] M. S. Rad, Y. Prawato and Z. Ahmad, “Analytical solution and finite element approach to the 3D re-entrant structures of auxetic materials”, *MECH. MATER.,* vol. 74, pp. 76-87, 2014.

[265] K. Wang, Y. H. Chang, Y. W. Chen, C. Zhang and B. Wang, “Designable dual-material auxetic metamaterials using three dimensional printing”, *Materials and Design,* vol. 67, pp. 159-164, 2015.

[266] K. L. Alderson, A. Alderson and K. E. Evans, “The interpretation of the strain-dependent Poisson’s ratio in auxetic polyethylene”, *J. STRAIN ANAL. ENG.,* vol. 32, pp. 201-212, 1997.

[267] N. Gaspar, C. W. Smith, A. Alderson, J. N. Grima and K. E. Evans, “A generalized three dimensional tethered-nodule model for auxetic materials”, *J. Mater. Sci.,* vol. 46, pp. 372-384, 2011.

[268] Z. K. Zhang, H. Hu, S. Liu and B. G. Xu, “Study of an auxetic structure made of tubes and corrugated sheets”, *Phys. Status Solidi B,* vol. 250, pp. 1996-2001, 2013.

[269] Z. K. Zhang, H. Hu and B. G. Xu, “An elastic analysis of a honeycomb structure with negative Poisson's ratio”, *Smart Mater. Struct.,* vol. 22, p. 084006, 2013.

[270] A. Alderson, K. L. Alderson, D. Attard, K. E. Evans, R. Gatt, J. N. Grima, W. Miller, N. Ravirala, C. W. Smith and K. M. Zied, “Elastic constants of 3-, 4- and 6-connected chiral and anti-chiral honeycombs subject to uniaxial in-plane loading”, *Composite Science and Technology,* vol. 70, pp. 1042-1048, 2010.

[271] J. N. Grima, R. Gatt and P. S. Farrugia, “On the properties of auxetic meta-tetrachiral structures”, *Phys. Status Solidi B,* vol. 245, pp. 521-529, 2008.

[272] A. Spadoni and M. Ruzzene, “Elasto-static micropolar behaviour of a chiral auxetic lattice”, *J. Mech. Phys. Solids,* vol. 60, pp. 156-171, 2012.

[273] A. Bacigalupo and L. Gambarotta, “Homogenization of periodic hexa- and tetrachiral cellular solids”, *Compos. Struct.,* vol. 116, pp. 461-476, 2014.

[274] R. Gatt, D. Attard, P. S. Farrugia, K. M. Azzopardi, L. Mizzi, J. P. Brincat and J. N. Grima, “A realistic generic model for antitetrachiral systems”, *Phys. Status Solidi B,* vol. 250, pp. 2012-2019, 2013.

[275] Y. Chen, X. Liu and G. Hu, “Micropolar modelling of planar orthotropic rectangular chiral lattices”, *Comptes Rendus Mecanique,* vol. 342, pp. 273-283, 2014.

[276] A. Lorato, P. Innocenti, F. Scarpa, A. Alderson, K. L. Alderson, K. M. Zied, N. Ravirala, W. Miller, C. W. Smith and K. E. Evans, “The transverse elastic properties of chiral honeycombs”, *Compos. Sci. Technol.,* vol. 70, pp. 1057-1063, 2010.

[277] F. Scarpa, S. Blain, T. Lew, D. Perrott, M. Ruzzene and J. R. Yates, “Elastic buckling of hexagonal chiral cell honeycomb”, *Composites Part A,* vol. 38, pp. 280-289, 2007.

[278] A. Spadoni, M. Ruzzene and F. Scarpa, “Global and local linear buckling behaviour of a chiral cellular structure”, *Phys. Status Solidi B,* vol. 242, pp. 695-709, 2005.

[279] W. Miller, C. W. Smith, F. Scarpa and K. E. Evans, “Flatwise buckling optimization of hexachiral and tetrachiral honeycombs”, *Compos. Sci. Technol.,* vol. 70, pp. 1049-1059, 2010.

[280] G. Cicala, G. Recca, L. Oliveri, Y. Perikleous, F. Scarpa, C. Lira, A. Lorato, D. J. Grube and G. Ziegmann, “Hexachiral truss-core with twisted hemp yarns: Out-of-plane shear properties”, *Compos. Struct.,* vol. 94, pp. 3556-3562, 2012.

[281] J. Dirrenberger, S. Forest and D. Jeulin, “Elastoplasticity of auxetic materials”, *Comput. Mater. Sci.,* vol. 64, pp. 57-61, 2012.

[282] R. Gatt, J. P. Brincat, K. M. Azzopardi, L. Mizzi and J. N. Grima, “On the effect of the mode of connection between the node and the ligaments in anti-tetrachiral systems”, *Adv. Eng. Mater.,* vol. 17, p. 189–198, 2014.

[283] A. A. Pozniak and K. W. Wojciechowski, “Poisson’s ratio of rectangular anti-chiral structures with size dispersion of circular nodes”, *Phys. Status Solidi B,* vol. 251, pp. 367-374, 2014.

[284] O. Sigmund, “Tailoring materials with prescribed elastic properties”, *Mech. Mater.,* vol. 20, pp. 351-368, 1995.

[285] Y. Ishibashi and M. Iwata, “A Microscopic Model of a Negative Poisson’s Ratio in Some Crystals”, *J. Phys. Soc. Japan,* vol. 69, pp. 2702-2703, 2000.

[286] J. N. Grima, A. Alderson and K. E. Evans, “Auxetic behaviour from rotating rigid units”, *Phys. status solidi B,* vol. 242, pp. 561-575, 2005.

[287] J. N. Grima, R. Gatt, A. Alderson and K. E. Evans, “On the Auxetic Properties of `Rotating Rectangles’ with Different Connectivity”, *J. Phys. Soc. Japan,* vol. 74, pp. 2866-2867, 2005.

[288] J. N. Grima and K. E. Evans, “Auxetic behavior from rotating triangles”, *J. Mater. Sci.*, vol. 41, pp. 3193-3196, 2006.

[289] J. N. Grima, P.-. S. Farrugia, R. Gatt and V. Zammit, “Connected Triangles Exhibiting Negative Poisson’s Ratios and Negative Thermal Expansion”, *J. Phys. Soc. Japan*, vol. 76, p. 25001, 2007.

[290] J. N. Grima, E. Chetcuti, E. Manicaro, D. Attard, M. Camilleri, R. Gatt and K. E. Evans, “On the auxetic properties of generic rotating rigid triangles”, *Proc. Royal Soc. A*, vol. 468, pp. 810-830, 2011.

[291] E. Chetcuti *et al.*, “Modeling auxetic foams through semi-rigid rotating triangles”, *Phys. status solidi B,* vol. 251, pp. 297-306, 2014.

[292] X.-. Q. Zhou, L. Zhang and L. Yang, “Negative linear compressibility of generic rotating rigid triangles”, *Chin. Phys. B,* vol. 26, 2017.

[293] J. J. Williams, C. W. Smith, K. E. Evans, Z. A. D. Lethbridge and R. I. Walton, “An analytical model for producing negative Poisson’s ratios and its application in explaining off-axis elastic properties of the NAT-type zeolites”, *Acta Mater.,* vol. 55, pp. 5697-5707, 2007.

[294] D. Attard, E. Manicaro and J. N. Grima, “On rotating rigid parallelograms and their potential for exhibiting auxetic behaviour”, *Phys. Status Solidi B,* vol. 246, pp. 2033-2044, 2009.

[295] J. N. Grima, P.-. S. Farrugia, R. Gatt and D. Attard, “On the auxetic properties of rotating rhombi and parallelograms: A preliminary investigation”, *Phys. Status Solidi B,* vol. 245, pp. 521-529, 2008.

[296] J. N. Grima, M. Bajada, S. Scerri, D. Attard, K. K. Dudek and R. Gatt, "Maximizing negative thermal expansion via rigid unit modes: a geometry-based approach", *Proc. R. Soc. A,* vol. 471, 2015.

[297] D. Attard, Investigation on materials and structures exhibiting negative mechanical properties, University of Malta, 2011.

[298] J. N. Grima, E. Manicaro and D. Attard, "Auxetic behaviour from connected different-sized squares and rectangles", *Proc. R. Soc. London A Math. Phys. Eng. Sci.,* vol. 467, 2010.

[299] H. Mitschke *et al.*, " Finding Auxetic Frameworks in Periodic Tessellations", *Adv. Mater.,* vol. 23, pp. 2669-2674, 2011.

[300] H. Mitschke, V. Robins, K. Mecke and G. E. Schröder-Turk, "Finite auxetic deformations of plane tessellations", *Proc. R. Soc. London A Math. Phys. Eng. Sci.,* vol. 469, 2012.

[301] H. Mitschke *et al.*, "Symmetry detection of auxetic behaviour in 2D frameworks", *Europhysics Lett.,* vol. 102, p. 66005, 2013.

[302] A. Alderson and K. E. Evans, "Rotation and dilation deformation mechanisms for auxetic behaviour in the α-cristobalite tetrahedral framework structure", *Phys. Chem. Miner.,* vol. 28, pp. 711-718, 2001.

[303] D. Attard and J. N. Grima, "A three-dimensional rotating rigid units network exhibiting negative Poisson's ratios", *Phys. Status Solidi B,* pp. 1-9, 2012.

[304] J. Shen, S. Zhou, X. Huang and Y. M. Xie, “Simple cubic three-dimensional auxetic metamaterials”, *Phys. Status Solidi B,* vol. 251, pp. 1515-1522, 2014.

[305] T. Bückmann *et al.*, “ On three-dimensional dilational elastic metamaterials”, *New J. Phys.*, vol. 16, p. 33032, 2014.

[306] R. Gatt, R. Caruana-Gauci, D. Attard, A. R. Casha, W. Wolak, K. Dudek, L. Mizzi and J. N. Grima, “On the properties of real finite-sized planar and tubular stent-like auxetic structures”, *Phys. Status Solidi B,* vol. 251, pp. 321-327, 2014.

[307] J. N. Grima, A. Alderson and K. E. Evans, “An Alternative Explanation for the Negative Poisson’s Ratios in Auxetic Foams”, *J. Phys. Soc. Japan,* vol. 74, pp. 1341-1342, 2005.

[308] S. A. McDonald, G. Dedreuil-Monet, Y. T. Yao, A. Alderson and P. J. Withers, “In situ 3D X-ray microtomography study comparing auxetic and non-auxetic polymeric foams under tension”, *Phys. Status Solidi B,* vol. 248, pp. 45-51, 2011.

[309] R. Cauchi, Modelling of the mechanical and thermal properties in zeolites and related frameworks, Ph.D. Thesis, 2013.

[310] R. Cauchi and J. N. Grima, “Modelling of the static and dynamic properties of THO-type silicates”, *TASK Q.*, vol. 18, pp. 5-65, 2014.

[311] J. N. Grima, R. N. Cassar and R. Gatt, “On the effect of hydrostatic pressure on the auxetic character of NAT-type silicates”, *J. Non. Cryst. Solids,* vol. 355, pp. 1307-1312, 2009.

[312] J. N. Grima *et al.*, "On the origin of auxetic behaviour in the silicate α-cristobalite", *J. Mater. Chem.,* vol. 15, p. 4003, 2005.

[313] J. N. Grima, R. Gatt, A. Alderson and K. E. Evans, "An alternative explanation for the negative Poisson's ratios in α-cristobalite", *Mater. Sci. Eng. A,* vol. 423, pp. 219-224, 2006.

[314] K. E. Evans and A. Alderson, "Rotation and dilation deformation mechanisms for auxetic behaviour in the α-cristobalite tetrahedral framework structure", *Phys. Chem. Miner.,* vol. 28, pp. 711-718, 2001.

[315] A. Alderson, J. Rasburn, K. E. Evans and J. N. Grima, "Auxetic polymeric filters display enhanced de-fouling and pressure compensation properties", *Membr. Technol.,* vol. 2001, pp. 6-8, 2001.

[316] R. Gatt, V. Zammit, C. Caruana and J. N. Grima, "On the atomic level deformations in the auxetic zeolite natrolite", *Phys. status solidi B,* vol. 245, pp. 502-510, 2008.

[317] J. N. Grima, M. Bajada, S. Scerri, D. Attard, K. K. Dudek and R. Gatt, "Maximizing negative thermal expansion via rigid unit modes: a geometry-based approach", *Proc. R. Soc. A,* vol. 471, 2015.

[318] T. Bückmann, N. Stenger, M. Kadic, J. Kaschke, A. Frölich, T. Kennerknecht, C. Eberl, M. Thiel and M. Wegener, "Tailored 3D Mechanical Metamaterials Made by Dip-in Direct-Laser-Writing Optical Lithography", *Adv. Mater.,* vol. 24, pp. 2710-2714, 2012.

[319] G. Cicala, G. Recca, L. Oliveri, Y. Perikleous, F. Scarpa, C. Lira, A. Lorato, D. J. Grube and G. Ziegmann, “Hexachiral truss-core with twisted hemp yarns: Out-of-plane shear properties”, *Compos. Struct.,* vol. 94, pp. 3556-3562, 2012.

[320] V. Kunin, S. Yang, Y. Cho, P. Deymier and D. J. Srolovitz, “Static and dynamic elastic properties of fractal-cut materials”, *Extreme Mechanics Letters,* vol. 6, pp. 103-114, 2016.

[321] T.-C. Lim, “Analogies across auxetic models based on deformation mechanism”, *Phys. Status Solidi RRL,* vol. 11, p. 1600440, 2017.

[322] R. Lakes, “Materials with structural hierarchy”, *Nature,* vol. 361, pp. 511-515, 1993.

[323] K. E. Easterling, R. Harrysson, L. J. Gibson and M. F. Ashby, “On the Mechanics of Balsa and Other Woods”, *Proc. R. Soc. London A Math. Phys. Eng. Sci.,* vol. 383, 1982.

[324] Y. Chen, X. Wang, H. Ren, H. Yin and S. Jia, “Hierarchical Dragonfly Wing: Microstructure-Biomechanical Behavior Relations”, *J. Bionic Eng.,* vol. 9, pp. 185-191, 2012.

[325] J.-. Y. Rho, L. Kuhn-Spearing and P. Zioupos, “ Mechanical properties and the hierarchical structure of bone”, *Med. Eng. Phys.,* vol. 20, pp. 92-102, 1998.

[326] R. Oftadeh, B. Haghpanah, D. Vella, A. Boudaoud and A. Vaziri, “Optimal Fractal-Like Hierarchical Honeycombs”, *Phys. Rev. Lett.,* vol. 113, p. 104301, 2014.

[327] D. Mousanezhad, S. Babaee, H. Ebrahimi, R. Ghosh, A. S. Hamouda, K. Bertoldi and A. Vaziri, “Hierarchical honeycomb auxetic metamaterials”, *Sci. Rep.,* vol. 5, p. 18306, 2015.

[328] Y. Sun and N. M. Pugno, “In plane stiffness of multifunctional hierarchical honeycombs with negative Poissonâ€TMs ratio sub-structures”, *Compos. Struct.,* vol. 106, pp. 681-689, 2013.

[329] Y. Cho, Y.-H. Shin, A. Costa, T. A. Kim, V. Kunin, J. Li, S. Y. Lee, S. Yang, H.-N. Han, I.-S. Choi and D. J. Srolovitz, “Engineering the shape and structure of materials by fractal cut”, *Proc. Natl. Acad. Sci.,* vol. 111, pp. 17390-17395, 2014.

[330] R. Gatt, L. Mizzi, J. I. Azzopardi, K. M. Azzopardi, D. Attard, A. Casha, J. Briffa and J. N. Grima, “Hierarchical Auxetic Mechanical Metamaterials”, *Sci. Rep.,* vol. 5, p. 8395, 2015.

[331] Y. Tang, G. Lin, L. Han, S. Qiu, S. Yang and J. Yin, “Design of Hierarchically Cut Hinges for Highly Stretchable and Reconfigurable Metamaterials with Enhanced Strength”, *Adv. Mater.,* vol. 27, pp. 7181-7190, 2015.

[332] K. Billon, M. Ouisse, E. Sadoulet-Reboul, F. Scarpa and M. Collet, “Parametric Study of Wave Propagation in Hierarchical Auxetic Perforated Metamaterials”, *Active and Passive Smart Structures and Integrated Systems,* vol. 9799, p. 979906, 2016.

[333] H. Seifi, A. R. Javan, A. Ghaedizadeh, J. Shen, S. Xu and Y. M. Xie , “Design of Hierarchical Structures for Synchronized Deformations”, *Sci. Rep.,* vol. 7, p. 41183, 2017.

[334] D. Li, J. Yin, L. Dong and R. S. Lakes, “Numerical analysis on mechanical behaviors of hierarchical cellular structures with negative Poisson’s ratio”, *Smart Mater. Struct.,* vol. 26, p. 025014, 2017.

[335] D. J. Gunton and G. A. Saunders, “The Young's modulus and Poisson's ratio of arsenic, antimony and bismuth”, *J. Mater. Sci.,* vol. 7, p. 1061, 1972.

[336] B. Morosin and J. E. Schirber, “Linear compressibilities and the pressure dependence of the atomic positional parameter of As”, *Solid State Commun.,* vol. 10, p. 249, 1972.

[337] S. Prawer, T. F. Smith and T. R. Finlayson, “The Room Temperature Elastic Behaviour of CsH2PO4”, *Aust. J. Phys.,* vol. 38, p. 63, 1985.

[338] E. F. Skelton, J. L. Feldman, C. Y. Liu and I. L. Spain, *Phys. Rev. B,* vol. 13, p. 2605, 1976.

[339] A. B. Cairns, J. Catafesta, C. Levelut, J. Rouqette, A. van der Lee, L. Peters, A. L. Thompson, V. Dmitriev, J. Haines and A. L. Goodwin, “Giant negative linear compressibility in zinc dicyanoaurate”, *Nature Mater.,* vol. 12, p. 212, 2013.

[340] A. B. Cairns, A. L. Thompson, M. G. Tucker, J. Haines and A. L. Goodwin, “Rational Design of Materials with Extreme Negative Compressibility: Selective Soft-Mode Frustration in KMn[Ag(CN)2]3”, *J. Am. Chem. Soc.,* vol. 134, p. 4454, 2012.

[341] A. D. Fortes, E. Suard and K. S. Knight, “Negative linear compressibility and massive anisotropic thermal expansion in methanol monohydrate”, *Science,* vol. 331, p. 742, 2011.

[342] C. N. Weng, K. T. Wang and T. Chen, “Design of microstructures and structures with negative linear compressibility in certain directions”, *Adv. Mat. Res.,* Vols. 33-37, pp. 807-814, 2008.

[343] J. N. Grima, D. Attard, R. Caruana-Gauci and R. Gatt, “Negative linear compressibility of hexagonal honeycombs and related systems”, *Scr. Mater.,* vol. 65, pp. 565-568, 2011.

[344] R. Caruana-Gauci, E. P. Degabriele, D. Attard and J. N. Grima, “Auxetic metamaterials inspired from wine-racks”, *J. Mater. Sci.,* vol. 53, pp. 5079-5091, 2018.

[345] Y. Yan, A. E. O’Connor, G. Kanthasamy, G. Atkinson, D. R. Allan, A. J. Blake and M. Schroder, “Unusual and Tunable Negative Linear Compressibility in the Metal–Organic Framework MFM-133(M) (M = Zr, Hf)”, *J. Am. Chem. Soc.,* vol. 140, pp. 3952-3958, 2018.

[346] X. Zhou, L. Zhang, H. Zhang, Q. Liu and T. Ren, “3D cellular models with negative compressibility through the wine-rack-type mechanism”, *Phys. Status Solidi B,* pp. 1-17, 2016.

[347] T.-C. Lim, “2D Structures Exhibiting Negative Area Compressibility”, *Phys. Status Solidi B,* vol. 254, p. 1600682, 2017.

[348] J. N. Grima, E. P. Degabriele and D. Attard, “Nano networks exhibiting negative linear compressibility”, *phys. status solidi b,* vol. 253, pp. 1419-1427, 2016.

[349] J. Qu, M. Kadic and M. Wegener, “Poroelastic metamaterials with negative effective static compressibility”, *Appl. Phys. Lett.,* vol. 110, p. 171901, 2017.

[350] J. Qu, A. Gerber, F. Mayer, M. Kadic and M. Wegener, “Experiments on Metamaterials with Negative Effective Static Compressibility”, *Phys. Rev. X,* vol. 7, p. 041060, 2017.

[351] J. N. Grima, D. Attard and R. Gatt, “Truss-type systems exhibiting negative compressibility”, *Phys. Status Solidi B,* vol. 245, pp. 2405-2414, 2008.

[352] T. A. M. Hewage, K. L. Alderson, A. Alderson and F. Scarpa, “Double-Negative Mechanical Metamaterials Displaying Simultaneous Negative Stiffness and Negative Poisson's Ratio Properties”, *Adv. Mater.,* vol. 28, pp. 10323-10332, 2016.

[353] D. Attard, R. Caruana-Gauci, R. Gatt and J. N. Grima, “Negative linear compressibility from rotating rigid units”, *Phys. Status Solidi B,* vol. 253, pp. 1410-1418, 2016.

[354] W. Molyneaux, Supports for vibration isolation, Great Britain: Aeronautical, 1957.

[355] C. Oran, “Tangent stiffness in space frames”, *J. Struct. Div.,* vol. 99, pp. 987-1001, 1973.

[356] J. M. T. Thompson, “Stability predictions through a succession of folds”, *Philos. Trans. Royal Soc. A,* vol. 292, pp. 1-23, 1979.

[357] S.-L. Chan and J.-X. Gu, “Exact Tangent Stiffness for Imperfect Beam-Column Members”, *Journal of Structural Engineering,* vol. 126, pp. 1094-1102, 2000.

[358] F. Falk, “Model free-energy, mechanics and thermodynamics of shape-memory alloys”, *Acta Metall.,* vol. 28, p. 1773, 1980.

[359] L. Kashdan, C. C. Seepersad, M. Haberman and P. S. Wilson, “Design, fabrication, and evaluation of negative stiffness elements using SLS”, *Rapid Prototyping Journal,* vol. 18, pp. 194-200, 2012.

[360] S. Cortes, J. Allison, C. Morris, M. R. Haberman, C. C. Seepersad and D. Kovar, “Design, manufacture and quasi-static testing of metallic negative stiffness structures within a polymer matrix”, *Experimental Mechanics,* vol. 57, pp. 1183-1191, 2017.

[361] D. M. Correa, C. C. Seepersad and M. R. Haberman, “Mechanical design of negative stiffness honeycomb materials”, *Integrating Materials and Manufacturing Innovation,* vol. 4, p. 10, 2015.

[362] D. M. Correa, T. Klatt, S. Cortes, M. Haberman, D. Kovar and C. Seepersad, “Negative stiffness honeycombs for recoverable shock isolation”, *Rapid Prototyping Journal,* vol. 21, pp. 193-200, 2015.

[363] R. S. Lakes, T. Lee, A. Bersie and Y. C. Wang, “Extreme damping in composite materials with negative-stiffness inclusions”, *Nature,* vol. 410, pp. 565-567, 2001.

[364] T.-. C. Lim, “In-Plane Stiffness of Semiauxetic Laminates”, *Journal of Engineering Mechanics,* vol. 136, 2010.

[365] R. S. Lakes, “Extreme Damping in Composite Materials with a Negative Stiffness Phase”, *Phys. Rev. Lett.,* vol. 86, pp. 2897-2900, 2001.

[366] R. S. Lakes, “Extreme damping in compliant composites with a negative-stiffness phase”, *Philos. Mag. Lett.,* vol. 81, pp. 95-100, 2001.

[367] R. S. Lakes and W. J. Drugan, “Dramatically stiffer elastic composite materials due to a negative stiffness phase?”, *J. Mech. Phys. Solids,* vol. 50, pp. 979-1009, 2002.

[368] Y. C. Wang, “Extreme thermal expansion, piezoelectricity, and other coupled field properties in composites with a negative stiffness phase”, *J. Appl. Phys.,* vol. 90, p. 6458, 2001.

[369] Y. C. Wang and R. S. Lakes, “Extreme thermal expansion, piezoelectricity, and other coupled field properties in composites with a negative stiffness phase”, *J. Appl. Phys.,* vol. 90, p. 6458, 2001.

[370] T. Jaglinski, D. Kochmann, D. Stone and R. S. Lakes, “Composite Materials with Viscoelastic Stiffness Greater Than Diamond”, *Science,* vol. 315, pp. 620-622, 2007.

[371] T-. C. Lim and U. R. Acharya, “Counterintuitive modulus from semi-auxetic laminates”, *Phys. Status Solidi B,* vol. 248, pp. 60-65, 2011.

[372] T. C. Lim, “Out-of-plane modulus of semi-auxetic laminates”, *European Journal of Mechanics - A/Solids,* vol. 28, pp. 752-756, 2009.

[373] W. J. Drugan, “Composite Materials Having a Negative Stiffness Phase Can Be Stable”, *Phys. Rev. Lett.,* vol. 98, p. 055502, 2007.

[374] D. M. Kochmann and W. J. Drugan, “Dynamic stability analysis of an elastic composite material having negative-stiffness phase”, *Journal of Mechanics and Physics of Solids,* vol. 57, pp. 1122-1138, 2009.

[375] D. M. Kochmann and W. J. Drugan, “Infinitely stiff composite via a rotation-stabilized negative-stiffness phase”, *Appl. Phys. Lett.,* vol. 99, p. 011909, 2011.

[376] A. V. Dyskin and E. Pasternak, “Elastic composite with negative stiffness inclusions in antiplane strain International”, *Journal of Engineering Science,* vol. 58, pp. 45-56, 2012.

[377] K. C. Jajam and H. V. Tippur, “Role of inclusion stiffness and interfacial strength on dynamic matrix crack growth: An experimental study”, *International Journal of Solids and Structures,* vol. 49, pp. 1127-1146, 2012.

[378] Y.-C. Wang and C.-C. Ko, “Stability of viscoelastic continuum with negative-stiffness inclusions in the low-frequency range”, *Phys. Status Solidi B,* vol. 250, p. 2070–2079, 2013.

[379] D. Chronopoulos, I. Antoniadis and T. Ampatzidis, “Enhanced acoustic insulation properties of composite metamaterials having embedded negative stiffness inclusions”, *Extreme Mechanics Letters,* vol. 12, pp. 48-54, 2017.

[380] T. Klatt and M. R. Haberman, “A nonlinear negative stiffness metamaterial unit cell and small-on-large multiscale material model”, *J. Appl. Phys.,* vol. 114, p. 033503, 2013.

[381] A. Carrella, M. J. Brennan and T. P. Waters, “On the design of a high-static–low-dynamic stiffness isolator using linear mechanical springs and magnets”, *J. Sound Vibr.,* vol. 315, pp. 712-720, 2008.

[382] C.-M. Lee, V. N. Goverdovskiy and A. I. Temnikov, “Design of springs with ”negative" stiffness to improve vehicle driver vibration isolation”, *J. Sound Vibr.,* vol. 302, pp. 865-874, 2007.

[383] R. A. Ibrahim, “Recent advances in nonlinear passive vibration isolators”, *J. Sound Vibr.,* vol. 314, pp. 371-452, 2008.

[384] F. Weber, C. Boston and M. Maslanka, “An adaptive tuned mass damper based on the emulation of positive and negative stiffness with an MR damper”, *Smart Mater. Struct.,* vol. 20, 2010.

[385] L. Dong and R. Lakes, “Advanced damper with negative structural stiffness”, *Smart Mater. Struct.,* vol. 21, 2012.

[386] L. Dong and R. Lakes, “Advanced damper with high stiffness and high hysteresis”, *Int. J. Solids Struct.,* vol. 50, pp. 2416-2423, 2013.

[387] C.-M. Lee and V. N. Goverdovskiy, “A multi-stage high-speed railroad vibration isolation system with "negative" stiffness”, *J. Sound Vibr.,* vol. 331, pp. 914-921, 2012.

[388] M. Feldman, “Non-linear free vibration identification via the Hilbert transform”, *J. Sound Vibr.,* vol. 208, pp. 475-489, 1997.

[389] W. S. Robertson, M. R. F. Kidner, B. S. Cazzolato and A. C. Zander, “Theoretical design parameters for a quasi-zero stiffness magnetic spring for vibration isolation”, *J. Sound Vibr.,* vol. 326, pp. 88-103, 2009.

[390] R. Ravaud, G. Lemarquand and V. Lemarquand, “Force and Stiffness of Passive Magnetic Bearings Using Permanent Magnets. Part 2: Radial Magnetization”, *IEEE TRANSACTIONS ON MAGNETICS,* vol. 45, pp. 3334-3342, 2009.

[391] Y. Zheng, X. Zhang, Y. Luo, Y. Zhang and S. Xie, “Analytical study of a quasi-zero stiffness coupling using a torsion magnetic spring with negative stiffness”, *Mech. Syst. Signal Process.*, vol. 100, pp. 135-151, 2018.

[392] N. Zhou and K. Liu, “A tunable high-static–low-dynamic stiffness vibration isolator”, *J. Sound Vibr.*, vol. 329, pp. 1254-1273, 2010.

[393] D. Xu, Q. Yu, J. Zhou and S. R. Bishop, “Theoretical and experimental analyses of a nonlinear magnetic vibration isolator with quasi-zero-stiffness characteristic”, *J. Sound Vibr.*, vol. 332, pp. 3377-3389, 2013.

[394] Q. Li, Y. Zhu, D. Xu, J. Hu, W. Min and L. Pang, “A negative stiffness vibration isolator using magnetic spring combined with rubber membrane”, *J. Sound Vibr.*, vol. 27, pp. 813-824, 2013.

[395] W. Wu, X. Chen and Y. Shan, “Analysis and experiment of a vibration isolator using a novel magnetic spring with negative stiffness”, *J. Sound Vibr.*, vol. 333, pp. 2958-2970, 2014.

[396] X. Shi and S. Zhu, “Magnetic negative stiffness dampers”, *Smart Mater. Struct.*, vol. 24, p. 072002, 2015.

[397] X. Shi and S. Zhu, “Simulation and optimization of magnetic negative stiffness dampers”, *Sens. Actuator A-Phys.*, vol. 259, pp. 14-33, 2017.

[398] T. D. Le and K. K. Ahn, “A vibration isolation system in low frequency excitation region using negative stiffness structure for vehicle seat”, *J. Sound Vibration*, vol. 330, pp. 6311-6335, 2011.

[399] T. D. R. Pasala, A. A. Sarlis, S. Nagarajaiah, A. M. Reinhorn, M. C. Constantinou and D. Taylor, “Adaptive negative stiffness: new structural modification approach for seismic protection”, *J. Struct. Eng.,* vol. 139, pp. 1112-23, 2012.

[400] S. Nagarajaiah, T. D. R. Pasala, A. Reinhorn, M. Constantinou, A. A. Sirilis and D. Taylor, “Adaptive Negative Stiffness: A New Structural Modification Approach for Seismic Protection”, *Advances in Civil Infrastructure Engineering,* vol. 639, pp. 54-66, 2013.

[401] F. Scarpa, W. A. Bullough and P. Lumley, “Trends in acoustic properties of iron particle seeded auxetic polyurethane foam”, *Proc. Inst. Mech. Eng. C,* vol. 218, pp. 241-244, 2004.

[402] F. Scarpa and F. C. Smith, “Passive and MR fluid-coated auxetic PU foam-mechanical, acoustic, and electromagnetic properties”, *J. Intell. Mater. Syst. Struct.,* vol. 15, pp. 973-979, 2004.

[403] F. C. Smith, F. Scarpa and B. Chambers, “The electromagnetic properties of re-entrant dielectric honeycombs”, *IEEE Microw. Guided Wave Lett,* vol. 10, pp. 451-453, 2000.

[404] M. R. Dudek and K. W. Wojciechowski, “Magnetic films of negative Poisson's ratio in rotating magnetic fields”, *Journal of Non-Crystalline Solids,* vol. 354, pp. 4304-4308, 2008.

[405] M. R. Dudek, B. Grabiec and K. W. Wojciechowski, “MOLECULAR DYNAMICS SIMULATIONS OF AUXETIC FERROGEL”, *Rev. Adv. Mater. Sci.,* vol. 14, pp. 167-173, 2007.

[406] J. N. Grima, R. Caruana-Gauci, M. R. Dudek, K. W. Wojciechowski and R. Gatt, "Smart metamaterials with tunable auxetic and other properties", *Smart Mater. Struct.*, vol. 22, p. 084016, 2013.

[407] K. Singh, C. R. Tipton, E. Han and T. Mullin, "Magneto-elastic buckling of an Euler beam", *Proc. Royal Soc. A,* vol. 469, p. 20130111, 2013.

[408] M. Schaeffer and M. Ruzzene, "Wave propagation in reconfigurable magneto-elastic kagome lattice structures", *J. Appl. Phys,* vol. 117, p. 194903, 2015.

[409] C. R. Tipton, E. Han and T. Mullin, "Magneto-elastic buckling of a soft cellular solid", *Soft Matter,* vol. 8, pp. 6880-6883, 2012.

[410] R. L. Harne, Z. Deng and M. J. Dapino, "Characterization of adaptive magnetoelastic metamaterials under applied magnetic fields", in *Proceedings of the ASME 2016 Conference on Smart Materials, Adaptive Structures and Intelligent Systems SMASIS2016,* 2016.

[411] M. Schaeffer and M. Ruzzene, "Wave propagation in multistable magneto-elastic lattices", *Int. J. Solid. Struct.,* Vols. 56-57, pp. 78-95, 2015.

[412] M. Schaeffer and M. Ruzzene, "Homogenization of 1D and 2D magnetoelastic lattices", *EPJ Applied Metamaterials,* vol. 2, p. 13, 2015.

[413] M. Feldman, "Non-linear free vibration identification via the Hilbert transform", *J. Sound Vibr.,* vol. 208, pp. 475-489, 1997.

[414] A. Carrella, M. J. Brennan and T. P. Waters, “Demonstrator to show the effects of negative stiffness on the natural frequency of a simple oscillator”, *Proc. Inst. Mech. Eng. C,* vol. 222, pp. 1189-1192, 2008.

[415] A. M. Bloch and J. E. Marsden, “Stabilization of rigid body dynamics by the Energy-Casimir method”, *Syst. Control Lett.,* vol. 14, pp. 341-346, 1990.

[416] Z. Ismail and R. Varatharajoo, “A study of reaction wheel configurations for a 3-axis satellite attitude control”, *Adv. Space Res.,* vol. 45, pp. 750-759, 2010.

[417] K. K. Dudek, R. Gatt, L. Mizzi, M. R. Dudek, D. Attard and J. N. Grima, “Global rotation of mechanical metamaterials induced by their internal deformation”, *AIP Adv.,* vol. 7, p. 095121, 2017.

[418] R. L. Burden and J. D. Faires, Numerical Analysis, PWS Publishers, 1985, p. 220.

[419] M. Sanami, N. Ravirala, K. Alderson and A. Alderson, “Auxetic Materials for Sports Applications”, *Procedia Engineering,* vol. 72, pp. 453-458, 2014.

[420] J. N. Grima and R. Gatt, “Perforated Sheets Exhibiting Negative Poisson’s Ratios”, *Adv. Eng. Mater.,* vol. 12, pp. 460-464, 2010.

[421] D. Attard, E. Manicaro, R. Gatt and J. N. Grima, “On the properties of auxetic rotating stretching squares”, *Phys. Status Solidi B,* vol. 246, pp. 2045-2054, 2009.

[422] N. H. Scott, “The incremental bulk modulus, young’s modulus and Poisson’s ratio in nonlinear isotropic elasticity: physically”, *Math. Mech. Solids,* vol. 12, pp. 526-542, 2007.

[423] C. W. Smith, R. J. Wootton and K. E. Evans, “Interpretation of experimental data for Poisson’s ratio of highly nonlinear materials”, *Exp. Mech.,* vol. 39, pp. 356-362, 1999.

[424] K. K. Dudek, R. Gatt, L. Mizzi, M. R. Dudek, D. Attard, K. E. Evans and J. N. Grima, “On the dynamics and control of mechanical properties of hierarchical rotating rigid unit auxetics”, *Sci. Rep.,* vol. 7, p. 46529, 2017.

[425] A. Alderson *et al.*, “An Auxetic Filter: A Tuneable Filter Displaying Enhanced Size Selectivity or Defouling Properties”, *Ind. Eng. Chem. Res.,* vol. 39, pp. 654-665, 2000.

[426] G. W. Milton, “Complete characterization of the macroscopic deformations of periodic unimode metamaterials of rigid bars and pivots”, *J. Mech. Phys. Solids,* vol. 61, pp. 1543-60, 2013.

[427] G. W. Milton and A. V. Cherkaev, “Which elasticity tensors are realizable?”, *J. Eng. Mater. Technol.,* vol. 117, pp. 483-93, 1995.

[428] G. W. Milton, “New examples of three-dimensional dilational materials”, *Phys. Status Solidi B,* vol. 252, pp. 1426-30, 2015.

[429] R. G. Hutchinson and N. A. Fleck, “The structural performance of the periodic truss”, *J. Mech. Phys. Solids,* vol. 54, pp. 756-82, 2006.

[430] V. Kapko, M. M. J. Treacy, M. F. Thorpe and S. D. Guest, “On the collapse of locally isostatic networks”, *Proc. R. Soc. A,* vol. 465, p. 3517–30, 2009.

[431] L. Cabras and M. Brun, “Auxetic two-dimensional lattice with Poisson’s ratio arbitrarily close to -1”, *Proc. R. Soc. A,* vol. 470, p. 20140538, 2014.

[432] K. K. Dudek, D. Attard, R. Caruana-Gauci, K. W. Wojciechowski and J. N. Grima, "Unimode metamaterials exhibiting negative linear compressibility and negative thermal expansion", *Smart Mater. Struct.,* vol. 25, p. 025009, 2016.

[433] R. H. Baughman, S. Stafstrom, C. Cui and S. O. Dantas, "Materials with negative compressibilities in one or more dimensions", *Science,* vol. 279, pp. 1522-4, 1998.

[434] P. R. L. Welche, V. Heine and M. T. Dove, "Negative thermal expansion in beta-quartz", *Phys. Chem. Miner.,* vol. 26, pp. 63-77, 1998.

[435] F. S. Tautz, V. Heine, M. T. Dove and X. Chen, "Rigid unit modes in the molecular dynamics simulation of quartz and the incommensurate phase transition", *Phys. Chem. Miner.,* vol. 18, pp. 326-336, 1991.

[436] A. K. A. Pryde, K. D. Hammonds, M. T. Dove, V. Heine, J. D. Gale and M. C. Warren, "Origin of the negative thermal expansion in ZrW2O8 and ZrV2O7", *J. Phys.: Condens. Matter,* vol. 8, pp. 10973-82, 1996.

[437] W. Miller, C. W. Smith, D. S. Mackenzie and K. E. Evans, "Negative thermal expansion: a review", *J. Mater. Sci.,* vol. 44, pp. 5441-51, 2009.

[438] J. N. Grima, M. Bajada, S. Scerri, D. Attard, K. K. Dudek and R. Gatt, "Maximizing negative thermal expansion via rigid unit modes: a geometry-based approach", *Proc. R. Soc. A,* vol. 471, p. 20150188, 2015.

[439] J. N. Grima, D. Attard, R. Caruana-Gauci and R. Gatt, "Negative linear compressibility of hexagonal honeycombs and related systems", *Scr. Mater,* vol. 65, pp. 565-8, 2011.

[440] A. Versluis, W. H. Douglas and R. L. Sakaguchi, “Thermal expansion coefficient of dental composites measured with strain gauges”, *Dent. Mater.,* vol. 12, pp. 290-4, 1996.

[441] O. Sigmund and S. Torquato, “Design of materials with extreme thermal expansion using a three-phase topology optimization method”, *J. Mech. Phys. Solids,* vol. 45, pp. 1037-67, 1997.

[442] F. Scarpa, G. Tagliafico and L. A. Tagliafico, “Classification proposal for room temperature”, *Int. J. Refrig.,* vol. 35, pp. 453-458, 2011.

[443] M. Kadic, R. Schittny, T. Bückmann, C. Kern and M. Wegener, “Hall-Effect Sign Inversion in a Realizable 3D Metamaterial”, *Phys. Rev. X,* vol. 5, p. 021030, 2015.

[444] D. Restrepo, N. D. Mankame and P. D. Zavattieri, “Phase transforming cellular materials”, *Extreme Mechanics Letters,* vol. 4, pp. 52-60, 2015.

[445] U. D. Larsen, O. Signund and S. Bouwsta, “Design and fabrication of compliant micromechanisms and structures with negative Poisson's ratio”, *J. Microelectromech. Syst.,* vol. 6, pp. 99-106, 1997.

[446] J. M. D. Coey, Magnetism and Magnetic Materials, Cambridge: Cambridge University Press, 2010.

[447] V. Z. C. Paes and D. H. Mosca, “Magnetostrictive contribution to Poisson ratio of galfenol”, *J. Appl. Phys.,* vol. 22, p. 084016, 2013.

[448] D. H. Mosca, F. Vidal and V. H. Etgens, “Strain engineering of the magnetocaloric effect in MnAs epilayers”, *Phys. Rev. Lett.,* vol. 101, p. 125503, 2008.

[449] E. Warburg, “Über einige Wirkungen der Coërcitivkraft”, *Ann. Phys.*, vol. 13, p. 141, 1881.

[450] A. de Oliveira and P. J. von Ranke, “Theoretical aspects of the magnetocaloric effect”, *Phys. Rep.*, vol. 489, pp. 89-159, 2010.

[451] A. M. Tishin and Y. I. Spichkin, The Magnetocaloric Effect and its Applications, Bristol: IOP Publishing, 2003.

[452] V. K. Pecharsky and K. A. Gschneidner, “Giant magnetocaloric effect in Gd5(Si2Ge2)”, *Phys. Rev. Lett.*, vol. 78, pp. 4494-7, 1997.

[453] O. Petracic, X. Chen, S. Bedanta, W. Kleemann, S. Sahoo, S. Cardoso and P. P. Freitas, “Collective states of interacting ferromagnetic nanoparticles”, *J. Magn. Magn. Mater.*, vol. 300, pp. 192-7, 2006.

[454] V. Markovich, I. Fita, A. Wisniewski, R. Puzniak, D. Mogilyansky, P. Iwanowski, P. Dluzewski and G. Gorodetsky, “Nanometer size effect on magnetic properties of Sm0.8Ca0.2MnO3 Nanoparticles”, *J. Phys. Chem. C*, vol. 116, pp. 435-47, 2012.

[455] D. Parker, I. Lisiecki and M. P. Pileni, “Do 8 nm Co nanocrystals in long-range-ordered face-centered cubic (fcc) supracrystals show superspin glass behavior?”, *J. Phys. Chem. Lett.*, vol. 1, pp. 1139-42, 2010.

[456] E. Skoropata, R. D. Desautels, B. W. Southern and J. van Lierop, “Comment on colossal reduction in Curie temperature due to finite-size effects in CoFe2O4 nanoparticles”, *Chem. Mater.*, vol. 25, pp. 1998-2000, 2013.

[457] L. Onsager, “Crystal statistics: I. A two-dimensional model with an order-disorder transition”, *Phys. Rev.*, vol. 65, p. 117–49, 1944.

[458] K. Huang, Statistical Mechanics, New York: Wiley, 1987.

[459] R. J. Baxter, Exactly Solved Models in Statistical Mechanics, New York: Academic, 1982.

[460] H. E. Stanley, Introduction to Phase Transitions and Critical Phenomena, Oxford: Oxford University Press, 1971.

[461] C. P. Bean and D. S. Rodbell, “Magnetic disorder as a first-order phase transformation”, *Phys. Rev.*, vol. 126, pp. 104-15, 1962.

[462] V. I. Mitsiuk, N. Y. Pankratov, G. A. Govor, S. A. Nikitin and A. I. Smarzhevskaya, “Magnetostructural phase transitions in manganese arsenide single crystals”, *Phys. Solid State*, vol. 54, pp. 1988-95, 2012.

[463] D. J. Huang, C. F. Chang, H.-. T. Jeng, G. Y. Guo, H.-. J. Lin, W. B. Wu, H. C. Ku, A. Fujimori, Y. Takahashi and C. T. Chen, “Spin and orbital magnetic moments of Fe3O4”, *Phys. Rev. Lett.*, vol. 93, p. 077204, 2004.

[464] E. Ising, *Z. Physik*, vol. 31, p. 253, 1925.

[465] L. Onsager, *Z. Physik*, vol. 31, p. 253, 1925.

[466] R. J. Baxter, Exactly Solved Models in Statistical Mechanics, New York: Academic, 1982.

[467] D. Stauffer, “Social applications of two-dimensional Ising models”, *Am. J. Phys.,* vol. 76, pp. 470-473, 2008.

[468] J. J. Hopfield, “Neural networks and physical systems with emergent collective computational abilities”, *Proc. Natl. Acad. Sci. USA,* vol. 79, pp. 2254-2558, 1982.

[469] S. Bornholdt and F. Wagner, “Stability of money: phase transitions in an Ising economy”, *Physica A,* vol. 316, pp. 453-468, 2002.

[470] S. M. Allen and J. W. Cahn, “A microscopic theory for antiphase boundary motion and its application to antiphase domain coarsening”, *Acta Metall.,* vol. 27, pp. 1085-1095, 1979.

[471] K. Humayun and A. J. Bray, “Non-equilibrium dynamics of the Ising model for T less-than/equal-toTc”, *J. Phys. A: Math. Gen.,* vol. 24, p. 1915, 1991.

[472] I. M. Lifshitz and V. V. Slyozov, “The kinetics of precipitation from supersaturated solid solutions”, *J. Phys. Chem. Solids,* vol. 19, pp. 35-50, 1961.

[473] J. G. Amar, F. E. Sullivan and R. D. Mountain, “Monte Carlo study of growth in the two-dimensional spin-exchange kinetic Ising model”, *Phys. Rev. B ,* vol. 37, pp. 196-208, 37.

[474] A. J. Bray, “Theory of phase-ordering kinetics”, *Adv. Phys.,* vol. 43, p. 357, 1994.

[475] A. D. Rutenberg and A. J. Bray, “Energy-scaling approach to phase-ordering growth laws”, *Phys. Rev. E,* vol. 51, p. 5499, 1995.

[476] G. A. Baker Jr. and J. W. Essam, “Effects of lattice compressibility on critical behavior”, *Phys. Rev. Lett.,* vol. 24, pp. 447-449, 1970.

[477] B. B. Machta, R. Chachra, M. K. Transtrum and J. P. Sethna, “Parameter space compression underlies emergent theories and predictive models”, *Science,* vol. 342, pp. 604-607, 2013.

[478] E. N. M. Cirillo, G. Gonnella and G. P. Saracco, “Monte Carlo results for the Ising model with shear”, *Phys. Rev. E,* vol. 72, p. 026139, 2005.

[479] N. Metropolis, A. Rosenbluth, M. Rosenbluth, A. Teller and E. Teller, “Equation of state calculations by fast computing machines”, *J. Chem. Phys.,* vol. 21, pp. 1087-1092, 1953.

[480] K. Binder and A. P. Young, “Spin glasses: Experimental facts, theoretical concepts, and open questions”, *Rev. Mod. Phys.,* vol. 58, pp. 801-976, 1986.

[481] D. J. Huang, C. F. Chang, H.-. T. Jeng, G. Y. Guo, H.-. J. Lin, W. B. Wu, H. C. Ku, A. Fujimori, Y. Takahashi and C. T. Chen, “Spin and Orbital Magnetic Moments of Fe3O4”, *Phys. Rev. Lett.,* vol. 93, p. 077204, 2004.

[482] T. L. Gilbert, "A phenomenological theory of damping in ferromagnetic materials", IEEE Transactions of Magnetics, vol. 40, pp. 3443-3449, 2004

[483] D. Kirsanov, "The book of Inkscape", publisher: William Pollock, 2009

Appendix I: Additional information related to the self-induced global rotation of the rotating square system

A) Derivation of the analytical formula allowing to determine moment of inertia of the system of rotating squares rotating with respect to its centre of mass

In this work, the general expression for moment of inertia of the discussed system rotating with respect to its centre of mass was defined as follows:

$$I_1 = \frac{1}{12}a^2\left[\left(N_S{}^2-1\right)M_L+\left(N_S{}^2+1\right)M_H\right]+ \\ +\frac{1}{4}d^2\left(N_S{}^2-1\right)\left[\left(\frac{N_S{}^2}{3}-1\right)M_L+\left(\frac{N_S{}^2}{3}+1\right)M_H\right]. \qquad \text{A1-1}$$

The above expression was derived by means of the induction procedure during which process certain number of initial values of N_S was taken under consideration. In order to further explain the way how equation A1-1 was derived, the expression for I_1 is going to be calculated for a few values of N_S (see Fig. A1-1).

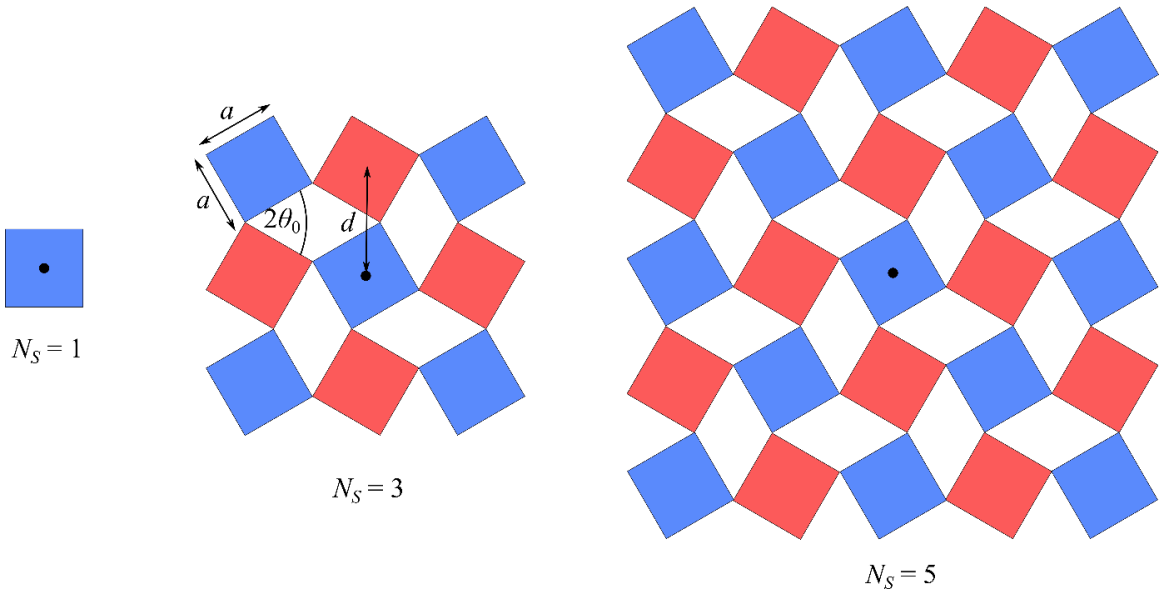

Figure A1-1 The system corresponding to $N_S = 1$, 3 and 5. The black point at the centre of the square is associated with the axis of rotation of the whole system.

Expression for I_1 calculated for the system corresponding to N_s=1

According to the assumption stated in the main text, the square corresponding to the centre of mass of the whole system is always associated with M_H. This means that the system corresponding to N_S=1 consists of only one square. Moreover, in this particular case, the axis of rotation of the whole system corresponds to the centre of the square (see Figure A1-1). In view of this, the moment of inertia I_1 can be written down as follows:

$$I_1 = \frac{1}{6} M_H a^2 \ . \qquad \text{A1-2}$$

At this point one may realise that upon substituting the variable N_S with 1 in equation A1-1 it is possible to obtain equation A1-2.

Expression for I_1 calculated for the system corresponding to N_s=3

Based on Figure A1-2, one can note that in the case of the system corresponding to $N_S = 3$, the moment of inertia associated with the centre square is the same as it was the case for the system in which $N_S = 1$. This means that in order to find the expression for I_1 it is sufficient to establish the contribution to its final value based on 8 remaining squares (highlighted part in Figure A1-2). This can be done by means of the parallel axes theorem in the following manner:

$$I_{1,N_s=3\ \text{contr}} = 4\left[\frac{1}{6} M_L a^2 + M_L d^2\right] + 4\left[\frac{1}{6} M_H a^2 + M_H \left(d\sqrt{2}\right)^2\right] . \qquad \text{A1-3}$$

This means that in the case of this system, the final expression for I_1 can be expressed in the following manner:

$$I_1 = \frac{1}{6} M_H a^2 + I_{1,N_s=3\ \text{contr}} = \frac{5}{6} M_H a^2 + \frac{2}{3} M_L a^2 + d^2\left(4M_L + 8M_H\right) . \qquad \text{A1-4}$$

At this point one may note that upon substituting the N_S variable in equation A1-1, the obtained expression is identical to equation A1-4.

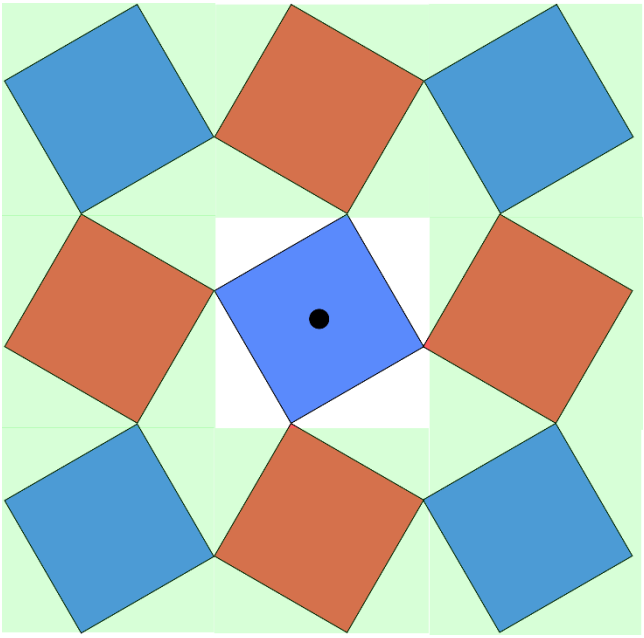

Figure A1-2 The system corresponding to $N_S = 3$. The highlighted part corresponds to the units which have not yet been considered in terms of their contribution to the final value of I_1.

Expression for I_1 calculated for the system corresponding to N_s=5

Analogically to the system corresponding to $N_S = 3$, in order to determine the expression for I_1 it is sufficient to calculate the moment of inertia associated with squares which were not present in the system corresponding to lower values of N_S. Such expression would assume the following form:

$$I_{1,N_s=5\ \text{contr}} = 4\left[\frac{1}{6}M_H a^2 + M_H\left(2d\right)^2\right] + 4\left[\frac{1}{6}M_H a^2 + M_H\left(2\sqrt{2}d\right)^2\right] + \\ +8\left[\frac{1}{6}M_L a^2 + M_L\left(d\sqrt{5}\right)^2\right]. \qquad \text{A1-5}$$

In view of this, the expression for I_1 can be expressed as shown in equation A1-6.

$$I_1 = \frac{1}{6} M_H a^2 + I_{1,N_s=3\ \text{contr}} + I_{1,N_s=5\ \text{contr}} = \frac{13}{6} M_H a^2 + \frac{12}{6} M_L a^2 + d^2 \left(44 M_L + 56 M_H\right) \qquad \text{A1-6}$$

After substituting the N_S variable with 5 in equation A1-6, it is easy to show that the obtained expression is identical to the one presented above.

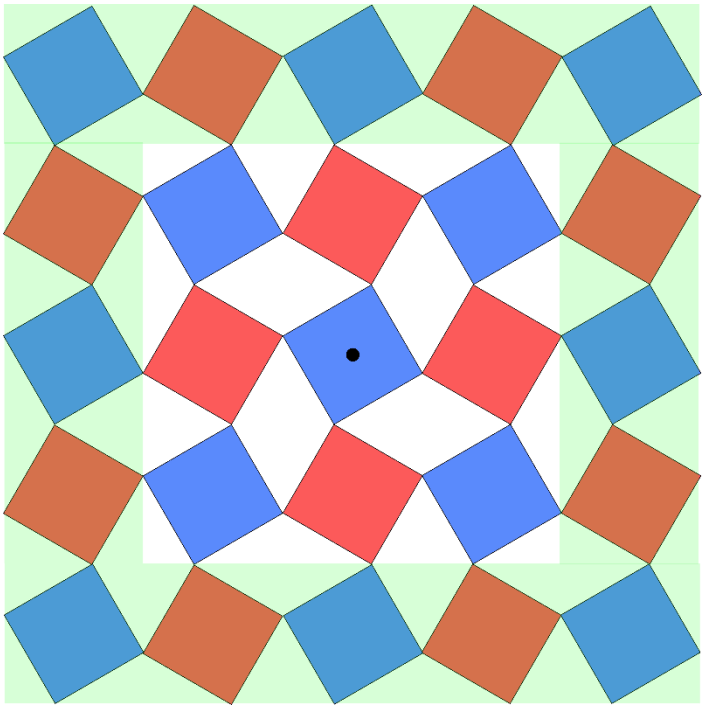

Figure A1-3 The system corresponding to $N_S = 3$. The highlighted part corresponds to the units which have not yet been considered in terms of their contribution to the final value of I_1.

Verification of the expression for I_1 for an arbitrary value of N_s

In order to show that the expression shown in equation A1-1 applies to an arbitrary value of N_S, the computer script was written in order to calculate the value of I_1 accordingly to the above procedure. The comparison of the results obtained by means of the script and analytical expression may be found in Figure A1-4. This graph was generated for an arbitrary set of parameters set to be: a = 5.16 m, M_L =1.2 kg, M_H = 3.4 kg and d = 4.17 m.

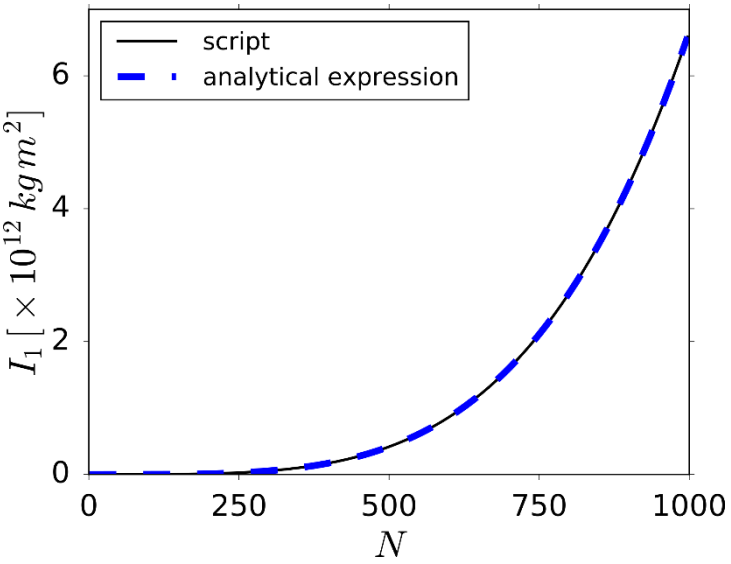

Figure A1-4 The system corresponding to $N_S = 3$. The highlighted part corresponds to the units which have not yet been considered in terms of their contribution to the final value of I_1.

Based on Figure A1-4, one may note that there is a perfect agreement between the values of I_1 generated by means of the analytical expression provided in the main text and the script.

B) Angular momentum associated with rigid units constituting the system

Before discussing a particular form of the angular momentum associated with rigid units constituting discussed systems, it is worth to write down a general expression for the angular momentum of the rigid body $\left(\vec{L}\right)$ moving with respect to an arbitrary point O. This can be done by means of the following formula:

$$\vec{L} = I\vec{\omega} + m\vec{r} \times \vec{\upsilon} \qquad \text{A1-7}$$

where, I and $\vec{\omega}$ stand for the moment of inertia and the angular velocity associated with the rotation of the rigid body with respect to its own centre of mass. The remaining quantities on the right hand side of the above equation represent the following: m is the mass, $\vec{r}$ stands for

the distance between point O and the centre of mass of the considered body and $\vec{\upsilon}$ represents the linear velocity measured with respect to the point O. Based on the above equation, one can easily note that the first term on the right hand side corresponds to the rotation of the body with respect to its own centre while the second term is associated with the translational motion. It should be highlighted that depending on the type of the exhibited motion, either first, second, both or none of these terms may assume the value of zero. At this point, one may also note that rigid unit systems considered in this thesis are a collection of rigid bodies where the angular momentum can be calculated separately for each of the units by means of the expression analogical to equation A1-7.

As discussed in this thesis, all of the considered systems are highly symmetric and due to their geometry the resultant angular momentum (calculated with respect to the centre of mass of the entire structure) associated with all of the units constituting the system does not depend on the linear velocity of respective units. This means that, upon denoting the respective quantities corresponding to one of the units within the system by means of the index *i*, the angular momentum $\vec{L}$ corresponding to the whole system may be rewritten from:

$$\vec{L} = \left(\sum_{i=1}^{\left(N_S^2+1\right)/2} I_H \vec{\omega}_0 + m_H \vec{r}_{H,i} \times \vec{\upsilon}_i \right) + \left(\sum_{j=1}^{\left(N_S^2-1\right)/2} I_L \left(-\vec{\omega}_0\right) + m_L \vec{r}_{L,j} \times \vec{\upsilon}_j \right) \qquad \text{A1-8}$$

to the following form:

$$\vec{L} = \left(\sum_{i=1}^{\left(N_S^2+1\right)/2} I_H \vec{\omega}_0 \right) + \left(\sum_{j=1}^{\left(N_S^2-1\right)/2} I_L \left(-\vec{\omega}_0\right) \right) \qquad \text{A1-9}$$

where, $\vec{r}_{H,i}$ and $\vec{r}_{L,j}$ correspond to the distance of centres of the respective heavy and light units from the centre of mass of the entire structure. Analogically, $\vec{\upsilon}_i$ and $\vec{\upsilon}_j$ stand for linear velocities associated with these units. One should note that the negative sign in front of $\vec{\omega}_0$ in the second

term of the above equation stems from the fact that one group of rigid units rotates in the clockwise direction while all of the remaining units rotate in the anticlockwise direction.

Appendix II: Solving differential equations by means of the fourth-order Runge-Kutta algorithm

In this thesis, there are a few chapters where it is necessary to solve a differential equation in order to describe the motion of the investigated system. In the literature, there are numerous algorithms which depending on the particular problem allow to estimate the exact solution of a differential equation with a varying accuracy. In the case of this thesis, a particular algorithm, i.e. the fourth-order Runge-Kutta method was selected in order to solve all of the differential equations (which could not be solved exactly) as it is normally considered as a stable method providing reliable results for a variety of different physical problems. However, it should be noted that due to a relative simplicity of considered problems and small time steps Δt, one could consider the use of lower order techniques which would also allow to correctly estimate the behaviour of investigated systems.

Before applying the Runge-Kutta method to a particular physical problem it is necessary to express equations of motion corresponding to a given system in terms of the velocity υ and acceleration *a*. It is also necessary to define initial parameters describing the system, i.e. $x_0\left(x_0 = x\left(t=0\right)\right)$ and $\upsilon_0\left(\upsilon_0 = \upsilon\left(t=0\right)\right)$, where *x* stands for the position of the system at a time *t*. In general, upon providing such information, the set of equations of motion corresponding to an arbitrary physical system could be solved by means of the fourth-order Runge-Kutta method in the following manner:

$$
\begin{aligned}
k_1 &= \Delta t a\left(x_n, \upsilon_n, t_n\right) & l_1 &= \Delta t \upsilon_n \\
k_2 &= \Delta t a\left(x_n + \frac{l_1}{2}, \upsilon_n + \frac{k_1}{2}, t_{n+1/2}\right) & l_2 &= \Delta t\left(\upsilon_n + \frac{k_1}{2}\right) \\
k_3 &= \Delta t a\left(x_n + \frac{l_2}{2}, \upsilon_n + \frac{k_2}{2}, t_{n+1/2}\right) & l_3 &= \Delta t\left(\upsilon_n + \frac{k_2}{2}\right) \\
k_4 &= \Delta t a\left(x_n + l_3, \upsilon_n + k_3, t_{n+1}\right) & l_4 &= \Delta t\left(\upsilon_n + k_3\right) \\
\upsilon_{n+1} &= y_n + \frac{1}{6}\left(k_1 + 2k_2 + 2k_3 + k_4\right) \\
x_{n+1} &= x_n + \frac{1}{6}\left(l_1 + 2l_2 + 2l_3 + l_4\right)
\end{aligned}
\qquad \text{A2-1}
$$

where, t_n, x_n and υ_n stand for time, position and velocity of a system at the *n*-th time step respectively.

Some examples of systems which in the case of this thesis were investigated from the point of view of their dynamic behaviour could be the rotating squares system and rotating rectangle systems. In both of those cases, the potential to induce a global rotational motion as a result of the rotation of their subunits was investigated which effect originates from the principle of the conservation of angular momentum. This means that in the case of the system which was initially at rest, one should expect that the net angular momentum would be always equal to zero irrespective of the stage of deformation. In order for that to happen, the resultant angular momentum associated with the motion of respective units would have to be equal to the angular momentum associated with the global rotation in terms of magnitude and have an opposite orientation. As the matter of fact, in order to verify whether the differential equations of motion describing the behaviour of the system are solved correctly, one could check whether the aforementioned conservation law is satisfied throughout the simulation. An example of such validation procedure is presented below for a particular example of the Type I rotating rectangles system with all of the parameters being the same as in the case of Chapter 6.

Based on equation A2-1, one may note that before applying the fourth-order Runge-Kutta method to a particular system, it is necessary to rewrite Newton's equations of motion in a

manner allowing to express them in terms of the acceleration and velocity. In the particular case of the Type I rotating rectangles system inducing its own global rotational motion, in order to describe the global rotation of the system, these quantities may be expressed as follows:

$$\omega_1 = \frac{d\theta_1}{dt} \qquad \varepsilon_1 = \frac{d^2\theta_1}{dt^2} = -\left(\frac{\tau_0 + \frac{dI_1}{dt}}{I_1} \right). \tag{A2-2}$$

It should be noted that all of the quantities used in the above equation were already defined in Chapter 4 and Chapter 6 of the thesis. It is also important to remember that in the case of this particular study, equations describing the movement of individual units constituting the system were solved exactly, hence only equations corresponding to the global rotation had to be solved numerically.

Based on Figure A2-1, one can clearly note that the angular momenta corresponding to the individual units composing the system and the entire system almost exactly cancel each other out which results in the system having the same net angular momentum at all times. This result confirms that the principle of the conservation of angular momentum is satisfied and proves the suitability of the considered numerical method to describe the motion of systems discussed in this thesis.

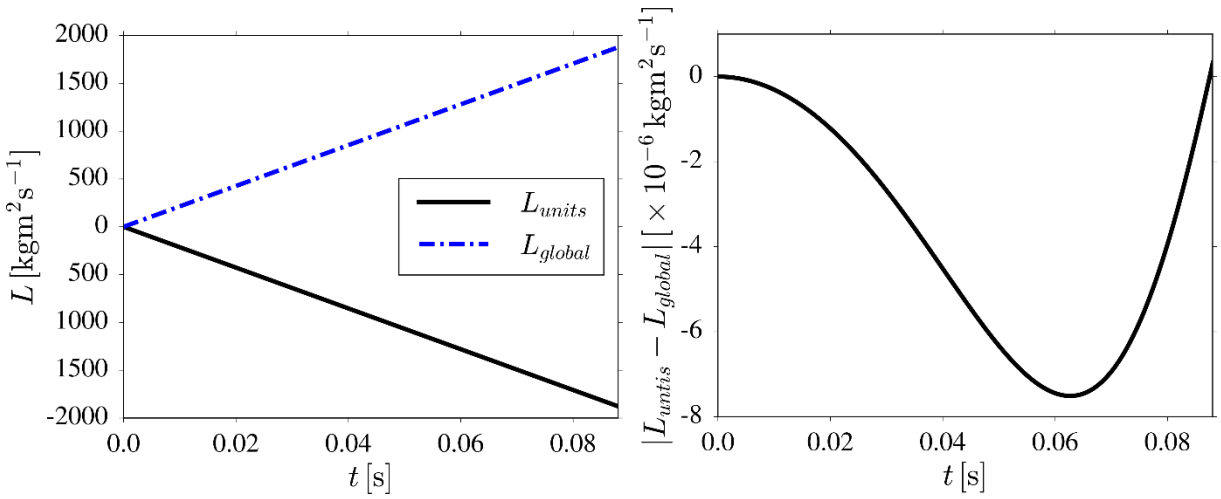

Figure A2-1 Panels show the variation in the magnitude of angular momenta associated with the rotation of individual units constituting the system and the global rotation of the system.

Appendix III: Additional results corresponding to the deformation of the hierarchical mechanical metamaterial system composed of rigid squares

A) Expressions for L_x and L_y

The geometry of a two-level hierarchical rotating square system may be described by the aperture between the Level 0 squares $\left(2\theta_0\right)$, the aperture between the Level 1 square-like units $\left(2\theta_1\right)$ and the number of Level 0 repeat units $\left(N_0\right)$. This means that the Level 1 building block is made up of $N_0 \times N_0$ Level 0 repeat units which corresponds to $2N_0 \times 2N_0$ squares. These parameters may be used to define the linear dimensions of the Level 1 square-like units, u_1 and υ_1, as follows: $u_1 = 2N_0 l\cos\left(\theta_0\right) + 2\left(N_0 - 1\right)l\sin\left(\theta_0\right)$ and $\upsilon_1 = 2N_0 l\left(\cos\left(\theta_0\right) + \sin\left(\theta_0\right)\right)$, where *l* stands for the length of the sides of the Level 0 squares. These dimensions can in turn be used to define the overall on-axis dimensions of the system:

$$L_x = 2\left(u_1\cos\left(\theta_1\right) + \upsilon_1\sin\left(\theta_1\right)\right) \qquad \text{A3-1}$$

$$L_y = 2\left(\upsilon_1\cos\left(\theta_1\right) + u_1\sin\left(\theta_1\right)\right) \qquad \text{A3-2}$$

B) Calculation of the moment of inertia corresponding to Level 0 and Level 1 of the system

The moment of inertia I_0 associated with Level 0 of the structure can be considered as the sum of moments of inertia of all of the Level 0 squares rotating with respect to their centres. Assuming that the rotating rigid units are made of a material having a surface density ρ, the moment of inertia of a single square can be expressed as $I_{sq} = \frac{1}{6}\rho l^4$. In such a case, I_0 can be calculated by means of the following expression: $I_0 = 16N_0^2 I_{sq}$.

The moment of inertia I_1, can be defined as four times the moment of inertia corresponding to the Level 1 building block $\left(I_{1,BB}\right)$ rotating with respect to its centre of mass (there are 4 Level 1 building blocks). The moment of inertia $I_{1,BB}$ depends on the contribution from each of the Level 0 squares, constituting the Level 1 building block and the distance from the centre of mass of the Level 1 building block to the centre of the particular square within the considered Level 1 unit d_m. Thus, I_1 can be expressed as follows:

$$I_1 = 4I_{1,BB} = 4\left(\sum_m^{4N^2} I_{sq} + \rho l^2 d_m^2\right). \qquad \text{A3-3}$$

C) Dependence of values of angles defining the considered system on strain

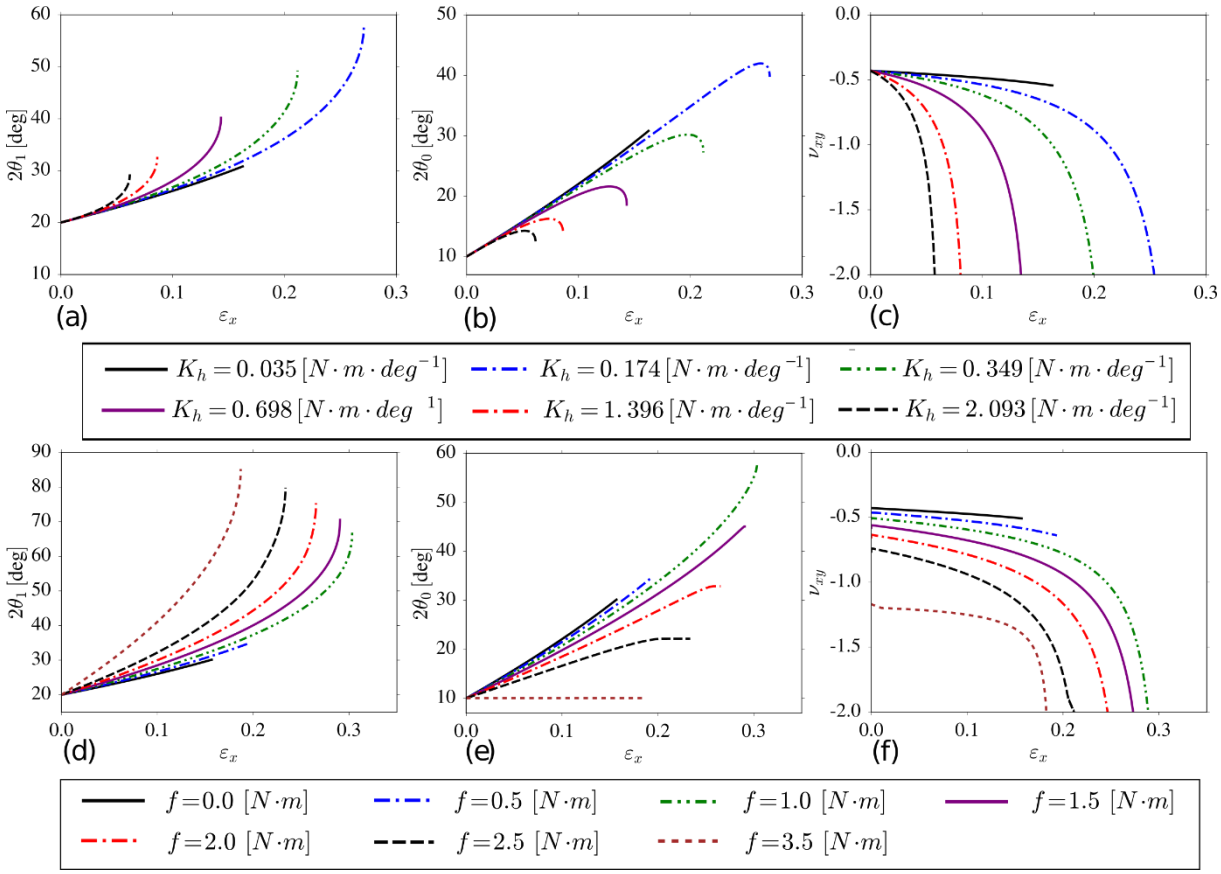

Figure A3-1 Behaviour of the system plotted with respect to strain (ε_x). Panels (a)-(c) correspond to the results where the resistance to the rotational motion of hinges was governed by the harmonic potential while panels (d)-(f) correspond to friction-based hinges. All of these results were generated for the analogical parameters as it was the case in Chapter 7.

D) The effect of the variation in the magnitude of the applied force in time on the behaviour of the system

The effect of a non-constant force on the deformation of the considered hierarchical system was also investigated. This was done by changing the magnitude of the force $\vec{F}$ as shown in Figure A3-2(a-e) and Figure A3-3 (a-e). These results indicate that although there are similar trends to the results obtained for the system subjected to the constant force $\left(\left|\vec{F}\right| = 500 \text{ N}\right)$, in this case, Level 0 opens to a greater extent for the same coefficients corresponding to the resistance to the rotational motion (See Figure A3-2). This stems from the fact that in this case, the initial force is very large and thus, the ratio of the torque generated by the applied force and the resistance torque is significantly greater than was the case for a constant force. This also indicates that in the case of the considered hierarchical system, one may apply a force to its vertices which changes in magnitude in time in order to gain an additional way of controlling the behaviour of the system.

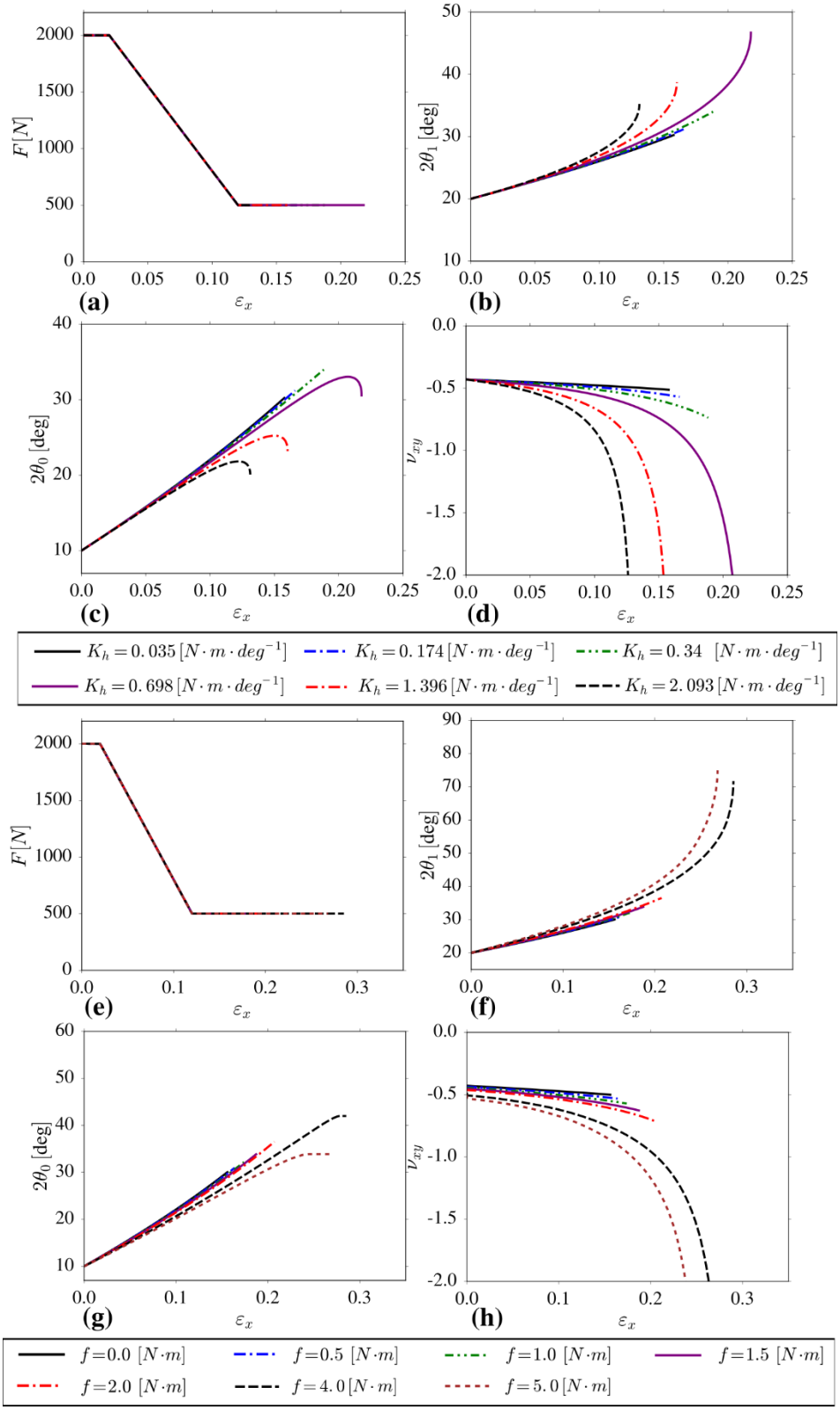

Figure A3-2 Deformation of the system (expressed in terms of the change in strain) subjected to the force *F* having its magnitude gradually changed from 2000N to 500N (which value was considered in Chapter 7). Panels (a)-(d) correspond to the system with hinges having their rotational motion governed by the harmonic potential while panels (e)-(h) correspond to friction-based hinges.

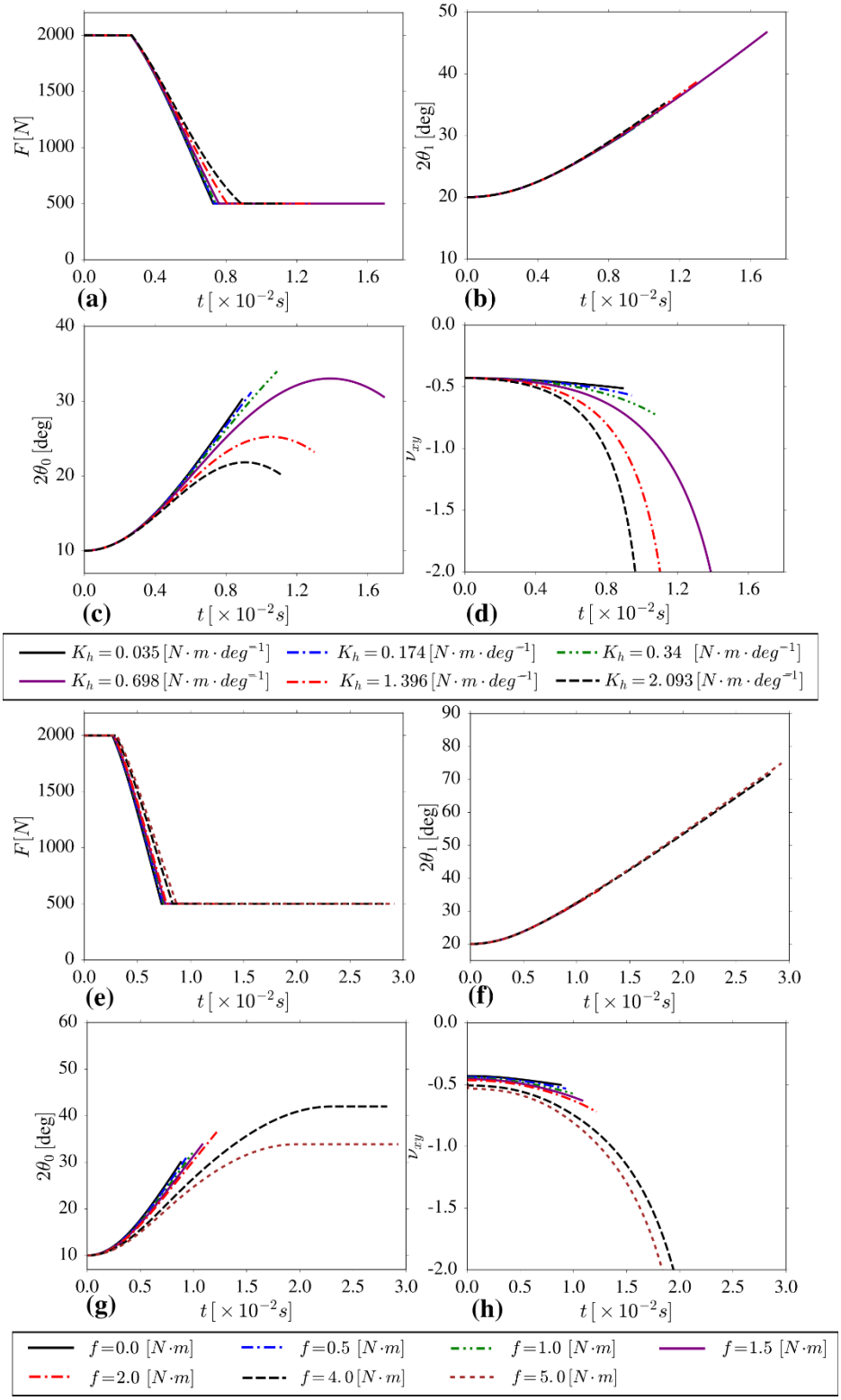

Figure A3-3 Deformation of the system (expressed in terms of the change in time) subjected to the force *F* having its magnitude gradually changed from 2000N to 500N (which value was considered in Chapter 7). Panels (a)-(d) correspond to the system with hinges having their rotational motion governed by the harmonic potential while panels (e)-(h) correspond to friction-based hinges.

E) Dependence of strain on time for all of the considered types of hinges

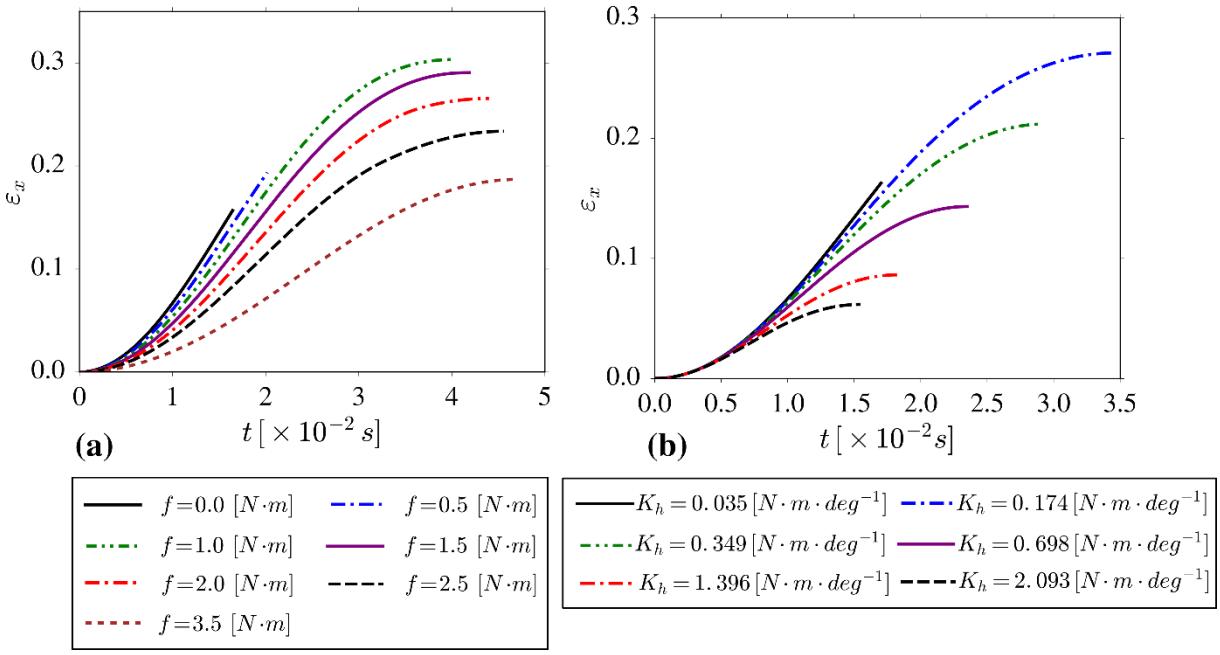

Figure A3-4 Dependence of the value of the strain on time for the considered types of hinges. Results shown in panel (a) correspond to hinges in which the resistance to the rotational motion is governed by friction whereas the results shown in panel (b) are associated with the harmonic potential.

F) Different loading directions

In Chapter 7, only loading in the *x*-direction (see Figure A3-5(a)) was discussed. This stems from the fact that for this type of connectivity, upon subjecting the structure to the uniaxial tensile load, both levels can open simultaneously. On the other hand, for loading in the *y*-direction, Level 0 squares tend to close when subjected to the same tensile load, while at the same time, Level 1 building blocks rotate in a way promoting the expansion of the structure in the loading direction. This effect can be explained based on the orientation of vectors $\vec{r}_i$ and $\vec{F}$.

Based on Figure A3-5(a), one can note that in the case of the vast majority of permissible values of θ_0 and θ_1, the torque corresponding to Level 1 building block and Level 0 squares to which the force is applied, has the same orientation. Based on the right hand rule, it is easy to

note that in both cases a clockwise rotation will occur. This in turn leads to the opening of both levels upon the application of the tensile load. In the case of connectivity II (see Figure A3-5(b)), in the majority of cases, the right hand rule implies that Level 0 and Level 1 building blocks will close and open respectively.

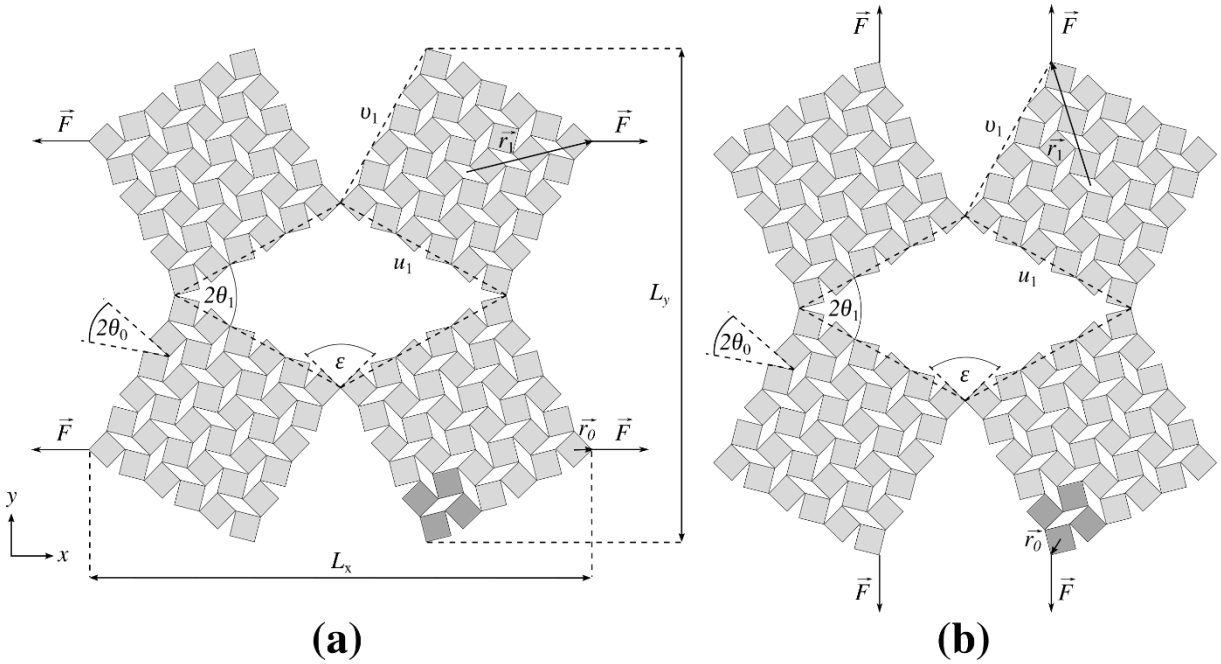

Figure A3-5 The system considered in this study for loading (a) in the *x*-direction and (b) in the *y*-direction.

In Figure A3-6, one may also note results associated with the considered system subjected to the loading in the *y* direction.

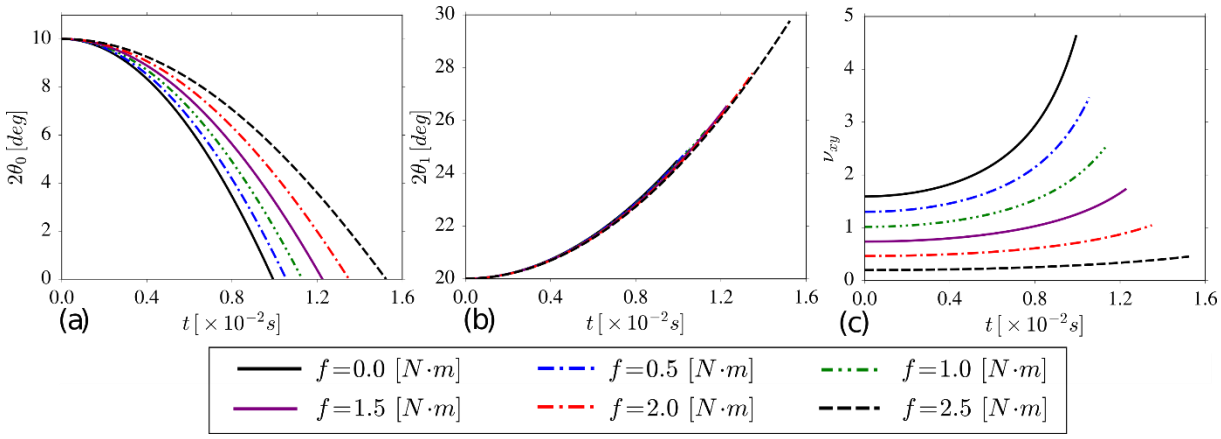

Figure A3-6 Plots show a variation in (a) θ_0, (b) θ_1 and (c) Poisson's ratio ν_{xy} as a function of time measured in the loading direction for systems corresponding to type II connectivity with *f* values ranging between 0.5 Nm and 2.5 Nm. Graphs shown here were generated for initial angles $2\theta_0$ and $2\theta_1$ set to be equal to $10°$ and $20°$ respectively.

Appendix IV: Details corresponding to the analysis of mechanical properties of unimode mechanical metamaterials composed of generic rigid triangles

A) Analytical transformation of the expression representing the unit-cell of the system required to determine the thermal expansion coefficient

The area of the unit-cell of the structure analysed in Chapter 8 from the point of view of its propensity to exhibit negative thermal expansion was expressed as follows:

$$A(\theta) = X_1 \cdot X_2 = b\left[a\cos\left(\frac{\theta}{2}\right)\sin\left(\gamma+\frac{\theta}{2}\right) - b\cos\left(\gamma+\frac{\theta}{2}\right)\sin\left(\gamma+\frac{\theta}{2}\right)\right] . \qquad \text{A4-1}$$

In this chapter, it was also mentioned that based on the assumption that vibrations of adjacent rigid units constituting the system are symmetric with respect to the equilibrium configuration associated with the angle $\theta_0 = \frac{\pi}{2}$ (which implies that $A(\theta_0+\Delta\theta) = A(\theta_0-\Delta\theta)$), it is possible to rewrite equation A4-1 in the form of equation A4-2, however the steps required to obtain the aforementioned expression were not provided.

$$A\left(\frac{\pi}{2}+\Delta\theta\right) = b\left[\frac{a}{2}\sin\left(\gamma+\frac{\pi}{2}+\Delta\theta\right)+\frac{a}{2}\sin\gamma-\frac{b}{2}\sin\left(2\gamma+\frac{\pi}{2}+\Delta\theta\right)\right] \qquad \text{A4-2}$$

Upon substituting $A(\theta_0+\Delta\theta) = A(\theta_0-\Delta\theta)$ and $\theta_0 = \frac{\pi}{2}$ into equation A4-1, it is possible to rewrite it as follows:

$$A(\theta_0+\Delta\theta)=ba\cos\left(\frac{\theta_0+\Delta\theta}{2}\right)\sin\left(\gamma+\frac{\theta_0+\Delta\theta}{2}\right) \\ -b^2\cos\left(\gamma+\frac{\theta_0+\Delta\theta}{2}\right)\sin\left(\gamma+\frac{\theta_0+\Delta\theta}{2}\right) \qquad \text{A4-3}$$

As shown in equation A4-4, the above expression can be divided into two parts denoted as term1 and term2 in order to consider them separately.

$$A\left(\frac{\pi}{2}+\Delta\theta\right)=b\left[\text{term1}-\text{term2}\right] \qquad \text{A4-4}$$

Expression denoted by term1 may be subsequently rearranged by means of the following trigonometric identity $\sin(x+y)=\sin x\cos y+\cos x\sin y$:

$$\text{term1}=a\cos\left(\frac{1}{2}\left(\frac{\pi}{2}+\Delta\theta\right)\right)\left[\sin\gamma\cos\left(\frac{1}{2}\left(\frac{\pi}{2}+\Delta\theta\right)\right)+\cos\gamma\sin\left(\frac{1}{2}\left(\frac{\pi}{2}+\Delta\theta\right)\right)\right] \qquad \text{A4-5}$$

$$\text{term1}=a\sin\gamma\cos^2\left(\frac{1}{2}\left(\frac{\pi}{2}+\Delta\theta\right)\right)+a\cos\gamma\cos\left(\frac{1}{2}\left(\frac{\pi}{2}+\Delta\theta\right)\right)\sin\left(\frac{1}{2}\left(\frac{\pi}{2}+\Delta\theta\right)\right). \qquad \text{A4-6}$$

Equation A4-6 can be further subdivided into terms term1a and term1b which leads to the following:

$$\text{term1}=\text{term1a}+\text{term1b}. \qquad \text{A4-7}$$

At this point one can use the following identity: $\cos^2\frac{x}{2}=\frac{1+\cos x}{2}$ to rewrite term1a into the following expression:

$$\text{term1a}=a\sin\gamma\left(\frac{1+\cos\left(\frac{\pi}{2}+\Delta\theta\right)}{2}\right). \qquad \text{A4-8}$$

It is also possible to rewrite term1b by means of the following identity

$\frac{1}{2}\sin(2x)=\sin x\cos x$ in order to express it as follows:

$$\text{term1b} = \frac{a}{2}\cos\gamma \sin\left(\frac{\pi}{2} + \Delta\theta\right) . \qquad \text{A4-9}$$

In view of this, term1 can be written down in terms of new expressions associated with term1a and term1b in the following manner:

$$\text{term1} = \frac{1}{2}a\sin\gamma + \frac{1}{2}a\left[\sin\gamma\cos\left(\frac{\pi}{2} + \Delta\theta\right) + \cos\gamma\sin\left(\frac{\pi}{2} + \Delta\theta\right)\right] . \qquad \text{A4-10}$$

As the result of the above transformations, and while remembering that $\text{term2} = \frac{b}{2}\sin\left(2\gamma + \frac{\pi}{2} + \Delta\theta\right)$, it is possible to obtain the desired form of the expression (equation A4-2) representing the area of the investigated unit-cell.

B) Transformations of systems composed of different types of triangles which were analysed in order to investigate their mechanical properties

As discussed in Chapter 8, three different types of triangles (i.e. equilateral, isosceles and scalene triangles) were selected in order to analyse mechanical properties of systems composed of such units. It was also discussed that in order for these systems to undergo a transformation at the whole range of θ between $0°$ and $360°$ such systems would have to undergo six transitions in their connectivity. In order to better visualise this concept, a diagram was prepared were the deformation of the systems considered in this work is presented.

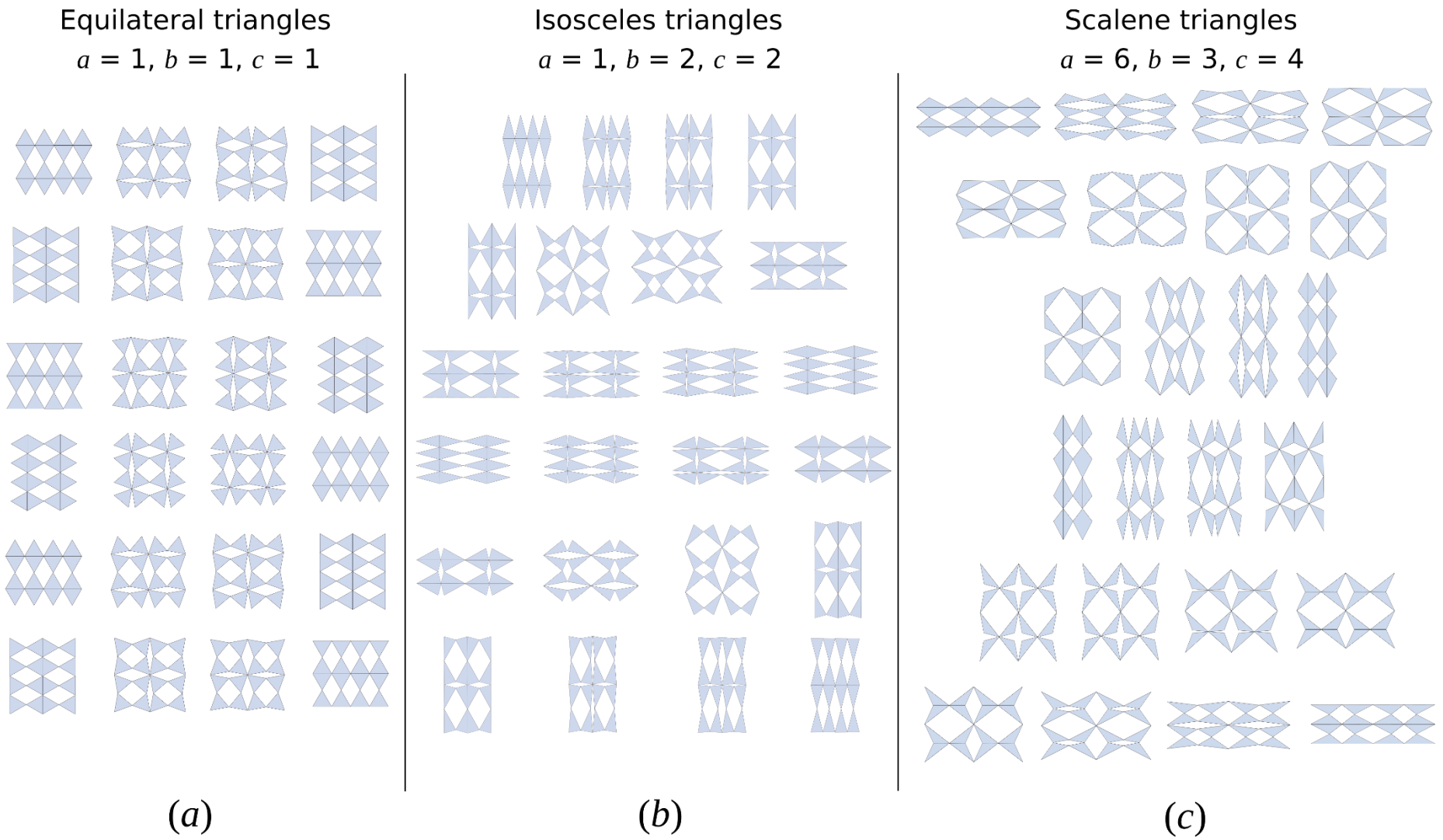

Figure A4-1 Transformation of different systems at the range of θ between $0°$ and $360°$. Each row corresponds to a different form of a given structure. Panels show examples of systems composed of: (a) equilateral, (b) isosceles and (c) scalene triangles.

C) Derivation of the relationship between the value of the Poisson's ratio and linear compressibility in a given direction

As discussed in Chapter 8, upon analysing the results generated for the considered systems, it was observed that whenever the value of the Poisson's ratio in a specific direction was exceeding the value of 1, then the system was also exhibiting negative linear compressibility in the same direction. This interesting observation can be confirmed analytically as shown below.

As written in Chapter 8, some of the general expressions describing mechanical properties of the discussed class of mechanical metamaterials can be defined as follows:

$$\nu_{12} = -\frac{1}{\nu_{21}} = -\frac{\varepsilon_2}{\varepsilon_1} \qquad E_i = \frac{K_h X_i^2}{X_1 X_2 z}\left(\frac{dX}{d\theta}\right)^{-2} \qquad \beta_{\mathrm{L}}\left[Ox_2\right] = \frac{1}{E_2} - \frac{\nu_{12}}{E_1}\ . \tag{A4-11}$$

Based on these expressions one can show that in order for a linear compressibility in a given direction to assume negative values (for example in the Ox_2 direction), the condition which can be obtained as the result of the following operations must be satisfied:

$$\beta_L\left[Ox_2\right] = \frac{1}{E_2} - \frac{\nu_{12}}{E_1} < 0 \Rightarrow \frac{1}{E_2} < \frac{\nu_{12}}{E_1} \Rightarrow 1 < \frac{E_2}{E_1}\nu_{12} \Rightarrow 1 < \frac{X_2^2}{\left(\frac{dX_2}{d\theta}\right)^2} \Big/ \frac{X_1^2}{\left(\frac{dX_1}{d\theta}\right)^2}\nu_{12} \tag{A4-12}$$

$$1 < \frac{X_2^2}{\left(\frac{dX_2}{d\theta}\right)^2} \Big/ \frac{X_1^2}{\left(\frac{dX_1}{d\theta}\right)^2}\nu_{12} \Rightarrow 1 < \frac{\varepsilon_1^2}{\varepsilon_2^2}\left(-\frac{\varepsilon_2}{\varepsilon_1}\right) \Rightarrow 1 < -\frac{\varepsilon_1}{\varepsilon_2} \Rightarrow 1 < \nu_{21}\ . \tag{A4-13}$$

Appendix V: Convergence test used in order to determine the size of the neighbourhood of the magnet in the considered magneto-mechanical system which is required to estimate its potential energy

As discussed in Chapter 9, in order to calculate the magnetic potential energy of a single magnet in the very large or infinite system, it is sufficient to consider the contribution made only by those of the magnets which are relatively close to the considered magnet for which the energy is being calculated. This stems from the fact that the magnitude of magnetic interactions between any two magnets decreases proportionally to their separation distance raised to the power of -3. In order to establish the size of such neighbourhood, one may conduct an appropriate convergence test as shown below.

Before conducting the convergence test, it is first necessary to define a particular nomenclature allowing to refer to a specific region within the system which consists of a certain number of magnets. One such approach is shown in Fig A5-1, where the auxiliary reference magnet for which the magnetic potential energy is being calculated is surrounded by a red dashed line. The highlighted background corresponds to the smallest possible neighbourhood considered in this chapter where magnets form a rectangle-like region composed of 3×3 magnets. In view of this, this type of neighbourhood will be referred to as $N_M = 3$. Should one consider extending this neighbourhood both in the horizontal and in the vertical direction by one "row of magnets", then the considered region would consist of 5×5 magnets and hence it would be referred to as $N_M = 5$.

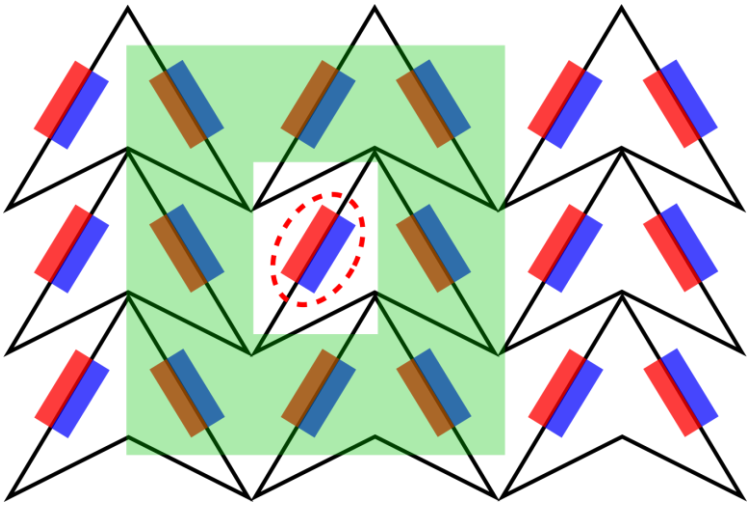

Figure A5-1 A fragment of the large / infinite system where the reference magnet for which the magnetic potential energy is calculated is encircled by means of the red dashed line. According to the proposed nomenclature, the highlighted background indicates the neighbourhood of the size $N_M \times N_M = 3 \times 3$.

In order to verify the sufficient size of the neighbourhood to calculate the energy of a given magnet, the energy U^{MAG} was calculated for different values of N_M. Based on Figure A5-2, one may clearly note that the neighbourhood composed of 7×7 magnets already gives a good estimation of the real value of the energy. However, in order to make the results even more reliable, in the case of all of results presented in Chapter 9, N_M was set to be equal to 15.

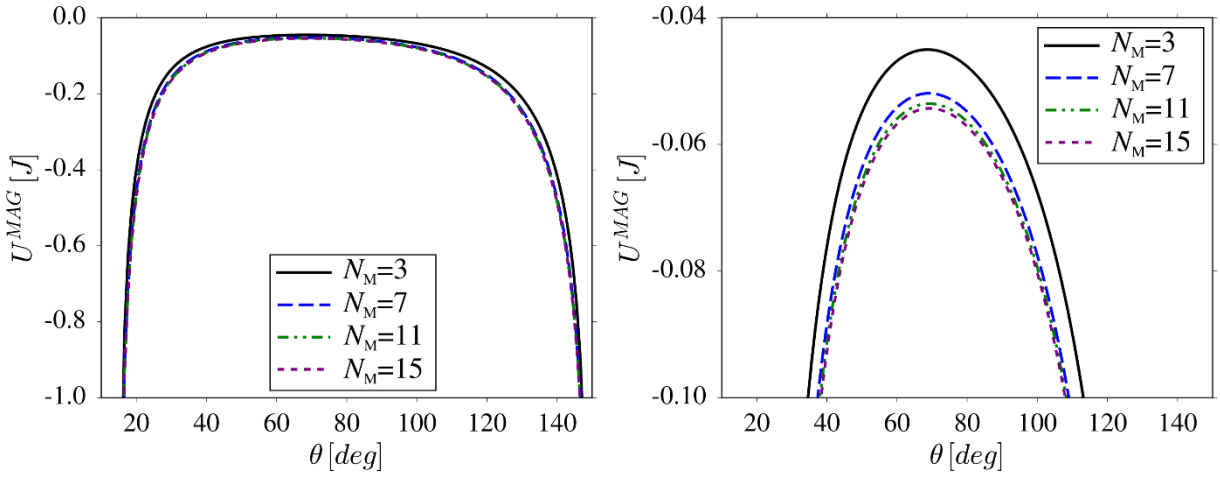

Figure A5-2 The results of the convergence test showing the magnetic potential energy of the system throughout the deformation process for the neighbourhood if a single magnet corresponding to different values of N_M.

Appendix VI: Details corresponding to the calculation of the extent of the magnetocaloric effect for the considered magneto-mechanical system

A) Change in entropy in the magneto-mechanical auxetic system

The extent of the magnetocaloric effect in the isothermal process corresponds to the change in the reduced magnetic entropy of the system (Δs_M). In order to calculate this quantity in the case of the system undergoing the transition from the configuration associated with a particular value of θ_i to the conformation corresponding to θ_f, it is first necessary to determine the reduced magnetic entropy s_M of these systems at certain temperature *T*. In order to do that, one must calculate reduced internal energy *u* and reduced Helmholtz free energy *f* associated with these configurations.

In Chapter 10, Ising spins defined on the matrix related to the particular mechanical metamaterial were defined on the square lattice at all times. The only geometric parameter which was changing as the system was undergoing the transition from configuration corresponding to one value of θ to another was the distance between Ising spins. In view of this, the reduced entropy s for the magneto-mechanical system discussed in Chapter 10, can be determined by means of the famous Onsager solution corresponding to the square lattice. According to this solution, both the reduced Helmholtz free energy and reduced internal energy can be expressed by means of the following expressions:

$$-f = \ln\left(2\cosh\left(2\frac{J}{k_B T}\right)\right) - \frac{1}{2\pi}\int_0^{\pi} d\varphi \ln\left(1+\sqrt{1-\kappa^2\sin^2\varphi}\right) \qquad \text{A6-1}$$

$$u = -2J \tanh\left(\frac{2J}{k_B T}\right) + \frac{d\kappa}{dT}\frac{2}{\pi}\int_0^{\pi/2} d\varphi \sqrt{1-\kappa^2 \sin^2\varphi} \qquad \text{A6-2}$$

where the parameter κ and its derivative with respect to the temperature *T* are defined as follows:

$$\kappa = 2\tanh\left(\frac{2J}{k_B T}\right)\cosh\left(\frac{2J}{k_B T}\right) \qquad \frac{d\kappa}{dT} = \frac{-J\left(\sinh^2\left(\frac{2J}{k_B T}\right)-1\right)}{\sinh\left(\frac{2J}{k_B T}\right)\cosh\left(\frac{2J}{k_B T}\right)} \; . \qquad \text{A6-3}$$

Upon substituting parameters provided in Chapter 10 into above equations, it is possible to calculate the reduced entropy *s* by means of equation A6-4.

$$s = -\left(f - \frac{u}{k_B T}\right) \qquad \text{A6-4}$$

Based on Figure A6-1, one can see that for a given temperature *T*, different systems correspond to very different values of the reduced entropy. The only exception are systems where $\theta = 0°$ and $\theta = 90°$, where as the result of the particular geometry of the considered system, the distance between Ising spins is exactly the same. It may also be noted that despite significant difference in the value of *s* associated with different system at a given temperature, the extent of the change in *s* for the entire range of temperature is approximately the same. It is also worth to highlight the fact that the maximum value of *s* assumed by each of the system does not exceed the value of $\ln(2)$ which condition must be satisfied for the Ising model.

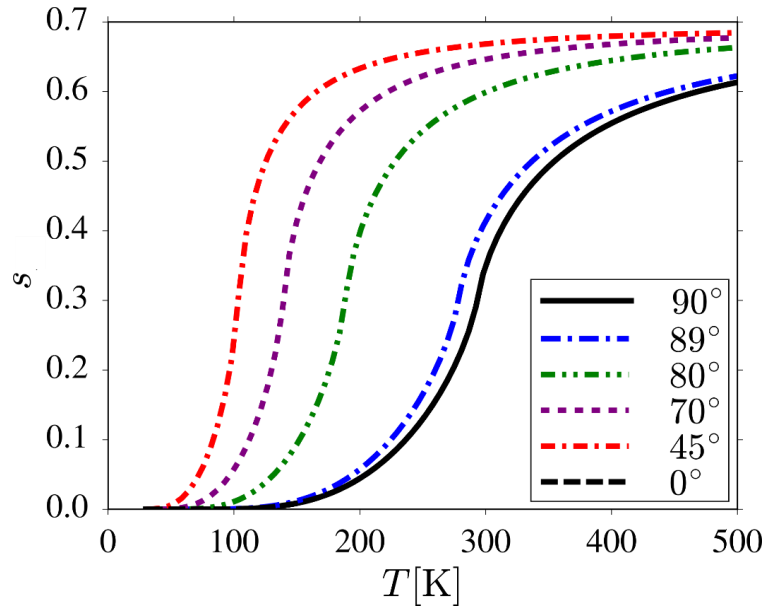

Figure A6-1 The variation of the reduced entropy in temperature for systems corresponding to different values of θ.

In order to determine the change in the magnetic entropy corresponding to the transition of the system from the configuration associated with the angle θ_i to the configuration associated with the angle θ_f, it is sufficient to subtract values corresponding to arbitrary two graphs from Figure A6-1. As the result of such subtraction, one can obtain results presented in Figure A6-2.

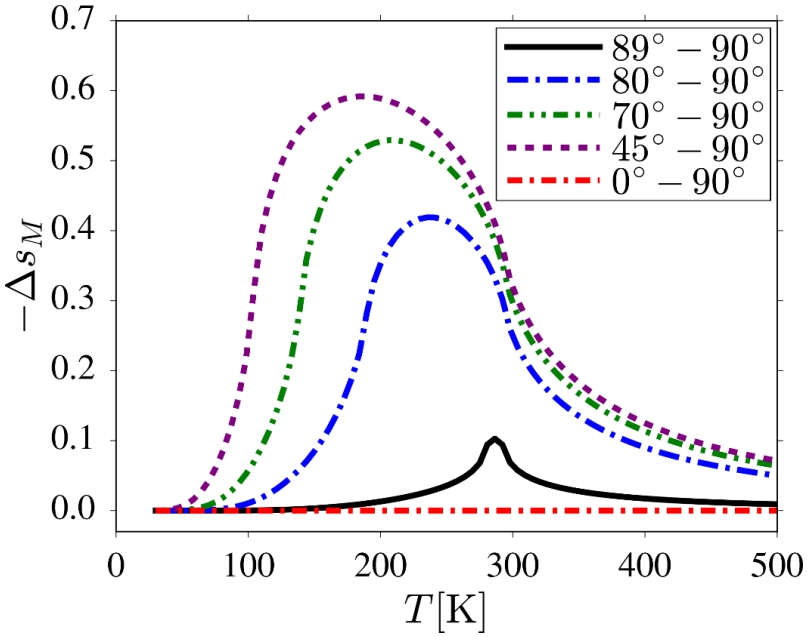

Figure A6-2 The variation of the reduced magnetic entropy in temperature for systems corresponding to different values of θ.

B) The extent of the magnetocaloric effect for the hypothetical experimental realisation of the considered theoretical model

As discussed in Chapter 10, the considered magneto-mechanical system was represented by means of the Ising model solely due to the fact that such approach made it possible to obtain exact results corresponding to the magnetic entropy of the system. Nonetheless, this does not mean that one cannot consider the use of actual magnetic nanoparticles to represent magnetic inclusions within the system. As the matter of fact, as discussed in Chapter 10, the extent of the magnetocaloric effect for the discussed hypothetical magneto-mechanical system can be better visualised upon considering the scenario where the Ising spins within the system would be replaced with magnetite nanoparticles $\left(Fe_3O_4\right)$. In this chapter, it was also mentioned that even very small magnetic Fe_3O_4 nanoparticles with a diameter of 5 nm (radius R=2.5 nm) can be sufficient for ordering processes at room temperature. However, in order to estimate the extent of the magnetocaloric effect for such a system, it is first necessary to determine the magnetic moment associated with each of the nanoparticles which can be achieved based on information regarding the considered compound as shown below.

A single unit cell of the magnetite (Fe_3O_4 which can be represented by formula $Fe^{2+}Fe^{3+}O_4^-$) consists of 32 Oxygen atoms which based on the chemical formula of this compound means that there are eight formula units (f. u.) per unit cell. The linear dimension of such unit cell a is equal to 8.397 Å which means that the volume of the entire unit cell V_u $\left(V_u = a^3\right)$ is approximately equal to 592.07 Å. Furthermore, based on the volume of a single unit cell $\left(V_u\right)$ and the volume of an entire nanoparticle $\left(V\right)$, it is possible to find a number of unit cells in a nanoparticle $\left(N\right)$ in the following manner:

$$N = V / V_u = \frac{4}{3}\pi R^3 \frac{1}{V_u} \approx 110 \ . \qquad \text{A6-5}$$

As already discussed, in each of the nanoparticles there would be $8N$ magnetic moments, which according to the above equation is approximately equal to 880. Furthermore, as reported by Huang *et al.* [481], the magnetic moment per formula unit $\left(\mu_{\text{fu}}\right)$ is equal to $4.33\,\mu_{\text{B}}$. Thus, the magnetic moment corresponding to the considered nanoparticle $\left(\mu\right)$ can be expressed as $\mu = 8N\mu_{\text{fu}} \approx 3830\mu_{\text{B}}$.

Once when knowing the magnetic moment $\mu\ \left(\mu = |\vec{\mu}|\right)$ associated with each of the magnetite nanoparticles, it is possible to determine the magnetic interaction energy for two adjacent nanoparticles having a magnetic moment μ where the distance between their centres d is assumed to be equal to 5 nm (nanoparticles are touching each other). In general, the energy *E* of interaction between two magnetic moments can be described by means of the following expression:

$$E = \frac{\mu_0}{4\pi|\vec{r}|^3}\left[\vec{\mu}\cdot\vec{\mu} - \frac{3}{|\vec{r}|^2}\left(\vec{\mu}\cdot\vec{r}\right)\left(\vec{\mu}\cdot\vec{r}\right)\right] \qquad \text{A6-6}$$

where, $\mu_0\ \left(\mu_0 \approx 1.257\times10^{-6}\ \text{NA}^{-2}\right)$ stands for vacuum permeability and $\vec{r}$ is the position vector (in this case, $|\vec{r}| = d$). One should note that in the case of the Ising model, the adjacent magnetic moments are always either parallel or antiparallel which means that the above equation can be simplified to the following form:

$$E = \frac{\mu_0}{4\pi|\vec{r}|^3}\mu^2 \ . \qquad \text{A6-7}$$

It should be noted that upon substituting the above numbers into equation A6-7 and dividing both of its sides by the Boltzmann constant $k_{\text{B}}\ \left(k_{\text{B}} \approx 1.38\times10^{-23}\ \text{JK}^{-1}\right)$, the reduced energy E/k_{B} describing the interaction between two particles is approximately equal to

73.1 K. Based on the fact that in the case of the considered two-dimensional square lattice each of the nanoparticles interacts with four of its nearest neighbours, the energy E / k_{B} per nanoparticle can be estimated as 292.3 K. It may be noted that this value is very close to the room temperature which suggests that magnetic dipole-dipole interactions in the considered system can be sufficiently large at such temperature to induce the ordering process if the magnetic inclusions on the non-magnetic matrix are densely packed.

It should be noted that the magnitude of the magnetocaloric effect depends on the strength of interaction between magnetic inclusions. This in turn means that the results corresponding to the hypothetical theoretical system discussed in chapter 10 of the thesis should be expected to be observed in reality only if sufficiently strong magnetic interactions between magnetic inclusions within the system could be achieved. In view of this, the fact that in this appendix it is shown that very strong interaction can be observed in the vicinity of the room temperature for a particular experimental realisation of the considered model indicates that the considered concept may indeed prove to be useful in the case of real life applications.

Appendix VII: Python script used in order to calculate the entropy of the investigated system

```
#!/usr/bin/env python
from scipy.interpolate import interp1d
from scipy.integrate import quad

import numpy as np
import sys


if __name__ == '__main__':

    kB=8.617342e-5 #eV/K
    J=0.01116#eV
    a_latt=1.0
    teta= 90.0/180.0*np.pi
    dist=(2*a_latt*a_latt)**0.5*np.sin(teta+np.pi/4.0)

    J=J/dist**3


    Tstart=30.0# K
    Tstop=600.0# K
    nT=100.0
    dT=(Tstop-Tstart)/nT

    nphi=1000


    x = np.linspace(0.0,np.pi,nphi)
    y = np.linspace(0.0,np.pi,nphi)

    xx = np.linspace(0.0,np.pi/2,nphi)
    yy = np.linspace(0.0,np.pi/2,nphi)



    T=Tstart

    with open('entropy_theta90', 'w') as g:
        while T<=Tstop:
            kBT=kB*T

            wyraz0=-np.log(2*np.cosh(2*J/kBT))

            for i in range(nphi):
                a=np.float64(x[i])
                K=2*np.sinh(2*J/kBT)/(np.cosh(2*J/kBT)*np.cosh(2*J/kBT))
                K2=K*K
                wyraz=(1.0-K2*np.sin(a)*np.sin(a))

                y[i]=np.log((1.0+np.sqrt(wyraz))/2)


            f = interp1d(x, y)
            ans, err = quad(f, 0.0, np.pi)

            #free energy
            free_energy=wyraz0-ans/(2*np.pi)
```

```
            print free_energy, "free_energy"


            K=2*np.sinh(2*J/kBT)/(np.cosh(2*J/kBT)*np.cosh(2*J/kBT))
            K2=K*K
            dK=-J*(np.sinh(2*J/kBT)*np.sinh(2*J/kBT)-
1.0)/(np.sinh(2*J/kBT)*np.cosh(2*J/kBT))


            u0=-2*J*np.tanh(2*J/kBT)

            for i in range(nphi):
                a=np.float64(xx[i])
                delta=np.sqrt(1.0-K2*np.sin(a)*np.sin(a))

                yy[i]=1/(delta)


            f = interp1d(xx,yy)
            ans, err = quad(f, 0.0, np.pi/2)

            energy=u0+dK*(ans*2/np.pi-1.0)
            print energy, "U"

            entropy=-(free_energy-energy/kBT)

            g.write(str(T))
            g.write(" ")
            g.write(str(entropy))
            g.write('\n')

            print T", ",entropy
            T+=dT

```

Appendix VIII: Python script allowing to generate all of the results related to the magnetic domain evolution in magneto-auxetic system associated with the rotating squares system

```
import numpy as np
import random
import time


class Initial_high_T():
    def __init__(self, l, J0, T, beta, Nx, N, N_monte_initial, theta_0):
        self.l = l
        self.J0 = J0
        self.Nx = Nx
        self.N = N
        self.theta_0 = theta_0
        self.N_monte_initial = N_monte_initial
        self.beta = beta

        lattice = self.initial_assignment()
        self.algorithm_input(lattice)


    def initial_assignment(self):

        lattice = np.zeros((self.Nx, self.Nx))

        for i in range(self.Nx):
            for j in range(self.Nx):

                possibilities = [-1, 1]
                spin = random.choice(possibilities)

                lattice[i][j] = spin

        return lattice


    def algorithm_input(self, lattice):

        r = self.l * ((2**0.5) / 2.0)
        d = 2.0 * r * np.sin(np.pi / 4.0 + self.theta_0 / 2.0)

        self.J = self.J0 / (d**3)
        lattice_old = lattice

        for i in range(int(self.N_monte_initial)):
            lattice_new = self.algorithm(lattice_old)

            lattice_old = lattice_new

        self.lattice_final_high_T = lattice_new


    def algorithm(self, lattice):
```

```
55.
56.         for i in range(int(self.N)):
57.             x_i = random.randint(0, self.Nx - 1)     #The x coordinate of the i-
    th spin is selected randomly from the given interval.
58.             y_i = random.randint(0, self.Nx - 1)
59.
60.             boundary_cond = self.periodic_boundary_conditions(x_i, y_i)
61.
62.             xl = boundary_cond[0]
63.             xr = boundary_cond[1]
64.             yt = boundary_cond[2]
65.             yb = boundary_cond[3]
66.
67.             nn_sum = lattice[x_i][y_i] * ( lattice[x_i][yb] + lattice[xl][y_i] + lat
    tice[x_i][yt] + lattice[xr][y_i] )
68.
69.             E1 = -self.J * nn_sum
70.             E2 = self.J * nn_sum    #The energy calculated for considered spins base
    d on the fact that the i-th spin changed its orientation
71.
72.             dE = E2 - E1
73.
74.             if dE < 0:
75.                 lattice[x_i][y_i] = lattice[x_i][y_i] * (-1) #flipping a spin
76.
77.             else:
78.                 r = random.random()     #A random number from the interval [0; 1)
79.
80.                 Boltzman_factor = np.exp(-self.beta * dE)
81.
82.                 if r < Boltzman_factor:
83.                     lattice[x_i][y_i] = lattice[x_i][y_i] * (-1) #flip the spin
84.                 else:
85.                     None
86.
87.         return lattice
88.
89.
90.
91.     def periodic_boundary_conditions(self, x_i, y_i):
92.         yt = y_i + 1
93.         yb = y_i - 1
94.         xr = x_i + 1
95.         xl = x_i - 1
96.
97.         if xl == -1:
98.             xl = self.Nx - 1
99.
100.                if xr == self.Nx:
101.                    xr = 0
102.
103.                if yt == self.Nx:
104.                    yt = 0
105.
106.                if yb == -1:
107.                    yb = self.Nx -1
108.
109.                return xl, xr, yt, yb
110.
111.
112.
113.            def results(self):
114.                return self.lattice_final_high_T
115.
116.
117.
```

```
118.
119.
120.
121.
122.
123.       class Deformation():
124.           def __init__(self, theta_0, theta_f, delta_theta, J0, l, T, beta, Nx, N,
    N_monte, lattice_initial, speed_factor):
125.               self.theta_0 = theta_0
126.               self.theta_f = theta_f
127.               self.delta_theta = delta_theta
128.
129.               self.iterations(J0, l, T, beta, Nx, N, N_monte, lattice_initial, spee
    d_factor)
130.
131.
132.
133.           def iterations(self, J0, l, T, beta, Nx, N, N_monte, lattice_initial, spe
    ed_factor):
134.
135.               lattice_old = lattice_initial
136.               self.list_of_lattices = []
137.               self.list_of_angles = []
138.               self.list_of_time = []
139.
140.               counter_time = 0
141.
142.               for theta in np.arange(theta_0, theta_f, delta_theta):
143.                   print theta * (180.0 / np.pi), "theta"
144.                   constructor = Spins(lattice_old, l, J0, T, beta, Nx, N, N_monte,
    theta, theta_0, speed_factor)
145.                   lattice_new = constructor.results()
146.
147.                   self.list_of_lattices.append(lattice_new * 1.0)
148.                   self.list_of_angles.append(theta * 1.0)
149.                   self.list_of_time.append(N_monte * speed_factor * counter_time)
150.                   lattice_old = lattice_new
151.                   counter_time += 1
152.
153.
154.           def results(self):
155.               return self.list_of_angles, self.list_of_time, self.list_of_lattices

156.
157.
158.
159.
160.
161.
162.       class Spins():
163.           def __init__(self, lattice_theta, l, J0, T, beta, Nx, N, N_monte, theta,
    theta_0, speed_factor):
164.               self.J0 = J0
165.               self.beta = beta
166.               self.theta = theta
167.               self.Nx = Nx
168.               self.N = N
169.               self.l = l
170.               self.theta_0 = theta_0
171.               self.speed_factor = speed_factor
172.
173.               self.metropolis_process(lattice_theta, N_monte)
174.
175.
176.
177.           def metropolis_process(self, lattice_old, N_monte):
```

```
178.
179.                 r = self.l * ((2**0.5) / 2.0)
180.                 d = 2.0 * r * np.sin(np.pi / 4.0 + self.theta / 2.0)
181.
182.                 self.J = self.J0 / (d**3)
183.
184.                 for i in range(N_monte):
185.                     lattice_new = self.algorithm(lattice_old)
186.                     lattice_old = lattice_new
187.
188.                 self.final_lattice = lattice_new
189.
190.
191.
192.             def algorithm(self, lattice):
193.
194.                 for i in range(int(self.N * self.speed_factor)):
195.                     x_i = random.randint(0, self.Nx - 1)     #The x coordinate of the
    i-th spin is selected randomly fron the given interval.
196.                     y_i = random.randint(0, self.Nx - 1)
197.
198.                     boundary_cond = self.periodic_boundary_conditions(x_i, y_i)
199.
200.                     xl = boundary_cond[0]
201.                     xr = boundary_cond[1]
202.                     yt = boundary_cond[2]
203.                     yb = boundary_cond[3]
204.
205.                     nn_sum = lattice[x_i][y_i] * ( lattice[x_i][yb] + lattice[xl][y_i
    ] +
206.                                         lattice[x_i][yt] + lattice[xr][y_i] )
207.
208.                     E1 = -self.J * nn_sum
209.                     E2 = self.J * nn_sum    #The energy calculated for considered spi
    ns based on the fact that the i-th spin changed its orientation
    with respect to the former definition. The surrounding spins retain their orientatio
    n.
210.                     dE = E2 - E1
211.
212.                     if dE < 0:
213.                         lattice[x_i][y_i] = lattice[x_i][y_i] * (-1) #flip a spin
214.
215.                     else:
216.                         r = random.random() #A random number from the interval [0; 1)
217.
218.                         Boltzman_factor = np.exp(-self.beta * dE)
219.
220.                         if r < Boltzman_factor:
221.                             lattice[x_i][y_i] = lattice[x_i][y_i] * (1)#flip the spin
222.                         else:
223.                             None
224.
225.                 return lattice
226.
227.
228.
229.             def periodic_boundary_conditions(self, x_i, y_i):
230.                 yt = y_i + 1
231.                 yb = y_i - 1
232.                 xr = x_i + 1
233.                 xl = x_i - 1
234.
235.                 if xl == -1:
236.                     xl = self.Nx - 1
237.
238.                 if xr == self.Nx:
```

```
                    xr = 0

                if yt == self.Nx:
                    yt = 0

                if yb == -1:
                    yb = self.Nx -1

                return xl, xr, yt, yb


            def results(self):
                return self.final_lattice




        class Correlation_length():
            def __init__(self, list_of_lattices, Nx, N):
                self.list_of_lattices = list_of_lattices
                self.Nx = Nx
                self.N = N

                self.initial_procedure()


            def initial_procedure(self):

                self.list_corr_lengths = []

                for i in range(len(self.list_of_lattices)):
                    avg_corr_length = self.procedure(self.list_of_lattices[i])
                    self.list_corr_lengths.append(avg_corr_length)


            def procedure(self, lattice):

                corr_length_given_time_step = []

                for i in range(self.Nx):
                    for j in range(self.Nx):

                        counter_left = 0
                        counter_right = 0
                        counter_top = 0
                        counter_bottom = 0

                        validator_r = 0
                        validator_l = 0
                        validator_t = 0
                        validator_b = 0

                        while validator_r == 0:
                            index_right = j + counter_right
                            indices_right_element = self.periodic_boundary_conditions
    _right(index_right)
                            right_elem_x = indices_right_element

                            index_more_to_the_right = self.periodic_boundary_conditio
    ns_right(j + counter_right + 1)
                            more_to_the_right_x = index_more_to_the_right
```

```
303.
304.                             if lattice[right_elem_x][i] == lattice[more_to_the_right_
    x][i]:
305.                                 counter_right += 1
306.                             else:
307.                                 validator_r = 1
308.                             if counter_right >= self.Nx - 1:
309.                                 validator_r = 1
310.
311.                         while validator_l == 0:
312.                             index_left = j - counter_left
313.                             indices_left_element = self.periodic_boundary_conditions_
    left(index_left)
314.                             left_elem_x = indices_left_element
315.
316.                             if lattice[j - counter_left][i] == lattice[j - counter_le
    ft - 1][i]:
317.                                 counter_left += 1
318.                             else:
319.                                 validator_l = 1
320.                             if counter_left >= self.Nx - 1:
321.                                 validator_l = 1
322.
323.
324.                         while validator_t == 0:
325.                             index_top = i + counter_top
326.                             indices_top_element = self.periodic_boundary_conditions_t
    op(index_top)
327.                             top_elem_y = indices_top_element
328.
329.                             index_higher_top = i + counter_top + 1
330.                             indices_higher_top_element = self.periodic_boundary_condi
    tions_top(index_higher_top)
331.                             higher_top_elem_y = indices_higher_top_element
332.
333.                             if lattice[j][top_elem_y] == lattice[j][higher_top_elem_y
    ]:
334.                                 counter_top += 1
335.                             else:
336.                                 validator_t = 1
337.                             if counter_top >= self.Nx - 1:
338.                                 validator_t = 1
339.
340.
341.                         while validator_b == 0:
342.                             index_bottom = i - counter_bottom
343.                             indices_bottom_element = self.periodic_boundary_condition
    s_bottom(index_bottom)
344.                             bottom_elem_y = indices_bottom_element
345.
346.                             index_below_bottom = i - counter_bottom - 1
347.                             indices_below_bottom_element = self.periodic_boundary_con
    ditions_bottom(index_below_bottom)
348.                             below_bottom_elem_y = indices_below_bottom_element
349.
350.                             if lattice[j][bottom_elem_y] == lattice[j][below_bottom_e
    lem_y]:
351.                                 counter_bottom += 1
352.                             else:
353.                                 validator_b = 1
354.                             if counter_bottom >= self.Nx - 1:
355.                                 validator_b = 1
356.
357.                         corr_length_given_item_avg = (counter_right + counter_left +
    counter_top + counter_bottom) / 4.0
```

```
                        corr_length_given_time_step.append(corr_length_given_item_avg
    )

                corr_length_final = sum(corr_length_given_time_step) / len(corr_lengt
    h_given_time_step)

                return corr_length_final


            def periodic_boundary_conditions_right(self, xr):
                if xr >= self.Nx:
                    xr = xr - self.Nx
                else:
                    None

                return xr


            def periodic_boundary_conditions_left(self, xl):
                if xl <= -1:
                    xl = self.Nx + xl
                else:
                    None

                return xl


            def periodic_boundary_conditions_top(self, yt):
                if yt >= self.Nx:
                    yt = yt - self.Nx
                else:
                    None

                return yt


            def periodic_boundary_conditions_bottom(self, yb):
                if yb <= -1:
                    yb = self.Nx + yb
                else:
                    None

                return yb


            def results(self):
                return self.list_corr_lengths



        class Energy_calculation():
            def __init__(self, list_of_lattices, Nx, N, list_of_angles, J0, l):
                self.list_of_lattices = list_of_lattices
                self.Nx = Nx
                self.N = N
                self.list_of_angles = list_of_angles
                self.J0 = J0
                self.l = l

                self.change_in_angle()

```

```
422.
423.         def change_in_angle(self):
424.
425.             self.list_of_energies = []
426.
427.             for i in range(len(self.list_of_angles)):
428.                 r = self.l * ((2**0.5) / 2.0)
429.                 theta = self.list_of_angles[i]
430.                 d = 2.0 * r * np.sin(np.pi / 4.0 + theta / 2.0)
431.                 J = self.J0 / (d**3)
432.
433.                 energy = self.calculation(i, J)
434.                 self.list_of_energies.append(energy / self.N)
435.
436.
437.         def calculation(self, i, J):
438.             lattice = self.list_of_lattices[i]
439.
440.             temporary_energy = 0
441.             for m in range(Nx):
442.                 for n in range(Nx):
443.                     indices = self.periodic_boundary_conditions(n, m)
444.                     y_bottom = indices[0]
445.                     x_right = indices[1]
446.
447.                     if lattice[n][m] * lattice[x_right][m] < 0:
448.                         energy_right = -
    J * (lattice[n][m] * lattice[x_right][m])
449.                     else:
450.                         energy_right = 0
451.
452.                     if lattice[n][m] * lattice[n][y_bottom] < 0:
453.                         energy_bottom = -
    J * (lattice[n][m] * lattice[n][y_bottom])
454.                     else:
455.                         energy_bottom = 0
456.
457.                     temporary_energy += (energy_right + energy_bottom)
458.
459.             return temporary_energy
460.
461.
462.
463.         def periodic_boundary_conditions(self, x_i, y_i):
464.             yb = y_i - 1
465.             xr = x_i + 1
466.
467.             if xr == self.Nx:
468.                 xr = 0
469.
470.             if yb == -1:
471.                 yb = self.Nx -1
472.
473.             return yb, xr
474.
475.
476.         def results(self):
477.             return self.list_of_energies
478.
479.
480.
481.
482.
483.
484.
485.     class Visualization():
```

```
486.           def __init__(self, lattices_for_all_angles):
487.               self.lattices = lattices_for_all_angles
488.
489.               self.new_files()
490.
491.
492.           def new_files(self):
493.               for i in range(len(self.lattices)):
494.                   np.savetxt("Ising_"+str(i)+".txt", self.lattices[i])
495.
496.
497.
498.       class Graphs():
499.           def __init__(self, time_list, list_of_angles, corr_lengths_list, list_of_
    energies):
500.
501.               self.time_list = time_list
502.               self.corr_lengths_list = corr_lengths_list
503.               self.list_of_angles = list_of_angles
504.               self.list_of_energies = list_of_energies
505.
506.               self.generation()
507.
508.           def generation(self):
509.               with open('avg_corr_length_speed_fac_0_1.dat', 'w') as g:
510.                   for i in range(len(self.time_list)):
511.                       g.write(str(self.time_list[i]))
512.                       g.write(" ")
513.                       g.write(str(self.list_of_angles[i]))
514.                       g.write(" ")
515.                       g.write(str(self.corr_lengths_list[i]))
516.                       g.write(" ")
517.                       g.write(str(self.list_of_energies[i]))
518.                       g.write('\n')
519.               print "BBB"
520.
521.
522.
523.       class Average():
524.           def __init__(self, all_list_of_time, all_lists_of_angle, all_lists_of_cor
    r_lengths, all_lists_of_energy, n_aux):
525.               self.all_lists_of_corr_lengths = all_lists_of_corr_lengths
526.               self.all_lists_of_energy = all_lists_of_energy
527.               self.all_list_of_time = all_list_of_time
528.               self.all_lists_of_angle = all_lists_of_angle
529.               self.n_aux = n_aux
530.
531.               self.calculation()
532.
533.
534.           def calculation(self):
535.               n_internal = len(self.all_lists_of_energy[0])
536.               self.corr_lengths = np.zeros(n_internal)
537.               self.energies = np.zeros(n_internal)
538.               self.angles = np.zeros(n_internal)
539.               self.times = np.zeros(n_internal)
540.
541.               for j in range(n_internal):
542.                   for i in range(self.n_aux):
543.                       self.corr_lengths[j] += self.all_lists_of_corr_lengths[i][j]

544.                       self.energies[j] += self.all_lists_of_energy[i][j]
545.                       self.angles[j] += self.all_lists_of_angle[i][j]
546.                       self.times[j] += self.all_list_of_time[i][j]
547.                   self.corr_lengths[j] = self.corr_lengths[j] / self.n_aux
548.                   self.energies[j] = self.energies[j] / self.n_aux
```

```
549.                     self.angles[j] = self.angles[j] / self.n_aux
550.                     self.times[j] = self.times[j] / self.n_aux
551.
552.
553.             def results(self):
554.                 return self.corr_lengths, self.energies, self.angles, self.times
555.
556.
557.
558.         if __name__ == '__main__':
559.
560.             Nx = 500
561.             N = Nx**2#number of units
562.             N_monte = 1#1
563.             l = 1.0#linear dimension of a square
564.             n_avg = 4
565.             J0 = 1.2
566.             T = 1.0#Tc=2.269 [J / kB]
567.             k_B = 1.0#1.38 * 10**(-23)
568.             beta = 1.0 / (k_B * T)
569.             theta_0 = 0.0 * (np.pi / 180.0)
570.             theta_f = 180.0 * (np.pi / 180.0)
571.             delta_theta = 1.0 * (np.pi / 180.0)#speed
572.
573.             speed_factor = 0.1
574.             print speed_factor, "speed_factor"
575.
576.             n_avg = 10
577.
578.             all_lists_of_angle = []
579.             all_list_of_time = []
580.             all_lists_of_corr_lengths = []
581.             all_lists_of_energy = []
582.
583.             for i in range(n_avg):
584.                     print i
585.                     T_initial_high = 10.0
586.                     beta_initial = 1.0 / (k_B * T_initial_high)
587.                     N_monte_initial = 5.0
588.
589.                     constructor_init_T = Initial_high_T(l, J0, T_initial_high, beta_i
    nitial, Nx, N, N_monte_initial, theta_0)
590.                     lattice_initial = constructor_init_T.results()
591.
592.                     constructor_deform = Deformation(theta_0, theta_f, delta_theta, J
    0, l, T, beta, Nx, N, N_monte, lattice_initial, speed_factor)
593.                     results_for_diff_angles = constructor_deform.results()
594.                     list_of_angles = results_for_diff_angles[0]
595.                     list_of_time = results_for_diff_angles[1]
596.                     list_of_lattices = results_for_diff_angles[2]
597.
598.                     if i == 0:
599.                         constr_vis = Visualization(list_of_lattices)
600.                     else:
601.                         None
602.
603.                     constructor_corr_length = Correlation_length(list_of_lattices, Nx
    , N)
604.                     list_of_corr_lengths = constructor_corr_length.results()
605.
606.                     constructor_energy = Energy_calculation(list_of_lattices, Nx, N,
    list_of_angles, J0, l)
607.                     list_of_energies = constructor_energy.results()
608.
609.                     all_lists_of_corr_lengths.append(list_of_corr_lengths)
610.                     all_lists_of_energy.append(list_of_energies)
```

```
611.                     all_lists_of_angle.append(list_of_angles)
612.                     all_list_of_time.append(list_of_time)
613.
614.
615.             constr_avg = Average(all_list_of_time, all_lists_of_angle, all_lists_of_c
    orr_lengths, all_lists_of_energy, n_avg)
616.             avg_results = constr_avg.results()
617.             avg_list_corr_lengths = avg_results[0]
618.             avg_list_energies = avg_results[1]
619.             avg_list_angles = avg_results[2]
620.             avg_list_times = avg_results[3]
621.
622.             constr_graps = Graphs(avg_list_times, avg_list_angles, avg_list_corr_leng
    ths, avg_list_energies)
```

Appendix IX: List of peer-reviewed publications co-authored by candidate throughout his Ph.D. studies[9]

1. R. Gatt, R. Caruana-Gauci, D. Attard, A. R. Casha, W. Wolak, **K. Dudek**, L. Mizzi, J. N. Grima, On the properties of real finite-sized planar and tubular stent-like structures *Phys. Status Solidi B* **251** 321-327 (2014)

2. A. R. Casha, A. Manche, R. Gatt, W. Wolak, **K. Dudek**, M. Gauci, P. Schembri-Wismayer, M.-T. Camilleri-Podesta, J. N. Grima, Is there a biomechanical cause for spontaneous pneumothorax? *Eur. J. Cardiothorac. Surg.* **45** 1011-1016 (2014)

3. A. R. Casha, L. Camilleri, A. Manche, R. Gatt, D. Attard, W. Wolak, **K. Dudek**, M. Gauci, C. Giordimaina, J. N. Grima, A hypothesis for reactivation of pulmonary tuberculosis: how thoracic wall shape affects the epidemiology of tuberculosis *Clin. Anat.* **28** 614-620 (2015)

4. J. N. Grima, M. Bajada, S. Scerri, D. Attard, **K. K. Dudek**, R. Gatt, Maximising thermal expansion via rigid unit modes: a geometry-based approach *Proc. R. Soc. A* **471** 20150188 (2015)

5. *M. R. Dudek, K. W. Wojciechowski, J. N. Grima, R. Caruana-Gauci, **K. K. Dudek,** Colossal magnetocaloric effect in magneto-auxetic systems *Smart Mater. Struct.* **24** 085027 (2015)

6. ***K. K. Dudek**, D. Attard, R. Caruana-Gauci, K. W. Wojciechowski, J. N. Grima, Unimode metamaterials exhibiting negative linear compressibility and negative thermal expansions *Smart Mater. Struct.* **25** 025009 (2016)

7. A. R. Casha, A. Manche, L. Camilleri, R. Gatt, **K. Dudek**, M. Pace-Bardon, M. Gauci, J. N. Grima, A biomechanical cause for the pathophysiology of apical lung disease *Med. Hypotheses* **92** 88-93 (2016)

8. ***K. K. Dudek**, R. Gatt, L. Mizzi, M. R. Dudek, D. Attard, K. E. Evans, J. N. Grima, On the dynamics and control of mechanical properties of hierarchical rotating rigid unit auxetics *Sci. Rep.* **7** 46529 (2017)

[9] Papers which form the core of the thesis are marked with an asterisk

9. T. Maslowski, **K. K. Dudek,** The Dependence of the Proton Conductivity on Concentration for Networks with Different Symmetry of Molecules *Acta Phys. Pol. A* **132** 129-131 (2017)

10. ***K. K. Dudek**, W. Wolak, M. R. Dudek, R. Caruana-Gauci, R. Gatt, K. W. Wojciechowski, J. N. Grima, Programmable magnetic domain evolution in magnetic auxetic systems *Phys. Status Solidi RRL* **11** 1700122 (2017)

11. ***K. K. Dudek**, R. Gatt, L. Mizzi, M. R. Dudek, D. Attard, J. N. Grima, Global rotation of mechanical metamaterials induced by their internal deformation *AIP Adv.* **7** 095121 (2017)

12. ***K. K. Dudek**, K. W. Wojciechowski, M. R. Dudek, R. Gatt, L. Mizzi, J. N. Grima, Potential of mechanical metamaterials to induce their own global rotational motion *Smart Mater. Struct.* (2018) DOI: https://doi.org/10.1088/1361-665X/aabbf6

Appendix X: List of cenferences and seminars

1. **K. K. Dudek**, D. Attard, R. Caruana-Gauci, K. W. Wojciechowski, J. N. Grima, Unimode metamaterials exhibiting negative linear compressibility (14-18 Spetember, 2015, Malta), 6th International Conference Auxetics and other materials and models with “negative” characteristics

2. **K. K. Dudek**, R. Gatt, L. Mizzi, M. R. Dudek , D. Attard, K. E. Evans, J. N. Grima, Hierarchical systems with tunable mechanical properties (12-16 September, 2016, Szymbark, Poland), 7th International Conference Auxetics and other materials and models with “negative” characteristics and 12th International Workshop Auxetics and related systems

3. **K. K. Dudek**, W. Wolak, The use of auxetic systems in medicine (15 October, 2013, Zielona Góra, Poland), Seminar of the Faculty of Physics and Astronomy at the University of Zielona Góra

4. **K. K. Dudek**, Novel approaches allowing to utilise propensity of mechanical metamaterials to exhibit anomalous mechanical behaviour (6 March, 2018, Zielona Góra, Poland), Seminar of the Faculty of Physics and Astronomy at the University of Zielona Góra